ANALYTICAL MODELING OF CONCRETE COLUMNS CONFINED BY FRP

by

Jurgen Becque

A Thesis Submitted to
the Faculty of Graduate Studies
in Partial Fulfillment of the
Requirements for the Degree of

Master of Science

Structural Engineering Division
Department of Civil and Geological Engineering
University of Manitoba
Winnipeg, Manitoba
Canada

THE UNIVERSITY OF MANITOBA

FACULTY OF GRADUATE STUDIES

*****

COPYRIGHT PERMISSION PAGE

Analytical Modeling of Concrete Columns Confined by FRP

BY

Jurgen Becque

A Thesis/Practicum submitted to the Faculty of Graduate Studies of The University of Manitoba in partial fulfillment of the requirements of the degree of Master of Science

Abstract

FRP-encased concrete columns benefit from a confining effect due to the restraint of the lateral expansion. This effect increases the strength and the ductility of the concrete inside the FRP shell.

A number of empirical models predicting the behaviour of steel- and FRP-confined concrete have been presented in literature. However, a more accurate model for FRP-confined columns is needed.

This thesis proposes a model for concrete columns confined by an FRP shell, where the axial load is applied to the concrete core only and the shell is used as a confining jacket. A second model is proposed for the case where both the FRP and the concrete carry the compressive axial load. The latter model is modified to include configurations with an inner centered void and configurations with a double shell. All of these models satisfy the conditions of equilibrium and strain compatibility between both materials.

Also a finite element model for FRP-confined columns, based on the Drucker-Prager criterion, is presented.

The proposed models are verified by comparing the predictions to experimental data published by different researchers, including an experimental program carried out at the University of Manitoba.

The proposed models are used to examine the influence of key parameters, believed to determine the behaviour of composite sections.

Aknowledgments

This research project was carried out under the supervision of Dr. Sami Rizkalla. The author wishes to express his sincere gratitude to Dr. Rizkalla for providing excellent support, advice and guidance throughout the research program.

Special appreciation is extended towards Moray McVey. His experience and expertise were greatly appreciated during the material testing.

Finally, special thanks go towards all members of the ISIS staff and administration and towards all graduate students for their support and advice and for making ISIS a team.

Table of Contents

List of Tables

List of Figures

List of Symbols

1,2,3 = indices denoting the axial, radial and circumferential direction respectively

A, B = coefficients in octahedral strength criterion (II-47)

A_1, A_2, A_3 = polynomial coefficients in Eq. (II – 20)

A_c = cross-sectional area occupied by the concrete

A_{FRP} = cross-sectional area occupied by the FRP

A_i = parameter in Eq. (III – 41)

A_s = cross-sectional area occupied by the steel

B, A = coefficients in octahedral strength criterion (III-46)

B_{ij} = matrix coefficients in Eq. (III – 63)

c = cohesion (Drucker-Prager model)

D = diameter of the concrete core

D_i = parameter in Eq. (III – 41)

E = elastic modulus

E_o = initial elastic modulus of the concrete

E_{oi} = initial slope of the (σ_1 - ε_i) curve

E_1, E_2 = first and second slope of the σ_1-ε_1 curve as defined in Eq. (II – 38)

E_{1r}, E_{2r} = first and second slope of the σ_1-ε_2 curve as defined in Eq. (II – 38)

E_{ip} = modulus defined by Eq. (III – 45)

E_{hoop} = modulus of the FRP shell material in the hoop direction

E_{long} = modulus of the FRP shell material in the longitudinal direction

E_{sec} = secant modulus of the concrete

f_0 = parameter in Mirmiran and Shahawy's Eq. (II – 38)

f_{0r} = parameter in Mirmiran and Shahawy's Eq. (II – 42)

f_c' = unconfined concrete strength

f_{cc}' = confined concrete strength

$f_{hoop,t}$ = (tensile) strength of the FRP material in the hoop direction

$f_{long,t}$ = (tensile) strength of the FRP material in the longitudinal direction

$f_{hoop,c}$ = compressive strength of the FRP in the hoop direction

$f_{long,c}$ = compressive strength of the FRP in the longitudinal direction

f_y = yield strength of the steel

G = shear modulus of the concrete

G_o = initial shear modulus of the concrete

G_s = secant shear modulus of the concrete

G_T = tangent shear modulus of the concrete

h = height of the cylindrical specimen

H = coupling modulus of the concrete

k = confinement effectiveness coefficient

K = concrete bulk modulus

K_o = initial concrete bulk modulus

K_s = secant concrete bulk modulus

K_T = tangent concrete bulk modulus

n = parameter in Mirmiran and Shahawy's Eq. (II – 38)

n_r = parameter in Mirmiran and Shahawy's Eq. (II – 42)

p_o = outer pressure on the concrete core

p_i = inner pressure on the concrete core

P = load force on the section

r = radial coordinate

R = radius of the concrete core

R_o = outside radius of the concrete core

R_i = inside radius of the concrete core

R_E, R_σ, R_ε = as defined in Eqs (III – 69) to (III –73)

t = thickness of the shell

t_{inner} = thickness of the inner shell

t_{outer} = thickness of the outer shell

T = circumferential tension force in the shell

u = denotes a displacement

U_{cc} = energy stored in the confined concrete

$U_{c,uncf}$ = energy stored in the unconfined concrete

U_{shell} = energy stored in the shell

x = dimensionless strain defined in Eq. (II – 10)

X = dimensionless principal strain defined by Eq. (III – 43)

Y = dimensionless principal stress defined by Eq. (III – 42)

γ_o = octahedral deviatoric strain

$(\gamma_o)_o$ = octahedral deviatoric strain at the peak for a uniaxial test

Δ = indicates an increment in the associated variable

ε = denotes a strain

ε_1, ε_2, ε_3 = principal strains in the concrete

ε_{1u}, ε_{2u} = equivalent uniaxial strains

ε_{cc} = peak strain of the confined concrete

ε_{cu} = strain at failure of the confined concrete

ε_{FRPu} = ultimate strain of the FRP material

ε_{hoop} = hoop strain in the shell

ε_{long} = hoop strain in the shell

ε_o = octahedral volumetric strain

$(\varepsilon_o)_o$ = octahedral volumetric strain at the peak for a uniaxial test

ε_{if} = defines a random point on the descending part of the stress-strain curve

ε_p = peak strain of the unconfined concrete

ε_{ip} = peak strain in the i-th principal direction of the confined concrete

ε_v = volumetric strain

θ = angular coordinate

μ = dilation rate of the concrete

μ_o = initial dilation rate of the concrete

μ_{max} = maximum dilation rate of the concrete

μ_u = ultimate dilation rate of the concrete

μ_{12}, μ_{23} = as defined in Eq. (III – 60)

ν = Poisson's ratio of the concrete

ν_f = major Poisson's ratio of the FRP

ν_f' = minor Poisson's ratio of the FRP

ν_o = initial Poisson's ratio of the concrete

ν_1, ν_2 = as defined in (III – 79)

ν_{ij} = Poisson's ratio of the concrete in direction i under loading in direction j

ξ = Tsai-Wu coefficient

ρ = reinforcement ratio

σ = denotes a stress

$\sigma_1, \sigma_2, \sigma_3$ = principal stresses in the concrete

$\sigma_{2,max}$ = maximum confining pressure

σ_{if} = defines a random point on the descending part of the stress-strain curve

σ_{ip} = concrete peak stress for direction i

σ_{hoop} = hoop stress in the shell

σ_{long} = longitudinal stress in the shell

σ_o = octahedral hydrostatic stress

τ_o = octahedral shear stress

$\tau_{o,max}$ = octahedral shear strength

ϕ = friction angle

ϕ_f = flow angle

ψ = behaviour parameter defined in (VII - 1)

ω_1, ω_2 = ratio variables defined in Eqs. (IV – 6) and (IV – 8)

Chapter I :

Introduction

1.1 Definition and Types of Hybrid Columns

The term 'hybrid column' or 'composite column' implies a column constructed from two or more different materials in such a way that they work together in resisting stresses and strains induced by forces or conditions external to the column. Strictly speaking, ordinary reinforced concrete columns fall within the scope of this definition. However, the term is normally used to indicate applications like either concrete-encased steel columns or concrete-filled tubes of square, rectangular or circular cross-section (Fig. I-1). Besides steel, newly emerging materials like Fiber Reinforced Plastics (FRPs) can be introduced as a tube material, providing an interesting field of study. In this way, concrete columns wrapped with FRP-sheets to provide confinement can also be attributed the name of 'hybrid column'.

In the column sections shown in Fig. I-2, the concrete is enclosed in such a way that axial loading of the column results in a triaxial stress state in the concrete. Axial loading

of any of these column sections will cause a tendency of the concrete to expand laterally which is counteracted by the shell. This will bring the concrete in a state of confinement and thus change its stress-strain behaviour and increase its compressive strength.

In this way, the composite column will act as a synergetic system where the confining pressure of the shell brings the concrete in a triaxial stress state, allowing it to reach higher strength, while the concrete prevents the shell from buckling. This will create a more-than-optimum engineering solution where the strength of the composite column is higher than the sum of its components.

Very little confinement has been experimentally observed in rectangular or square sections. In these sections, a lateral expansion of the concrete will result in bending of the shell walls rather than in the development of membrane stresses equivalent to the hoop stresses in a circular section (Tomii et al. (1988)).

The different aspects of hybrid columns considered in this thesis are :

materials : an important portion of this work will be devoted to FRP-confined concrete columns. However, the models will be evaluated for conventional steel-confined columns as well.

loading : the shell can be solely used as a 'jacket' with the purpose of providing lateral confinement, or in other cases, the shell can contribute in the axial load carrying capacity.

configuration : the shell can be totally filled with concrete, contain a void inside or consist of the double 'sandwich' shell with concrete in between.

1.2 Advantages and Disadvantages of Composite Columns

Concrete filled steel or FRP tubes offer a number of advantages in both design and construction :

1. The tube confines the concrete. This results in an increased strength and ductility of the concrete.

2. The concrete prevents the tube from local buckling.

3. The tube provides well-distributed reinforcement. The reinforcement is located in the most efficient position to resist secondary bending moments.

4. The tube protects the surface of the concrete from physical damage and deterioration by environmental effects such as carbonation and chloride penetration.

5. The tube provides a formwork for the casting of the concrete, which stays in place and doesn't need to be removed. This results in time and cost savings on site.

6. The load-carrying capacity of a composite column is increased when compared to an ordinary reinforced concrete column of the same cross-sectional dimensions. In buildings therefore, more floor area is available for the occupants.

The major disadvantage of a composite column is the exposure of the tube to environmental effects (heat, cold, UV,...). For steel tubes this rises concerns related to susceptibility to corrosion and fire safety. The fire resistance of a concrete-filled steel column is significantly less than that of ordinary reinforced column. There is no reason however why a fire-retardant coating cannot be applied to the surface.

1.3 FRP-Concrete Composite Columns

Substantial progress has been made in the use of composites in the construction industry over the last few years, including the introduction of mass-produced FRP structural members in civil engineering. They have emerged as a potential solution to the problems associated with corrosion and deterioration of the infrastructure.

FRPs consist of continuous fibers of glass, aramid or carbon, embedded in a polymer resin matrix such as polyester, epoxy or vinylester. Tubes of FRP material can be easily produced by filament winding. GFRP (Glass Fiber Reinforced Plastic) appears to be the more economical material.

Properties of interest to engineers offered by composites are high tensile strength for low weight, corrosion immunity, high fatigue strength, high damping and electromagnetic neutrality. The additional benefits of using FRP are :

1. The tubes are light-weight and easy to handle, now providing the ideal formwork.

2. Susceptibility to corrosion is no longer a problem.

3. FRP is an anisotropic material. By changing the winding angles, thicknesses and the number of the different layers a different material can be obtained with a different ratio of axial to circumferential material properties. In other words, the properties in the axial and hoop direction are uncoupled and can be optimized.

4. Glass fiber jackets have been used as insulators in severe conditions e.g. in a hot oil pipeline project over the water on the Gulf of Mexico.

1.4 Objectives

The main objective of the thesis is to develop reliable models to predict the behaviour and load carrying capacity of FRP/concrete hybrid columns. The first model will deal with the loading case when the load is applied only to the concrete core and the shell provides only the confinement effect. The second model covers all the cases where the

applied load is resisted by the entire FRP/concrete hybrid system. This includes the totally filled column, the column with an inner void and the sandwich system.

Based on the established reliability of the model, parametric studies will be performed to study the effect of the void size, the shell material properties and the amount of hoop fibre reinforcement.

Based on the finding, design guidelines will be provided.

1.5 Scope

The thesis will review the current models for hybrid systems presented in the literature. This includes steel/concrete and FRP/concrete hybrid systems. These models will be calibrated to experimental work conducted by others to evaluate their validity to predict the response and ultimate load carrying capacity.

Chapter III will review the material constitutive relationship of FRP and concrete. The constitutive relations for the concrete involve complete triaxial material laws presented by different authors. These material laws are employed in the proposed models based on strain compatibility and equilibrium. In Model 1, strain compatibility in the lateral direction is assured between the concrete and the outer shell. In Model 2, strain compatibility is assured in both the lateral and the longitudinal direction.

The proposed models, using different constitutive relations, will be verified using experimental data. Based on the findings, the best model will be recommended.

Model 2 will be further modified to predict the behaviour of different configurations. The modified model will be verified using an experimental program conducted at the University of Manitoba.

A finite element model is proposed to model solid hybrid FRP-concrete sections and compared to the proposed models as well as the experimental data.

A summary of the work and design recommendations are presented in chapter VIII.

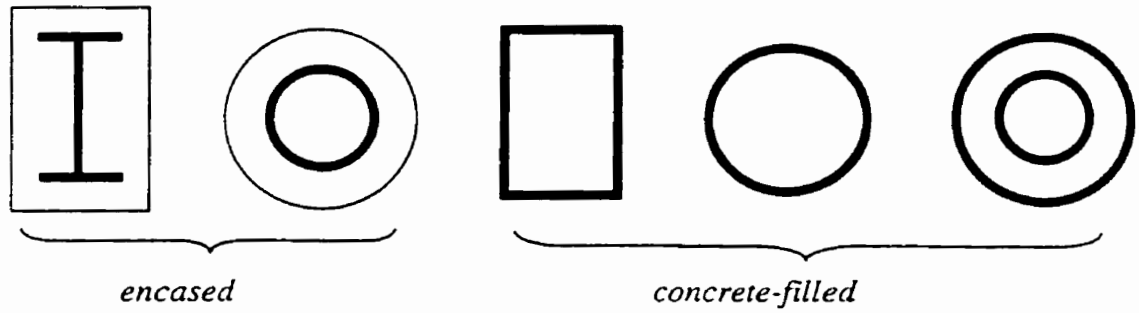

Fig. I – 1 : Different types of hybrid columns

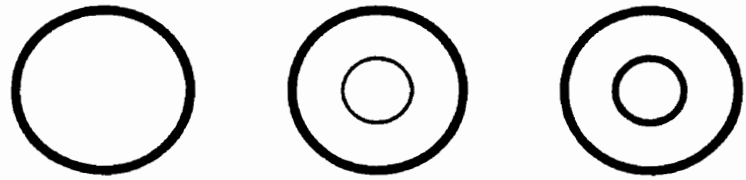

Fig. I – 2 : Examples of confined hybrid columns

Chapter II :

Literature Review

2.1 Introduction

This chapter provides an overview of the models currently available to predict the behaviour of hybrid sections. Behaviour of FRP-confined concrete columns will also be compared to the behaviour of a steel-confined concrete column.

2.2 Conventions

The sign convention in this thesis assumes a positive sign for compressive stresses and consequently a negative sign for tensile stresses.

The coordinate axes system assumed for the cylinder uses axis 1 for the longitudinal direction, axis 2 for the radial direction and axis 3 for the circumferential direction, as shown in Fig. (II - 1).

The three axes are also the directions of the principal stresses under applied compressive axial loading. In this thesis, σ_1 and ε_1 represent the concrete stress and strain in the longitudinal direction, σ_2 and ε_2 are the concrete stress and strain in the radial direction, and σ_3 and ε_3 are the concrete stress and strain in the circumferential direction.

2.3 Comparison between Steel- and FRP - confined Concrete

Fig. (II - 2) shows the axial stress-strain behaviour of a steel-confined concrete cylinder together with the typical axial stress-strain behaviour of a GFRP-confined concrete cylinder. The data for the steel-confined cylinder is based on tests by Orito (1987) while the FRP-confined cylinder was tested by Mirmiran (1997).

Because of the high modulus of elasticity of the steel, confinement of the concrete core is initiated at relatively low load levels. Only small lateral straining of the concrete is needed to develop significant hoop stresses, resulting in a confining pressure. It can be seen from Fig. (II – 2) that the steel-confined concrete experiences only mild softening before it reaches a maximum strength. It has been shown (Ahmad (1980)) that this peak strength occurs shortly after the steel tube yields. After reaching its maximum strength the curve follows a gradual postpeak descending branch.

On the other hand, the FRP-confined concrete displays a distinct bilinear response with a sharp softening and a transition zone at the level of its unconfined strength f_c', after

which the tangent stiffness stabilizes at a constant value until reaching the ultimate strength.

Because of the low modulus of GFRP material in comparison to steel, the GFRP material is little effective in providing lateral confining pressures at low load levels. This is evident from the behaviour in the first part of the stress-strain curve, which is almost identical to the unconfined curve. At a stress level near the unconfined compressive strength of the concrete, f_c', the concrete expands extensively in the lateral direction due to the formation of microcracks. This results in activation of the confinement and an increase in strength. Because of the linear nature of its material behaviour the FRP will apply a continuously increasing pressure on the concrete core until the tube reaches failure due to fiber rupture. This behaviour is unlike the steel tube where the confining pressure remains constant after yielding of the steel.

Alternatively, the behaviour can be examined by considering the volumetric strain behaviour shown in Fig (II - 3). Volumetric strains can be calculated as :

$$\begin{aligned} \varepsilon_v &= \varepsilon_1 + \varepsilon_2 + \varepsilon_3 \\ &= \varepsilon_1 + 2\varepsilon_2 \end{aligned} \qquad (\text{II} - 1)$$

where ε_1, ε_2 and ε_3 are the principal strains of the concrete.

For an unconfined concrete cylinder the volumetric strain becomes unstable and randomly large near failure. Fig. (II – 3) shows that a steel shell effectively confines the concrete until the concrete dilation becomes unstable shortly after yielding of the steel tube.

In the case of an FRP tube, the concrete tends to expand when the unconfined strength is reached and the FRP becomes effective at curtailing the lateral expansion shortly after. The FRP shell then reverses the direction of volumetric response and failure of the concrete core is associated with large volume contraction.

Fig. (II - 4) shows the dilation rate curves of concrete for the two confinement mechanisms, as well as a typical dilation curve for an unconfined concrete cylinder. The dilation rate μ is defined as :

$$\mu = \frac{d\varepsilon_2}{d\varepsilon_1} \qquad (II-2)$$

The dilation rate for the unconfined concrete increases drastically with the growth of microcracks and becomes unstable near its peak strength. The dilation rate of steel-confined concrete, on the other hand, is delayed until the steel tube yields , after which the confined concrete behaves much in the same way as the unconfined concrete. The behaviour of the FRP-confined concrete however is totally different. Once the tube becomes fully activated, it not only contains the dilation rate of the concrete core, but also reduces the dilation rate to an asymptotic value.

Mirmiran and Shahawy (1998) experimentally formulated the maximum dilation rate μ_{max} and the ultimate dilation rate μ_u as follows :

$$\mu_{max} = -0.977\ Ln\left(\frac{2E_{hoop}t}{f_c'D}\right) + 3.938 \qquad (II-3)$$

$$\mu_u = -0.187\ Ln\left(\frac{2E_{hoop}t}{f_c'D}\right) + 0.881 \qquad (II-4)$$

where D is the diameter of the concrete core, t is the thickness of the GFRP shell and E_{hoop} is the elastic modulus of the GFRP material in the hoop direction.

The following section will highlight some of the well-known models for confined concrete.

2.4 Mander

2.4.1 Introduction

The model for confined concrete proposed by Mander (1988) is the most widely used one to date. Although it was originally developed for conventionally reinforced concrete columns, it can be used to model steel-jacketed columns.

2.4.2 Stress-strain behaviour

According to Mander's theory the axial compressive strength of confined concrete f_{cc}' can be determined as follows :

$$f'_{cc} = 2.254\sqrt{1+7.94\frac{\sigma_{2,max}}{f'_c}} - 2\frac{\sigma_{2,max}}{f'_c} - 1.254 \qquad (II-5)$$

where f_c' is the unconfined concrete strength. $\sigma_{2,max}$ is the maximal lateral confining stress induced on the concrete core by the shell. In case of a steel shell, the maximum lateral confinement stress is related to the yield strength f_y of the steel as follows :

$$\sigma_{2,\max} = \frac{f_y t}{R} \qquad (II-6)$$

In case of an FRP shell, the maximum confinement stress is proportional to the ultimate strength of the FRP jacket in the hoop direction, f_{hoop}, as follows :

$$\sigma_{2,\max} = \frac{f_{hoop} t}{R} \qquad (II-7)$$

The strain ε_{cc} corresponding to the maximum confined concrete stress f_{cc}' can be calculated as follows :

$$\varepsilon_{cc} = \varepsilon_p \left(1 + 5 \left(\frac{f_{cc}'}{f_c'} - 1 \right) \right) \qquad (II-8)$$

where ε_p is the strain of the unconfined concrete at peak stress, which can be taken as 0.002.

The actual stress-strain curve is based on an equation proposed by Popovics (1973) :

$$\sigma_1 = \frac{f_{cc}' \, x \, r}{r - 1 + x^r} \qquad (II-9)$$

where the variables in the above equation are defined by :

$$x = \frac{\varepsilon_1}{\varepsilon_{cc}} \qquad (II-10)$$

$$r = \frac{E_o}{E_o - E_{\sec}} \qquad (II-11)$$

$$E_{\sec} = \frac{f'_{cc}}{\varepsilon_{cc}} \qquad (II-12)$$

E_o and E_{sec} are the initial tangent modulus of the unconfined concrete and the secant modulus at peak strength of the confined concrete respectively.

2.4.3 Energy Balance

In the case of steel encased concrete, the steel at some point will yield in the hoop direction, subsequently providing a constant confining pressure. The concrete will reach its confined peak strength f_{cc}' at a strain ε_{cc}. Failure of an FRP confined cylinder on the other hand is determined by rupture of the fibers in the hoop direction. This occurs at a concrete longitudinal strain ε_{cu} which is not necessarily equal to ε_{cc}.

To calculate the concrete longitudinal strain ε_{cu} for FRP confined concrete, an energy balance approach is used. Mander proposed the idea is that the additional strain energy which is stored in the concrete when it is confined, is provided by energy built up in the confining shell. In other words, the difference in area under the confined and the unconfined stress-strain curves is set to be equal to the strain energy of the confining shell U_{shell} (Fig. II - 5) :

$$U_{shell} = U_{cc} - U_{c,uncf} \qquad (II-13)$$

U_{cc} denotes the energy of the confined concrete, $U_{c,uncf}$ is the energy of the unconfined concrete.

In the case of an FRP shell, the stress-strain behaviour of the shell is linear up to failure. The energy stored in the shell at failure, integrated over the cross-section is then given by :

$$U_{shell} = A_{FRP} E_{hoop} \int_0^{\varepsilon_{FRPu}} \varepsilon_{hoop} d\varepsilon_{hoop}$$

$$= A_{FRP} E_{hoop} \frac{\varepsilon_{FRPu}^2}{2} \qquad (II-14)$$

where ε_{FRPu} is the ultimate strain of the FRP material in the hoop direction, A_{FRP} is the cross-sectional area occupied by the FRP, ε_{hoop} stands for the FRP strain in the hoop direction and E_{hoop} is the elastic modulus of the FRP material in the hoop direction.

The total energy of the unconfined concrete, up to failure, is obtained by integration of the unconfined concrete stress-strain curve :

$$U_{c,uncf} = A_c \int_0^{0.0035} \sigma_1 d\varepsilon_1 \qquad (II-15)$$

where A_c is the cross-sectional area occupied by the concrete.

A parabolic stress-strain behaviour is assumed for the unconfined concrete :

$$\sigma_1 = f_c' \left(\frac{2\varepsilon_1}{0.002} - \left(\frac{\varepsilon_1}{0.002} \right)^2 \right) \qquad (II-16)$$

The strain energy of the confined concrete can be found by (numerical) integration over the stress-strain equation given by Eq. (II - 9) :

$$U_{cc} = A_c \int_0^{\varepsilon_{cu}} \sigma_1 d\varepsilon_1 \qquad (II-17)$$

Substituting Eqs. (II - 17), (II - 15) and (II - 14) into Eq. (II - 13) and solving for ε_{cu}, the concrete strain at the point of fracture of the FRP jacket can be calculated. Accordingly, the complete stress-strain curve of the confined concrete can be determined.

It should be noted that an additional term should be added to the right-hand side of Eq. (II - 13), accounting for the lateral strain energy of the confined concrete :

$$U'_{cc} = 2A_c \int \sigma_2 d\varepsilon_2 \qquad (II-18)$$

However this term will be negligible compared to U_{cc}.

2.5 A modified Mander theory

2.5.1 Introduction

Recently, it was found that Mander's model was unable to predict the typical response of FRP-confined concrete (Parent and Labossiere (1999)). The two researchers proposed a modification to Mander's theory to account for the varying confining pressure under FRP confinement.

It should be noted that Mander's model, in the format presented in section 2.4, has been used by Purba and Mufti (1998) to model the behaviour of carbon fibre wrapped columns and has even been extended towards the calculation of theoretical interaction diagrams for combined bending and axial load. Reasonable results in comparison to the

measured values were reported. However, the reported values of the elastic modulus of the carbon sheets were 231 to 373 GPa, which is even higher than the modulus of steel. For this reason the shape of the stress-strain relationship for the carbon wrapped columns was similar to that of steel confined columns and the bilinear stress-strain relationship typically observed for a low modulus confining medium was not observed.

2.5.2 Radial Strains

The dilation rate μ was previously introduced by Eq. (II – 2) and is related to the concrete Poisson's ratio ν by the equation :

$$\mu = \frac{\nu}{\left(1-\nu-2\nu^2\right)\frac{\alpha}{E_c}-1} \qquad (II-19)$$

where :

$$\alpha = \frac{t}{R} E_{hoop}$$

A cubic polynomial formula was proposed by Parent and Labossiere to express the relation between the radial and the axial strains of the concrete as follows :

$$\varepsilon_2 = A_1\varepsilon_1 + A_2\varepsilon_1^2 + A_3\varepsilon_1^3 \qquad (II-20)$$

where the polynomial coefficients A_1 to A_3 can be determined using limit conditions :

1. $$\left.\frac{d\varepsilon_2}{d\varepsilon_1}\right|_{(\varepsilon_1 = 0)} = \mu_0 \qquad (II-21)$$

2. $\varepsilon_2 = \varepsilon_{FRPu} \quad for \quad \varepsilon_1 = \varepsilon_{cu}$ (II – 22)

3. $\left.\frac{d\varepsilon_2}{d\varepsilon_1}\right|_{(\varepsilon_1 = \varepsilon_{cu})} = \mu_u$ (II – 23)

With :

ε_{cu} = the concrete axial strain at the failure point of the FRP

μ_0 , μ_u = the initial and ultimate dilation rates respectively

ε_{FRPu} = the ultimate hoop strain of the FRP

Conditions 1-3 result in :

$$A_1 = \mu_0 \tag{II – 24}$$

$$A_2 = \frac{\varepsilon_{FRPu} - A_3\varepsilon_{cu}^3 - A_1\varepsilon_{cu}}{\varepsilon_{cu}^2} \tag{II – 25}$$

$$A_3 = \frac{\mu_u\varepsilon_{cu} - 2\varepsilon_{FRPu} + A_1\varepsilon_{cu}}{\varepsilon_{cu}^3} \tag{II – 26}$$

$$\mu_u = \frac{\nu_u}{\left(1 - \nu_u - 2\nu_u^2\right)\frac{\alpha}{E_c} - 1} \qquad \mu_o = \frac{\nu_o}{\left(1 - \nu_o - 2\nu_o^2\right)\frac{\alpha}{E_c} - 1} \qquad \alpha = \frac{t}{R}E_{hoop}$$

where :

ν_o = the initial Poisson's ratio of the concrete

ν_u = the Poisson's ratio of the concrete for a concrete strain $\varepsilon_1 = \varepsilon_{cu}$

Under the assumption that the ultimate strain of the confined concrete ε_{cu} is known, Eq. (II - 20) can be used to calculate the radial strain for any given axial strain.

2.5.3 Calculation Method

A flow chart of the calculations for the modified Mander model introduced by Parent and Labossiere is shown in Fig. (II – 6). To start the calculations a value for ε_{cu} , the concrete strain at failure, is assumed. Using this value the coefficients A_1, A_2 and A_3 of Eq. (II – 20) can be determined using Eqs. (II – 24), (II – 25) and (II – 26). The complete axial stress-strain curve can then be calculated as follows :

For a certain value of ε_1, the radial strain ε_2 (= ε_3) can be evaluated using Eq. (II - 20). Using the value of ε_2, the confining pressure σ_2 can be determined using Eq. (II – 28) which is based on the equilibrium of forces shown in Fig. (II – 7). The equilibrium equation can be written as follows :

$$\sigma_2 = \frac{T}{R} = \frac{\sigma_{hoop} t}{R} \qquad (II-27)$$

and :

$$\sigma_2 = \frac{\varepsilon_2 E_{hoop} t}{R} \qquad (II-28)$$

R is the radius of the core, t is the thickness of the shell.

Using Eq. (II - 9), σ_1 can be determined for the chosen ε_1.

When the complete stress-strain curve is established, an energy balance given by Eq. (II - 13) can be used to determine the new value for ε_{cu}. All steps are then repeated to establish a new stress-strain curve.

2.6 Razvi and Saatcioglu

2.6.1 Confined Concrete Strength

Razvi & Saatcioglu (1992) theoretically examined the confinement effect on a perfectly elastic material. A combination of lateral and axial compression will counteract the tendency of the material to expand laterally. Assuming a linearly elastic and isotropic material, the following relationship can be written between the uniaxial and the triaxial stresses at a given lateral strain level :

$$\frac{-\nu\sigma_{1u}}{E} = \frac{\sigma_{2t} - \nu(\sigma_{2t} + \sigma_{1t})}{E} \qquad (II-29)$$

where the extra indices u and t denote whether the stress is related to the uniaxial or the triaxial stress state respectively.

Eq. (II - 29) can be written as :

$$\sigma_{1t} = \sigma_{1u} + k'\sigma_{2t} \qquad (II-30)$$

with :

$$k' = \frac{1-\nu}{\nu} \qquad (II-31)$$

Thus k' is a function of the Poisson's ratio ν, and results in higher values for lower values of ν.

For concrete, the elastic modulus and the Poisson's ratio vary with loading due to material nonlinearity. Furthermore, it was found that microcracking induces anisotropy so that the stress-strain characteristics and Poisson's ratios may be different in all three orthogonal directions. Therefore the aforementioned expressions are not applicable to concrete. However, an expression of the same form as Eq. (II - 30) was written to express the triaxial strength of concrete in terms of uniaxial strength and lateral confining pressure :

$$f'_{cc} = f'_c + k\sigma_2 \qquad (II-32)$$

where f_{cc}' and f_c' are the confined and unconfined compressive strengths respectively. k is named the confinement effectiveness coefficient. While the coefficients k and k' are not identical, Razvi and Saatcioglu expect that k, like k' is a function of the Poisson's ratio and has lower values for higher values of the Poisson's ratio. Since higher values of the Poisson's ratio occur near failure, at which the lateral pressure is maximum, lower values of the coefficient k correspond to higher values of the lateral pressure. An expression reflecting the variation of k with lateral pressure was obtained by Richart (1982) based on regression analysis of experimental data an is as follows :

$$k = 6.7(\sigma_2)^{-0.17} \qquad (II-33)$$

with σ_2 the confining pressure in MPa.

Fig. (II - 8) shows that indeed k exhibits lower values for higher values of the lateral pressure, approaching an almost constant value slightly higher than 4 for the high pressure range.

2.6.2 Stress-strain relationship

For a certain confining pressure σ_2 Eqs. (II - 32) and (II - 33) can be used to predict the peak stress. At the peak point Razvi and Saatcioglu propose the following equation for the corresponding strain ε_{cc} :

$$\varepsilon_{cc} = \varepsilon_p (1 + 5K_1) \qquad (II-34)$$

where :

$$K_1 = \frac{k\sigma_2}{f'_c} \qquad (II-35)$$

ε_p is the peak strain of unconfined concrete, which, in the absence of experimental data, can be assumed to be 0.002.

Popovics' equation is used to represent the ascending branch of the stress-strain relationship as follows :

$$\sigma_1 = \frac{f'_{cc}\left(\frac{\varepsilon_1}{\varepsilon_{cc}}\right)r}{r - 1 + \left(\frac{\varepsilon_1}{\varepsilon_{cc}}\right)^r} \qquad (II-36)$$

where :

$$r = \frac{E_c}{E_c - E_{sec}} \qquad E_{sec} = \frac{f'_{cc}}{\varepsilon_{cc}} \qquad (II-37)$$

2.7 Mirmiran and Shahawy

2.7.1 Introduction

Mirmiran and Shahawy (1998) presented is an empirical model that is applicable to predict the behaviour of concrete columns confined by FRP.

The researchers realized that the response of FRP confined concrete is essentially bilinear. They presented a model based on a four-parameter relationship and calibrated that model according to experimental results.

2.7.2 Proposed Confinement Model

To represent the bilinear response of concrete confined with an FRP tube, the following model, shown in Fig. (II – 9), is proposed :

$$\sigma_1 = \frac{(E_1 - E_2)\varepsilon_1}{\left[1 + \left(\frac{(E_1 - E_2)\varepsilon_1}{f_0}\right)^n\right]^{1/n}} + E_2\varepsilon_1 \qquad (II-38)$$

where :

ε_1 and σ_1 = axial concrete strain and stress respectively

E_1 and E_2 = the first and second slopes respectively

f_0 = reference stress at the intercept of the second slope with the stress axis

n = a parameter that mainly controls the curvature of the curve in the transition zone

As noted before, the confining effect of the FRP shell is mainly activated at the level of lateral expansion, that is usually in the vicinity of the peak strength of the unconfined concrete f_c'. Therefore, the first slope depends almost solely on the concrete stiffness. Mirmiran and Shahawy evaluate the first slope E_1, based on an equation by Ahmad and Shah (1982), as follows :

$$E_1 = 3950\sqrt{f_c'} \qquad (II-39)$$

As the concrete core approaches its unconfined strength, the formation of microcracks causes a significant increase in the lateral expansion and the FRP jacket becomes the restraining device against failure. Therefore, the second slope E_2 is a function of the stiffness of the confining tube, and to a lesser extent, of the unconfined strength of the concrete. The slope of the second part of the curve, E_2, can be estimated as :

$$E_2 = 245.61\,(f_c')^{0.2} + 1.3456\left(\frac{E_{hoop}t}{D}\right) \qquad (II-40)$$

where E_{hoop} is the modulus of elasticity of the tube in the hoop direction, D is the core diameter and t is the thickness of the tube.

The reference stress, f_0, is a function of the strength of the unconfined concrete and the confining pressure provided by the tube and was therefore estimated as :

$$f_0 = 0.872 f_c' + 0.371 \sigma_{2,\max} + 6.258 \qquad (II-41)$$

where $\sigma_{2,\max}$ is given by Eq. (II - 7).

It can be shown that the model is not very sensitive to the curve-shape parameter n. A value of 1.5 is proposed by Mirmiran and Shahawy.

2.7.3 Modeling of lateral strains

Mirmiran and Shahawy realized that the axial stress vs. lateral strain curve is also bilinear. Therefore the same Eq. (II – 38) can be used to represent the behaviour in the lateral direction. The four parameters defining the shape of the curve, E_1, E_2, f_0 and n, will receive an extra subscript r denoting the radial direction, as follows :

$$\sigma_1 = \frac{(E_{1r} - E_{2r})\varepsilon_2}{\left[1 + \left(\frac{(E_{1r} - E_{2r})\varepsilon_2}{f_{0r}}\right)^{n_r}\right]^{1/n_r}} + E_{2r}\varepsilon_2 \qquad (II-42)$$

The first slope E_{1r} is simply obtained as follows :

$$E_{1r} = \frac{E_1}{\nu} \qquad (II-43)$$

E_{1r} is calculated in a similar way, using the dilation rate μ_u, as follows :

$$E_{2r} = \frac{E_2}{\mu_u} \qquad (II-44)$$

The curve-shape parameter n_r is determined as follows :

$$n_r = \frac{n}{\mu_u} \qquad (II-45)$$

and finally, the reference stress f_{0r} is calibrated in a form similar to f_0, as follows :

$$f_{0r} = 0.636 f_c' + 0.233 \sigma_{2,\max} + 4.561 \qquad (II-46)$$

2.7.4 Confinement effectiveness

As part of their work, Mirmiran and Shahawy also presented an expression for the confinement effectiveness coefficient k for FRP-confined concrete. From their experiments they calibrated an expression analoguous to Richart's equation (II – 33) :

$$k = 6.0(\sigma_2)^{-0.3} \qquad (II-47)$$

where σ_2 is the confining pressure, measured in MPa.

Eq. (II – 47) again represents the experimentally observed fact that confinement is not as effective at high lateral pressures as compared to the lower lateral pressures.

2.8 Evaluation of the existing models

2.8.1 Introduction

This section provides a calibration of the various models that have been previously discussed, using experimental data. The first example deals with a concrete cylinder, confined by a steel shell. The two other examples examine the behaviour of concrete confined by FRP tubes. In all three cases the load was applied to the concrete only.

2.8.2 Example 1 (Steel shell)

2.8.2.1 Properties

The experimental work was conducted by Orito (1987). The specimen is a heavily steel-confined column stub. The wall-thickness of the steel tube is 5.2 mm for a concrete core diameter of 114.3 mm. Arrangements were made to have the steel shell work as a jacket in unidirectional (circumferential) tension. The load is applied to the concrete core only. The specimen's dimensions and material properties are listed in Table (II – 1). All values from Table (II – 1) were experimentally measured, with the exception of the steel modulus, which was assumed to be 200 GPa, and the concrete modulus, which was calculated using the ACI formula :

$$E_c = 4500\sqrt{f'_c}$$

2.8.2.2 Mander

The application of Mander's original theory, presented in section 2.5, is quite straightforward and the prediction can be based on Eqs. (II - 5) to (II - 12). The axial stress-strain curve predicted by Mander's model is shown in Fig. (II - 10), together with the experimental data by Orito (1987). The peak strength, determined by Eq. (II - 5), was found to be 159.7 MPa, in comparison to the measured value of 172 MPa. Therefore the error is 7.1 percent. The peak strain, based on Eq. (II - 8) was found to be 0.023, in comparison to the measured value of 0.028 . The overall shape of the axial stress-strain curve, based on Eq. (II - 9), compares well with the experimental results.

2.8.2.3 Razvi & Saatcioglu

The predictions according to Razvi and Saatcioglu's model are shown in Fig. (II - 11). The predicted behaviour was based on Eqs. (II - 32) to (II - 37).

The peak stress, based on Eq. (II - 33), results in a value of 178.2 MPa, in comparison to the measured value of 172 MPa. Therefore the error is 3.6 percent.

The confined peak strain, predicted by Eq. (II - 34), is 0.026, in comparison to the measured value of 0.028. Therefore the error is 7.1 percent.

2.8.3 Example 2

2.8.3.1 Properties

Mirmiran and Shahawy (1998) tested several concrete cylinders confined with GFRP in compression. The FRP tubes were made of polyester resin with unidirectional E-glass fibers at a $\pm 75^{\circ}$ winding angle. The GFRP jacket was used to provide confinement only and not to share the applied axial load. The specimen details are listed in Table (II – 2).

2.8.3.2 Mander

Mander's model was applied using the data from Table (II – 2). The results are shown in Fig. (II - 12). According to Mander's theory, failure is determined using an energy balance. The energy stored in the FRP shell is given by Eq. (II – 14) :

$$U_{shell} = A_{FRP}\frac{f_{hoop}^2}{2E_{hoop}} = 4543 \quad Nm/m$$

The energy of the unconfined concrete is given by Eq. (II – 16) :

$$U_{c,uncf} = A_c f_c' \int_0^{0.0035}\left(\frac{2\varepsilon}{0.002} - \left(\frac{\varepsilon}{0.002}\right)^2\right)d\varepsilon = 1113 \quad Nm/m$$

The energy of the confined concrete can then be determined using Eq. (II – 13) :

$$U_{cc} = 5656 \quad Nm/m$$

Numerical integration of the area under the curve eventually determines the failure point at 69.0 MPa, in comparison to a measured value of 74.6 MPa. Therefore the error is 7.5 percent. The axial strain at failure is predicted to be 0.0077, in comparison to a measured value of 0.043.

2.8.3.3 Razvi and Saatcioglu

An attempt can be made to apply Razvi and Saatcioglu's model to the FRP-confined cylinder using the material properties from Table (II – 2). The axial stress-strain curve is presented in Fig. (II - 13). Failure is predicted for an axial concrete stress of 71.0 MPa, in comparison to a measured value of 74.6 MPa. Therefore the error is 4.8 percent. The axial concrete strain at failure is predicted to be 0.019, in comparison to a measured value of 0.043.

2.8.3.4 Modified Mander Model

The modified Mander model proposed by Parent and Labossiere was applied, using the equations presented in 2.5.2.

Fig. (II - 14) shows the calculated results. Failure occurs at an axial stress of 78.5 MPa, in comparison to a measured value of 74.6 MPa. Therefore the error is 5.2 percent. The energy balance, including the term from Eq. (III - 100), yields an ultimate concrete strain of 0.0124, compared to a measured value of 0.043, and proves to be unsuccessful.

2.8.3.5 Mirmiran and Shahawy

Fig. (II - 15) shows the results of Mirmiran and Shahawy's theory. Both first and second slopes are well estimated by the model. However, the confinement effect is slightly overestimated.

The point of failure can be determined by setting the radial (= circumferential) strain ε_2 in Eq. (II - 42) equal to the rupture strain ε_{FRPu} for the FRP. This results in a predicted failure at an axial stress of 83.2 MPa, in comparison to a measured value of 74.6 MPa. This corresponds to an error of 11.5 percent. The corresponding axial strain at failure is predicted to be 0.0388, in comparison to a measured value of 0.043. The error is 9.7 percent.

2.8.4 Example 3

2.8.4.1 Properties

Nanni and Bradford (1995) tested a 152.5 mm x 305 mm concrete cylinder, wrapped with four plies of E-glass fibers and vinylester resin. The modulus of elasticity of the FRP jacket has been reported as 52,000 MPa. The jacket has hoop fibres only (90° orientation). The hoop strength of the FRP shell is not accurately known. Details are provided by Table (II - 3).

2.8.4.2 Mirmiran and Shahawy

The predictions of Mirmiran and Shahawy's model are presented in Fig. (II - 16). Eq. (II - 39) somewhat overestimates the elastic modulus of the concrete and consequently the first slope of the stress-strain curve. However, the second slope of the curve matches well with the measured behaviour.

2.9 Conclusions

Both the predictions by Mander and Razvi and Saatcioglu are in good agreement with the experimental data for the steel-confined cylinder. Both models are easy to apply. However, they supply no information on lateral or volumetric concrete strains. Neither can they be used to determine the load level where the steel of the shell starts yielding in the circumferential direction.

When applied to FRP-confined concrete, Mander's model as well as Razvi and Saatcioglu's, fail to predict the response of the confined concrete.

Parent and Labossiere proposed a modification of Mander's theory, based on an energy approach. However, this model is unsuccessful as well in predicting the behaviour of FRP-confined concrete. This conclusion has been confirmed by Spoelstra and Monti (1999) and by Mirmiran and Shahawy (1998).

Mirmiran and Shahawy presented a model which is empirical in nature, but which yielded reasonably good results in the case of the examples that were considered.

All models presented in literature apply to the case where the compressive load is applied to the concrete core only and the shell is used as a confining jacket. No model has been presented yet to describe the case where both the concrete and the shell are loaded and the shell contributes directly in the load carrying capacity.

It is concluded that more research work is necessary in order to present models that provide accurate predictions and a full and detailed understanding of the behaviour of both steel- and FRP-confined concrete columns.

Property	*Value*
Core Diameter D	114.3 mm
Tube Thickness t	5.2 mm
Unconfined Concrete Strength f'_c	52.4 MPa
Confined Concrete Strength f'_{cc}	172 MPa
Ultimate (Confined) Strain ε_{cu}	0.036
Concrete Elastic Modulus E_c	32.6 GPa
Steel Yield Strength f_y	376.7 MPa
Steel Elastic Modulus E_s	200 GPa

Table II – 1 : Specimen Properties (Example 1)

Property	*Value*
Core Diameter D	145 mm
Tube Thickness t	2.2 mm
Unconfined Concrete Strength f'_c	26.4 MPa
Confined Concrete Strength f'_{cc}	74.6 MPa
Ultimate (Confined) Strain ε_{cu}	0.043
Concrete Elastic Modulus E_c	23.1 GPa
FRP Hoop Strength f_{hoop}	579.2 MPa
FRP Circumferential Elastic Modulus E_{hoop}	37 GPa

Table II - 2 : Specimen Properties (Example 2)

Property	*Value*
Core Diameter D	152.5 mm
Tube Thickness t	1.2 mm
Unconfined Concrete Strength f'_c	36.3 MPa
Concrete Elastic Modulus E_c	27.1 GPa
FRP Circumferential Elastic Modulus E_{hoop}	52 GPa

Table II – 3 : Specimen Properties

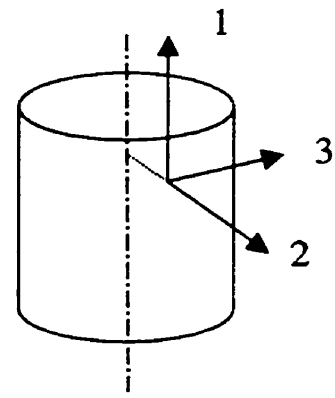

Fig. II – 1 : Orientation of the coordinate axes

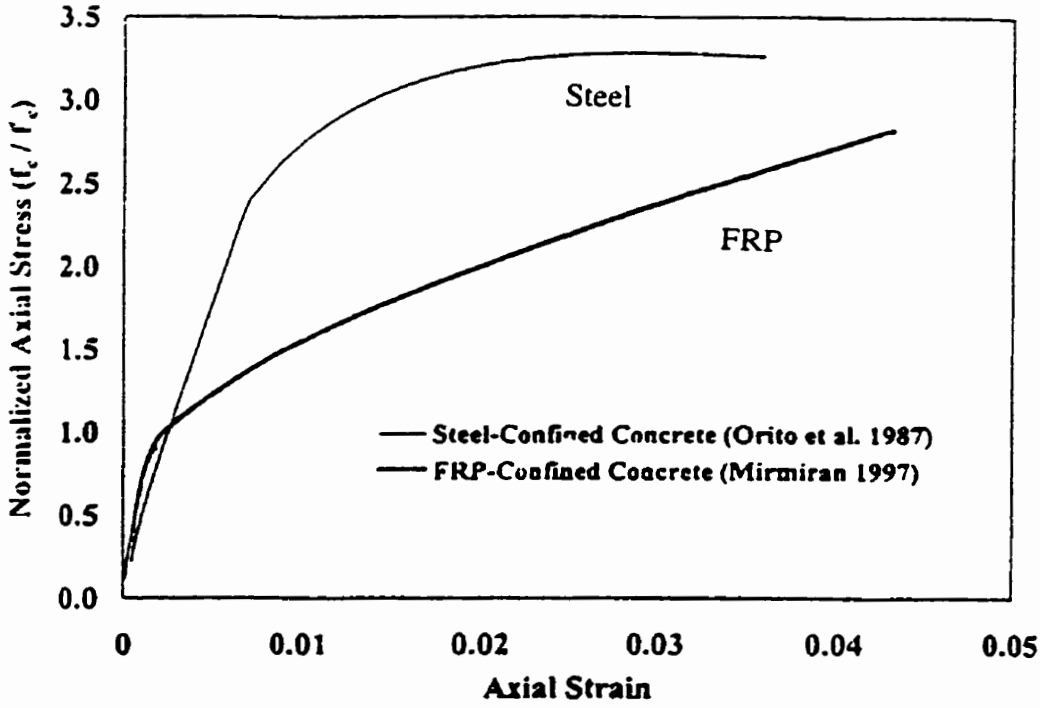

Fig. II - 2 : Axial stress-strain curves for steel- and FRP-confined concrete

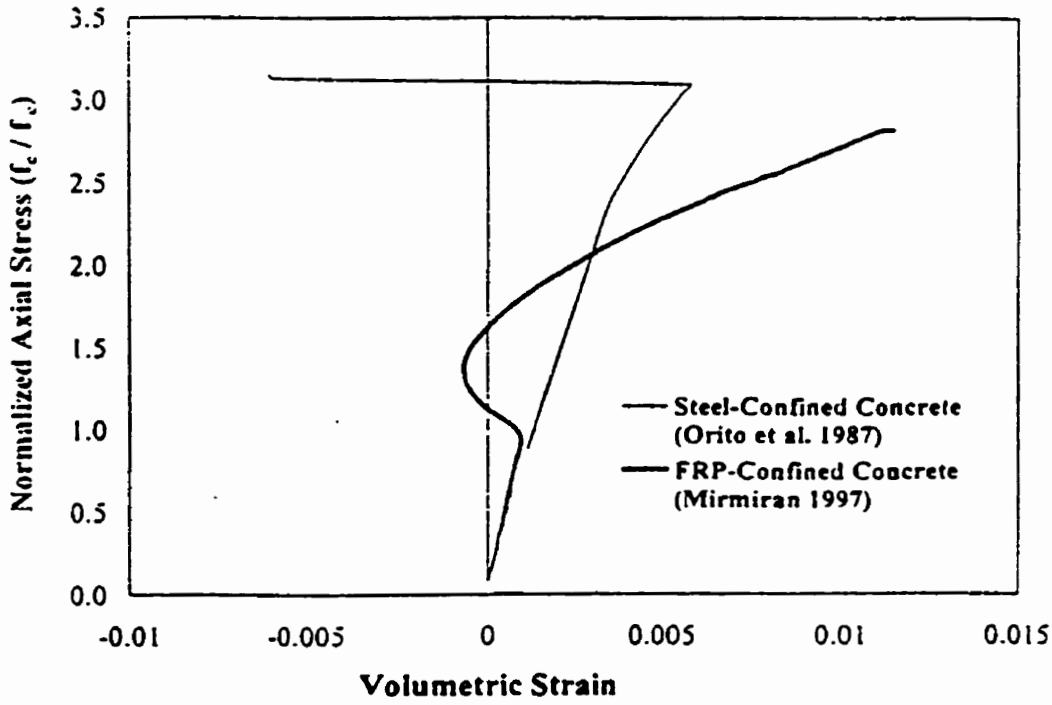

Fig. II - 3 : Axial stress-volumetric strain curves for steel- and FRP-confined concrete

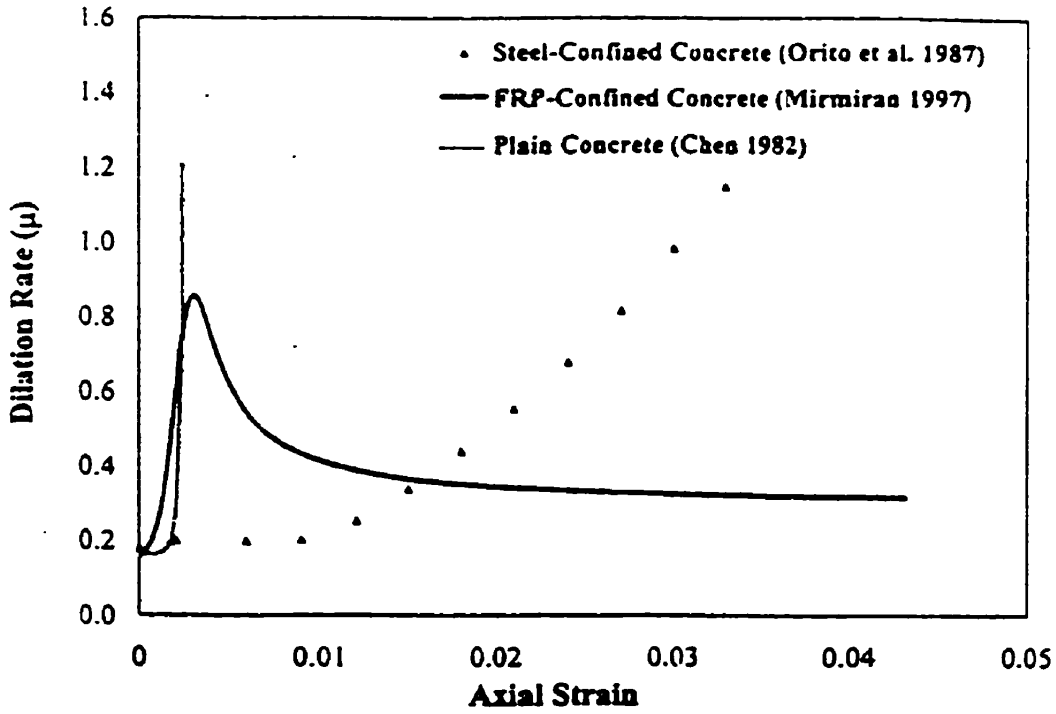

Fig. II – 4 : Dilation curves for steel- and FRP-confined concrete

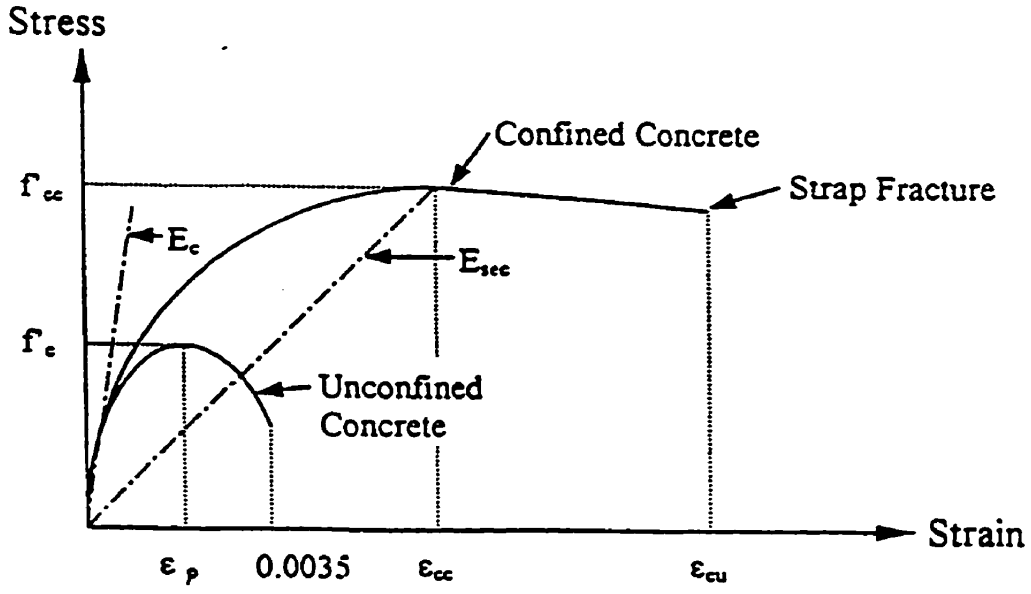

Fig. II – 5 : Confined and unconfined concrete curves (Mander)

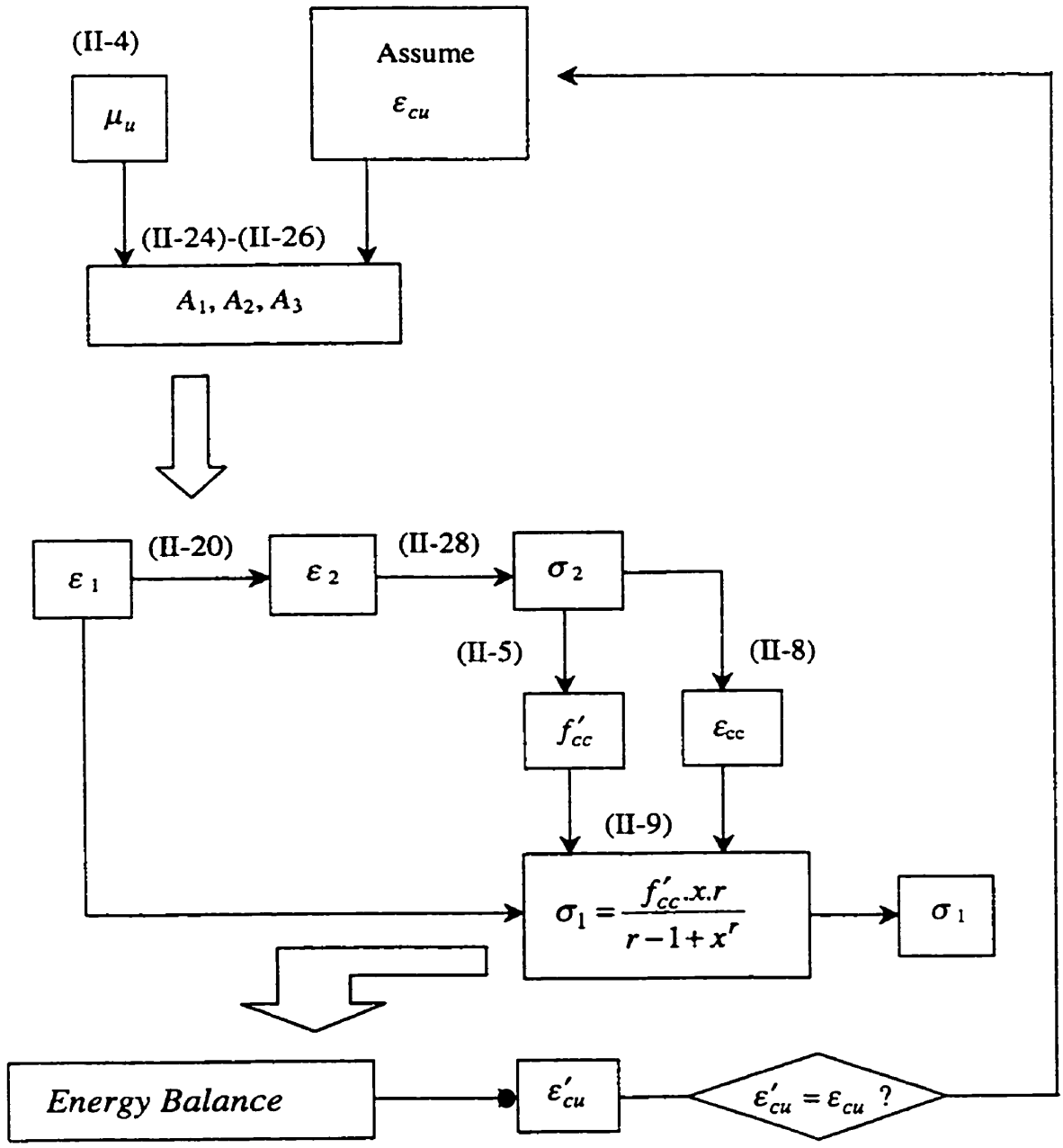

Fig. II - 6 : Flowchart for a modified Mander model (Parent & Labossiere)

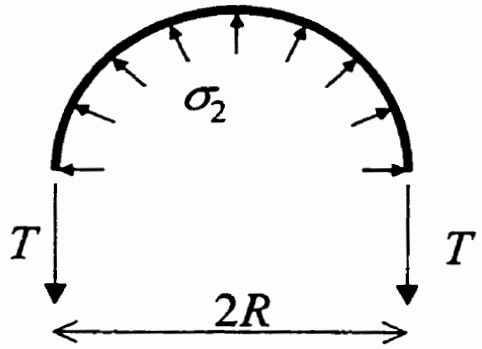

Fig. II - 7 : Equilibrium equation

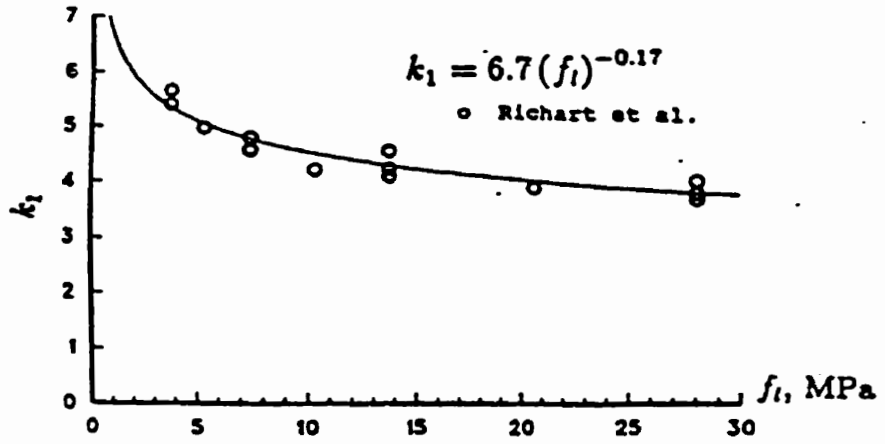

Fig. II – 8 : Confinement effectiveness vs. lateral pressure (Richart)

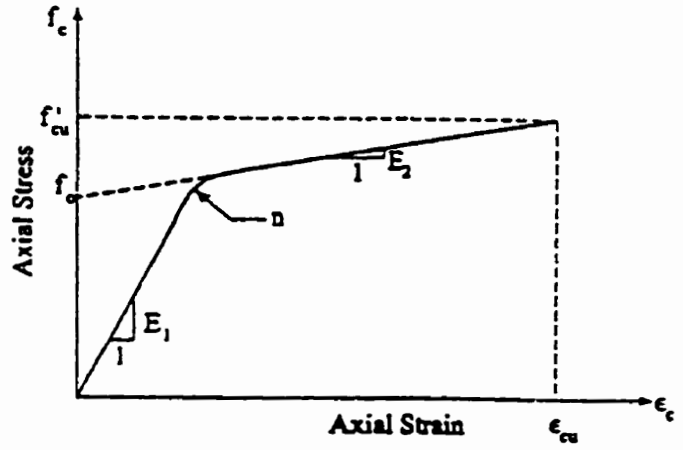

Fig. II – 9 : Bilinear confinement model (Mirmiran & Shahawy)

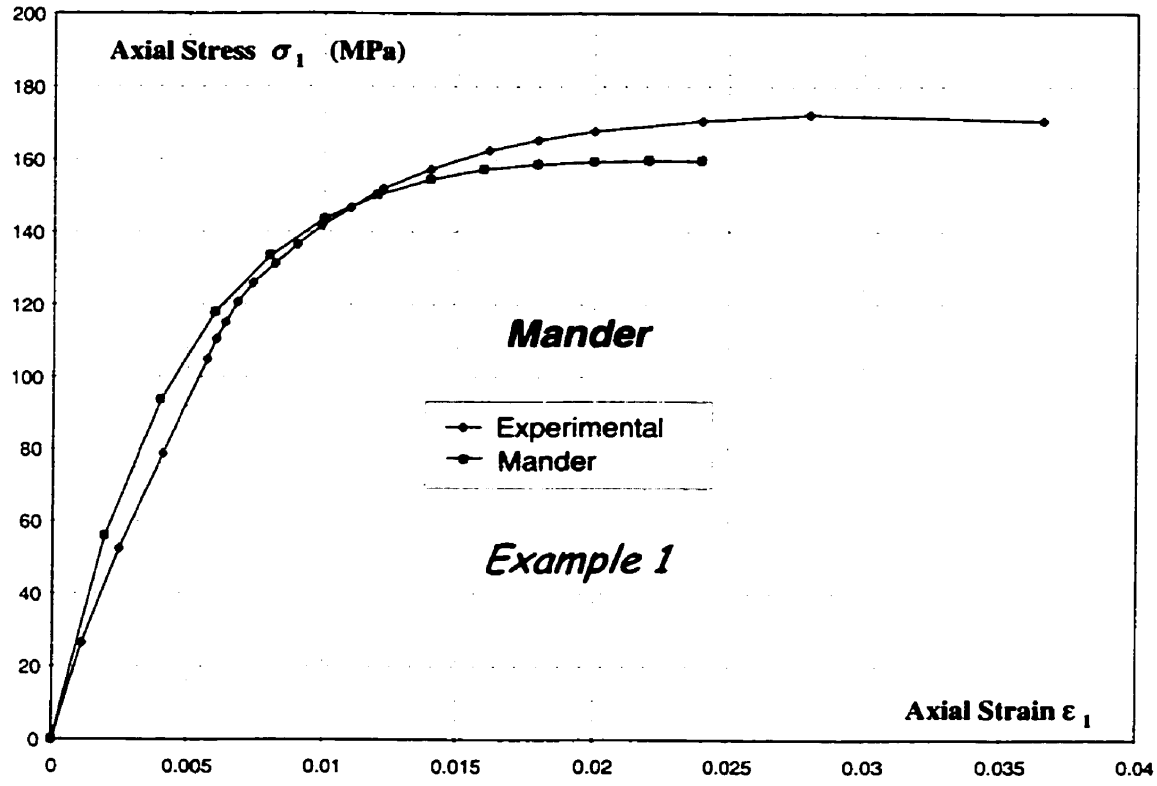

Fig. II - 10 : Axial concrete stress-strain curve : Mander

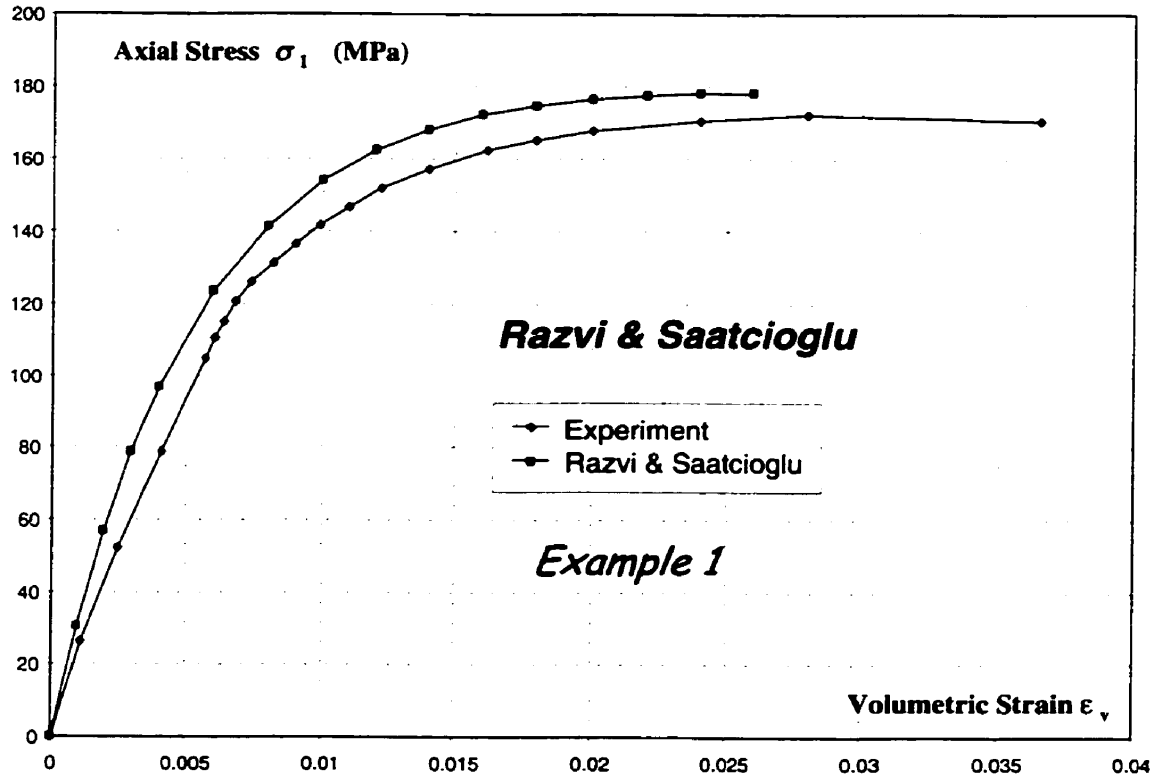

Fig. II - 11 : Axial concrete stress-strain curve : Razvi & Saatcioglu

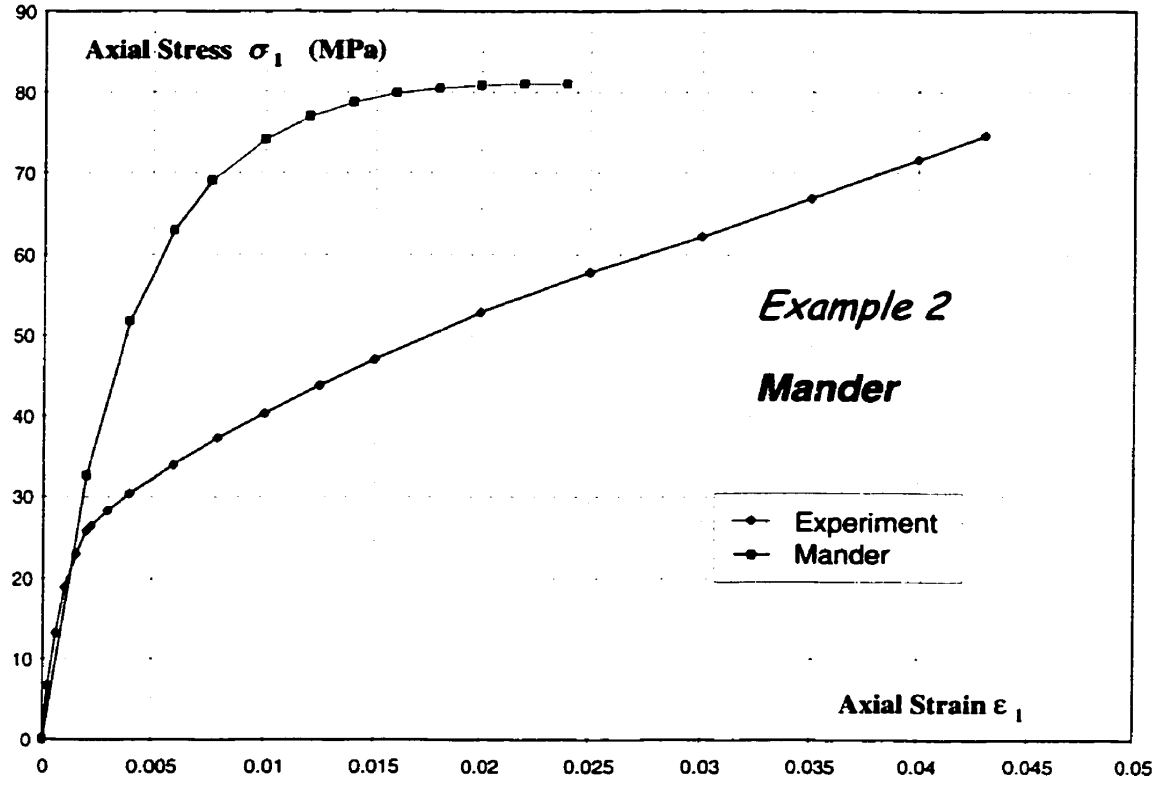

Fig. II - 12 : Axial concrete stress-strain curve : Mander

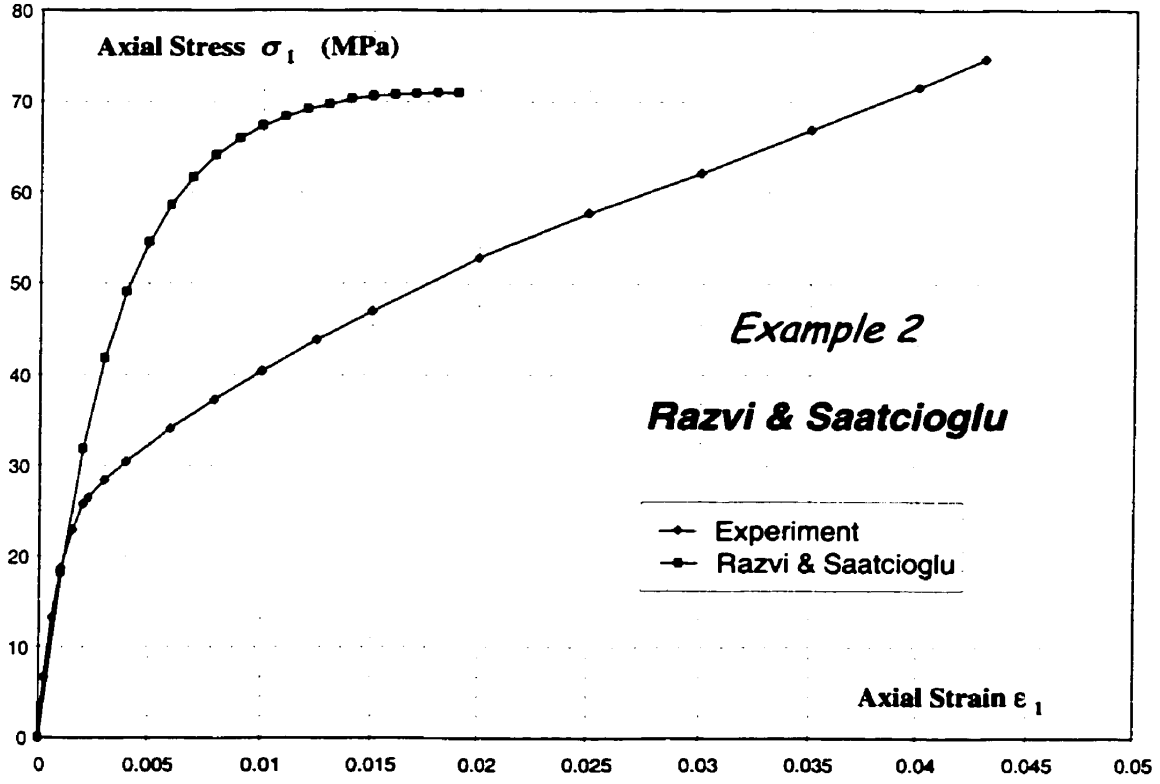

Fig. II - 13 : Axial concrete stress-strain curve : Razvi & Saatcioglu

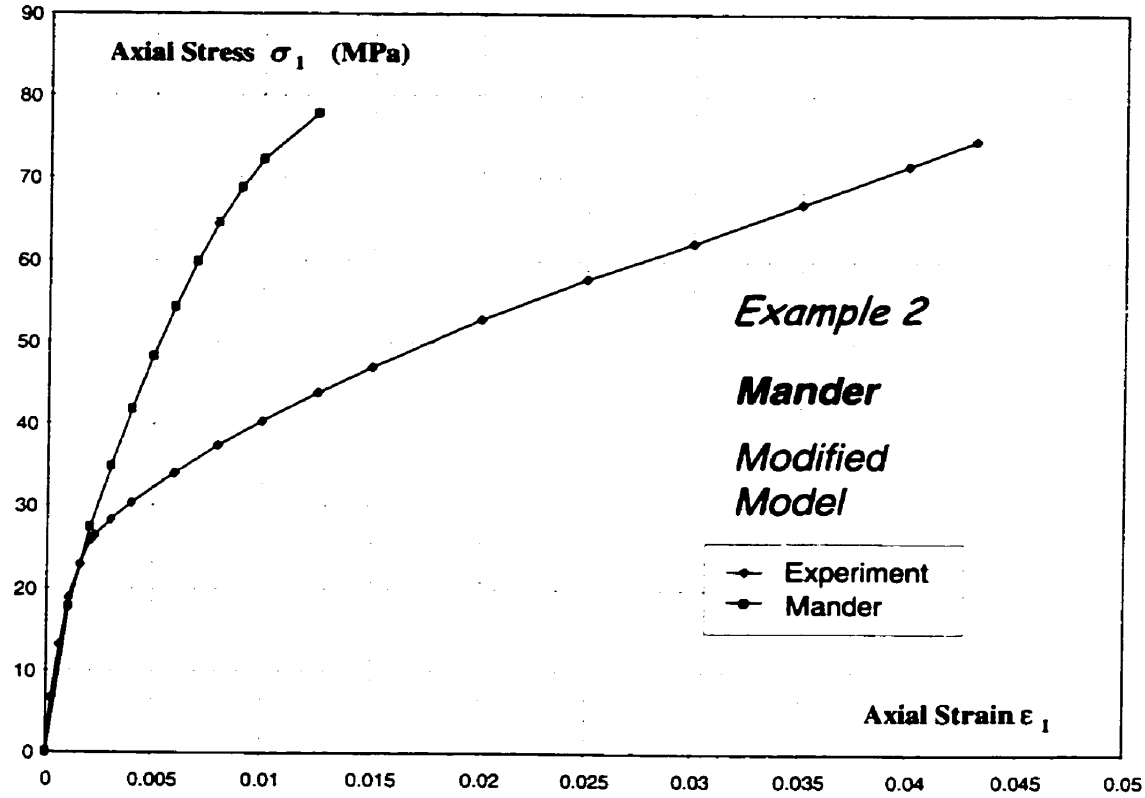

Fig. II - 14 : Axial concrete stress-strain curve : Mander (Modified)

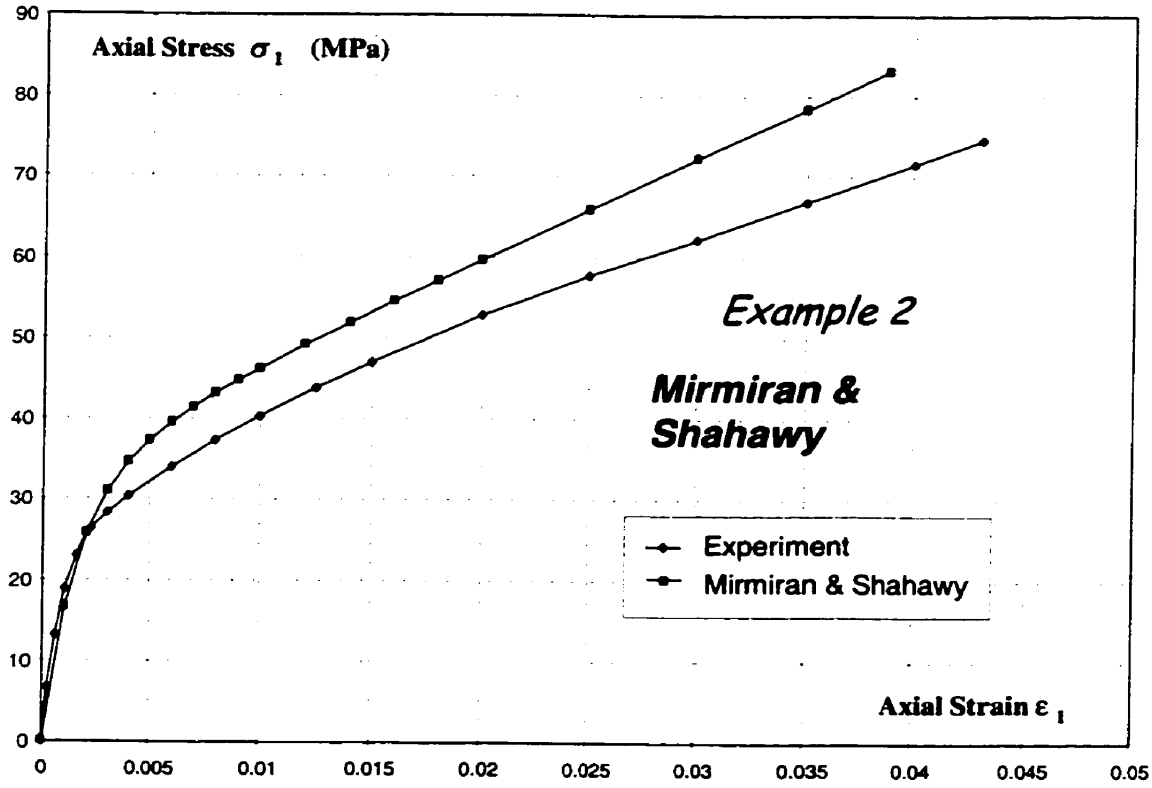

Fig. II -15 : Axial concrete stress-strain curve : Mirmiran & Shahawy

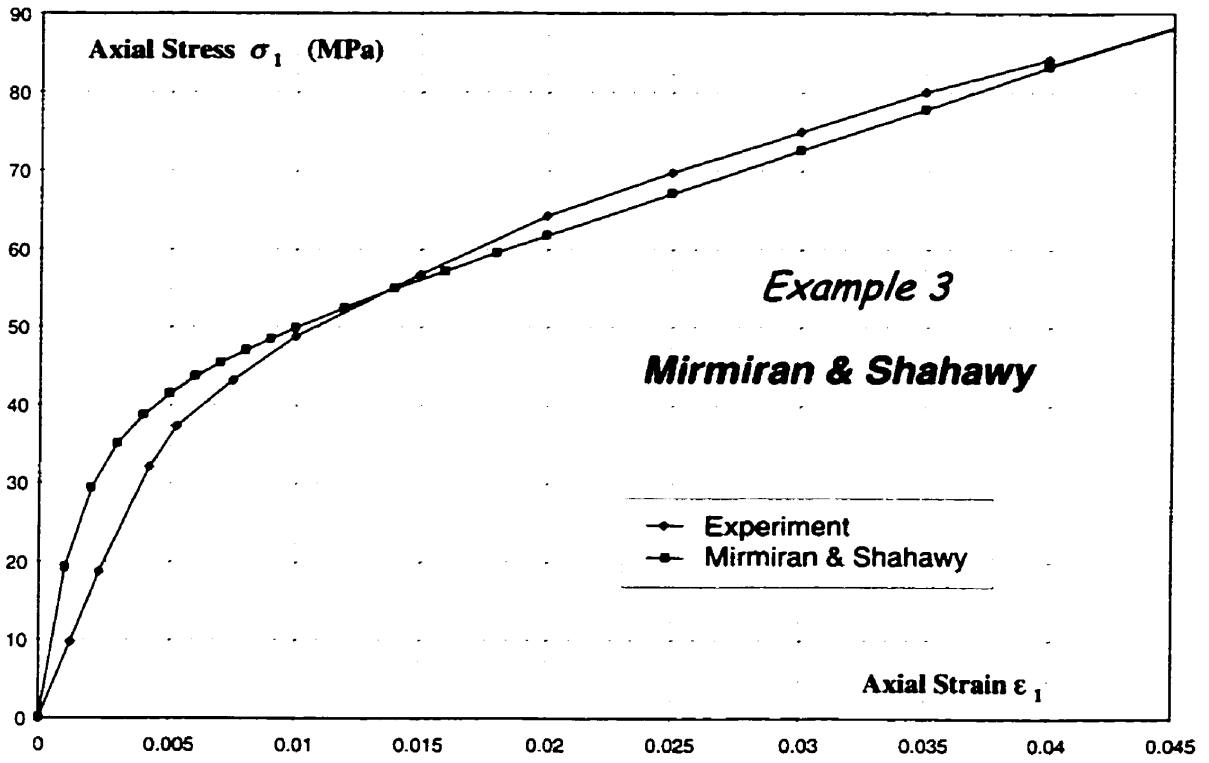

Fig. II - 16 : Axial concrete stress-strain curve : Mirmiran & Shahawy

Chapter III :

Material Constitutive Relations

3.1 Constitutive Relationship for the FRP

3.1.1 Elastic Equations

The FRP material is characterized by a linear behaviour up to failure. However, the properties of the material are different in different directions and depend on the orientation of the fibres in the different layers. The FRP material can be modeled as an orthotropic material.

When the shell is subjected to a longitudinal strain, ε_{long}, and a hoop strain, ε_{hoop}, the stresses in the shell can be determined by the following equations :

$$\sigma_{long} = \frac{(\varepsilon_{long} + \nu_f \varepsilon_{hoop}) E_{long}}{1 - \nu_f \nu'_f} \qquad \text{(III-1)}$$

$$\sigma_{hoop} = \frac{(\varepsilon_{hoop} + \nu'_f \varepsilon_{long}) E_{hoop}}{1 - \nu_f \nu'_f} \qquad \text{(III-2)}$$

where σ_{long} and σ_{hoop} are the longitudinal and hoop stresses in the shell respectively ; v_f and v_f' are the Poisson's ratios of the FRP material in the hoop and the longitudinal directions respectively ; and E_{hoop} and E_{long} are the elastic moduli of the FRP material in the hoop direction and the longitudinal directions respectively.

3.1.2 Biaxial failure criterion

When the FRP material is subjected to stresses in both the longitudinal and the hoop direction, a biaxial strength criterion is required to determine failure. The most widely used criterion in the analysis of composite materials is the Tsai-Wu criterion (1971). In this formulation, failure will occur when the variable ξ reaches a value of 1 :

$$\xi = A + B \tag{III-3}$$

where :

$$A = -\frac{(\sigma_{long})^2}{f_{long,t} f_{long,c}} - \frac{(\sigma_{hoop})^2}{f_{hoop,t} f_{hoop,c}} - \frac{\sigma_{long}\sigma_{hoop}}{\sqrt{f_{long,t} f_{long,c} f_{hoop,t} f_{hoop,c}}} \tag{III-4}$$

$$B = \left(\frac{1}{f_{long,t}} + \frac{1}{f_{long,c}}\right)\sigma_{long} + \left(\frac{1}{f_{hoop,t}} + \frac{1}{f_{hoop,c}}\right)\sigma_{hoop} \tag{III-5}$$

with the following notations :

$f_{hoop,t}$ = the ultimate tensile strength of the material in the hoop direction

$f_{hoop,c}$ = the ultimate compressive strength of the material in the hoop direction

$f_{long,t}$ = the ultimate tensile strength of the material in the longitudinal direction

$f_{long,c}$ = the ultimate compressive strength of the material in the longitudinal direction

In the case that $f_{hoop,t} = -f_{hoop,c}$ and $f_{long,t} = -f_{long,c}$ the previous equations (III - 4) and (III - 5) can be reduced into the following relationship :

$$A = \left(\frac{\sigma_{long}}{f_{long}}\right)^2 + \left(\frac{\sigma_{hoop}}{f_{hoop}}\right)^2 - \frac{\sigma_{long}\sigma_{hoop}}{f_{long}f_{hoop}} \qquad (III-6)$$

$$B = 0 \qquad (III-7)$$

where $f_{long} = f_{long,t}$ and $f_{hoop} = f_{hoop,t}$.

3.2 Triaxial Behaviour of Concrete

Experimental results of multiaxial compressive tests of plain concrete show a large scatter. This scatter can be attributed mainly to the variation in the materials itself and the variation of the test methods. An extensive research program has been undertaken by Gerstle (1980), involving different laboratories in order to investigate the influence of the test method on the results of triaxial tests. Various systems have been used in these tests like unlubricated metal platens, flexible platen systems, lubricated metal platens, brush bearing platens or fluid cushions. The main difference lies in the

boundary conditions. At one extreme, the boundaries may be perfectly flexible (e.g. fluid cushions), in which case a stress-controlled boundary condition prevails. The specimen will be in a state of uniform stress throughout, failure is controlled by the weakest point and is typically brittle. On the other hand, rough and unlubricated end conditions, such as thick steel plates, will impose specified displacements on the specimen. The specimen is subjected to non-uniform stresses and local distress, leading to an apparently higher strength and a more ductile failure mode.

The scatter of the results of triaxial tests might be one of the reasons why a triaxial concrete behaviour model is not widely used. It should also be mentioned that the experimental constants obtained from multiaxial tests usually apply to one type of concrete. Using another concrete type would require an extensive testing program to determine the material factors. In addition, the proposed triaxial material laws possess a higher order of complexity than a simple uniaxial stress-strain representation.

In the following sections a number of triaxial concrete models are presented, proposed by different authors. A group of three theories based on the same concept of octahedral stresses is presented in section 3.3. It includes the theories proposed by Gerstle (1981), Kotsovos and Newman (1978), and Cedolin (1977). Section 3.4 discusses the triaxial model proposed by Ahmad and Shah. Section 3.5 includes the model by Elwi and Murray.

3.3 Octahedral Theories

3.3.1 Definition

When using the concept of octahedral stresses, the triaxial stress state of the concrete is translated into two equivalent octahedral stresses : a hydrostatic stress σ_o (also called octahedral normal or mean normal stress) and a deviatoric stress τ_o (or octahedral shear stress). The hydrostatic stress is related to the volume change of the material whereas the deviatoric stress causes the distortional or shape change portions of the strains.

With σ_1, σ_2 and σ_3 being the principal stresses in the concrete, the octahedral stresses are given by the following equations :

$$\sigma_o = \frac{1}{3}(\sigma_1 + \sigma_2 + \sigma_3) \qquad \text{(III-8)}$$

$$\tau_o = \frac{1}{3}\sqrt{(\sigma_1 - \sigma_2)^2 + (\sigma_2 - \sigma_3)^2 + (\sigma_1 - \sigma_3)^2} \qquad \text{(III-9)}$$

The octahedral volumetric strain ε_o and the octahedral deviatoric strain γ_o are then :

$$\varepsilon_o = \frac{1}{3}(\varepsilon_1 + \varepsilon_2 + \varepsilon_3) \qquad \text{(III-10)}$$

$$\gamma_o = \frac{1}{3}\sqrt{(\varepsilon_1 - \varepsilon_2)^2 + (\varepsilon_2 - \varepsilon_3)^2 + (\varepsilon_1 - \varepsilon_3)^2} \qquad \text{(III-11)}$$

where ε_1, ε_2 and ε_3 are the principal strains of the concrete.

3.3.2 Octahedral stress-strain relations

The previous equations will further be used in incremental form with $\Delta\sigma_1$, $\Delta\sigma_2$ and $\Delta\sigma_3$ representing the principal stress increments and $\Delta\varepsilon_1$, $\Delta\varepsilon_2$ and $\Delta\varepsilon_3$ representing the corresponding principal strain increments :

$$\Delta\sigma_o = \frac{1}{3}(\Delta\sigma_1 + \Delta\sigma_2 + \Delta\sigma_3) \tag{III-12}$$

$$\Delta\tau_o = \frac{1}{3}\sqrt{(\Delta\sigma_1 - \Delta\sigma_2)^2 + (\Delta\sigma_2 - \Delta\sigma_3)^2 + (\Delta\sigma_1 - \Delta\sigma_3)^2} \tag{III-13}$$

and

$$\Delta\varepsilon_o = \frac{1}{3}(\Delta\varepsilon_1 + \Delta\varepsilon_2 + \Delta\varepsilon_3) \tag{III-14}$$

$$\Delta\gamma_o = \frac{1}{3}\sqrt{(\Delta\varepsilon_1 - \Delta\varepsilon_2)^2 + (\Delta\varepsilon_2 - \Delta\varepsilon_3)^2 + (\Delta\varepsilon_1 - \Delta\varepsilon_3)^2} \tag{III-15}$$

The following constitutive relations relating stress increments and strain increments are proposed by Gerstle :

$$\Delta\varepsilon_o = \frac{\Delta\sigma_o}{3K(\sigma_o)} + \frac{\Delta\tau_o}{H(\sigma_o)} \tag{III-16}$$

$$\Delta\gamma_o = \frac{\Delta\tau_o}{2G(\tau_o)} \tag{III-17}$$

The three moduli K, G and H are tangent values which depend on the current stresses or strains. K is called the bulk modulus and G is the shear modulus. They relate volumetric and deviatoric stress and strain respectively. The coupling modulus H becomes only

important for higher hydrostatic stresses, which exceed the range of 15 MPa, and accounts for the experimentally observed fact that the deviatoric stress also causes a decrease in volume. This effect can be neglected for low hydrostatic pressures and the volume changes and distortions are considered to be totally uncoupled.

The bulk modulus is a function only of the volumetric stress or strain level and the shear modulus is a function only of the deviatoric stress or strain.

The fundamental elastic theory gives the following relationship :

$$\varepsilon_1 = \frac{\sigma_1}{E} - \nu\frac{\sigma_2}{E} - \nu\frac{\sigma_3}{E}$$

With equivalent expressions for ε_2 and ε_3, K and G are related to the tangent modulus E and the Poisson's ratio ν as follows :

$$K = \frac{\Delta\sigma_o}{3\Delta\varepsilon_o}$$

$$= \frac{E}{3(1-2\nu)} \qquad \text{(III-18)}$$

$$G = \frac{\Delta\tau_o}{2\Delta\gamma_o}$$

$$= \frac{E}{2(1+\nu)} \qquad \text{(III-19)}$$

Given the triaxial stress increments $\Delta\sigma_1$, $\Delta\sigma_2$ and $\Delta\sigma_3$, the corresponding strain increments can be determined as follows :

1. Transform the given principal stress increments to octahedral stress increments $\Delta\sigma_o$ and $\Delta\tau_o$ using Eq. (III - 12) and (III - 13).
2. Calculate the octahedral strain increments $\Delta\varepsilon_o$ and $\Delta\gamma_o$ from the octahedral stress increments using Eq. (III - 16) and (III - 17). The calculation of the moduli K, G and H will be subject of the next sections, since different formulas are provided by different authors.
3. Transform the octahedral strains into principal strain increments $\Delta\varepsilon_1$, $\Delta\varepsilon_2$ and $\Delta\varepsilon_3$ using Eq. (III - 14) and (III - 15). The additional condition required to determine the three unknowns is based on the coincidence of the deviator stress increment vector s and the deviator strain increment vector e, as follows :

$$\frac{\Delta s_2}{\Delta s_1} = \frac{\Delta e_2}{\Delta e_1}$$

or :

$$\frac{\Delta\sigma_2 - \Delta\sigma_o}{\Delta\sigma_1 - \Delta\sigma_o} = \frac{\Delta\varepsilon_2 - \Delta\varepsilon_o}{\Delta\varepsilon_1 - \Delta\varepsilon_o} = B \qquad \text{(III-20)}$$

By solving Eqs. (III - 14), (III - 15) and (III - 20) for the principal strains, the following relations can be obtained :

$$\Delta\varepsilon_1 = \Delta\varepsilon_o + C.\Delta\gamma_o \qquad \text{(III-21)}$$

$$\Delta\varepsilon_2 = \Delta\varepsilon_o + B.C.\Delta\gamma_o \qquad \text{(III-22)}$$

$$\Delta\varepsilon_3 = \Delta\varepsilon_o - (B+1)C.\Delta\gamma_o \qquad \text{(III-23)}$$

Where $C = \sqrt{\frac{3}{2}\frac{1}{(1+B+B^2)}}$

3.3.3 Gerstle's Model (1981)

Gerstle carried out an experimental program on concrete subjected to triaxial stresses, where the load was applied in two parts : first a hydrostatic compression $\sigma_1 = \sigma_2 = \sigma_3 = \sigma_o$ up to a specified hydrostatic stress level $\overline{\sigma}_o$, followed by stress deviation within that octahedral plane $\sigma_o = \overline{\sigma}_o$ along three different paths :

Path 1 : Triaxial compression : $\Delta\sigma_1 = \Delta\sigma_2 = -\,{}^1/_2\,\Delta\sigma_3$

Path 2 : Simple shear : $\Delta\sigma_2 = 0,\ \Delta\sigma_3 = -\,\Delta\sigma_1$

Path 3 : Triaxial extension : $\Delta\sigma_3 = -\,2\,\Delta\sigma_1 = -\,2\,\Delta\sigma_2$

All of the test specimens were carried to failure.

From these tests the volumetric stress-strain curves (σ_o - ε_o), as well as the deviatoric stress-strain curves (τ_o - γ_o) can be plotted. They are given in Figs. (III – 1) and (III – 2). The different notations stand for the different end conditions which were examined.

3.3.3.1. Deviatoric stress-strain relations

Gerstle carried out tests for different values of the hydrostatic stress level $\overline{\sigma}_o$ in order to study the influence of $\overline{\sigma}_o$ on the (τ_o - γ_o) relations. Fig. III - 3 shows the different deviatoric stress-strain curves for different octahedral planes. The curves are closely

bunched with no systematic ordering according to $\overline{\sigma}_o$. It is concluded that the (τ_o - γ_o) relations are independent of the mean normal stress $\overline{\sigma}_o$, which justifies Eq. (III - 17).

To explore the path-dependence of the deviatoric stress-strain relations, the individual (τ_o - γ_o) curves were separated according to the different paths and averaged. The curves for the three paths coincide sufficiently closely, as shown in Fig. (III – 4). Therefore, the (τ_o - γ_o) relations can be assumed to be path-independent.

Gerstle approximated the (τ_o - γ_o) curves by the following exponential form :

$$\tau_o = \tau_{o,\max}\left(1 - e^{\left(\frac{-2G_o}{\tau_{o,\max}}\right)\gamma_o}\right) \qquad \text{(III–24)}$$

in which $\tau_{o,\max}$ is the octahedral shear strength and G_o is the initial shear modulus.

The tangent shear modulus can be obtained by differentiation of Eq. (III – 24) as follows :

$$2G = \frac{d\tau_o}{d\gamma_o} = 2G_o e^{\left(\frac{-2G_o}{\tau_{o,\max}}\right)\gamma_o} \qquad \text{(III–25)}$$

Solving Eq. (III - 24) and (III - 25) to eliminate γ_o provides the following relation between G and τ_o :

$$G = G_o\left(1 - \frac{\tau_o}{\tau_{o,\max}}\right) \qquad \text{(III–26)}$$

This means that the shear modulus G decreases linearly from its initial value G_o for $\tau_o = 0$ to 0 at failure. This represents a ductile failure. Gerstle notes that other, brittle modes of failure may take place for tests with unconstrained boundaries. It is also observed in tests that the shear modulus decreases somewhat slower than indicated by Eq. (III – 26) and this is shown in Fig. (III – 5).

The initial shear modulus G_o can be determined from Eq. (III – 19) using the initial tangent modulus E_o and Poisson's ratio v, which is assumed to be 0.2. The deviator strength $\tau_{o,max}$ can be obtained from a triaxial strength criterion which will be discussed later in this chapter.

3.3.3.2 Volumetric stress-strain relations

It has been generally accepted that under increasing triaxial compression the material first compacts and eventually, close to failure, dilates due to microcracking. Only the former effect is taken into account in the octahedral models that were studied, as the latter is highly affected by the details of load application and measurement.

Test results indicate volumetric behaviour that can be expressed by a linearly varying bulk modulus, using the following equation :

$$K = K_o(1 - \alpha\, \sigma_o) \qquad \text{(III–27)}$$

in which K_o is the initial bulk modulus at zero confining pressure and α is an experimentally obtained constant.

An approximation can be made by assuming a constant bulk modulus :

$$K = C_1 K_o \qquad C_1 < 1 \tag{III-28}$$

3.3.3.3 Coupling relations

The coupling modulus H, which establishes the volume change due to stress deviation, can be obtained from the measured volume change during deviatoric loading. Its variation with the hydrostatic stress σ_o can be represented analytically by the following expression :

$$H = \left(10 + \frac{300}{\sigma_o - 10}\right) 10^3 \text{ MPa}, \qquad \sigma_o \geq 10 \text{ MPa} \tag{III-29}$$

According to this formulation, the coupling modulus is a constant within an octahedral plane, where σ_o is constant. Its value increases radically with decreasing hydrostatic stress, and the coupling effect becomes negligible for low hydrostatic stresses ($\sigma_o < 15$ to 20 MPa). Gerstle notes that the data base for H must be considered as very preliminary.

Finally it should be mentioned that the proposed formulation is restricted to monotonically increasing stress and strain levels. It also excludes load histories for which stress-induced anisotropy due to cracking becomes important. The material remains at any time isotropic.

3.3.4 Kotsovos and Newman (1978)

Kotsovos and Newman set up a triaxial test program with concrete cylinders where the load was applied in two stages :

1 - increase the hydrostatic stress up to a given value

2 - apply an axial and a lateral stress in one of the following ways :

1. $\Delta\sigma_2 = \Delta\sigma_3 = -\,{}^1/_2\,\Delta\sigma_1$ causing failure to occur under a state of stress

   $\sigma_1 > \sigma_2 = \sigma_3$

2. $\Delta\sigma_3 = -\,2\,\Delta\sigma_1 = -\,2\,\Delta\sigma_2$ causing failure to occur under a state of stress

   $\sigma_1 = \sigma_2 > \sigma_3$

3. $\Delta\sigma_2 = \Delta\sigma_3 = 0$ with $\Delta\sigma_1 > 0$. The axial stress increases until failure occurs under constant lateral pressure.

4. $\Delta\sigma_2 = \Delta\sigma_3 = 0$; $\Delta\sigma_1 < 0$. The axial stress decreases until failure occurs under constant lateral pressure.

Kotsovos and Newton recognized that the volumetric strain ε_o varies with the hydrostatic stress σ_o, whereas both deviatoric γ_o and volumetric strains ε_o vary with deviatoric stress τ_o. The (τ_o - γ_o) relationship is practically independent of the hydrostatic stress level and there appears to be no statistically significant difference between the (τ_o - γ_o) curves for the different load paths.

A process of curve fitting was applied to the experimental stress-strain data, so that mathematical expressions for the secant bulk modulus K_s and the secant shear modulus

G_s could be derived, as shown in Fig. (II – 6) and Fig. (II – 7) respectively. K_s and G_s are given by the following equations :

$$\frac{K_s}{K_o} = \frac{1}{1+0.52\left(\frac{\sigma_o}{f_c'}\right)^{1.09}} \qquad \text{(III–30)}$$

$$\frac{G_s}{G_o} = \frac{1}{1+3.57\left(\frac{\tau_o}{f_c'}\right)^{1.7}} \qquad \text{(III–31)}$$

For use in incremental form the tangent bulk modulus, K_T, and the tangent shear modulus, G_T, are given by the following equations :

$$\frac{K_T}{K_o} = \frac{1}{1+1.08\left(\frac{\sigma_o}{f_c'}\right)^{1.09}} \qquad \text{(III–32)}$$

$$\frac{G_T}{G_o} = \frac{1}{1+9.63\left(\frac{\tau_o}{f_c'}\right)^{1.7}} \qquad \text{(III–33)}$$

3.3.5 Cedolin's Model (1977)

Cedolin combined experimental data from a considerable number of triaxial test programs conducted by different researchers. As such, different concrete strengths, specimen sizes, testing methods, boundary conditions and load paths are inherently included in the results. After processing the results, using regression analysis

techniques, Cedolin proposed the following expressions for the tangent bulk and shear moduli, K_T and G_T, as functions of the octahedral strains :

$$\frac{K_T}{K_o} = 0.85(1 - 654\varepsilon_o)(2.5)^{-\varepsilon_o/0.0014} + 0.15 \qquad \text{(III-34)}$$

$$\frac{G_T}{G_o} = 0.81(1 - 347\gamma_o)(2.0)^{-\gamma_o/0.002} - 4\gamma_o + 0.19 \qquad \text{(III-35)}$$

3.3.6 Failure Criterion Formulation

This section presents a triaxial failure criterion in terms of the octahedral stresses.

The octahedral shear strength $\tau_{o,max}$ appears to be a function not only of the hydrostatic stress level but also of the deviatoric load path.

Gerstle (1981) presented three parabolic relationships $\tau_{o,max} = f(\sigma_o)$, one according to each load path that was investigated, but these cannot be generalized since they apply only to one type of concrete with a specified uniaxial strength. A better formulation was proposed by Mills and Zimmerman (1971). In this formulation the failure envelope of the concrete was approximated by straight lines, as shown in Fig. (III – 8) :

$$\frac{\tau_{o,max}}{f'_c} = 0.199 + \frac{0.843\sigma_o}{f'_c} \quad ; \quad \sigma_1 > \sigma_2 = \sigma_3$$

$$\frac{\tau_{o,max}}{f'_c} = 0.147 + \frac{0.550\sigma_o}{f'_c} \quad ; \quad \sigma_1 = \sigma_2 > \sigma_3 \qquad \text{(III-36)}$$

Mills and Zimmerman recognized the fact that confinement becomes less effective for higher hydrostatic stresses. Therefore they recommend to use the following expressions at higher stress levels, as also shown in Fig. (III – 8) :

$$\frac{\tau_{o,max}}{f_c'} = 0.760 + \frac{0.525\sigma_o}{f_c'} \quad ; \quad \sigma_1 > \sigma_2 = \sigma_3$$

$$\frac{\tau_{o,max}}{f_c'} = 0.930 + \frac{0.297\sigma_o}{f_c'} \quad ; \quad \sigma_1 = \sigma_2 > \sigma_3 \qquad \text{(III–37)}$$

Kotsovos and Newman provide a lower bound bilinear failure criterion, which is associated with the onset of failure and the initiation of continuous cracks rather than the ultimate load :

$$\left.\begin{aligned} \frac{\tau_{o,max}}{f_c'} &= 1.417\frac{\sigma_o}{f_c'} \quad \text{for} \quad \frac{\sigma_o}{f_c'} \le 0.283 \\ \frac{\tau_{o,max}}{f_c'} &= 0.671\frac{\sigma_o}{f_c'} + 0.211 \quad \text{for} \quad \frac{\sigma_o}{f_c'} > 0.283 \end{aligned}\right\} \quad \sigma_1 > \sigma_2 = \sigma_3$$

(III–38)

$$\left.\begin{aligned} \frac{\tau_{o,max}}{f_c'} &= 0.707\frac{\sigma_o}{f_c'} \quad \text{for} \quad \frac{\sigma_o}{f_c'} \le 0.624 \\ \frac{\tau_{o,max}}{f_c'} &= 0.496\frac{\sigma_o}{f_c'} + 0.131 \quad \text{for} \quad \frac{\sigma_o}{f_c'} > 0.624 \end{aligned}\right\} \quad \sigma_1 = \sigma_2 > \sigma_3$$

In literature the following expression is often encountered, related to failure of a cylindrical specimen under lateral confining pressure :

$$f'_{cc} = f'_c + k.\sigma_2 \qquad \text{(III-39)}$$

Where f_{cc} is the confined concrete strength and σ_2 is the lateral confining pressure. k is the confinement effectiveness coefficient, which is given values in literature ranging from 4 to 7.

Eq. (II - 35) can be translated into an octahedral failure criterion, by substituting the following stresses into Eq. (III - 8) and Eq. (III - 9) :

$$(\sigma_1, \sigma_2, \sigma_3) = (f'_c + k\sigma_l, \sigma_l, \sigma_l)$$

where σ_l is the lateral confining pressure. By eliminating σ_l from Eq. (III - 8) and Eq. (III - 9), the following expression can be obtained :

$$\frac{\tau_{o,\max}}{f'_c} = \frac{\sqrt{2}}{k+2} + \sqrt{2}\frac{k-1}{k+2}\frac{\sigma_o}{f'_c} \qquad \text{(III-40)}$$

For instance, for $k = 6$ Eq. (II - 41) becomes :

$$\frac{\tau_{o,\max}}{f'_c} = 0.176 + 0.884\frac{\sigma_o}{f'_c}$$

3.4 Ahmad and Shah

In this section Ahmad and Shah's (1982) model for triaxial concrete behaviour is discussed. Instead of using a varying modulus approach, Ahmad and Shah propose a closed analytical expression for the triaxial stress-strain curves.

3.4.1 Proposed form of the stress-strain relations

Ahmad and Shah present the following analytical form for the stress-strain curves of concrete under triaxial compression :

$$Y = \frac{A_i X_i + (D_i - 1)X_i^2}{1 + (A_i - 2)X_i + D_i X_i^2} \qquad \text{(III-41)}$$

There are three equations of the same form (i = 1,2,3), one for each principal direction. The model includes the descending parts of the stress-strain curves. The symbols in Eq. (III - 41) stand for :

$$Y = \frac{\sigma_1}{f'_{cc}} \qquad \text{(III-42)}$$

σ_1 = the most principal compressive stress

f'_{cc} = the most principal compressive strength under confinement

$$X = \frac{\varepsilon_i}{\varepsilon_{ip}} \qquad \text{(III-43)}$$

ε_i = the strain in the i-th principal direction (i = 1, 2 or 3)

ε_{ip} = the strain at the peak compressive strength in the i-th principal direction

$$A_i = \frac{E_{oi}}{E_{ip}} \qquad \text{(III-44)}$$

E_{oi} = the initial slope of the (σ_1 - ε_i) curve

$$E_{ip} = \frac{f'_{cc}}{\varepsilon_{ip}} \qquad \text{(III-45)}$$

D_i = a parameter which controls the descending part of the (σ_1 - ε_i) curve

The following remarks should be made :

1. For the analytical modeling of a cylinder under compression only two stress-strain curves are needed, one in the axial direction and one in the lateral direction, because $\sigma_2 = \sigma_3$.

2. Eq. (III - 37) implies that the stress-strain curve has a zero slope at the peak.

3. Eq. (III - 37) has been used by many researchers to represent the uniaxial stress-strain relation of concrete. In this case Eq. (III – 37) is rewritten as follows :

$$Y = \frac{AX + (D-1)X^2}{1 + (A-2)X + DX^2}$$

$$Y = \sigma / f'_c \; ; \; X = \varepsilon / \varepsilon_p \; ; \; A = E_o / E_{sec} \; ; \; E_{sec} = f'_c / \varepsilon_p$$

where ε_p is the strain value at the peak and E_o is the initial Young's modulus. E_{sec} is the secant modulus at the peak. Hognestad's (1951) parabola can be obtained by using A = 2 and $D = 0$. The equation by Saenz (1964) can be obtained by using $D = 1$.

4. To predict the stress-strain curves using Eq. (III - 37), the following parameters need to be determined :

i. the most principal compressive strength f'_{cc}

ii. the three principal strains ε_{ip} at the peak

iii. the initial slope E_{oi} of the (σ_i - ε_i) curves

iv. the parameters D_i

The following sections will discuss these parameters.

3.4.2 Strength Criteria

Ahmad and Shah suggest that f'_{cc} can be obtained from an octahedral strength criterion, which in the case that $\sigma_1 > \sigma_2 = \sigma_3$, is represented by an equation of the same form as Eqs. (III - 36) to (III - 38), as follows :

$$\frac{\tau_{o,\max}}{f'_c} = A + B\frac{\sigma_o}{f'_c} \qquad \text{(III-46)}$$

where τ_o and σ_o are the octahedral shear and normal stresses as previously defined in Eq. (III - 8) and (III - 9). Ahmad and Shah propose the following values for A and B :

$A = 0.2261$; $B = 0.7360$ for $\sigma_o \leq 1.75 f'_c$

This corresponds to a confinement effectiveness coefficient of 4.255 in Eq. (III - 40). Basically any other strength criterion can be used in combination with Ahmad & Shah's theory e.g. the Mills-Zimmerman equations (III - 37) or, more generally, Eq. (III - 40) with a suitable value for k.

3.4.3 Peak Strain Criteria

Analysis of experimental data shows that a unique relationship exist between the octahedral normal strain and the octahedral normal stress at the compressive peak strength and also between the octahedral shear strain and the octahedral shear stress at the peak. Based on regression analysis, the following equations are proposed by Ahmad and Shah :

$$\frac{\gamma_o}{(\gamma_o)_o} = -4.8629 + 12.756\left(\frac{\tau_o}{f_c'}\right) \qquad \text{(III-47)}$$

$$\frac{\varepsilon_o}{(\varepsilon_o)_o} = 0.510375\left(\frac{\sigma_o}{f_c'}\right) \qquad \text{(III-48)}$$

$(\gamma_o)_o$ and $(\varepsilon_o)_o$ are the octahedral shear and normal strains at the peak for a uniaxial test. From a regression analysis of experimental data their values were determined by the following formulas :

$$(\gamma_o)_o = 0.001178(f_c')^{0.12817} \qquad \text{(III-49)}$$

$$(\varepsilon_o)_o = 0.001648 + 0.000114(f_c') \qquad \text{(III-50)}$$

These values can be combined with Eqs. (III - 47) and (III - 48) to obtain γ_o and ε_o at the peak. The strains in the principal directions ε_{1p} and $\varepsilon_{2p} = \varepsilon_{3p}$ can be determined from the definitions (III - 10) and (III - 11) for the octahedral shear and normal strain as follows :

$$\gamma_o = \frac{\sqrt{2}}{3}(\varepsilon_{1p} - \varepsilon_{2p}) \qquad \text{(III-51)}$$

$$\varepsilon_o = \frac{1}{3}(\varepsilon_{1p} + 2\varepsilon_{2p}) \qquad \text{(III-52)}$$

3.4.4 Initial Slope

Ahmad and Shah proposed the following formula for the initial slope of the stress-strain curve in the major principal direction (σ_1 - ε_1) :

$$E_{o1} = 4500\sqrt{f_c'}\left[1 + 0.31\left(\frac{\sigma_2}{f_c'} + \frac{\sigma_3}{f_c'}\right)\right] \qquad \text{(III-53)}$$

The factor between square brackets represents the effect of the confining stresses on the initial slope of the curve.

To obtain the initial slope of the (σ_1 - ε_2) curve, an elastic relationship can be used :

$$E_{o2} = \frac{E_{o1}}{\nu} = \frac{E_{o1}}{0.2} \qquad \text{(III-54)}$$

3.4.5 Parameter D_i

Ahmed and Shah calibrated the parameter D_i from their experiments and found :

i. - For the (σ_1 - ε_1) curve :

$$D_i = 1.111 + 0.876\,A_1 - 4.0883\frac{\tau_o}{f_c'} \qquad \text{(III-55)}$$

ii. - For the (σ_1 - ε_2) curve :

$$D_2 = 3.300 + 0.153 A_2 - 4.466 \frac{\tau_o}{f_c'} \qquad \text{(III-56)}$$

3.5 Elwi and Murray

A. A. Elwi and D. W. Murray (1979) developed a three-dimensional stress-strain relationship for concrete, based on the equivalent uniaxial strain concept. The model is defined in the form of an incremental stress-strain equation in which the material parameters are obtained from relations between stress and an equivalent uniaxial strain. The concrete is assumed to behave as an orthotropic material. This orthotropy is the consequence of stress-induced (micro)cracking affecting the material properties.

3.5.1 Form of the constitutive relations

Assuming an axisymmetric, cylindrical column, the following constitutive equations are presented by Elwi and Murray :

$$\begin{Bmatrix} d\varepsilon_1 \\ d\varepsilon_2 \end{Bmatrix} = \begin{bmatrix} \frac{1}{E_1} & -\frac{\nu_{12}}{E_2} \\ -\frac{\nu_{21}}{E_1} & \frac{(1-\nu_{23})}{2E_2} \end{bmatrix} \begin{Bmatrix} d\sigma_1 \\ 2d\sigma_2 \end{Bmatrix} \qquad \text{(III-57)}$$

E_1 and E_2 are the tangent elastic moduli in directions 1 and 2. ν_{ij} is the Poisson's ratio of the concrete in direction i when the load is applied in direction j.

Due to the symmetry of the matrix, the following equation has to be satisfied :

$$\nu_{12}E_1 = \nu_{21}E_2 \tag{III-58}$$

This brings the total of independent material properties, including the (irrelevant) shear modulus G down to five.

Eq. (II - 57) can be rewritten in an explicitly symmetric form as :

$$\begin{Bmatrix} d\varepsilon_1 \\ d\varepsilon_2 \end{Bmatrix} = \begin{bmatrix} \frac{1}{E_1} & -\frac{\mu_{12}}{\sqrt{E_1E_2}} \\ -\frac{\mu_{12}}{\sqrt{E_1E_2}} & \frac{(1-\mu_{23})}{2E_2} \end{bmatrix} \begin{Bmatrix} d\sigma_1 \\ 2d\sigma_2 \end{Bmatrix} \tag{III-59}$$

With :

$$\mu_{12}^2 = \nu_{12}\nu_{21}$$

$$\mu_{23} = \nu_{23} \tag{III-60}$$

The inverse relationship is then given by the following matrix equation :

$$\begin{Bmatrix} d\sigma_1 \\ d\sigma_2 \end{Bmatrix} = \frac{1}{\phi} \begin{bmatrix} E_1(1-\mu_{23}^2) & \sqrt{E_1E_2}(1+\mu_{23})\mu_{12} \\ \sqrt{E_1E_2}(1+\mu_{23})\mu_{12} & \frac{E_2(1+\mu_{23})}{2} \end{bmatrix} \begin{Bmatrix} d\varepsilon_1 \\ 2d\varepsilon_2 \end{Bmatrix} \tag{III-61}$$

With :

$$\phi = (1+\mu_{23})(1-\mu_{23}-2\mu_{12}^2) \tag{III-62}$$

3.5.2 Equivalent Uniaxial Strain

Following the definition of the incremental constitutive relations, this section describes how the four material properties of the model can be determined. Elwi and Murray used

the concept of equivalent uniaxial strains, which was developed by Darwin and Pecknold (1977), to rewrite Eq. (III - 61) as follows :

$$\begin{Bmatrix} d\sigma_1 \\ d\sigma_2 \end{Bmatrix} = \begin{bmatrix} E_1 B_{11} & E_1 B_{12} \\ E_2 B_{21} & E_2 B_{22} \end{bmatrix} \begin{Bmatrix} d\varepsilon_1 \\ 2d\varepsilon_2 \end{Bmatrix} \qquad (III-63)$$

where the coefficients B_{ij} can be defined by identifying the matrix terms of Eq. (III - 61) with the corresponding terms in Eq. (III - 63).

Eq. (III - 63) can be written as follows :

$$\begin{aligned} d\sigma_1 &= E_1 (B_{11} d\varepsilon_1 + 2B_{12} d\varepsilon_2) \\ d\sigma_2 &= E_2 (B_{21} d\varepsilon_1 + 2B_{22} d\varepsilon_2) \end{aligned} \qquad (III-64)$$

or, in matrix form :

$$\begin{Bmatrix} d\sigma_1 \\ d\sigma_2 \end{Bmatrix} = \begin{bmatrix} E_1 & 0 \\ 0 & E_2 \end{bmatrix} \begin{Bmatrix} d\varepsilon_{1u} \\ d\varepsilon_{2u} \end{Bmatrix} \qquad (III-65)$$

The vector on the right-hand side of Eq. (III - 65) may be defined as the vector of "equivalent incremental uniaxial strains", whose components are defined in terms of actual incremental strains by identifying with the appropriate terms of Eqs. (III - 64) :

$$\begin{aligned} d\varepsilon_{1u} &= B_{11} d\varepsilon_1 + 2B_{12} d\varepsilon_2 \\ d\varepsilon_{2u} &= B_{21} d\varepsilon_1 + 2B_{22} d\varepsilon_2 \end{aligned} \qquad (III-66)$$

The total equivalent uniaxial strain may be determined by integration over the load path:

$$\varepsilon_{iu} = \int d\varepsilon_{iu} = \int \frac{d\sigma_i}{E_i} \qquad (III-67)$$

As can be seen from Eq. (II - 65), the incremental uniaxial strain is the increment in strain in direction i that the material would exhibit if subjected to a stress increment $d\sigma_i$ with all other stress increments equal to zero.

The proposed constitutive relationship has the form :

$$d\sigma = F\left(d\varepsilon, \int d\sigma\right)$$

in which F implies a functional relationship. This kind of relationship is path-dependent and is called a hypoelastic law.

3.5.3 Equivalent Uniaxial Stress-Strain Relation

The uniaxial compressive stress-strain relation that was used is a generalized form of the Saenz equation (1964) :

$$\sigma_i = \frac{E_o \varepsilon_{iu}}{1 + (R + R_E - 2)\frac{\varepsilon_{iu}}{\varepsilon_{ip}} - (2R - 1)\left(\frac{\varepsilon_{iu}}{\varepsilon_{ip}}\right)^2 + R\left(\frac{\varepsilon_{iu}}{\varepsilon_{ip}}\right)^3} \qquad \text{(III-68)}$$

with $i = 1$ or 2, and in which the following definitions apply :

$$R_E = \frac{E_o}{E_s} \qquad \text{(III-69)}$$

$$E_s = \frac{\sigma_{ip}}{\varepsilon_{ip}} \qquad \text{(III-70)}$$

$$R_\sigma = \frac{\sigma_{ip}}{\sigma_{if}} \qquad \text{(III-71)}$$

$$R_\varepsilon = \frac{\varepsilon_{if}}{\varepsilon_{ip}} \tag{III-72}$$

$$R = R_E \frac{R_\sigma - 1}{(R_\varepsilon - 1)^2} - \frac{1}{R_\varepsilon} \tag{III-73}$$

and, as shown in Fig. (III - 9) :

E_o = the initial modulus of elasticity

σ_{ip} = the maximum stress, associated with direction i, that occurs for the current principal stress ratio

ε_{ip} = the corresponding equivalent uniaxial strain

σ_{if}, ε_{if} = the coordinates of a point on the descending branch of the stress-equivalent strain curve

The tangent elastic modulus can be found as follows :

$$E_i = \frac{d\sigma_i}{d\varepsilon_{iu}} \tag{III-74}$$

Differentiating Eq. (III - 68) with respect to ε_{iu} results in the following equation :

$$E_i = E_o \frac{1 + (2R - 1)\left(\frac{\varepsilon_{iu}}{\varepsilon_{ip}}\right)^2 - 2R\left(\frac{\varepsilon_{iu}}{\varepsilon_{ip}}\right)^3}{\left[1 + (R + R_E - 2)\frac{\varepsilon_{iu}}{\varepsilon_{ip}} - (2R - 1)\left(\frac{\varepsilon_{iu}}{\varepsilon_{ip}}\right)^2 + R\left(\frac{\varepsilon_{iu}}{\varepsilon_{ip}}\right)^3\right]^2} \tag{III-75}$$

This equation defines the required moduli.

3.5.4 Poisson's Ratios

The tangent elastic moduli of Eq. (III - 65) can now be determined from Eq. (III - 75) provided that the parameters from Fig. (III - 9) are known. However, to calculate real strain increments, it is also necessary to determine the values of the Poisson's ratios appearing in Eq. (III - 60).

Kupfer, Hilsdorf and Rusch (1969) determined an expression for the Poisson's ratio in a uniaxial compression test by fitting the experimental data with a cubic polynomial :

$$\nu = \nu_0 \left[1 + 1.3763 \frac{\varepsilon}{\varepsilon_p} - 5.3600 \left(\frac{\varepsilon}{\varepsilon_p} \right)^2 + 8.586 \left(\frac{\varepsilon}{\varepsilon_p} \right)^3 \right] \qquad \text{(III-76)}$$

or :

$$\nu = \nu_0 f \left(\frac{\varepsilon}{\varepsilon_p} \right) \qquad \text{(III-77)}$$

with :

ε = the uniaxial strain

ε_p = the uniaxial peak strain, which can be assumed as 0.002

ν_0 = the initial Poisson's ratio of the concrete, which can be assumed as 0.2

It is then postulated by Elwi and Murray that the Poisson's ratios in each direction i can be calculated by replacing ε with ε_{iu} and ε_p with ε_{ip} :

$$\nu_i = \nu_0 f \left(\frac{\varepsilon_{iu}}{\varepsilon_{ip}} \right) \qquad \text{(III-78)}$$

and with Eqs. (III - 60) modified into :

$$\mu_{12}^2 = \nu_1 \nu_2$$
$$\mu_{23} = \nu_2 \qquad \text{(III-79)}$$

Elwi and Murray also recommend to place a maximum limit of 0.5 on the Poisson's ratio in order to get realistic predictions.

3.5.5 Failure Surface

A surface in the 3D stress space is needed to define the ultimate strengths σ_{ip} for any ratio of stresses. Elwi and Murray suggest to use the failure surface proposed by Argyris (1976), based on an octahedral formulation, but basically any other proposal for the failure surface can be adopted.

Eqs. (III - 70) and (II – 72) also require the evaluation of the equivalent uniaxial strains ε_{ip}, associated with the ultimate strength points σ_{ip}. Elwi and Murray postulate an equivalent strain surface in the 3D equivalent uniaxial strain space that has the same form as the failure surface for the stresses in the 3D stress space. The formulation for this corresponding strain surface is thus obtained by replacing the octahedral shear stress τ_o and the octahedral normal stress σ_o in an equation of the form (III – 46) by the octahedral shear strain γ_o and the octahedral normal strain ε_o respectively. f'_c is replaced by the uniaxial peak strain ε_p.

3.5.6 Descending branch

The remaining parameters required by Eq. (III - 75) are the values of σ_{if} and ε_{if} on the descending branch of the stress-equivalent uniaxial strain curve. However, this portion

of the stress-strain curve is highly test-dependent and unavailable from load controlled test. Therefore, it was simply assumed by Elwi and Murray that :

$$\varepsilon_{if} = 4\varepsilon_{ip} \qquad \sigma_{if} = \frac{\sigma_{ip}}{4} \tag{III-80}$$

3.6 Summary

In this chapter the material constitutive relations for the FRP material were presented. Also a number of models representing the behaviour of concrete under a triaxial state of stresses were discussed. These models include the octahedral theories proposed by Gerstle, Kotsovos and Newman, and Cedolin, and the models proposed by Ahmad and Shah, and Elwi and Murray.

The material constitutive relations of the FRP and the concrete will be used in the next chapters to construct models for FRP/concrete composite sections.

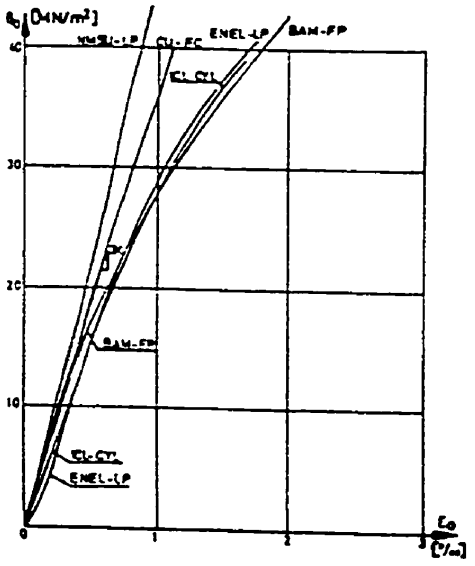

Fig. III - 1 : Variation of σ_o with ε_o

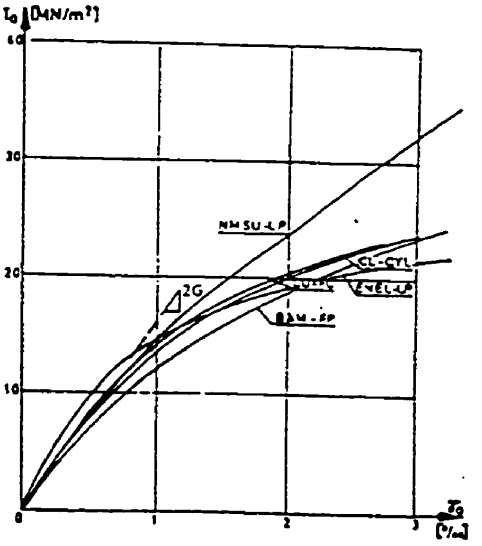

Fig. III - 2 : Variation of τ_o with γ_o

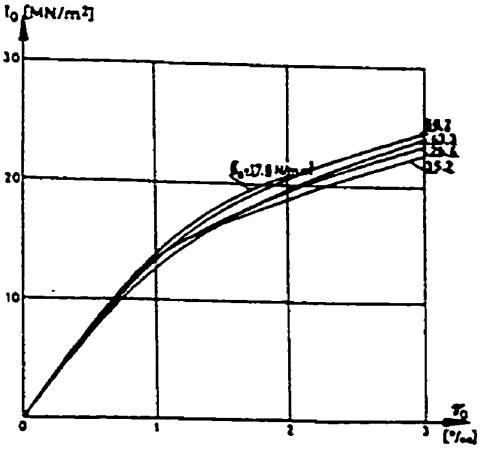

Fig. III - 3 :

Dependence of the τ_o-γ_o relation on σ_o

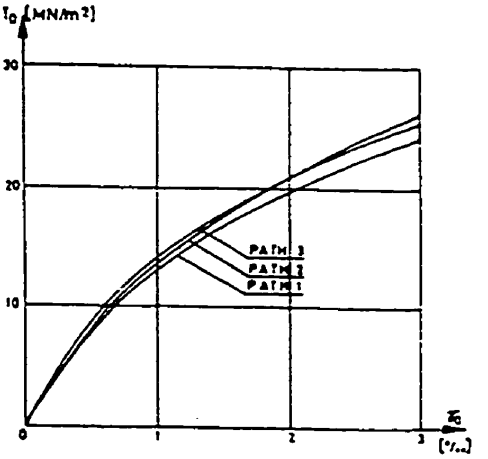

Fig. III - 4 :

Path-dependence of the τ_o-γ_o relation

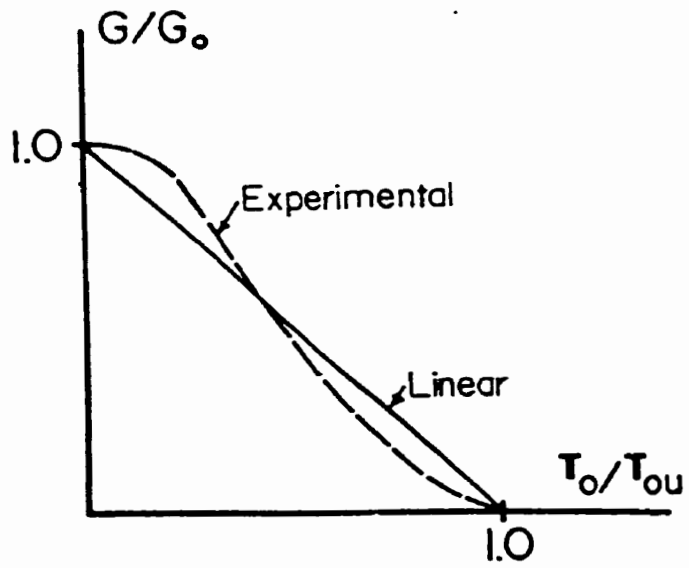

Fig. III - 5

Variation of the shear modulus G with τ_o

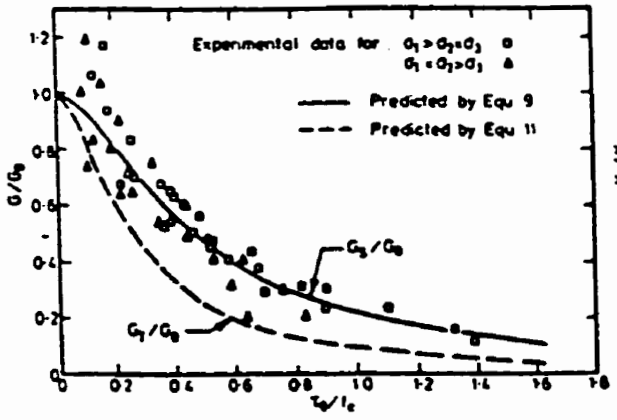

Fig. III - 6

Variation of G_s with τ_o (Kotsovos)

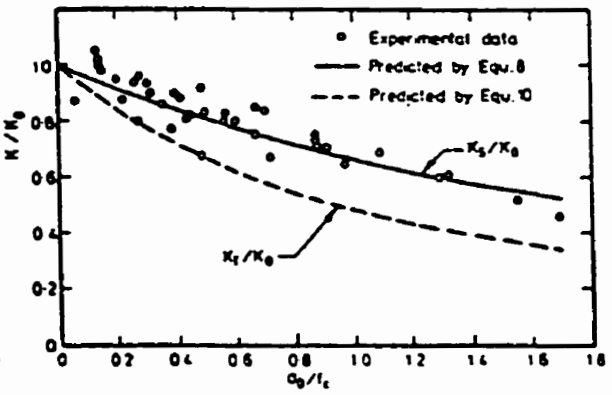

Fig. III - 7

Variation of K_s with σ_o (Kotsovos)

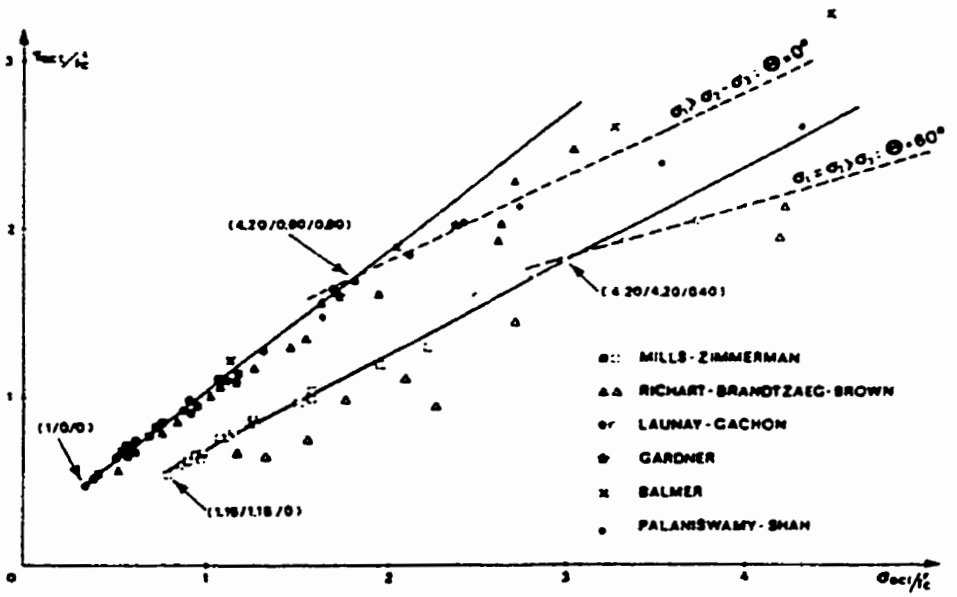

Fig. III - 8

Mills – Zimmerman strength criterion

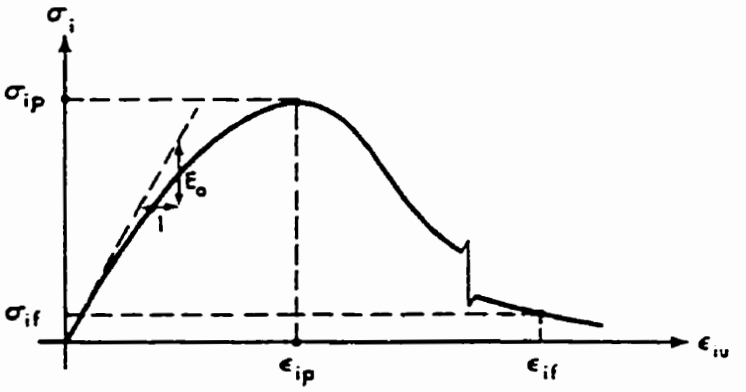

Fig. III - 9

Uniaxial stress-strain relation

Chapter IV :

Proposed Model 1

4.1 Introduction

This chapter deals with hybrid sections where the axial load is applied to the concrete core only. The shell carries no load in the axial direction and is used only to provide confinement to the core. This implies that arrangements have to be made to minimize the bond at the interface between the shell and the core to avoid transfer of stresses into the shell through bond at the interface.

The proposed model is based on the principles of equilibrium and strain compatibility in the lateral direction between the shell and the core. These principles will be applied using the different triaxial constitutive relations for the concrete presented in chapter III. In each case the performance of the model will be evaluated by comparing the predictions of the model to experimental data.

4.2 Equilibrium Equation

The basic equilibrium equation is given by Eq. (II - 27) : for a thin-walled shell with radius R and thickness t, subjected to an inner pressure σ_2, the following equation applies:

$$\sigma_2 = \frac{\sigma_{hoop} t}{R}$$

and :

$$\sigma_2 = \frac{\varepsilon_{hoop} E_{hoop} t}{R}$$

Lateral strain compatibility in the interface leads to the following equality :

$$\begin{aligned} \varepsilon_{hoop} &= \varepsilon_3 \\ &= \varepsilon_2 \end{aligned}$$

This results in the following equation :

$$\sigma_2 = \frac{\varepsilon_2 E_{hoop} t}{R} \qquad (\text{IV} - 1)$$

4.3 Confinement Mechanism

Consider a hybrid section where the concrete core is subjected to axial load.

As the load increases, the concrete cylinder expands laterally due to the Poison's effect. This expansion will be restrained by the shell which develops hoop stresses in the

circumferential direction resulting in a lateral confining pressure σ_2 (= σ_3) to the concrete. Unlike standard triaxial concrete tests where the confining pressure remains constant during testing, the confining pressure provided by the shell will build up during the test as the concrete keeps straining laterally.

In the case of a steel shell, the steel will be subjected to uniaxial circumferential tension, eventually reaching its full plastic strength f_y in the circumferential direction. Maximum confinement is established when the steel starts yielding. Referring to Eq. (II - 27), this will happen when :

$$\sigma_{2,\max} = \frac{f_y t}{R} \qquad (IV-2)$$

If no strain hardening is assumed for the steel, the confining stresses remain constant after yielding of the steel.

In the case of an FRP shell, the concrete core will be subjected to a monotonically increasing confining pressure up to failure, due to the linear material properties of the FRP. Failure will occur due to rupture of the FRP fibers under hoop tension forces. This happens when the hoop strength f_{hoop} of the FRP material is reached :

$$\sigma_{2,\max} = \frac{f_{hoop} t}{R} \qquad (IV-3)$$

This mechanism where increasing confining stresses develop as a consequence of a restraint provided by the shell is often referred to in literature as passive confinement. This is opposed to active confinement, where a constant lateral pressure is applied to the specimen, as in the case of steel-confined concrete after yielding of the steel.

4.4 Strain Compatibility Model using Gerstle

4.4.1 Proposed Methodology

In this section the principles of strain compatibility and equilibrium are combined with the concrete constitutive relationship proposed by Gerstle.

In the case of passive confinement, the confining pressure varies monotonically over the loading history. Therefore a step-wise approach is used, where the axial loading pressure σ_1 is applied in increments $\Delta\sigma_1$. An iterative procedure is required within each step to determine the confining stress increment $\Delta\sigma_2$. A detailed flow chart of the proposed methodology is presented in Fig. (IV - 1).

Using an assumed value of $\Delta\sigma_2$, the incremental deformations of the concrete cylinder can be calculated using Eqs. (III – 12) to (III – 23) of the octahedral theory. Specifically the concrete's radial and circumferential strain increments $\Delta\varepsilon_2$ and $\Delta\varepsilon_3$, which are equal in magnitude, can be determined. Subjecting the outer shell to the same circumferential strain increment, the hoop stress increment and corresponding confining pressure increment $\Delta\sigma'_2$ can be computed using Eq. (IV - 1) :

$$\Delta\sigma_2' = \frac{\Delta\varepsilon_2 E_{hoop} t}{R} \qquad (IV-4)$$

If $\Delta\sigma'_2$ is equal to the assumed $\Delta\sigma_2$, the assumed value is correct. Otherwise a new value for $\Delta\sigma_2$ is assumed and the same steps are repeated. The average of the original value of $\Delta\sigma_2$ and $\Delta\sigma'_2$ is used.

In case of a steel-confined concrete cylinder, $\Delta\sigma_2 = 0$ beyond the yield limit of the steel and therefore no iterations are necessary.

For the correct value of $\Delta\sigma_2$, the solution will satisfy both equilibrium and strain compatibility between the concrete core and the shell at every step.

Stresses and strains are related to each other via their octahedral forms. To obtain the shear modulus G for every step, Eq. (III - 26) is used. The coupling effect is not taken into account due to the absence of an accurate formula for the coupling modulus H. By lack of the experimental results, Gerstle's theory is further applied with a constant value for $K = K_o$.

The initial values K_o and G_o were obtained from Eq. (III - 18) and (III - 19).

Application of Gerstle's theory requires a value for $\tau_{o,max}$ in each step. This is achieved by using Eq. (III - 40).

4.4.2 Example 1

The proposed model 1 is illustrated by predicting the behaviour of the steel-jacketed concrete cylinder tested by Orito and introduced in Chapter II as example 1. All properties are listed in Table (II – 1).

The maximum confining pressure is determined by using Eq. (IV - 2) :

$$\sigma_{2,\max} = \frac{f_y t}{R} = \frac{(376.7)(5.2)}{57.15} = 34.3 \quad MPa$$

Failure criterion (III – 40) requires a value for the confinement effectiveness coefficient k. An estimation for k is given by Eq. (II - 33) :

$$k = 6.7(34.3)^{-0.17} = 3.67$$

The experimental value is given by the following calculation :

$$k = \frac{f'_{cc} - f'_c}{\sigma_{2,\max}} = \frac{172 - 52.4}{34.3} = 3.49$$

The calculations are performed according to Fig. (IV - 1).

The step size $\Delta\sigma_1$ is chosen as 10 MPa. The initial values of K and G are given by Eqs. (III – 18) and (III – 19) :

K = 18.1 GPa

G = 13.6 GPa

A value of 1 MPa is initially assumed for $\Delta\sigma_2$. The incremental octahedral state of stresses is then defined by Eqs. (III – 12) and (III – 13) :

$\Delta\sigma_o$ = 4.00 MPa

$\Delta\tau_o$ = 4.24 MPa

The constitutive relations Eqs. (III – 16) and (III –17) define the incremental octahedral strains as follows :

$\Delta\varepsilon_o$ = 0.074 millistrain

$\Delta\gamma_o$ = 0.16 millistrain

The principal strain increments are given by Eqs. (III – 21) to (III – 23) :

$\Delta\varepsilon_1$ = 0.29 millistrain

$\Delta\varepsilon_2$ = -0.037 millistrain

Eq. (IV – 4) yields :

$\Delta\sigma_2'$ = 0.67 MPa

All steps are now repeated with a newly assumed value for $\Delta\sigma_2$. $\Delta\sigma_2$ is set equal to the average of 1 MPa and 0.67 MPa, being 0.83 MPa. The consecutive values of $\Delta\sigma_2$ are 0.83 MPa, 0.79 MPa and 0.77 MPa. For a value of 0.77 MPa, $\Delta\sigma_2'$ equals 0.77 MPa and the iterations are stopped.

The new value for G, used in load step 2, is given by Eq. (III – 26), which yields a value of 9.8 GPa. The previously explained method is now repeated for the second load step.

The calculations are presented in table form in the Appendix (page A-1).

The theoretical predictions for Orito's test are shown in Fig. (IV - 2) and Fig. (IV - 3).

Fig. (IV – 2) shows the axial stress vs. axial strain relationship ($\sigma_1 - \varepsilon_1$) while Fig. (IV – 3) shows the axial stress vs. volumetric strain relationship ($\sigma_1 - \varepsilon_v$). The volumetric strain is given by :

$$\varepsilon_v = \varepsilon_1 + \varepsilon_2 + \varepsilon_3$$

$$= \varepsilon_1 + 2\varepsilon_2$$

An ultimate strength of 178.2 MPa was predicted, compared to an experimentally measured value of 172 MPa. This means an overestimation by only 3.6 %.

The axial stress-strain behaviour was predicted quite accurately. The actual, experimentally observed load level where the steel tube yields in the circumferential direction corresponds to an axial concrete stress of 125 MPa. The predicted value is 122.9 MPa, which is an underestimation by only 1.7 %. Also the volumetric strains match fairly well, though the model underestimates the volumetric strains at higher load levels due to neglecting the coupling effect. As pointed out in Chapter II, the octahedral theory does not account for the strong concrete dilation which happens just prior to failure.

4.4.3 Example 2

Example 2 was previously introduced in Chapter II and refers to a GFRP-confined specimen tested by Mirmiran and Shahawy. The specimen properties are listed in Table II - 2.

Using Eq. (IV - 3), the maximum confining pressure was determined as :

$$\sigma_{2,\max} = \frac{f_{hoop}\, t}{R} = \frac{(579.2)(2.2)}{(72.5)} = 17.6 \quad \text{MPa}$$

Using Eq. (II - 33) the confinement effectiveness coefficient k was found to be 2.54 . The experimentally obtained value is 2.74.

With $k = 2.54$ the coefficients A and B in the failure criterion given by Eq. (III – 46) are found to be 0.312 and 0.480 respectively. The calculations follow again the scheme explained in Fig. (IV - 1).

As mentioned before, this scheme is valid up to failure as the FRP material remains linearly elastic at all times and no yielding of the tube occurs. The calculations are presented in table form in the Appendix (page A-15).

The results of the calculations are presented in Fig (IV - 4) in the form of an axial concrete stress vs. axial concrete strain curve. The overall behaviour is closely matched. Failure as predicted by the model occurs at an axial concrete stress of 68.7 MPa, which is an underestimation by 7.9 %. The axial strain at failure is predicted to be 0.0345 which is an underestimation of 19.7 %.

4.4.4 Refinement of the calculations

In 4.4.3 the confinement effectiveness k is calculated using Eq. (II - 33) where σ_2 is taken as the maximum confining pressure σ_{2max}. In reality, σ_2 changes monotonically with increasing axial load. Therefore we can propose a refined model where k is

recalculated in every step using the current value of the confining pressure σ_2. As a result the coefficients A and B, used to compute $\tau_{o,max}$ will change from step to step (Eq. III - 46).

The results of this model are shown in Fig. (IV - 5). The upper branch matches the experimental behaviour in a slightly better way. The stiffness of the lower branch however is somewhat underestimated due to initial low values of σ_2 and corresponding high values of k, in a range where the application of Eq. (II - 33) is questionable.

Failure is predicted at an axial concrete stress of 69.7 MPa, which is an underestimation by 6.6 %. The axial strain at failure is predicted to be 0.035 which is an underestimation by 18.6 %.

4.4.5 Example 3

Example 3 was introduced in Chapter II. It is a GFRP-confined specimen tested by Nanni and Bradford. The specimen properties are shown in Table (II-3).

Since the hoop strength of the FRP shell is not accurately known, a failure point will not be predicted. A value of 3.09 for k was based on a conservative value of 583 MPa for the FRP hoop strength.

Fig. (IV - 6) shows the predicted axial stress-strain behaviour. Fig. (IV - 7) shows the axial stress-strain behaviour obtained by using the refined method discussed in section 4.4.4.

4.5 Strain Compatibility Models based on other Octahedral Theories

4.5.1 Introduction

The octahedral theories presented by either Kotsovos and Newman, or Cedolin, can be applied in a strain compatibility model in the same way as Gerstle's theory was used in section 4.4 and presented in Fig. (IV - 1). Both theories are only different from Gerstle's theory in the way the shear and bulk modulus are calculated. Instead of using Eqs. (III - 26) and (III - 27) for G and K respectively, Kotsovos and Newman proposed Eqs. (III - 32) and (III - 33), whereas Cedolin proposed Eqs. (III - 34) and (III - 35). All other steps in the calculations are identical to what was explained for Gerstle's theory.

4.5.2 Kotsovos and Newman

Kotsovos and Newman's constitutive relationships are used to predict the behaviour of Example 1, 2 and 3, previously introduced in Chapter II.

4.5.2.1 Example 1 (Orito)

The theoretical predictions are presented in Fig. (IV – 8), which shows the axial concrete stress vs. the axial concrete strain, and Fig. (IV – 9), which shows the axial concrete stress vs. the volumetric strain. The predicted behaviour initially exhibits a lower stiffness than the experimental observations, but predicts a higher stiffness after

yielding. The predicted yield level is 126.7 MPa, in comparison to a measured value of 125 MPa. This means an overestimation by 1.4 %.

4.5.2.2 Example 2 (Mirmiran & Shahawy)

The predicted axial stress-strain curve of the concrete is illustrated in Fig. (IV - 10). It is obvious that the effect of the confining pressures on the concrete strength is greatly overestimated. The ultimate axial stress was predicted to be 117.5 MPa. This is an overestimation of 57.5 %. The ultimate axial strain was predicted to be 0.0041, which is an underestimation by 4.6 %.

4.5.2.3 Example 3 (Nanni & Bradford)

Fig. (IV - 11) shows the predicted axial concrete behaviour. Again the confinement effect is overestimated.

4.5.3 Cedolin

4.5.3.1 Example 1 (Orito)

The predicted axial and volumetric behaviour of the concrete are shown in Fig. (IV - 12) and Fig. (IV - 13) respectively. The model behaves poorly, both in estimating axial and volumetric deformations. This can be explained by the fact that Cedolin calibrated his equations for the moduli K and G from a large number of tests on specimens with concrete strengths ranging from 7 to 39 MPa. In Cedolin's theory K and G do not directly depend on f_c, only indirectly through the concrete elastic modulus E. Therefore,

the application of Eqs. (III - 34) and (III - 35) for K and G cannot be extended towards higher concrete strengths. The unconfined strength in example 1 is 52.4 MPa.

4.5.3.2 Example 2 (Mirmiran & Shahawy)

The predicted concrete behaviour is shown in Fig. (IV - 14). Unlike example 1, the unconfined concrete strength lies within the range where Cedolin's theory applies. However, a major overestimation of the confinement effect can be noticed.

4.5.3.3 Example 3 (Nanni & Bradford)

The predicted axial stress-strain curve of the concrete is shown in Fig. (IV - 15). The confinement effect is overestimated.

4.6 Strain Compatibility Model based on Ahmad & Shah

4.6.1 Calculation method

In this section Ahmad and Shah's theory is combined with the principles of strain compatibility and equilibrium at the interface.

Using the lateral strain ε_2 as the governing parameter the axial stress-strain curve of the concrete can be calculated point by point, without iterations. The proposed methodology is shown in Fig. (IV - 16).

Eq. (III – 39) is used to determine the peak strength f_{cc}'. k is determined by Eq. (II - 33).

For any value of ε_2, the confining pressure σ_2 can be determined using Eq. (IV - 1) :

$$\sigma_2 = \frac{\varepsilon_2 E_{hoop}\, t}{R}$$

Starting from a selected value for ε_2, X_2 can be determined as follows :

$X_2 = \varepsilon_2 / \varepsilon_{2p}$

Y can be found using Eq. (III - 41), and consequently σ_1 can be determined using Eq. (III – 42). A quadratic equation (III - 41) in X_1 has then to be solved to obtain ε_1.

4.6.2 Example 1

The predicted axial stress-strain behaviour of the concrete is presented in Fig. (IV - 17). Fig. (IV - 18) shows the volumetric strain vs. the axial stress of the concrete.

The axial deformations are well predicted, though circumferential yielding occurs for a higher axial stress level than experimentally observed : a theoretical value of 139.5 MPa was found, which is an overestimation of 11.6 %. The ultimate load was calculated to be 178.2 MPa, in comparison to a measured value of 172 MPa, which is an overestimation by 3.6 %.

Also the volumetric strains, dependent on both lateral and axial strains, could be fairly well predicted.

4.6.3 Example 2

The predicted axial stress-strain curve of the GFRP-confined concrete is shown in Fig. (IV - 19). Initially matching the experimental data fairly well the curve gradually moves away from it, predicting failure at an axial stress of 66.9 MPa, which is an underestimation of 10.3 %, and an axial strain of 0.08.

4.6.4 Example 3

The predictions of the axial concrete stress-strain curve for Example 3 are presented in Fig. (IV - 20). Again, no good agreement was obtained between the predicted response and the experimental behaviour.

4.7 Strain Compatibility Model based on Elwi and Murray

4.7.1 Calculations

Using the strain compatibility approach combined with the material constitutive relationship proposed by Elwi and Murray, the proposed step-wise approach is given in Fig. (IV - 21).

In the first step, the initial concrete material properties are assumed as follows :

$$\nu_1 = \nu_2 = 0.2$$

and :

$$E_1 = E_2 = E_0 = 4500\sqrt{f_c'}$$

At the end of each step these material properties are updated and used in the following step.

First, a stepsize $\Delta\sigma_1$ is chosen and a value for $\Delta\sigma_2$ is assumed. Using the material properties from the previous step the real strain increments $\Delta\varepsilon_1$ and $\Delta\varepsilon_2$ can be calculated. $\Delta\varepsilon_1$ and $\Delta\varepsilon_2$ are obtained from the equivalent uniaxial strain increments $\Delta\varepsilon_{1u}$ and $\Delta\varepsilon_{2u}$ by solving Eqs. (II - 66), where the following equations apply :

$$B_{11} = \frac{1}{\phi}\left(1-\mu_{23}^2\right) \qquad B_{12} = \frac{1}{\phi}\sqrt{\frac{E_2}{E_1}}(1+\mu_{23})\mu_{12}$$

$$B_{21} = \frac{1}{\phi}\sqrt{\frac{E_1}{E_2}}(1+\mu_{23})\mu_{12} \qquad B_{22} = \frac{1}{2\phi}(1+\mu_{23}) \qquad \text{(IV-5)}$$

$\Delta\varepsilon_2$ is related to a confining pressure $\Delta\sigma_2'$ according to Eq. (IV - 4). If the correct $\Delta\sigma_2$ was assumed, then $\Delta\sigma_2'$ equals $\Delta\sigma_2$. If not, $\Delta\sigma_2$ has to be reassumed.

$(\sigma_{1p},\sigma_{2p})$ by definition is the point on the failure surface for the current principal stress ratio ω_1, defined as :

$$\frac{\sigma_{1p}}{\sigma_{2p}} = \frac{\sigma_1}{\sigma_2} = \omega_1 \qquad \text{(IV-6)}$$

Solving Eq. (III - 46) and Eq. (IV - 6) :

$$\begin{cases} \tau_o = Af_c' + B\sigma_o \\ \dfrac{\sigma_{1p}}{\sigma_{2p}} = \omega_1 \end{cases}$$

results in :

$$\sigma_{2p} = \frac{3Af_c'}{\sqrt{2}(\omega_1 - 1) - B(\omega_1 + 2)} \quad ; \quad \sigma_{1p} = \omega_1 \sigma_{2p} \qquad (IV-7)$$

And, in an analogous way, ω_2 is defined as :

$$\frac{\varepsilon_{1p}}{\varepsilon_{2p}} = \frac{\varepsilon_{1u}}{\varepsilon_{2u}} = \omega_2$$

This results in the following equation :

$$\varepsilon_{2p} = \frac{3(0.002)A}{\sqrt{2}(\omega_2 - 1) - B(\omega_2 + 2)} \quad ; \quad \varepsilon_{1p} = \omega_2 \varepsilon_{2p} \qquad (IV-8)$$

4.7.2 Example 1

The predicted axial stress-strain behaviour of the confined concrete is shown in Fig. (IV - 22), the volumetric behaviour of the concrete is presented in Fig. (IV - 23).

The complexity of the model does not pay off in an accurate estimation of strains and deformations. The axial and volumetric stiffnesses are overestimated for low and intermediate stress levels. Therefore, at a concrete stress level of 160 MPa, still no yielding of the steel has occurred. Convergence is lost beyond this stress level.

4.7.3 Example 2

Fig. (IV - 24) shows the predicted axial concrete behaviour of example 2. Convergence is lost at an axial stress level of 37 MPa, i.e. somewhat above the unconfined strength. The same problem occurs in the modeling of example 3.

4.8 Conclusions

It is concluded from this chapter that the proposed model, based on strain compatibility and equilibrium at the interface between the concrete and the shell, combined with Gerstle's constitutive relations for the concrete, provides the most realistic results in predicting the behaviour of FRP-confined concrete where the load is applied only to the concrete core.

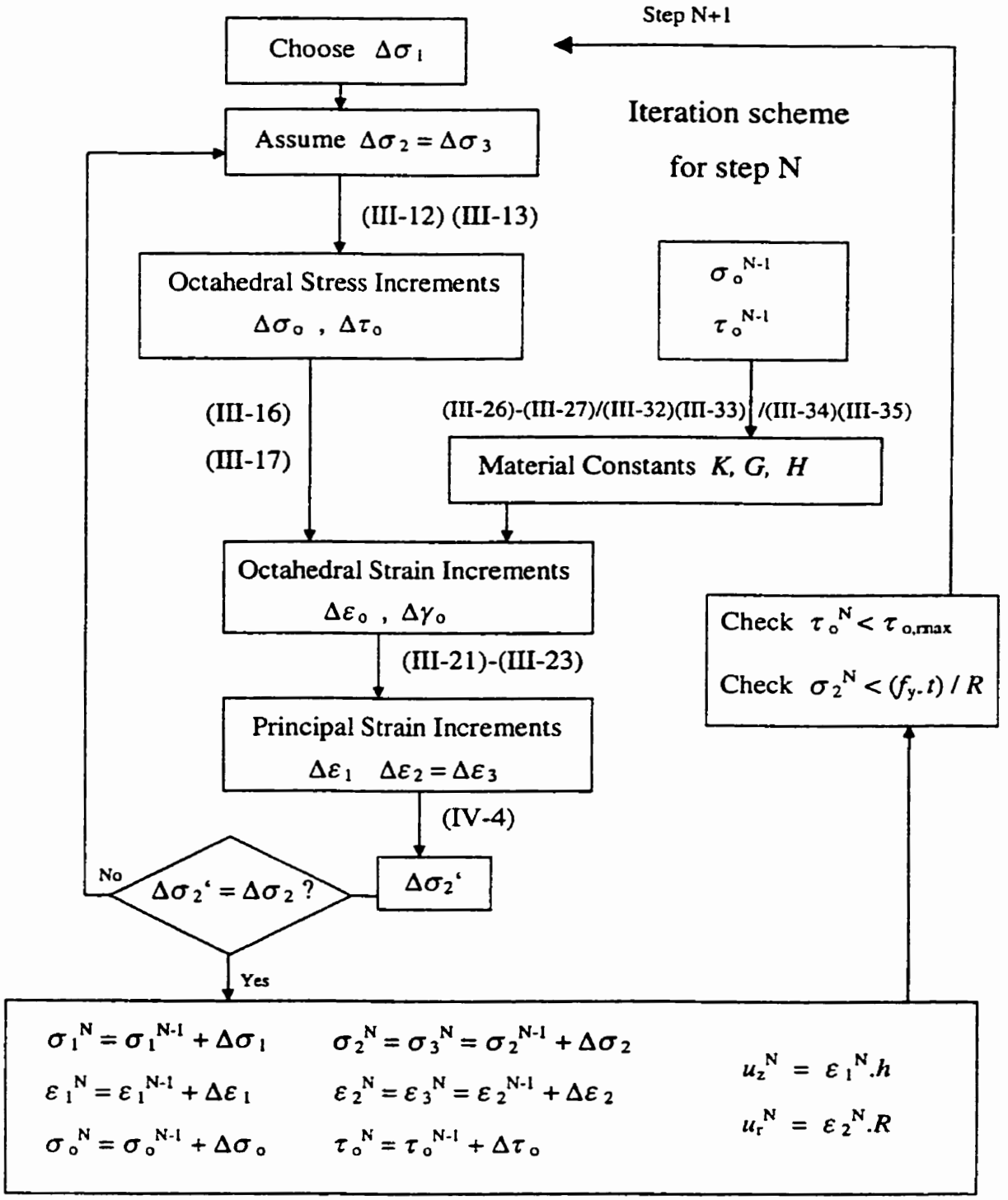

Fig. IV - 1 : Flowchart for a model based on an octahedral theory

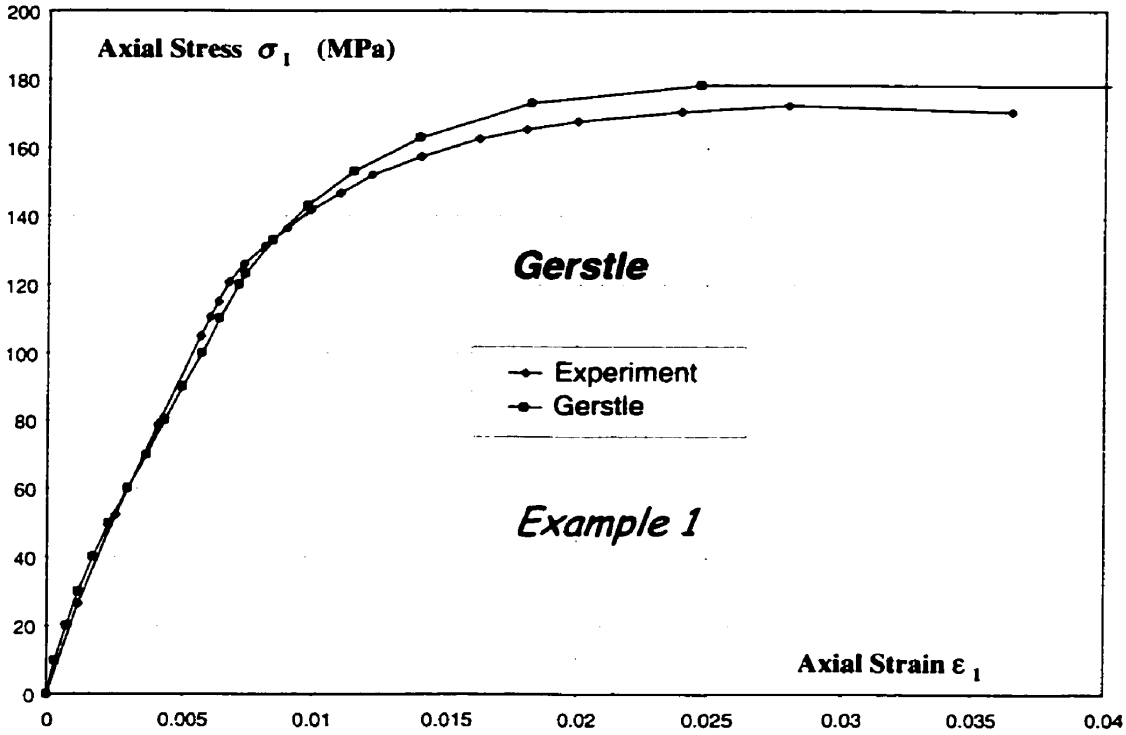

Fig. IV - 2 : Axial concrete stress-stress curve : Gerstle

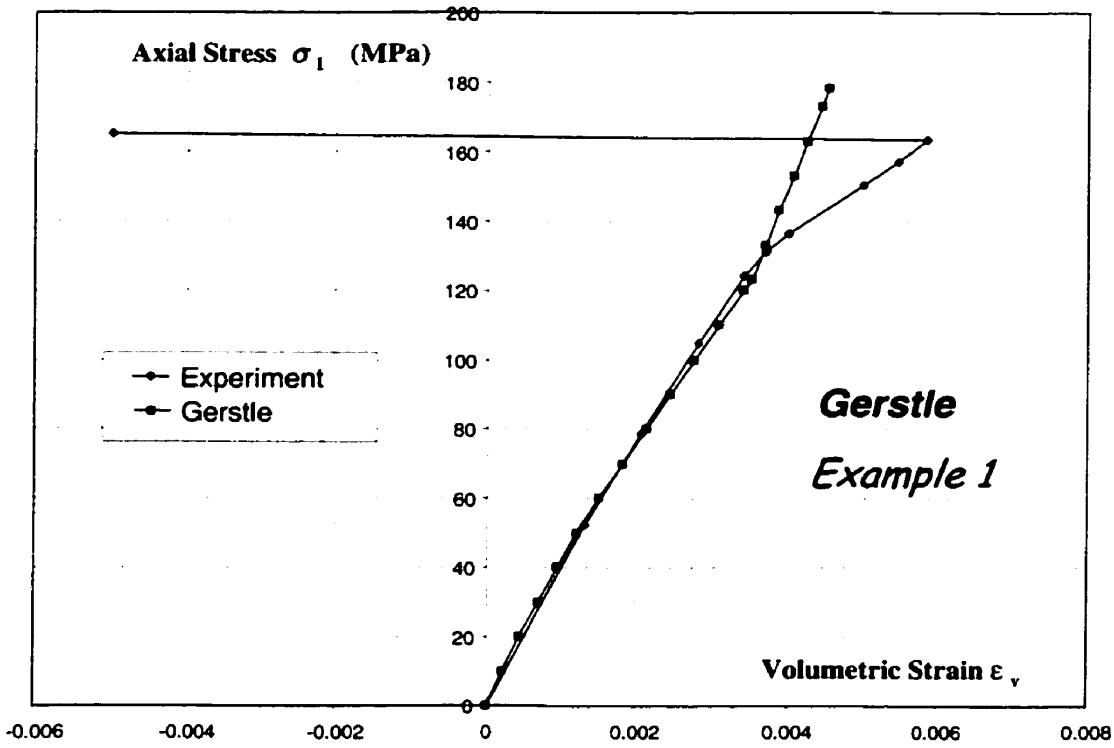

Fig. IV - 3 : Axial concrete stress vs. volumetric concrete strain : Gerstle

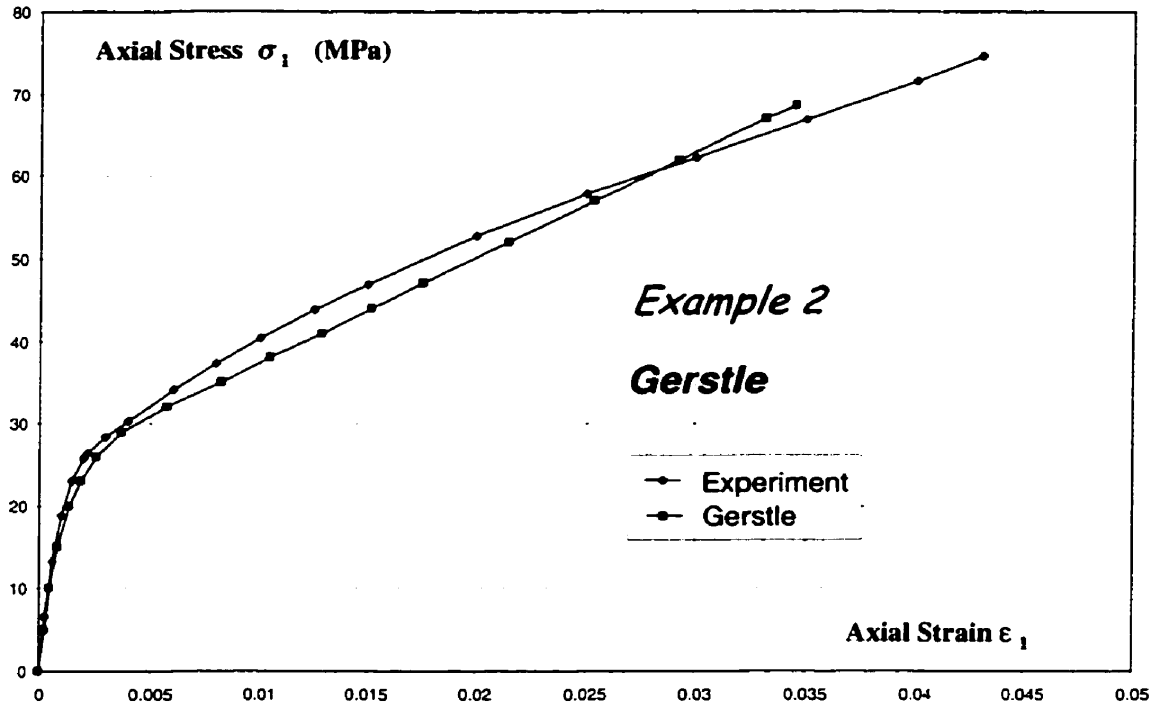

Fig. IV - 4 : Axial concrete stress-strain curve : Gerstle

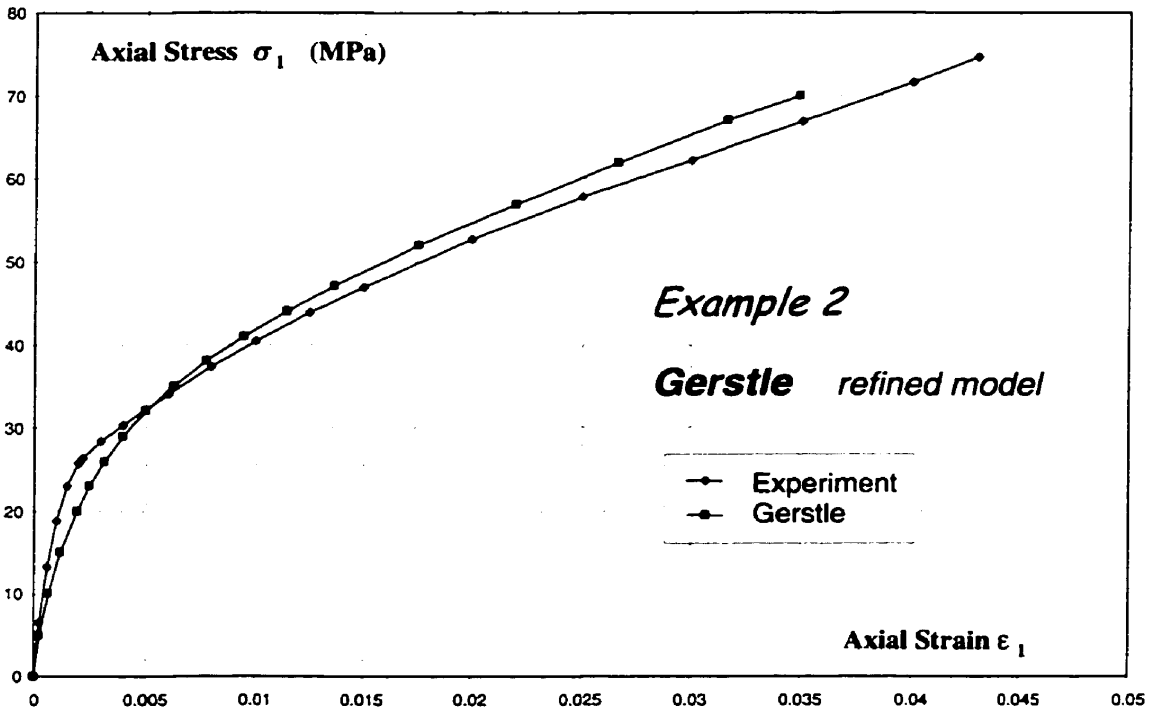

Fig. IV - 5 : Axial concrete stress-strain curve : Gerstle (refined)

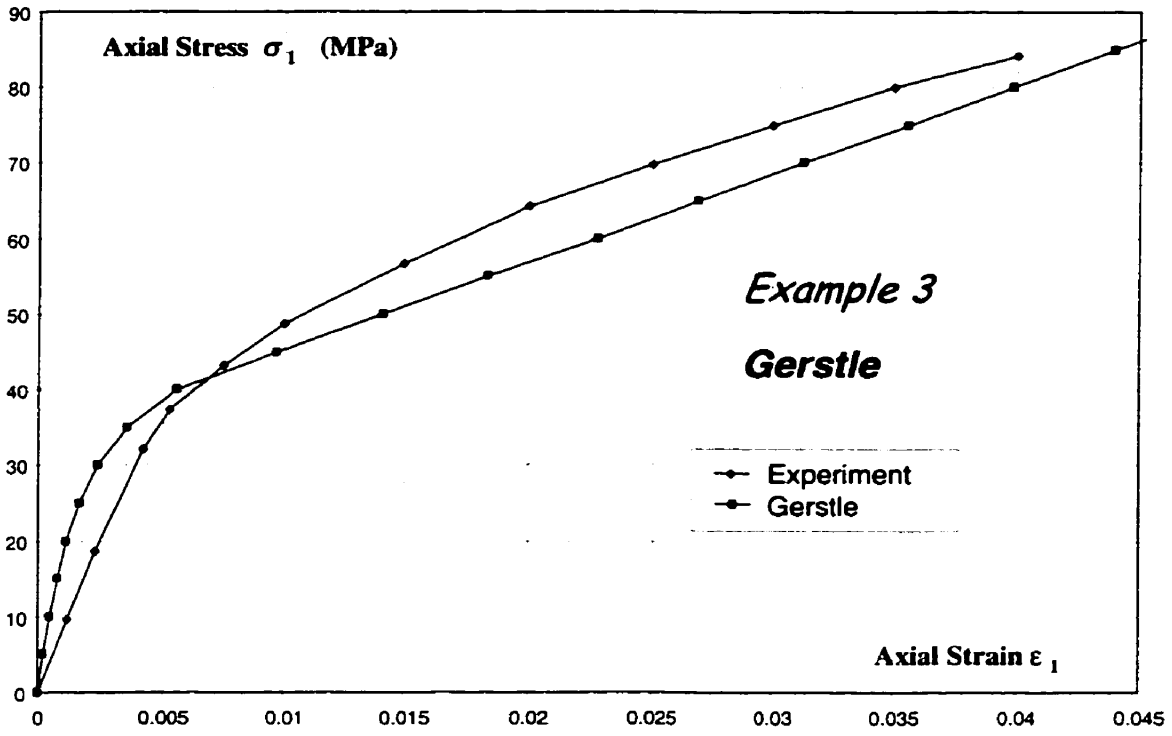

Fig. IV - 6 : Axial concrete stress-strain curve : Gerstle

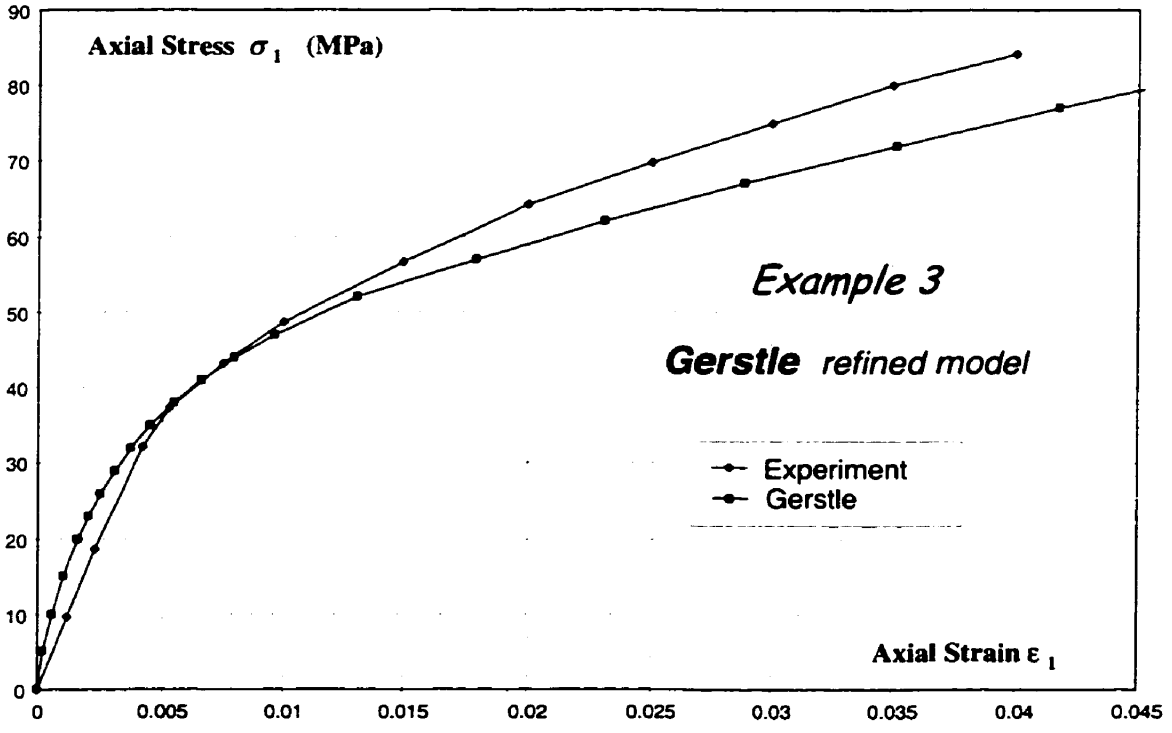

Fig. IV - 7 : Axial concrete stress-strain curve : Gerstle (refined)

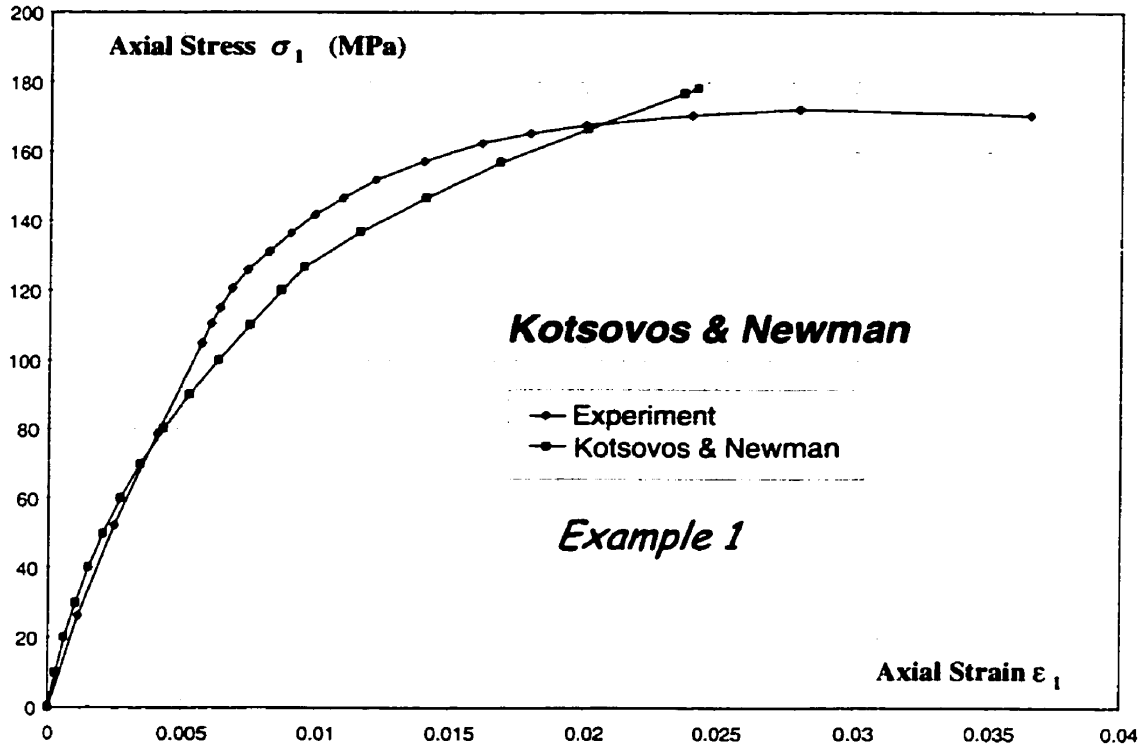

Fig. IV - 8 : Axial concrete stress-strain curve : Kotsovos & Newman

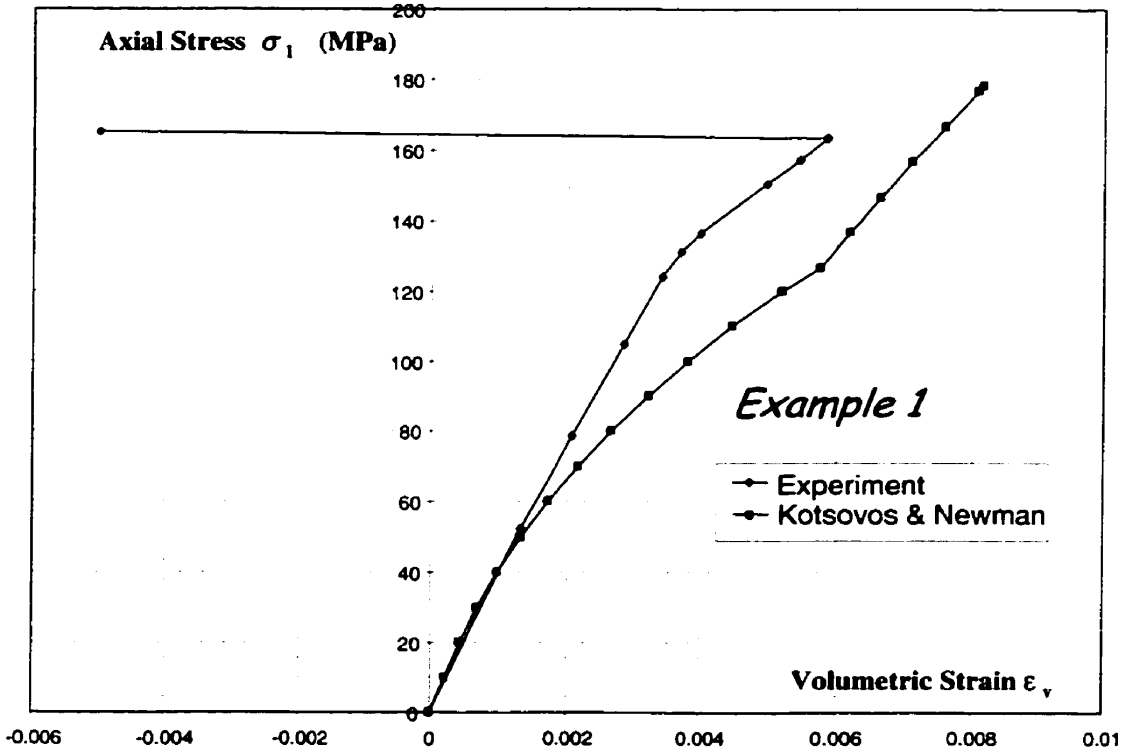

Fig. IV - 9 : Axial stress-volumetric strain curve : Kotsovos & Newman

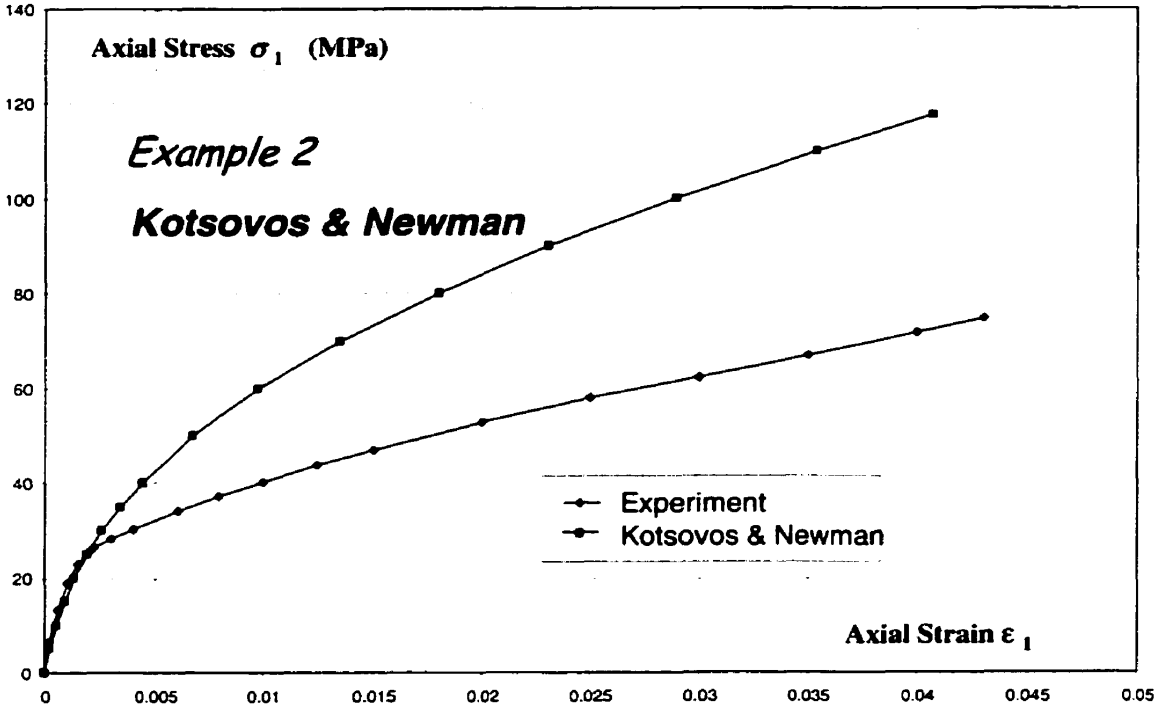

Fig. IV - 10 : Axial concrete stress-strain curve : Kotsovos & Newman

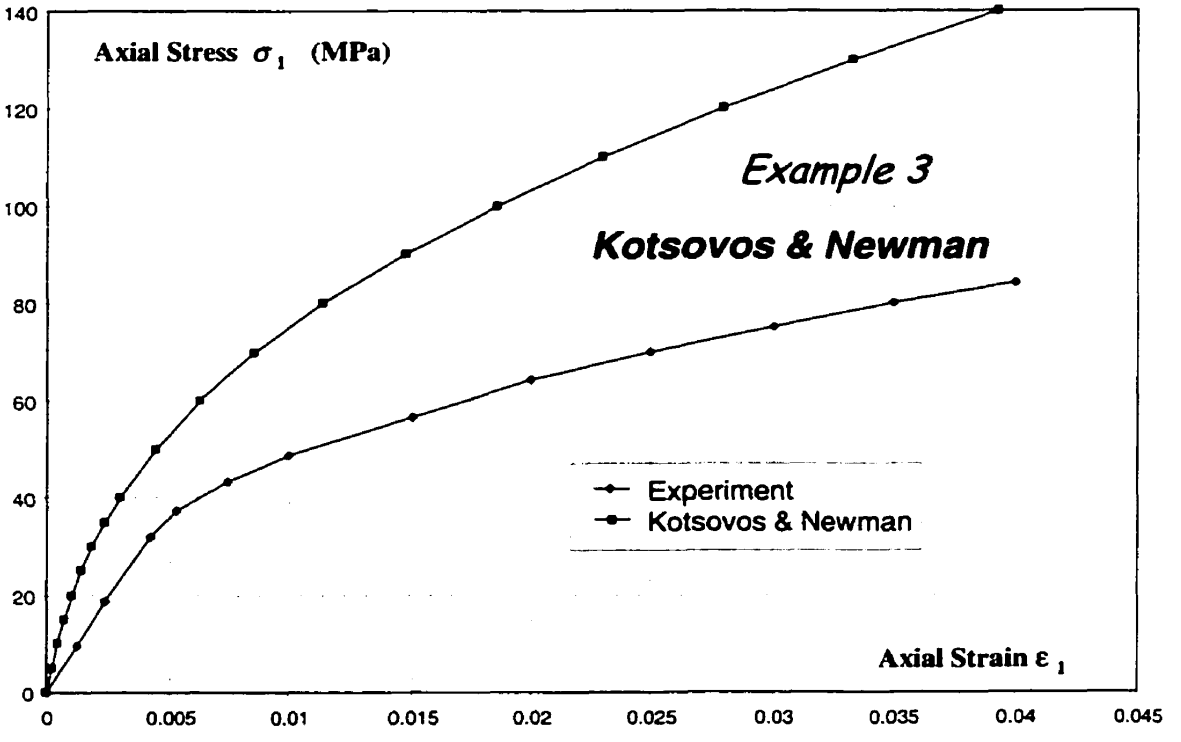

Fig. IV - 11 : Axial concrete stress-strain curve : Kotsovos & Newman

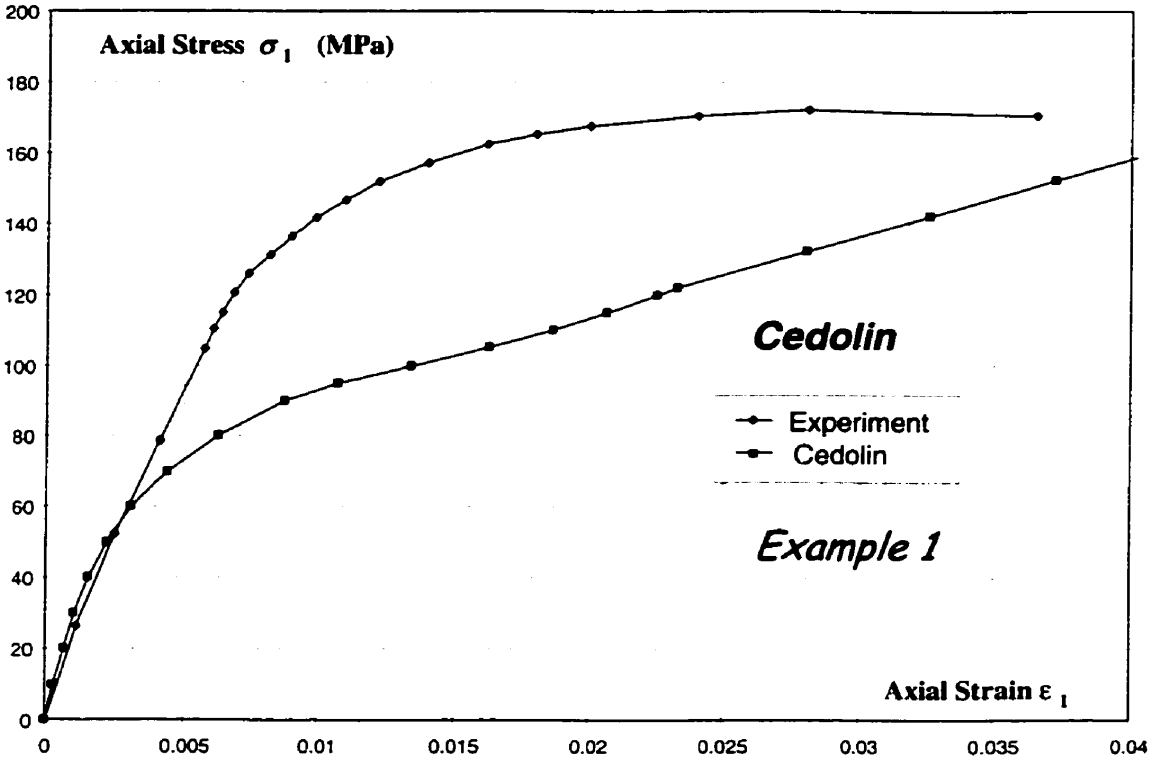

Fig. IV - 12 : Axial concrete stress-strain curve : Cedolin

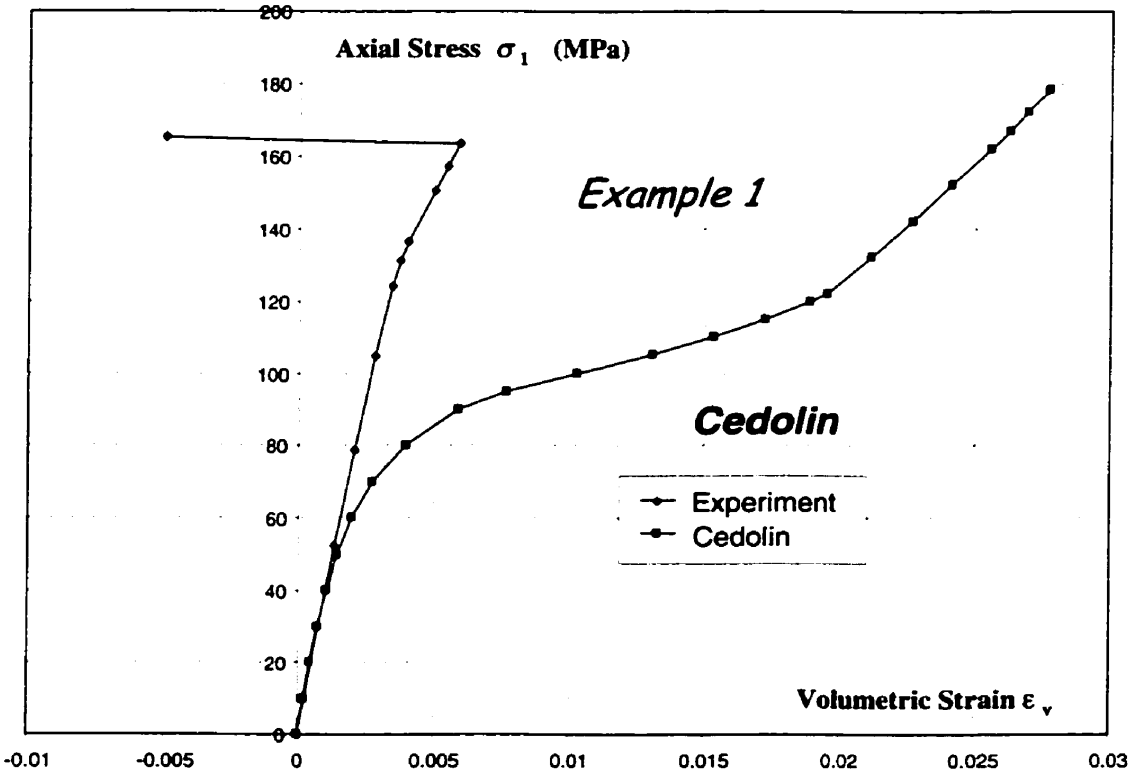

Fig. IV - 13 : Axial stress - volumetric strain curve : Cedolin

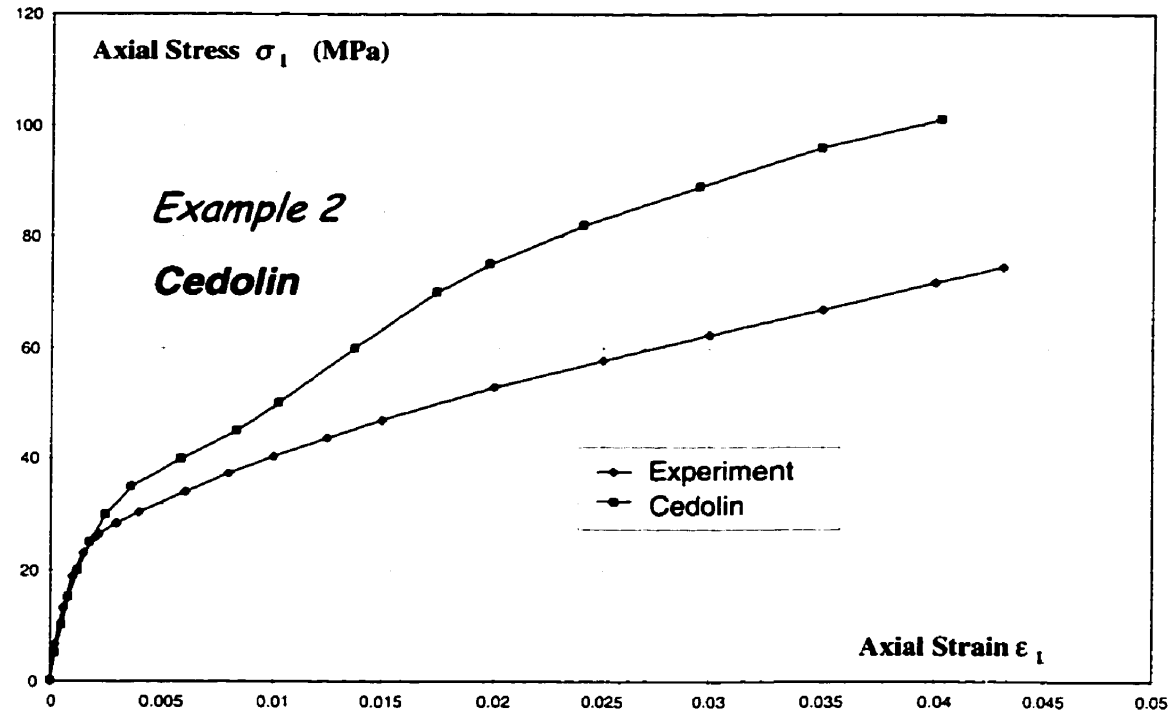

Fig. IV - 14 : Axial concrete stress-strain curve : Cedolin

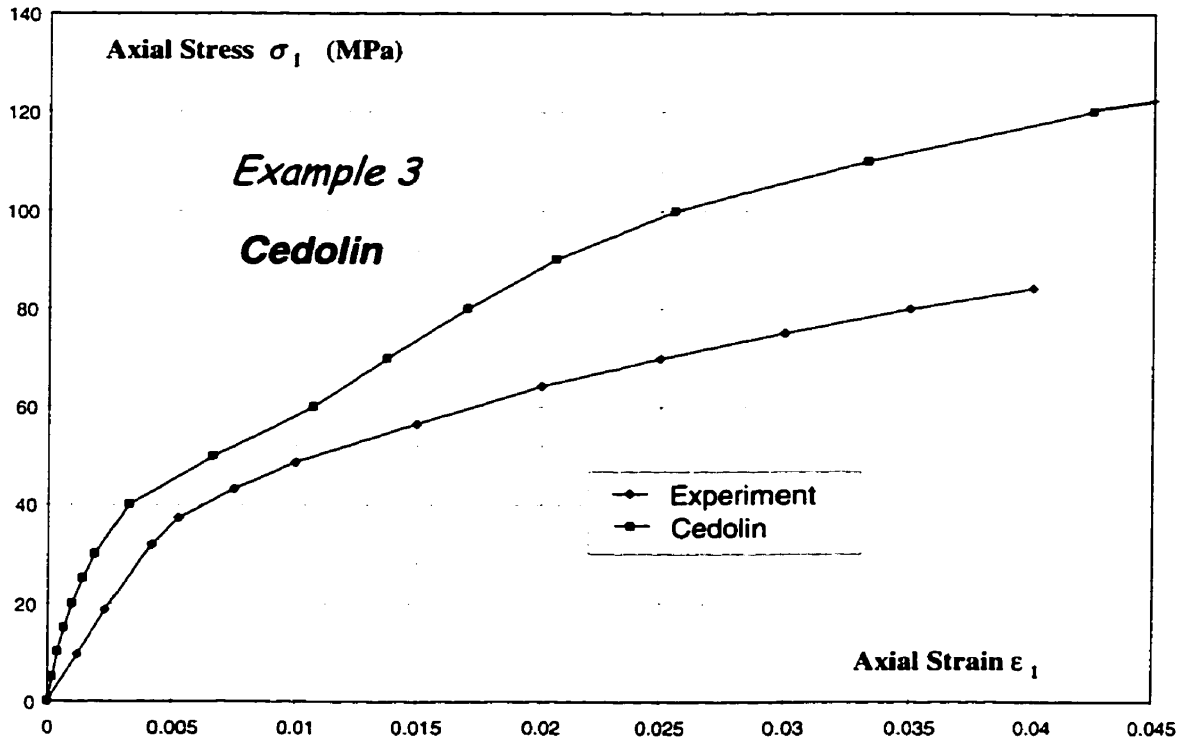

Fig. IV - 15 : Axial concrete stress-strain curve : Cedolin

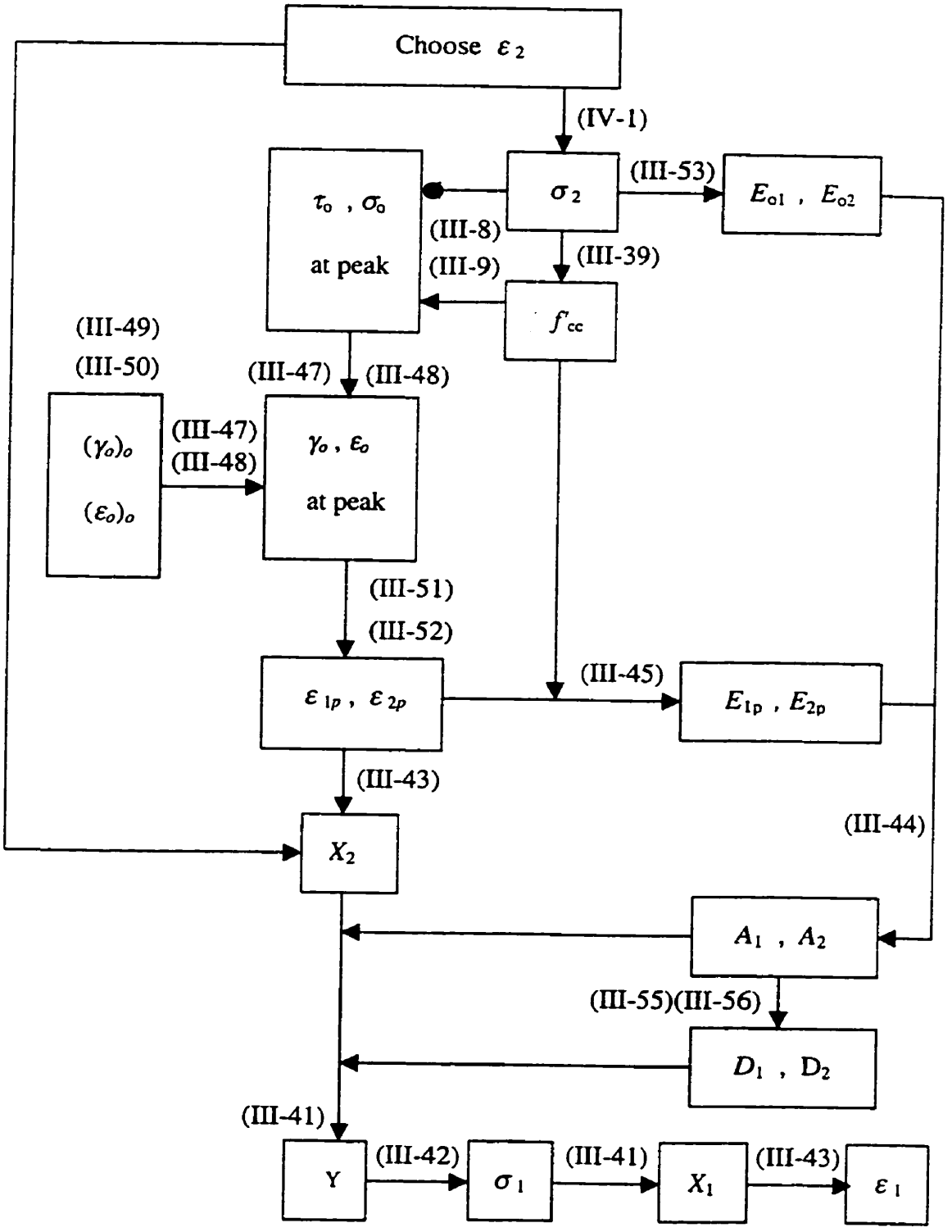

Fig. IV - 16 : Flowchart for Ahmad and Shah

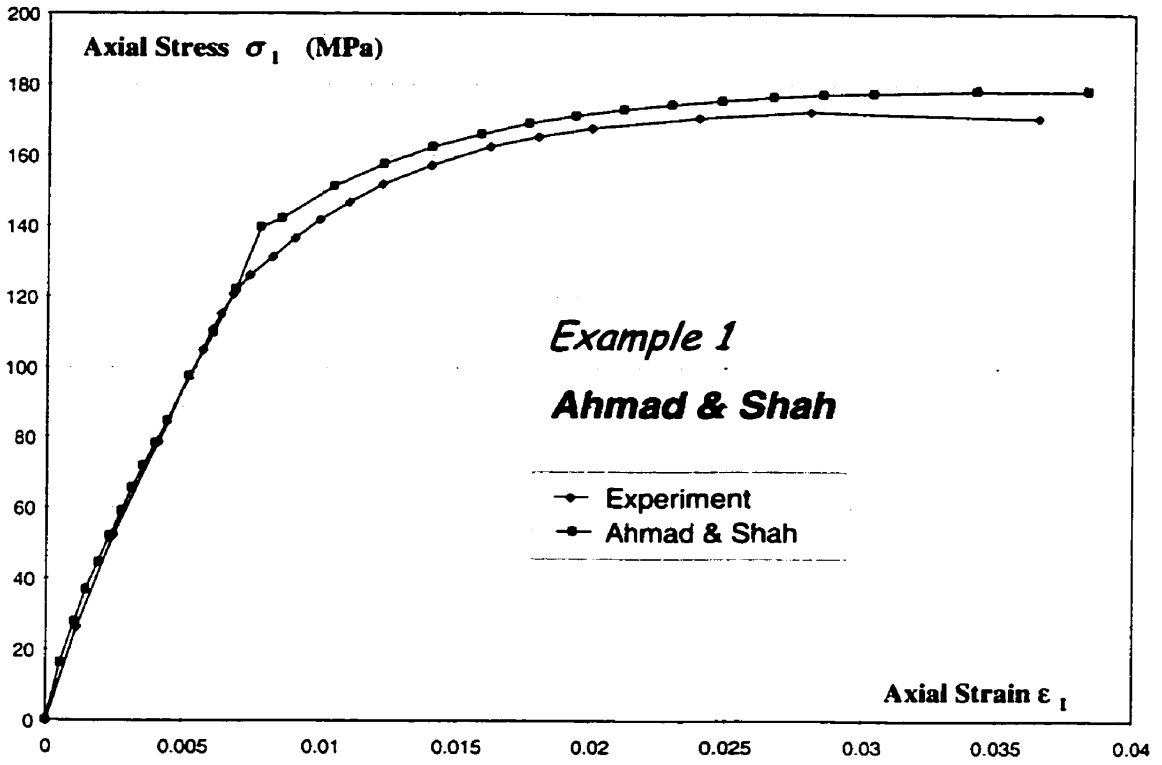

Fig. IV - 17 : Axial concrete stress-strain curve : Ahmad and Shah

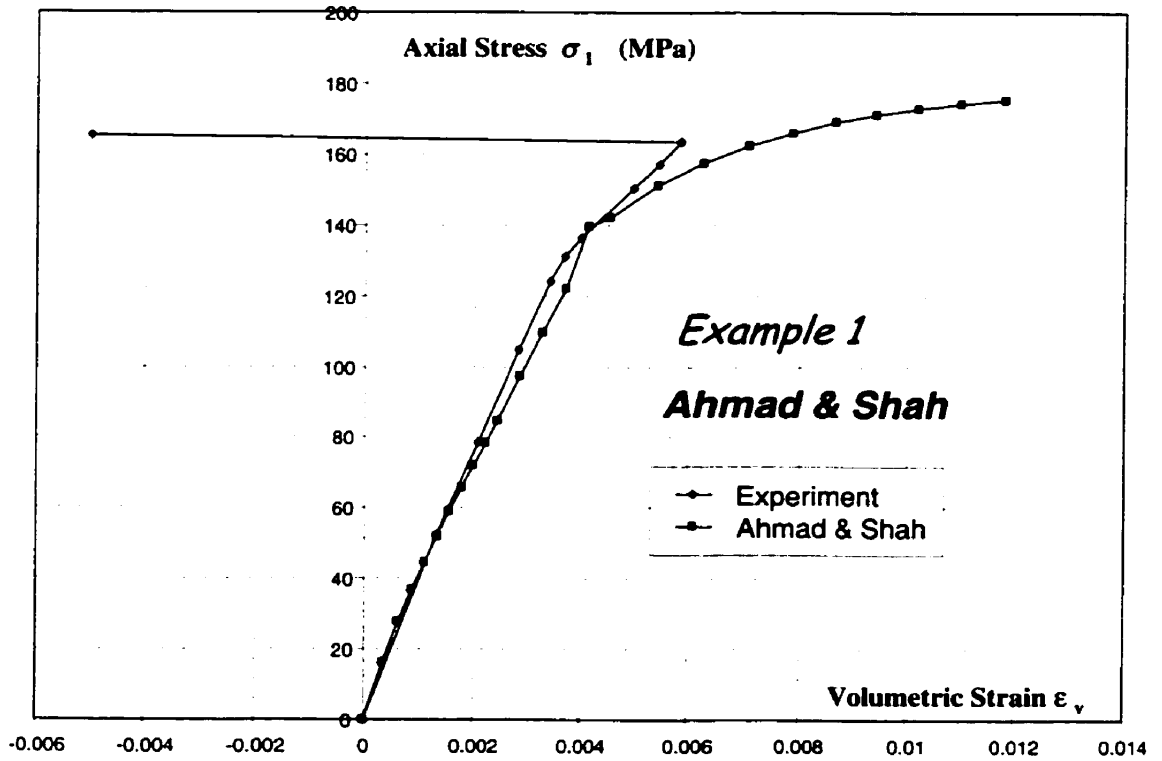

Fig. IV - 18 : Axial stress - volumetric strain curve : Ahmad and Shah

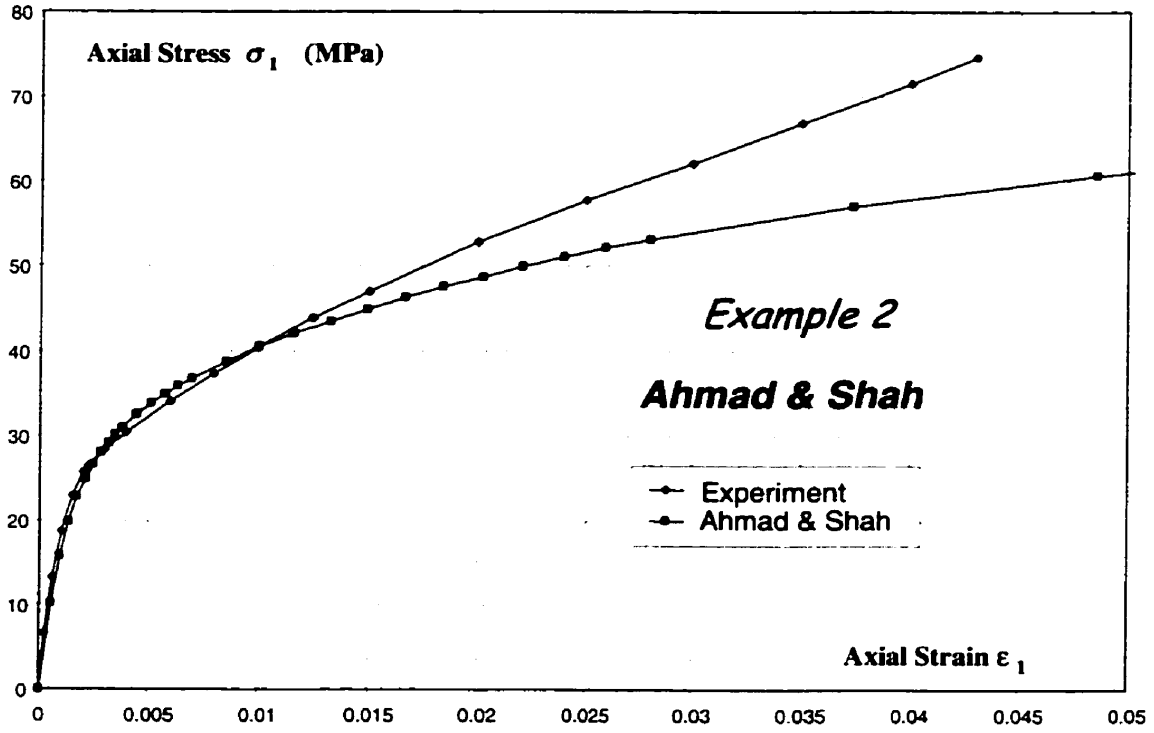

Fig. IV - 19 : Axial concrete stress-strain curve : Ahmad & Shah

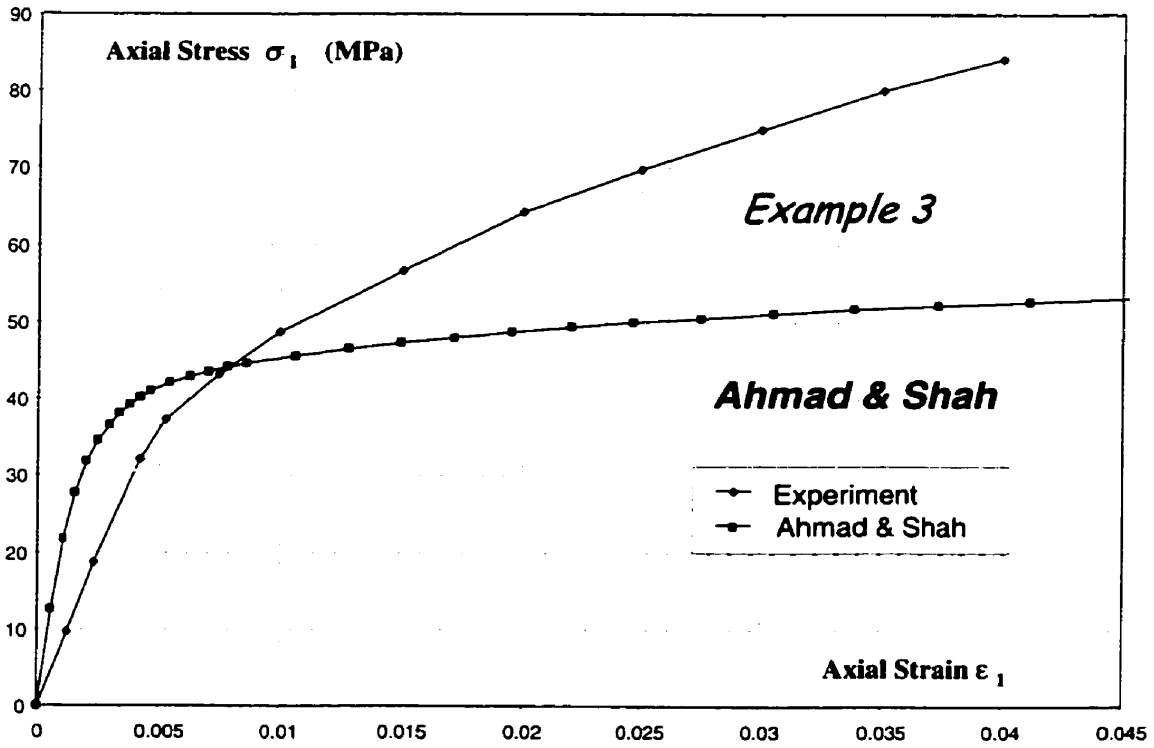

Fig. IV - 20 : Axial concrete stress-strain curve : Ahmad & Shah

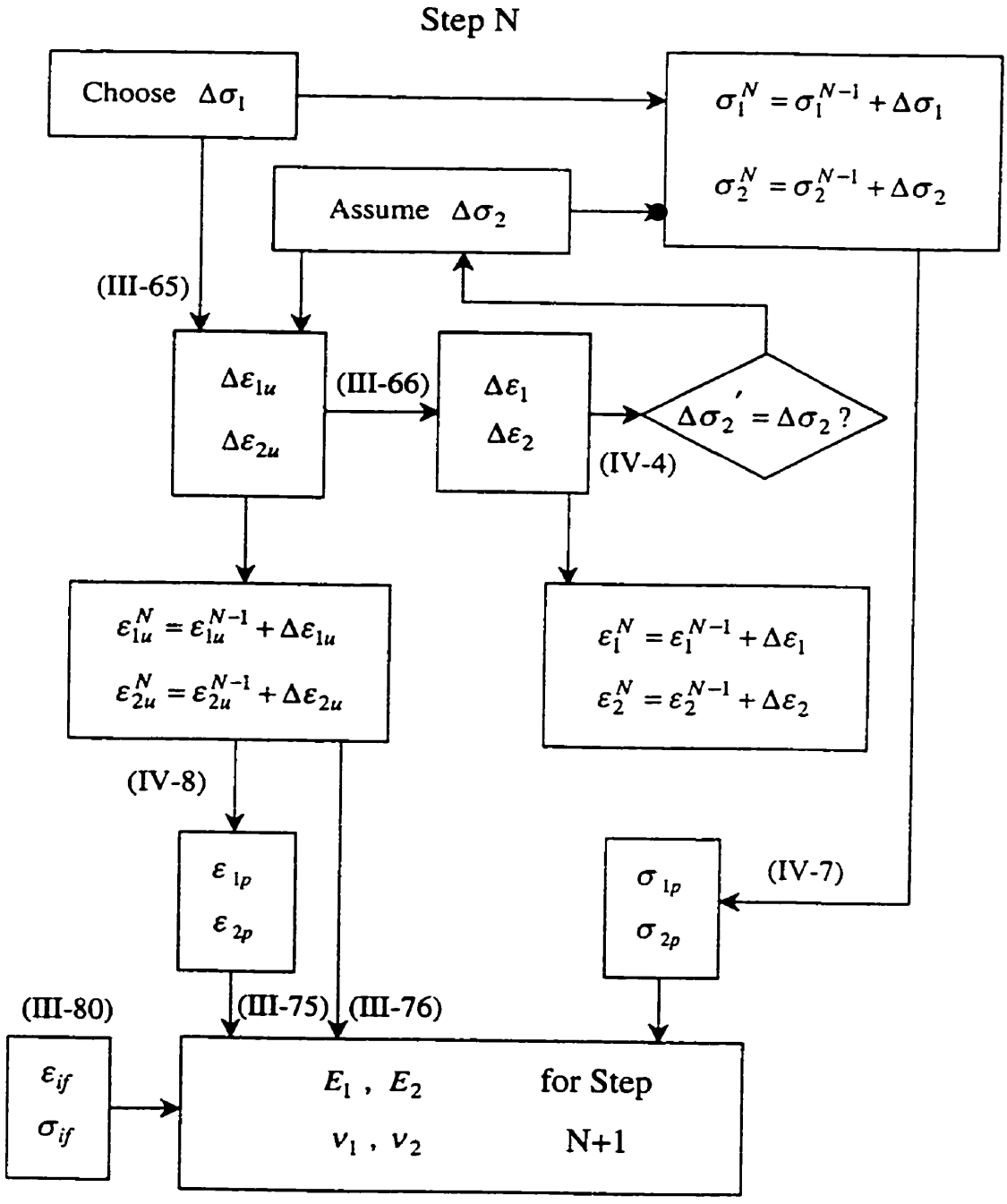

Fig. IV - 21 : Flowchart for Elwi and Murray

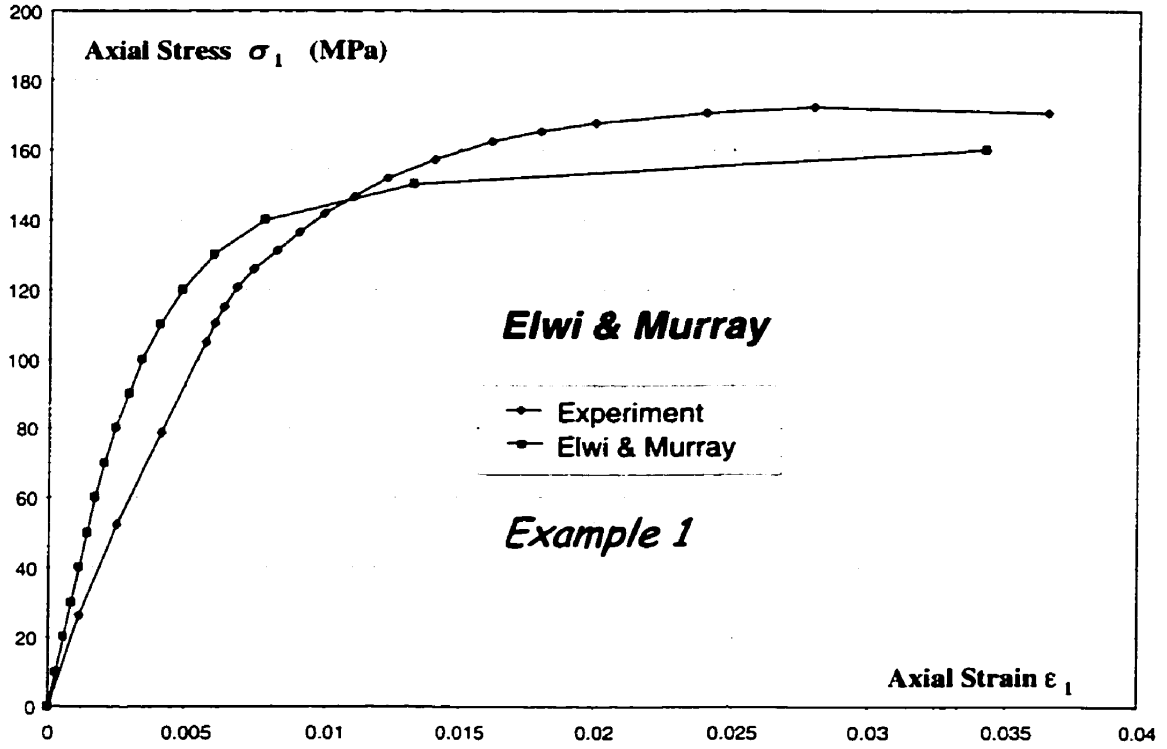

Fig. IV - 22 : Axial concrete stress-strain curve : Elwi & Murray

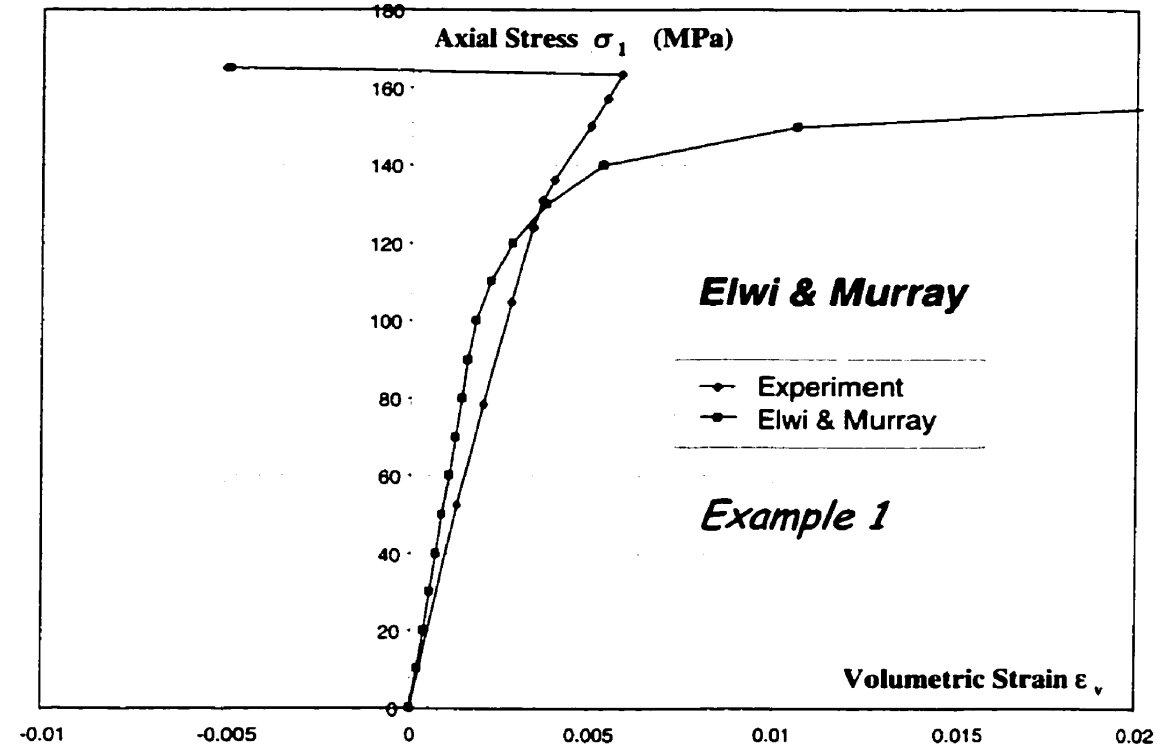

Fig. IV - 23 : Axial stress - volumetric strain curve : Elwi & Murray

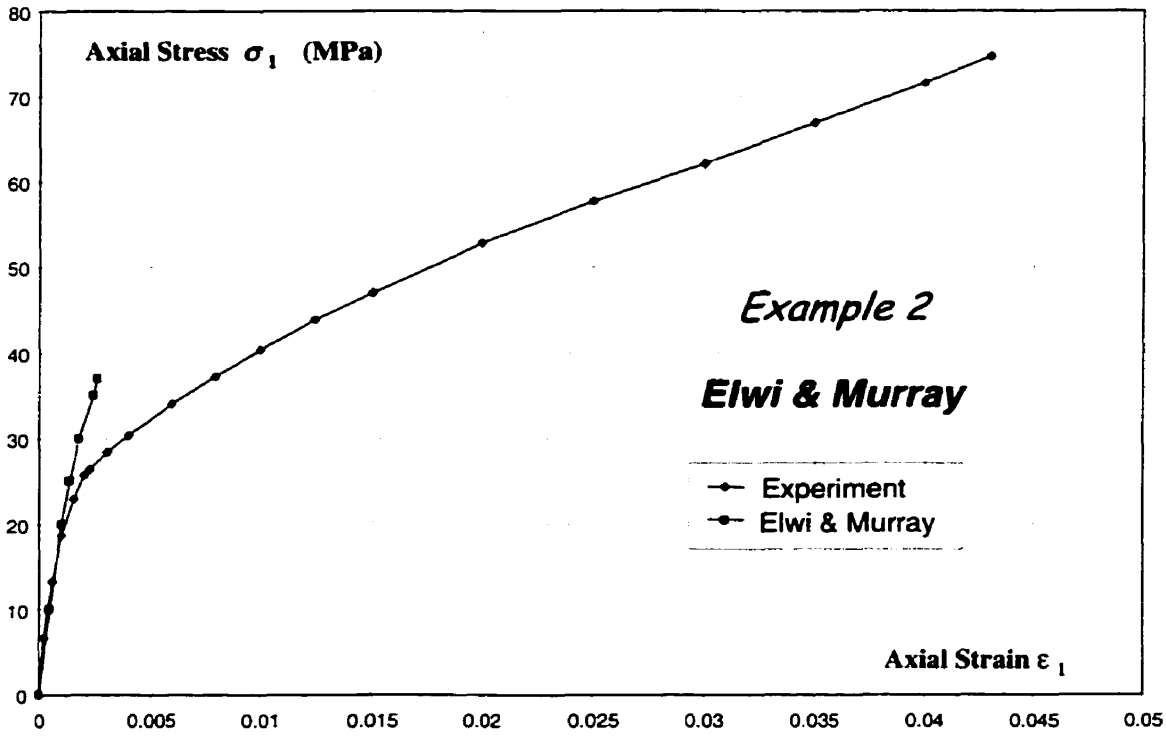

Fig. IV - 24 : Axial concrete stress-strain curve : Elwi & Murray

Chapter V :

Proposed Model 2

5.1 Introduction

In this chapter an analytical model is proposed for FRP composite sections where the axial compressive load is applied to both the concrete core and the shell. The FRP shell is subjected to a biaxial state of stresses, as a result of both longitudinal stresses in the loading direction and hoop stresses due to the lateral expansion of the core.

The model is based on strain compatibility and equilibrium between the concrete core and the shell. Strain compatibility is satisfied in both the lateral and the longitudinal directions.

The triaxial concrete constitutive relations proposed by Gerstle are used in the proposed model.

The model is modified to include also composite sections with an inner void and double shell configurations.

5.2 Totally filled section

A flowchart of the proposed methodology is shown in Fig. (V – 1). The proposed step-wise approach is based on application of the load in increments of $\Delta\sigma_1$. Assuming an initial value for $\Delta\sigma_2$, the octahedral state of stresses of the concrete can be determined using Eqs. (III - 12) and (III - 13). The corresponding incremental octahedral strains can be determined using Eqs. (III - 16) and (III - 17).

The principal strain increments $\Delta\varepsilon_1$ and $\Delta\varepsilon_2$ of the concrete can be calculated using Eqs. (III - 21) and (III - 22). To satisfy the strain compatibility between the concrete core and the shell, the shell should have the same strain increments $\Delta\varepsilon_1$ and $\Delta\varepsilon_2$. The incremental stress state in the shell can then be determined using Eqs. (III – 1) and (III – 2) :

$$\Delta\sigma_{long} = \frac{(\Delta\varepsilon_1 + \nu_f \Delta\varepsilon_2)E_{long}}{1-\nu_f\nu'_f} \qquad (V-1)$$

$$\Delta\sigma_{hoop} = \frac{(\Delta\varepsilon_2 + \nu'_f \Delta\varepsilon_1)E_{hoop}}{1-\nu_f\nu'_f} \qquad (V-2)$$

where E_{long} and E_{hoop} represent the moduli of the FRP material and where $\Delta\sigma_{long}$ and $\Delta\sigma_{hoop}$ are the stress increments of the shell in the longitudinal and circumferential direction respectively.

Based on equilibrium, Eq. (II - 27) is used to determine the incremental confining pressure corresponding to the incremental hoop tensile stress in the shell :

$$\Delta\sigma_2' = \frac{\Delta\sigma_{hoop}\, t}{R} \qquad (V-3)$$

The iteration process continues until the incremental hoop stress $\Delta\sigma'_2$ is equal to the assumed $\Delta\sigma_2$.

In every load step, the total longitudinal stress in the FRP shell can be determined as follows :

$$\sigma_{long}^{N} = \sigma_{long}^{N-1} + \Delta\sigma_{long} \qquad (V-4)$$

The total load on the specimen can be determined as the sum of the load carried by the concrete and the load carried by the shell, as follows :

$$P^{N} = A_{FRP}.\sigma_{long}^{N} + A_c.\sigma_1^{N} \qquad (V-5)$$

where A_c and A_{FRP} are the cross-sectional area of the concrete and the FRP respectively. Since the FRP shell is in a biaxial state of stresses, the Tsai-Wu criterion, Eq. (III – 3), is used to determine the failure of the FRP shell.

5.3 Composite Sections with a Void

In this section the proposed model is modified to predict the behaviour of sections with an inner void, as illustrated in Fig. (V – 2 b).

The presence of an inner void complicates the model since the state of stresses in a plane perpendicular to the axis is no longer uniform. This can be easily understood by considering the distribution of the radial stress, σ_2, which is equal to the confining pressure induced by the shell at the outer surface, but must be zero at the inner free surface.

The following section discusses the state of stresses in a confined cylinder with a void, using the thick-walled cylinder model. The principal state of stresses is then translated into an octahedral state of stresses.

5.3.1 Thick-Walled Cylinders under Internal/External Pressure

The theory of a thin-walled cylinder assumes that the hoop stress is constant through the thickness of the wall and the radial stress is negligible. For thick-walled cylinders, this assumption is not valid.

Fig. (V - 3) shows the cross-section of a thick-walled cylinder subjected to internal and external pressures p_i and p_o. The internal and external radii are denoted by R_i and R_o. Equilibrium of forces of an isolated element from the cylinder is shown in Fig. (V - 4).

The radial and circumferential stress components σ_2 and σ_3 are in equilibrium with the applied pressures p_i and p_o.

It should be noted that both the stress and strain components, as well as the displacements are independent of θ.

5.3.1.1 Radial and circumferential stresses

Consider the equilibrium of forces acting on the differential element in Fig. (V - 4). Equilibrium in the circumferential direction is satisfied. Equilibrium of forces in the radial direction can be expressed as follows :

$$\frac{d}{dr}(r\sigma_2)d\theta\, dr - \sigma_3 d\theta\, dr = 0 \qquad (V-6)$$

or :

$$\frac{d\sigma_2}{dr} + \frac{\sigma_2 - \sigma_3}{r} = 0 \qquad (V-7)$$

Eq. (V - 7) contains two unknown stresses σ_2 and σ_3. Therefore, these stress components cannot be determined from equilibrium considerations only. Equilibrium equation (V - 7) must be augmented with the constitutive relations of the cylinder material and with the strain-displacement relations to ensure geometrically compatible displacements.

The stress-strain relations can be written as follows :

$$\sigma_2 = \frac{E}{1-\nu^2}(\varepsilon_2 + \nu\varepsilon_3)$$

$$\sigma_3 = \frac{E}{1-\nu^2}(\varepsilon_3 + \nu\varepsilon_2) \qquad (V-8)$$

The required strain-displacement relations are obtained from the basic definitions of ε_2 and ε_3. If $u(r)$ is the radial displacement of an arbitrary point in the cylinder, the following equation can be written :

$$\varepsilon_2(r) = \lim_{\Delta r \to 0} \frac{\Delta u}{\Delta r} = \frac{du}{dr} \qquad (V-9)$$

while for the circumferential strain the following equation applies :

$$\varepsilon_3(r) = \frac{2\pi(r+u) - 2\pi r}{2\pi r} = \frac{u(r)}{r} \qquad (V-10)$$

Thus :

$$\varepsilon_2 = \frac{du}{dr} \qquad (V-11)$$

$$\varepsilon_3 = \frac{u}{r}$$

The strain-displacement relations (V - 11) together with the equilibrium equation (V - 7) and the stress-strain relations (V – 8) can be combined into a single differential equation for the radial displacement $u(r)$. Having determined $u(r)$, the strains ε_2 and ε_3 can be determined using Eq. (V - 11) and consequently the stresses σ_2 and σ_3 can be determined using Eq. (V - 8).

Substituting Eqs. (V - 11) into Eqs. (V - 8) yields the following equation :

$$\sigma_2 = \frac{E}{1-\nu^2}\left(\frac{du}{dr} + \nu\frac{u}{r}\right)$$

$$\sigma_3 = \frac{E}{1-\nu^2}\left(\frac{u}{r} + \nu\frac{du}{dr}\right) \qquad (V-12)$$

Eqs. (V - 12) and (V - 7) are combined to obtain the equilibrium equation in terms of the displacement $u(r)$ as follows :

$$\frac{d^2u}{dr^2} + \frac{1}{r}\frac{du}{dr} - \frac{u}{r^2} = 0 \qquad (V-13)$$

The general solution of this ordinary second-order differential equation is as follows :

$$u(r) = C_1 r + \frac{C_2}{r} \qquad (V-14)$$

where C_1 and C_2 are constants of integration to be determined from the boundary conditions. Substituting Eq. (V - 14) into Eqs. (V - 8) leads to :

$$\sigma_2 = \frac{E}{1-\nu^2}\left[(1+\nu)C_1 - \frac{(1-\nu)C_2}{r^2}\right]$$

$$\sigma_3 = \frac{E}{1-\nu^2}\left[(1+\nu)C_1 + \frac{(1-\nu)C_2}{r^2}\right] \qquad (V-15)$$

At the internal and external surfaces the boundary conditions must be satisfied :

$$\sigma_2(R_i) = p_i \qquad (V-16)$$

$$\sigma_2(R_o) = p_o$$

which eventually results in the following equations for the constants of integration :

$$C_1 = \frac{(1-\nu)}{E}\frac{\left(p_o R_o^2 - p_i R_i^2\right)}{\left(R_o^2 - R_i^2\right)} \qquad (V-17)$$

$$C_2 = \frac{(1+\nu)}{E}\frac{(p_o - p_i)R_o^2 R_i^2}{\left(R_o^2 - R_i^2\right)}$$

Consequently, using (Eq. V - 14), the following equation is obtained :

$$u(r) = \frac{(1-\nu)}{E}\frac{r}{\left(R_o^2 - R_i^2\right)}\left[\left(p_o R_o^2 - p_i R_i^2\right) + \frac{1+\nu}{1-\nu}(p_o - p_i)\frac{R_o R_i^2}{r^2}\right] \qquad (V-18)$$

The state of stresses is determined using (Eq. V- 8) as follows :

$$\begin{Bmatrix}\sigma_2\\ \sigma_3\end{Bmatrix} = \frac{\left(p_o R_o^2 - p_i R_i^2\right) \pm (p_i - p_o)\frac{R_o^2 R_i^2}{r^2}}{\left(R_o^2 - R_i^2\right)} \qquad (V-19)$$

5.3.1.2 External pressure only

In case $p_i = 0$, we obtain the following formulas :

$$u(r) = \frac{(1-\nu)}{E}\frac{p_o R_o^2}{\left(R_o^2 - R_i^2\right)}r\left[1 + \frac{1+\nu}{1-\nu}\left(\frac{R_i}{r}\right)^2\right] \qquad (V-20)$$

$$\begin{Bmatrix}\sigma_3\\ \sigma_2\end{Bmatrix} = \frac{p_o R_o^2}{\left(R_o^2 - R_i^2\right)}\left\{1 \pm \left(\frac{R_i}{r}\right)^2\right\} \qquad (V-21)$$

The maximum circumferential stress occurs at $r = R_i$, and the maximum radial stress occurs at $r = R_o$:

$$(\sigma_2)_{\max} = \frac{2p_o R_o^2}{R_o^2 - R_i^2} \qquad (\sigma_3)_{\max} = p_o \tag{V - 22}$$

5.3.2 Octahedral Stress State

For a cylinder with an inner void, confined by an outer shell and with an inner free surface, Eqs. (V – 21) and (V – 22) are applicable.

Now consider a hollow core column with an outside radius R_o and an inside radius R_i, subjected to a combination of an axial loading stress σ_1 and a outer lateral pressure p_o. In this case σ_2 and σ_3 ca be determined by Eq. (V - 21).

The octahedral hydrostatic stress at any point in the cylinder can be calculated as follows:

$$\begin{aligned} \sigma_o &= \frac{1}{3}(\sigma_1 + \sigma_2 + \sigma_3) \\ &= \frac{1}{3}\left(\sigma_1 + 2\frac{p_o R_o^2}{(R_o^2 - R_i^2)}\right) \end{aligned} \tag{V - 23}$$

σ_o is independent of r and θ and thus constant within the cylinder. Although σ_2 and σ_3 vary with r, their sum is constant. In this way the confining pressure is still uniform in octahedral terms.

The octahedral deviatoric stress at any point is given by the following equation :

$$\tau_o = \frac{1}{3}\sqrt{(\sigma_1-\sigma_2)^2+(\sigma_1-\sigma_3)^2+(\sigma_2-\sigma_3)^2}$$
$$= \frac{\sqrt{2}}{3}\sqrt{\left(\sigma_1 - p_o\frac{R_o^2}{\left(R_o^2-R_i^2\right)}\right)^2 + 3p_o\frac{R_o^2}{\left(R_o^2-R_i^2\right)}\frac{R_i^2}{r^2}} \qquad (V-24)$$

τ_o depends on r but the dependence is minor. In our examples τ_o will never vary more than 4% over the cross-section. Therefore, considering the column to be in a uniform octahedral stress state is quite acceptable.

5.3.3 Proposed Methodology

Since $\Delta\sigma_2$ is no longer constant over the cross-section, an incremental confining pressure Δp_o will be assumed to initiate the iteration process, instead of assuming $\Delta\sigma_2$. The following procedure is proposed :

1. Using the assumed Δp_o, determine the octahedral stress increments $\Delta\sigma_o$ and $\Delta\tau_o$ using Eq. (V - 23) and (V - 24), where r is set equal to R_o.
2. Determine $\Delta\sigma_2$ and $\Delta\sigma_3$ for $r = R_o$ using Eq. (V – 21)
3. Determine the octahedral strains using Eqs. (III – 16) and (III – 17).
4. Using Eqs. (III – 22) and (III – 23), determine $\Delta\varepsilon_2$ and $\Delta\varepsilon_3$ for $r = R_o$.
5. Use Eq. (V – 2) to determine $\Delta\sigma_{hoop}$.

6. $\Delta\sigma_{hoop}$ relates to a confining pressure $\Delta p'_o$ as follows:

$$\Delta p'_o = \frac{\Delta\sigma_{hoop}\, t}{R_o} \qquad (V-25)$$

The iteration process continues until $\Delta p'_o$, obtained from Eq. (V – 25), equals the assumed Δp_o. The material properties K and G for the next step can then be calculated and a new load step $\Delta\sigma_1$ is applied. The flow of the calculations is illustrated in Fig. (V – 5).

5.4 Sandwich Section

This section deals with the double shell configuration, illustrated in Fig. (V - 2 c).

At a certain stage of axial loading the encased concrete will experience an outer pressure from the outer shell as well as an inner pressure from the inner shell. Consequently, Eqs (V – 18) and (V – 19) will be used to determine the stress state.

5.4.1 Proposed Methodology

Fig. (V - 6) gives a schematic overview of the proposed methodology. The method starts by assuming an increment for both the outer and the inner pressures Δp_o and Δp_i. Through Eq. (V - 19) the incremental state of stresses in the cylinder is completely known and can be translated into an octahedral state of stresses using Eqs. (III - 12) and (III - 13). The octahedral hydrostatic stress σ_o is constant over the concrete section. The

analysis indicates that the variation of the shear stress τ_o between inner and outer surface is very small and the octahedral state of stresses can be considered uniform over the section.

Using the material properties K and G from the previous load step the octahedral strain increments $\Delta\varepsilon_o$ and $\Delta\gamma_o$ can then be calculated.

Consequently, the strain increments $\Delta\varepsilon_2$ and $\Delta\varepsilon_3$ at both the inner and outer surface of the concrete can be determined, using Eqs. (III - 22) and (III - 23) for $r = R_i$ and $r = R_o$.

Using Eq. (V – 2), the hoop stress increments in both inner and outer shell can be determined. The corresponding increments in confining pressures $\Delta p_o'$ and $\Delta p_i'$ can be calculated using the following equations :

$$\Delta p_o' = \frac{\Delta\sigma_{hoop,outer}\, t_{outer}}{R_o} \qquad (V-26)$$

$$\Delta p_i' = \frac{\Delta\sigma_{hoop,inner}\, t_{inner}}{R_i} \qquad (V-27)$$

Where t_{inner} and t_{outer} are the thickness of the inner and the outer shell respectively.

The iterations continue until the values of $\Delta p_o'$ and $\Delta p_i'$ equal the assumed values of Δp_o and Δp_i.

The increment in load carried by the composite section is given by the following equation:

$$\Delta P = \Delta\sigma_1 . A_c + \Delta\sigma_{long,inner} . 2\pi R_i t_{inner} + \Delta\sigma_{long,outer} . 2\pi R_o t_{outer} \qquad (V-28)$$

5.5 Verification of the Proposed Model

The proposed model is verified using the results of an experimental program carried out at the University of Manitoba (Amir Fam, 1999).

The experimental program includes a total of nine hybrid FRP-concrete cylindrical column stubs of different configurations and diameters. The following three configurations were considered :

C1 : (Fig V - 2a) The FRP tube is solidly filled with concrete.

C2 : (Fig V – 2b) The column consists of an outer FRP tube partly filled with concrete but with an inner centered void, which is practically realized by inserting a cardboard tube before casting.

C3 : (Fig V - 2c) The configuration consists of an outer FRP shell and a concentric inner FRP shell with the space in between filled with concrete.

Table (V - 1) shows an overview of the geometric properties of the different test specimens. These sections were built using three different sizes of FRP tubes : a 3.5" tube, a 6.625" tube and a 8.625" tube. These are outside diameters. The material properties of the different tubes will be discussed in the next section.

Also the effect of the bond at the FRP-concrete interface was studied. For the specimens marked as 'normal bond' no specific measures were taken to enhance the bond between

the tube and the concrete. For the specimens marked 'enhanced bond' the interface was prepared with a sand-epoxy mix.

All specimens were tested under compression till failure occurred in a stroke-controlled 5000 kN capacity MTS machine. In all cases, both the concrete core and the FRP shell were loaded simultaneously.

5.6 FRP Material Properties

Three different products were purchased from Lancaster Composite, these being filament wound FRP tubes with (outside) diameters of 3.5 inches, 6.625 inches and 8.625 inches. The following information was provided by the manufacturer :

- The fiber type is E-glass. The matrix material is MTHPA (Anhydride) cured bis-phenol-A epoxy.

- The layer sequence and the angles and thickness of the different layers are shown in Table (V – 2) :

- The fiber weight fraction is 68 %. By using the ratio of the densities, the fiber weight fraction can be converted to a fiber volume fraction, which is found to be 50.7 %.

$$\frac{\rho_{fiber}}{\rho_{matrix}} = 2.067$$

where ρ_{fiber} and ρ_{matrix} are the densities of the fibers and the matrix respectively.

• The filament winding process used to make the tubes is a continuous process yielding a cylindrical shape. The 8.625" tube also has an intermediate wall of sand to give it extra circumferential stiffness for external loads encountered when the pipe is buried. The sand thickness (0.035") does not contribute to the tensile strength of the pipe but does add to the moment of inertia calculation when considering ring stiffness.

• The pipes were designed with a nominal 2:1 strength ratio with twice as much reinforcement in the circumferential direction as in the longitudinal direction.

• The mechanical properties of the pipe, as tested by the manufacturer, are listed in Table (V – 3).

5.6.1 Material Testing

5.6.1.1 Circumferential Properties

The circumferential modulus and strength of the FRP material are the governing parameters in the confinement effect and are therefore the most important properties of the FRP. Consequently, a specially designed test setup was used to determine the modulus and strength in the hoop direction.

Four test specimens were prepared each consisting of a ring of about 4 cm wide that was sliced out of the tube. Two samples M1 and M2 were taken out of the 6.625" tube, two samples M3 and M4 were taken from the 8.625" tube.

Fig. (V - 7) illustrates the test setup. A steel disk that fits the inside diameter of the FRP ring was split into two halves. Those two stiff halves were pulled away from each other over hinges and the hoop strains in the FRP were measured at the gap.

Since the circumferential fibers include a small angle with the circumference due to the winding process, the rings were cut at a reasonable width to include a maximum amount of continuous fibers.

The material testing was performed on a 60 kips machine.

All specimens were instrumented with a strain gauge on the left side and another strain gauge on the right side, both measuring the strain in the circumferential direction. Specimen M2 also had a strain gauge on the left side measuring the strain in the tube's axial direction to determine the minor Poisson's ratio ν_f'. The instrumentation of specimen M2 is shown in Fig. (V - 8).

The strains were read out using a multi-channel strain indicator box.

Hinges allowed the specimen to line up with the direction of the tensile force. Nevertheless, the forces P_1 and P_2 in the left and right cross-section respectively are not exactly the same. However, considering Fig. (V - 9), the following equation can be written :

$$P_1 + P_2 = P \qquad (V-29)$$

and :

$$\frac{P_1}{A_1} = E_{hoop}\varepsilon_1 \qquad \frac{P_2}{A_2} = E_{hoop}\varepsilon_2 \tag{V-30}$$

where A_1 and A_2 are the left and right cross-sectional areas respectively.

Combination of Eqs. (V - 29) and (V - 30) results in the following equation :

$$(A_1\varepsilon_1 + A_2\varepsilon_2)E_{hoop} = P \tag{V-31}$$

Since the FRP material is linear up to failure, its elastic modulus E_{hoop} is a constant and Eq. (V - 31) represents a linear relationship between the tensile force P of the machine and the variable :

$$\Lambda = A_1\varepsilon_1 + A_2\varepsilon_2$$

The experimental $\Lambda - P$ relation for specimen M1 is shown in Fig. (V - 10). Some of the initial deformations of the setup will be taken up by the rubber fillings and due to the many hinges the system will need some initial self-adjustment, but the end portion of the diagram is fairly linear and a reliable modulus value can be derived from this part.

It should be noted that the initial strain readings from the strain indicator were not zero. However this does not affect the value of E_{hoop}.

5.6.1.2 Test Results

Table (V - 4) shows the measured values of the circumferential elastic modulus E_{hoop} and the circumferential strength f_{hoop} for the different specimens.

The measured values are slightly lower but fairly close to those provided by the manufacturer.

The Poisson's ratio v_f' determined from specimen M2 is 0.111.

5.6.2 Laminate Theory

Table (V – 2) shows the layer configuration of the FRP tubes. Knowing the different winding angles and thicknesses of the individual layers, the classical laminate theory can be used to compute the mechanical properties of the tube.

Software has been developed by J.J. Kibler (Materials Sciences Corporation) to address this type of problems. Using the layer information provided by manufacturer, the program gives the following results :

1. for the 6.625" diameter tube :

E_{hoop} = 27,710 MPa

E_{long} = 17,434 MPa

G = 3,662 MPa

v_f = 0.098

v_f' = 0.155

f_{hoop} = 442 MPa

f_{long} = 281 MPa

2. for the 8.625" diameter tube :

E_{hoop} = 27,770 MPa

E_{long} = 17,855 MPa

G = 3,600 MPa

v_f = 0.0836

v_f' = 0.130

f_{hoop} = 430 MPa

f_{long} = 260 MPa

These values for the moduli and material strengths seem to coincide fairly well with those indicated by the manufacturer.

5.7 Concrete Material Properties

Using standard concrete cylinder compression tests the compressive strength was determined and found to have an average value of 58.3 MPa. As well, testing was performed to establish the complete uniaxial stress-strain curve. This curve was found to coincide almost perfectly with Hognestad's (1951) parabolic expression for a peak strain ε_p of 0.002 and a peak strength f'_c of 58.3 MPa. Therefore, the initial modulus can be calculated as follows :

$$E_o = \frac{2f'_c}{\varepsilon_p} \qquad (V-32)$$

5.8 Test S1

In this section, specimen S1, listed in Table (V – 1), is used to verify the proposed model. The specimen consists of a large diameter FRP tube (8.625") solidly filled with concrete. Both the concrete core and the FRP shell are loaded simultaneously in the axial direction.

The behaviour was predicted using the proposed model, according to the methodology explained in Fig. (V – 1). Since the FRP shell is subjected to a biaxial stress state, the biaxial strength criterion of Tsai-Wu is used to determine failure.

Properties of specimen S1 are listed in Table (V – 5) and Table (V – 6). Tsai-Wu's failure criterion is used in the form of Eq. (III - 6) and (III - 7). The assumption that $f_{long,t} = f_{long,c}$ (equal strength in tension and compression in the longitudinal direction) is justified by the manufacturer's test data. A test on the FRP material to determine the circumferential compressive strength $f_{hoop,c}$ would be a technical challenge and therefore $f_{hoop,c}$ was assumed to equal the tensile strength $f_{hoop,t}$. This can be justified by the presence of the concrete core, which prevents the shell from local buckling.

The step-wise calculations are presented in table form in the appendix (A – 29).

The results of the calculations are presented in Fig (V - 11). Excellent agreement with the experimental results is obtained for the axial load-strain curve. The Tsai-Wu criterion predicts failure for an axial load of 2795 kN and an axial strain of 11 millistrain, in comparison to measured values of 2636 kN and 10.52 millistrain

respectively. These values translate into an error of 6 percent on the predicted ultimate load and an error of 4.6 percent on the ultimate axial strain.

The lateral strains however are somewhat underestimated at load levels close to failure.

5.9 Tests S2 and S3

The two similar specimens S2 and S3 are used also to verify the model proposed in 5.2. Both specimens are constructed from smaller diameter GFRP tubes (6.625") and solidly filled with concrete.

Specimen S2 underwent a treatment to enhance the bond in the interface and demonstrates a slightly higher strength than specimen S3 although the load-strain curves for both specimens were very similar.

The geometric and material properties are listed in Table (V – 7) and (V – 8).

The predictions are presented in Fig. (V – 12). The measured failure load is 2154 kN for specimen S2 and 2089 kN for specimen S3, with an average of 2121 kN. The ultimate axial strain is 13 ms, the ultimate lateral strain is −12 ms.

Using the Tsai-Wu criterion, the predicted failure load is 1727 kN. The error is 18.6 percent. The predicted ultimate axial strain is 10.5 ms, which represents an error of 19.2 percent.

In this case, the model somewhat underestimates the effect of the confinement, although the slope of the curve was well predicted.

5.10 Tests S4 and S5

Specimens S4 and S5 were also used to verify the proposed model. The two specimens were constructed with an outer GFRP shell of 6.625 inches diameter and have an inner void of 3.5 inches diameter and no inner shell.

The material properties of the concrete and the FRP shell are listed in Table (V – 7). The inside radius R_i was measured to be 46 mm, for an outside radius R_o of 82 mm.

The analytical predictions, according to the model proposed in section 5.3, are shown in Fig. (V – 13). It can be seen, experimentally as well as theoretically, that the confinement effect in the concrete is fairly small. However the predicted curve for the total load rises well beyond the experimentally measured values.

This can be explained by the fact that Gerstle's triaxial model assumes totally ductile failure resulting in a never descending stress-strain curve of the concrete. In reality the curve indicating the contribution of the concrete will have a descending branch, because of the minor effect of confinement.

5.11 Test S6

Specimen S6 has a large diameter FRP shell (8.625") with an inner void of 3.5" and no inner shell. R_o and R_i were measured and found to be 106 mm and 47 mm respectively. The properties of the concrete and the FRP shell are listed in Table (V – 5).

The analytical predictions are shown in Fig. (V - 14). Again the ductility of the concrete is overestimated in a way that the predicted concrete curve has no descending branch but remains horizontal after reaching its maximum strength.

5.12 Test S7

Specimen S7 has an outer FRP shell of 8.625" diameter and a large inner void of 5" diameter and no inner shell. R_o and R_i were measured and found to be 106 mm and 66 mm respectively.

The predicted behaviour is presented in Fig. (V - 15). It confirms the conclusions drawn from sections 5.10 and 5.11 are confirmed.

5.13 Effect of an inner void

Fig. (V - 16) shows the predicted axial stress-strain curve of the concrete for specimen S7, compared to the predicted axial stress-strain curve for the equivalent solid section S1.

Fig. (V - 17) compares the predicted axial stress-strain curves of the concrete for specimens S4 and S2.

The behaviour indicates obvious reduction of the confinement. Based on the model, this can be explained by the two following reasons :

1. The radial stiffness of a cylinder with an inner void is lower than the radial stiffness of its solid equivalent. Therefore, a lower equilibrium pressure in the interface is needed to establish strain compatibility between the shell and the concrete core. A hollow cylinder subjected to a lateral pressure p undergoes a radial displacement that is determined by Eq. (V - 20) :

$$u_1(R_o) = \frac{1-\nu}{E} pR_o \frac{R_o^2}{\left(R_o^2 - R_i^2\right)}\left[1 + \frac{1+\nu}{1-\nu}\left(\frac{R_i}{R_o}\right)^2\right] \qquad (V-33)$$

$$\text{with :} \quad \frac{R_o^2}{R_o^2 - R_i^2} > 1 \qquad \text{and} \qquad \frac{1+\nu}{1-\nu}\left(\frac{R_i}{R_o}\right)^2 > 0$$

Whereas the radial displacement of a solid cylinder under a lateral pressure p is given by the following equation :

$$u_2(R_o) = \frac{1-\nu}{E} pR_o \qquad (V-34)$$

2. The cylinder with an inner void is subjected to a non-uniform confinement state with $\sigma_2 \neq \sigma_3$. This will result in higher values for the octahedral deviatoric stress τ_o, which is a function of the differences of the principal stresses :

$$\tau_o = \frac{1}{3}\sqrt{(\sigma_1 - \sigma_2)^2 + (\sigma_1 - \sigma_3)^2 + (\sigma_2 - \sigma_3)^2}$$

The deviatoric stress τ_o is responsible for the distortional strains of the specimen.

Higher values of τ_o will bring the specimen closer to failure and result in a reduced slope of the stress-strain curve (See Eq. III - 26).

5.14 Tests S8 and S9

Specimens S8 and S9 were constructed using a 6.625 inches diameter outer FRP shell and a 3.5 inches diameter inner FRP shell. The space in between is filled with concrete. Specimen S8 has enhanced bond properties.

The model proposed in section 5.4 and illustrated in Fig. (V - 6) is used to predict the behaviour.

The material properties of the concrete and the 6.625" diameter FRP outer tube are listed in Table (V – 5). The outside diameter of the concrete core was measured to be 164 mm and the inside diameter is 88 mm. The specimen height is 341 mm.

The properties of the inner shell were calculated using the classical laminate theory, using the layer properties listed in Table (V – 2) and the following values were obtained:

E_{hoop} = 25,366 MPa

E_{long} = 16,000 MPa

G = 3,945 MPa

v_f = 0.157

v_f' = 0.248

f_{hoop} = 466 MPa

f_{long} = 302 MPa

The inner shell thickness is 2 mm.

Fig. (V - 18) compares the predicted behaviour to the measured behaviour. Good agreement with the experiment was obtained, especially for specimen S8. This is the specimen with the better bond.

The measured failure load of specimen S8 was 1357.4 kN for an axial strain of 11.48 ms and a lateral strain of 7.2 ms. The predicted values are 1410.6 kN, 11.92 ms and 6.92 ms respectively. The errors are 3.9 percent, 3.8 percent and 3.9 percent respectively. The failure load of specimen S9 was 1336.3 kN.

The analysis indicates that initially, all points in the concrete move away from the centerline of the cylinder, causing a negative radial strain. Assuming total bond at the interfaces, this will bring the inner shell in a state of hoop tension, thus introducing negative confining pressures into the concrete at that interface. However, with increasing load levels and increasing dilation of the concrete in the core, the sign of Δp_i will reverse from negative into positive and eventually bring the inner shell in a state of hoop compression, beneficial to the confinement effect.

The Tsai-Wu failure criterion was applied to both shells and eventually detects failure in the outer shell, thus confirming the experimental findings.

5.15 Conclusions

A model is proposed for a totally filled FRP/concrete composite section for the case where the FRP shell contributes directly in carrying the axial load. The model is based on strain compatibility and equilibrium of stresses at the interface. Gerstle's triaxial constitutive relations are used to model the concrete.

The model was modified to account for the presence of an inner void with or without an inner FRP shell.

Verification of the proposed model using experimental data indicates that the model can be recommended to predict the behaviour of solidly filled columns under simultaneous loading of the concrete and the shell. The model also yields good predictions of the behaviour of the double shell configuration. In the case of a column with an inner void and no inner shell, the concrete is subjected to a state of low confinement and the model is likely to overestimate the strength of the section. This is due to the assumption of totally ductile failure of the concrete.

Specimen	Config.	Outside D	Inside D	Interface
S1	C1	8.625"	solid	normal
S2	C1	6.625"	solid	enhanced
S3	C1	6.625"	solid	normal
S4	C2	6.625"	3.5"	enhanced
S5	C2	6.625"	3.5"	normal
S6	C2	8.625"	3.5"	normal
S7	C2	8.625"	5"	normal
S8	C3	6.625"	3.5"	enhanced
S9	C3	6.625"	3.5"	normal

Table V – 1 : Overview Test Program

3.5"			6.625"			8.625"		
#	α	"	#	α	"	#	α	"
1	14.7	.007	1	7.7	.003	1	-87.7	.010
2	-82.5	.013	2	-86.4	.014	2	-87.7	.010
3	-82.5	.010	3	-86.4	.011	3	4.5	.013
4	14.7	.007	4	7.7	.010	4	-87.7	.017
5	-82.5	.010	5	-86.4	.015	5	-87.7	.020
6	14.7	.007	6	7.7	.010	6	4.5	.013
7	-82.5	.010	7	-86.4	.014	7	-87.7	.020
8	14.7	.007	8	7.7	.010	8	4.5	.013
9	-82.5	.010	9	-86.4	.014	9	-87.7	.017

(Note : The liner is not considered in the structural wall of the pipe)

Table V – 2 : Layer Properties

Property	Minimum value	ASTM Method
Tensile Strength Longitudinal Circumferential	 224 MPa 448 MPa	 D2105 D1599
Tensile Modulus Longitudinal Circumferential	 19.3 GPa 27.6 GPa	 D2105 -
Compressive Strength Longitudinal	224 MPa	D695
Compressive Modulus Longitudinal	19.3 GPa	D695

Table V – 3 : Mechanical Properties of the FRP

Specimen	E_{hoop} (MPa)	f_{hoop} (MPa)
M1	26,270	442.8
M2	27,235	436.8
Average	26,753	439.8

Specimen	E_{hoop} (MPa)	f_{hoop} (MPa)
M3	24,781	466.2
M4	28,108	373.3
Average	26,445	419.8

Table V - 4 : Measured material properties

Property	*Value*
Core Diameter D	212 mm
Tube Thickness t	3.5 mm
Specimen Height h	440 mm
Unconfined Concrete Strength f'_c	58.3 MPa
Concrete Initial Elastic Modulus E_o	58.3 GPa
FRP Longitudinal Elastic Modulus E_{long}	19 GPa
FRP Longitudinal Strength f_{long}	220 MPa
FRP Circumferential Elastic Modulus E_{hoop}	27 GPa
FRP Circumferential Strength f_{hoop}	440 MPa

Table V – 5 : Material Properties of specimen S1

$\sigma_{2,max}$ = 15.50 MPa	
k = 2.64	
A = 0.305	B = 0.500
μ_u = 0.371	

Table V – 6 : Calculated Properties of specimen S1

Property	*Value*
Core Diameter D	162 mm
Tube Thickness t	3.2 mm
Specimen Height h	340 mm
Unconfined Concrete Strength f'_c	58.3 MPa
Concrete Initial Elastic Modulus E_o	58.3 GPa
FRP Longitudinal Elastic Modulus E_{long}	19 GPa
FRP Longitudinal Strength f_{long}	220 MPa
FRP Circumferential Elastic Modulus E_{hoop}	27 GPa
FRP Circumferential Strength f_{hoop}	440 MPa

Table V – 7 : Specimen Properties for S2 and S3

$\sigma_{2,max}$ = 17.38 MPa	
k = 2.55	
A = 0.311	B = 0.482
μ_u = 0.333	μ_{max} = 1.077

Table V – 8 : Calculated Properties for S2 and S3

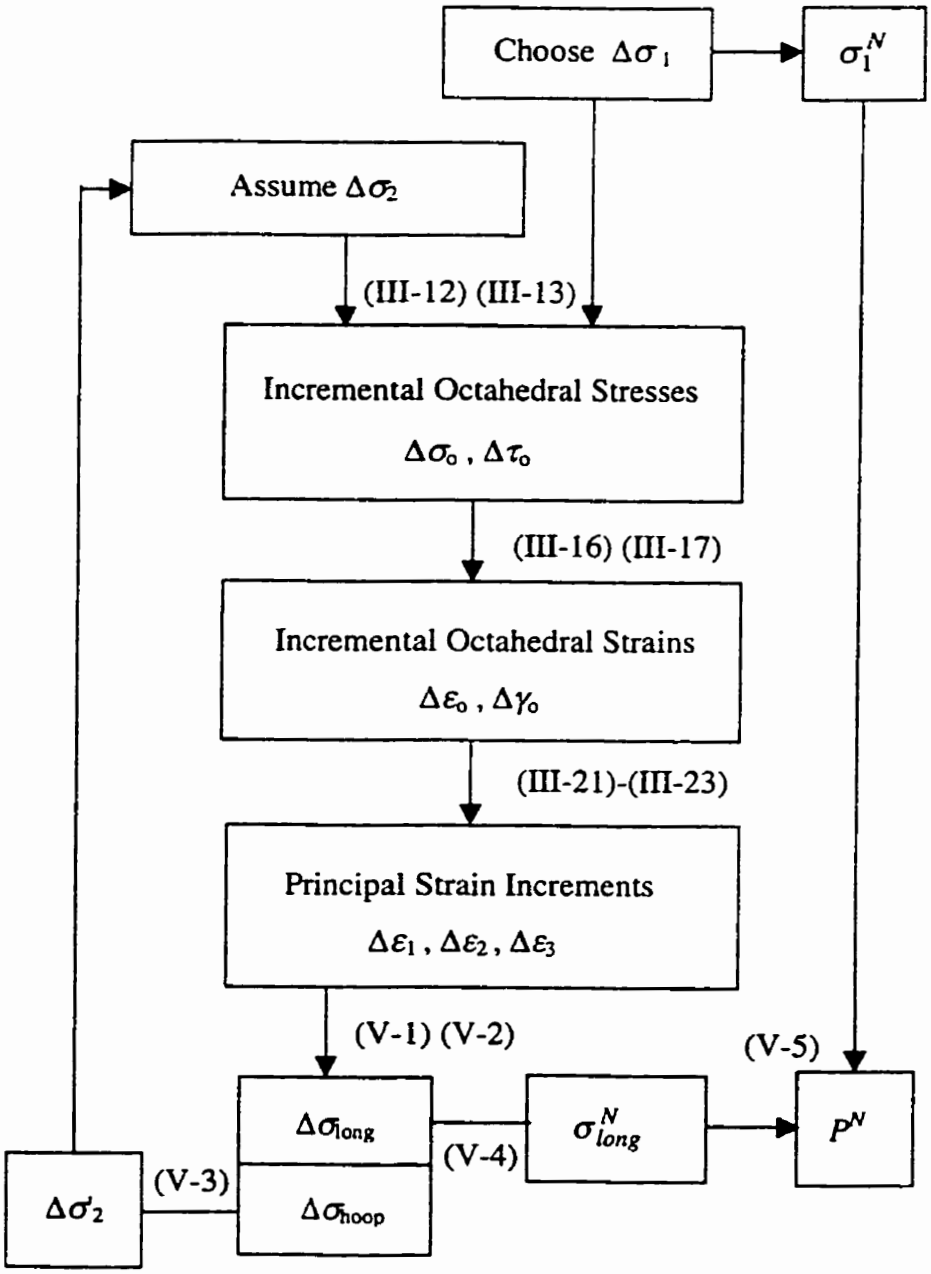

Fig. V - 1 : Flowchart for a totally filled section under combined loading

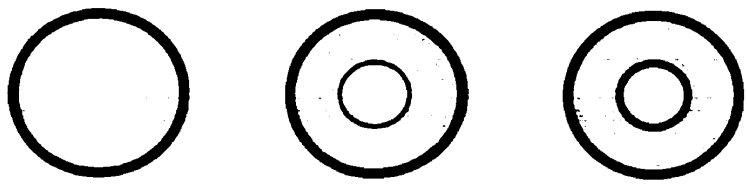

- a - - b - - c -

Fig. V - 2 : Different cross-sectional configurations

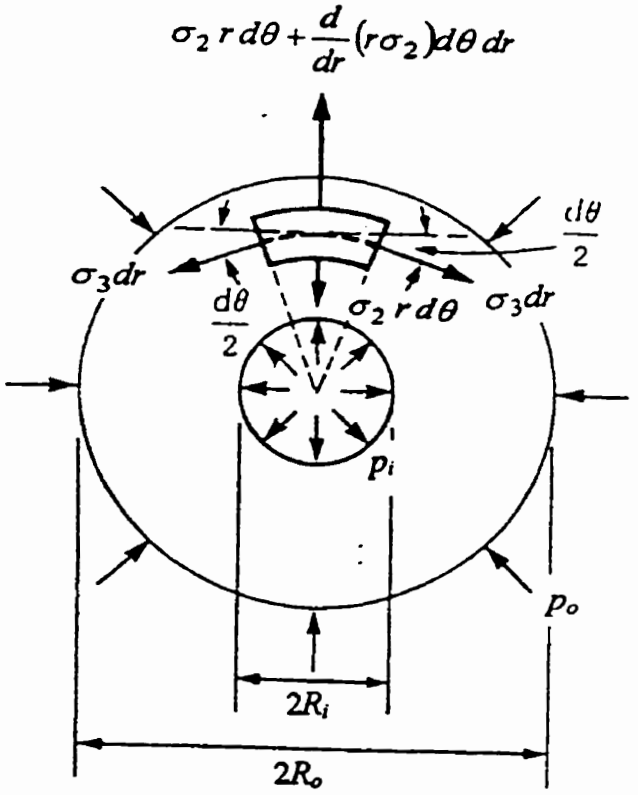

Fig. V – 3 : Thick-walled cylinder under inner and outer pressure

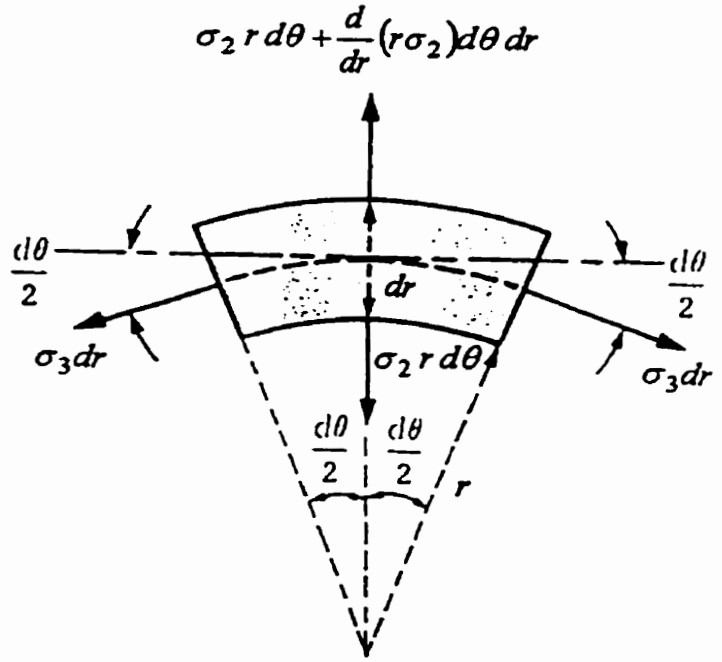

Fig. V – 4 : Equilibrium of an isolated element

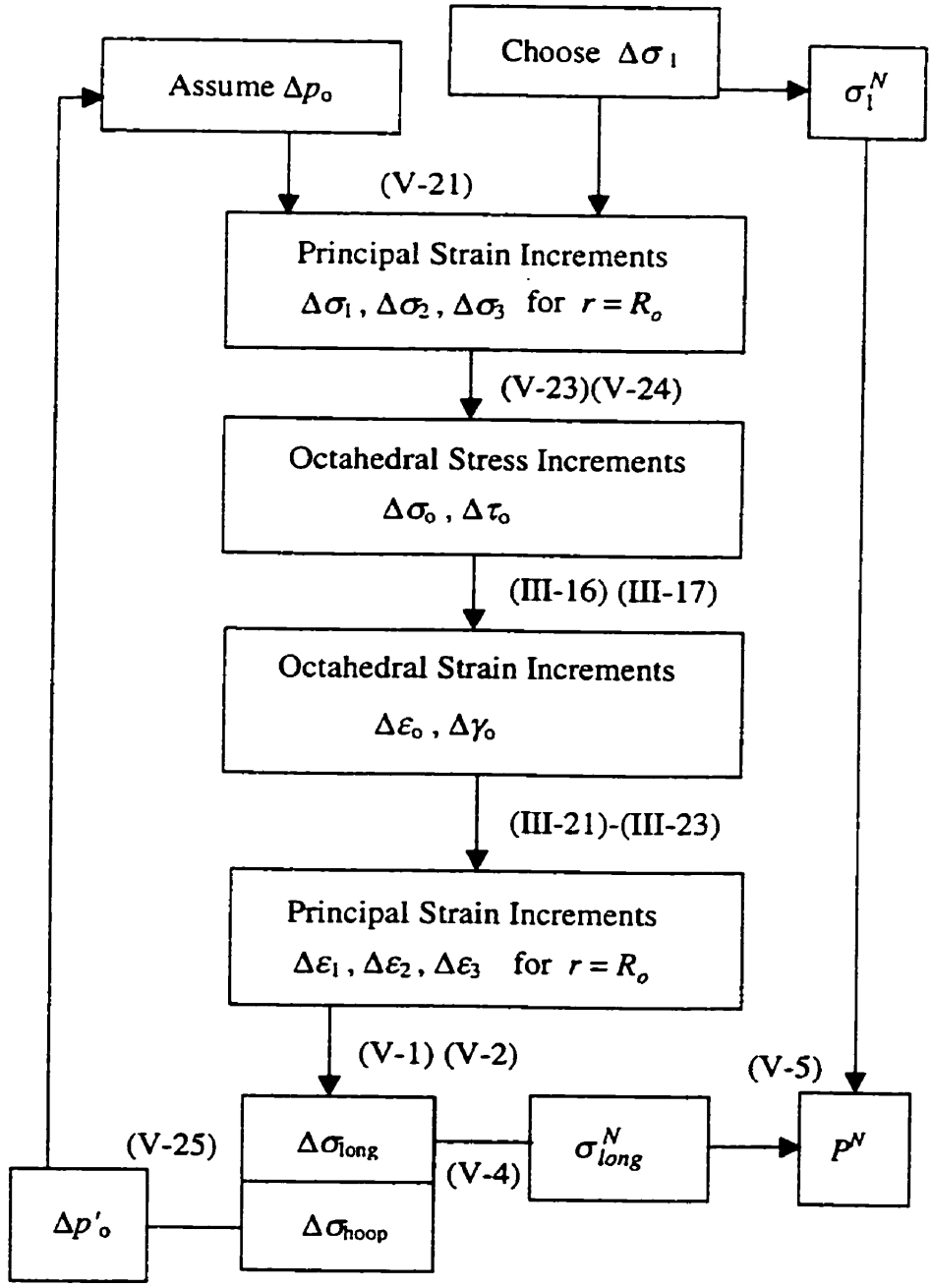

Fig. V - 5 : Flowchart for a section with an inner void under combined loading

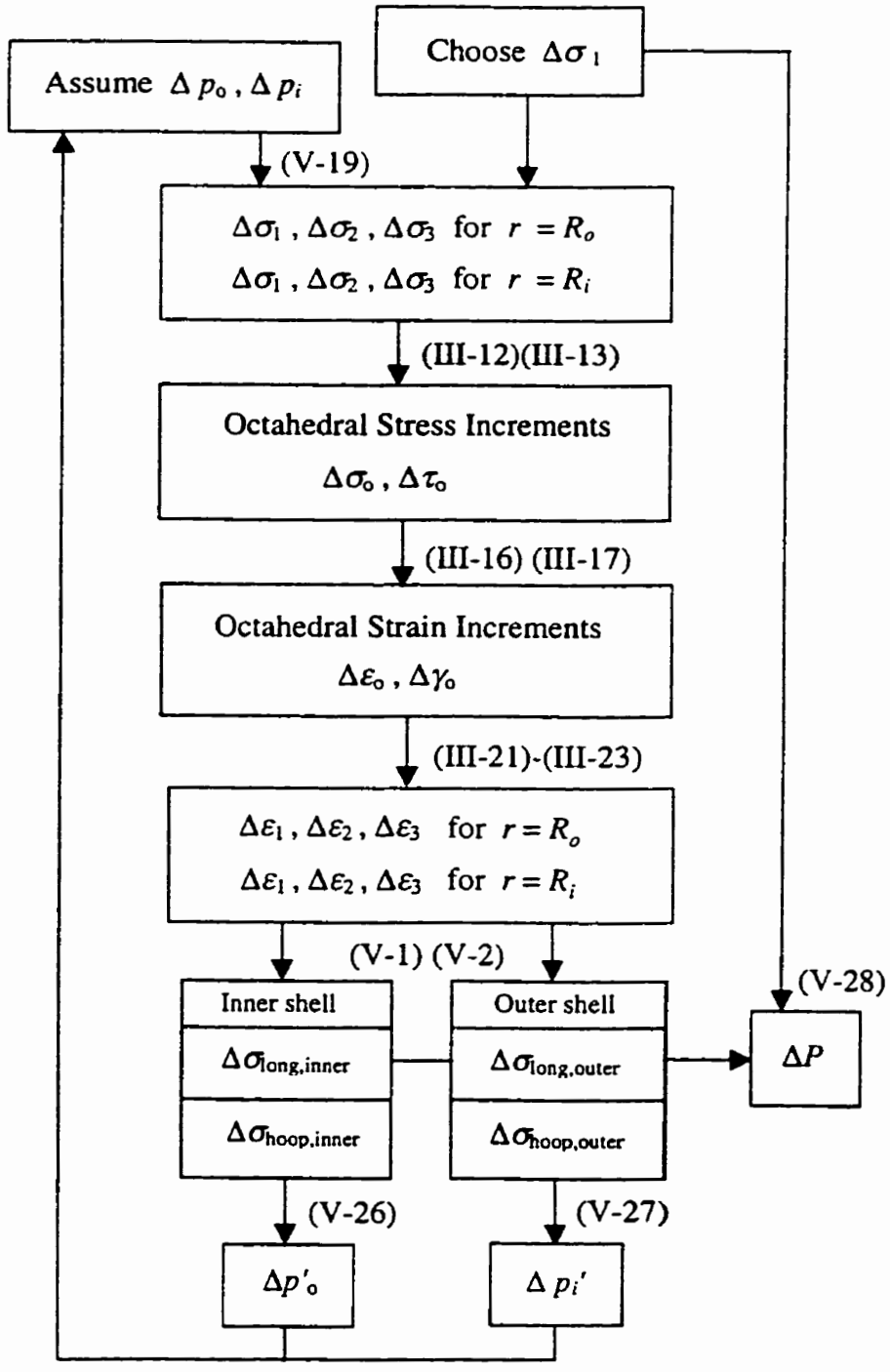

Fig. V - 6 : Flowchart for double shell configuration under combined loading

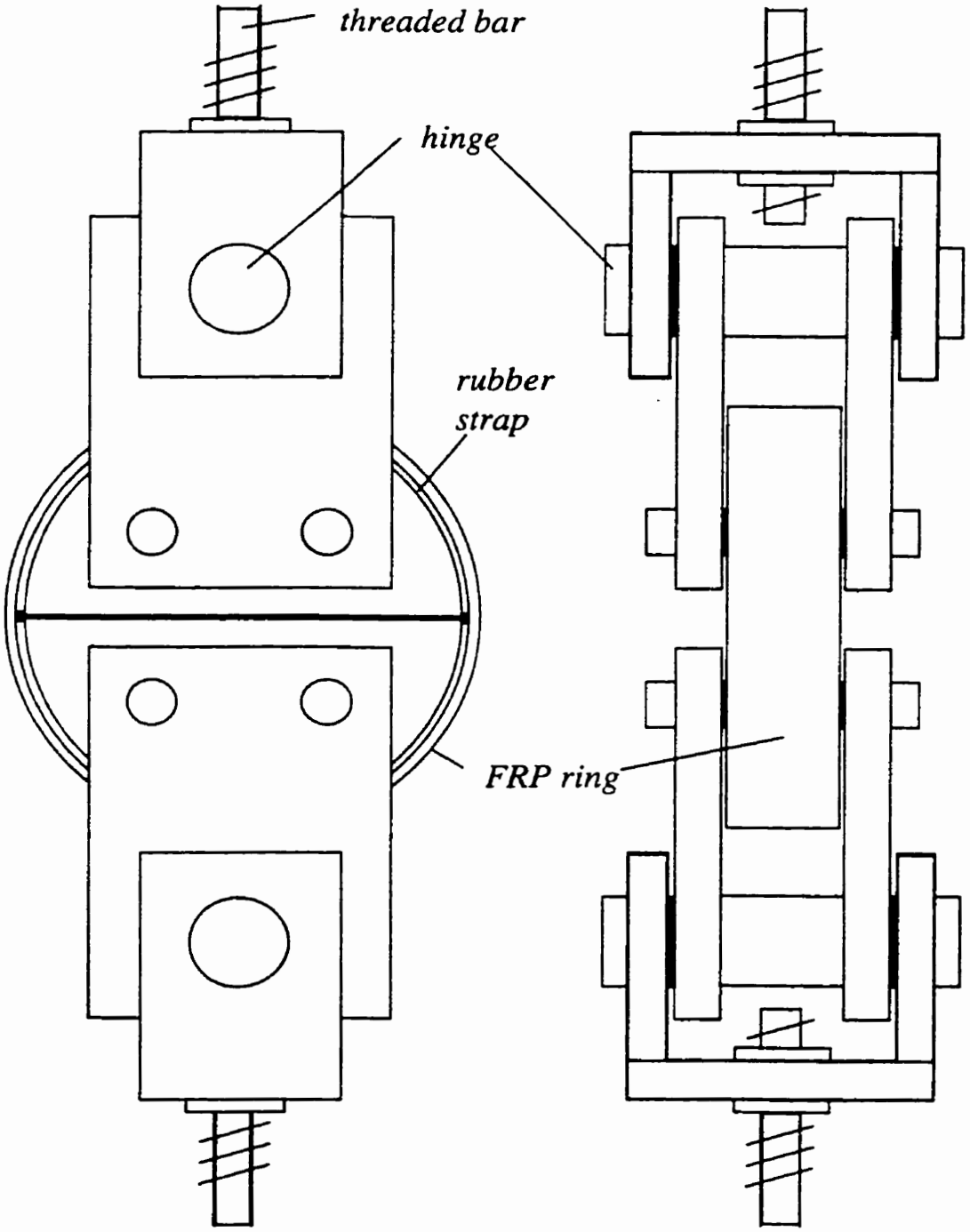

Fig. V - 7 : Tension Test Setup

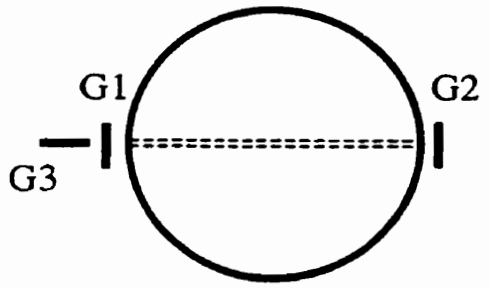

Fig. V - 8 : Instrumentation of M2

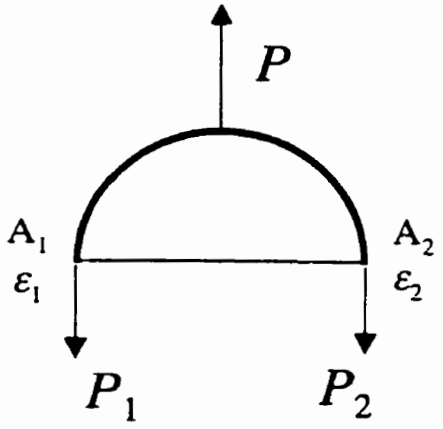

Fig. V - 9 : Equilibrium of forces

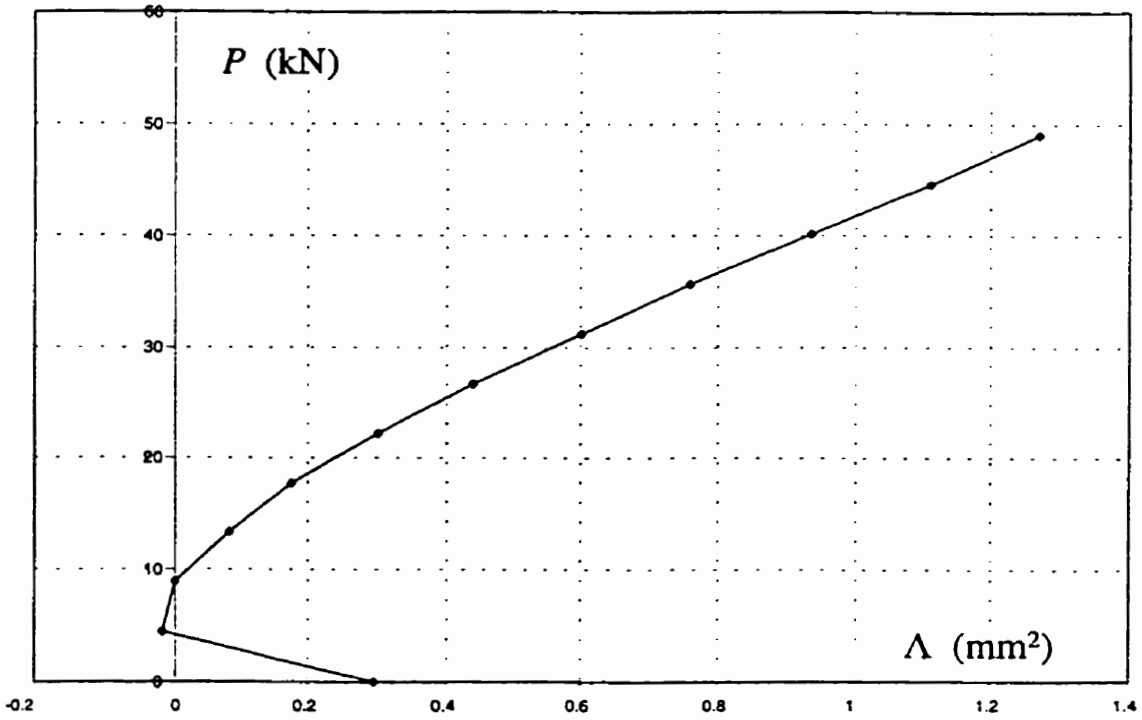

Fig. V - 10 : P - Λ relation for M1

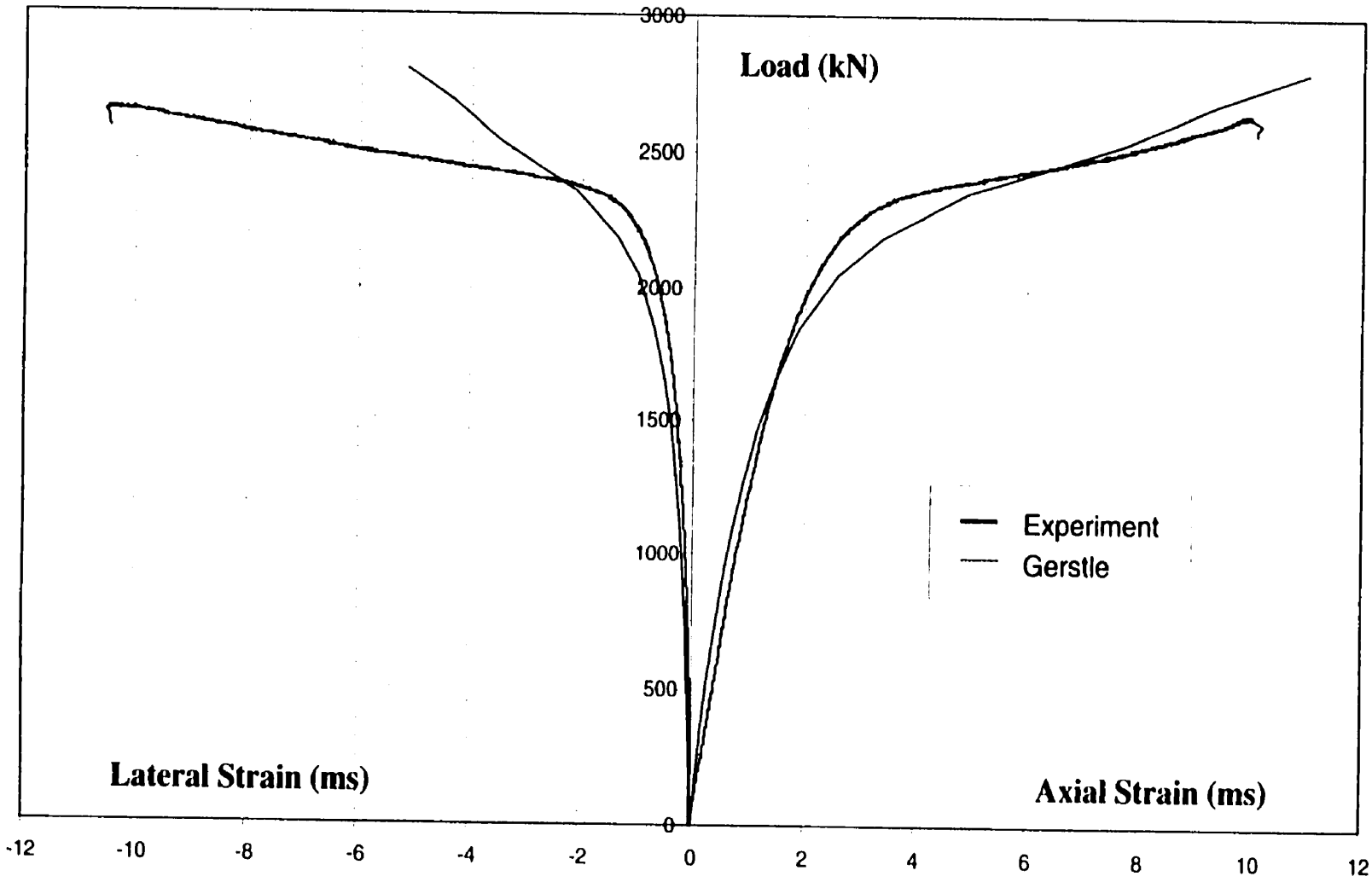

Fig.* V - 11 : *Modeling of Stub Column Test S1

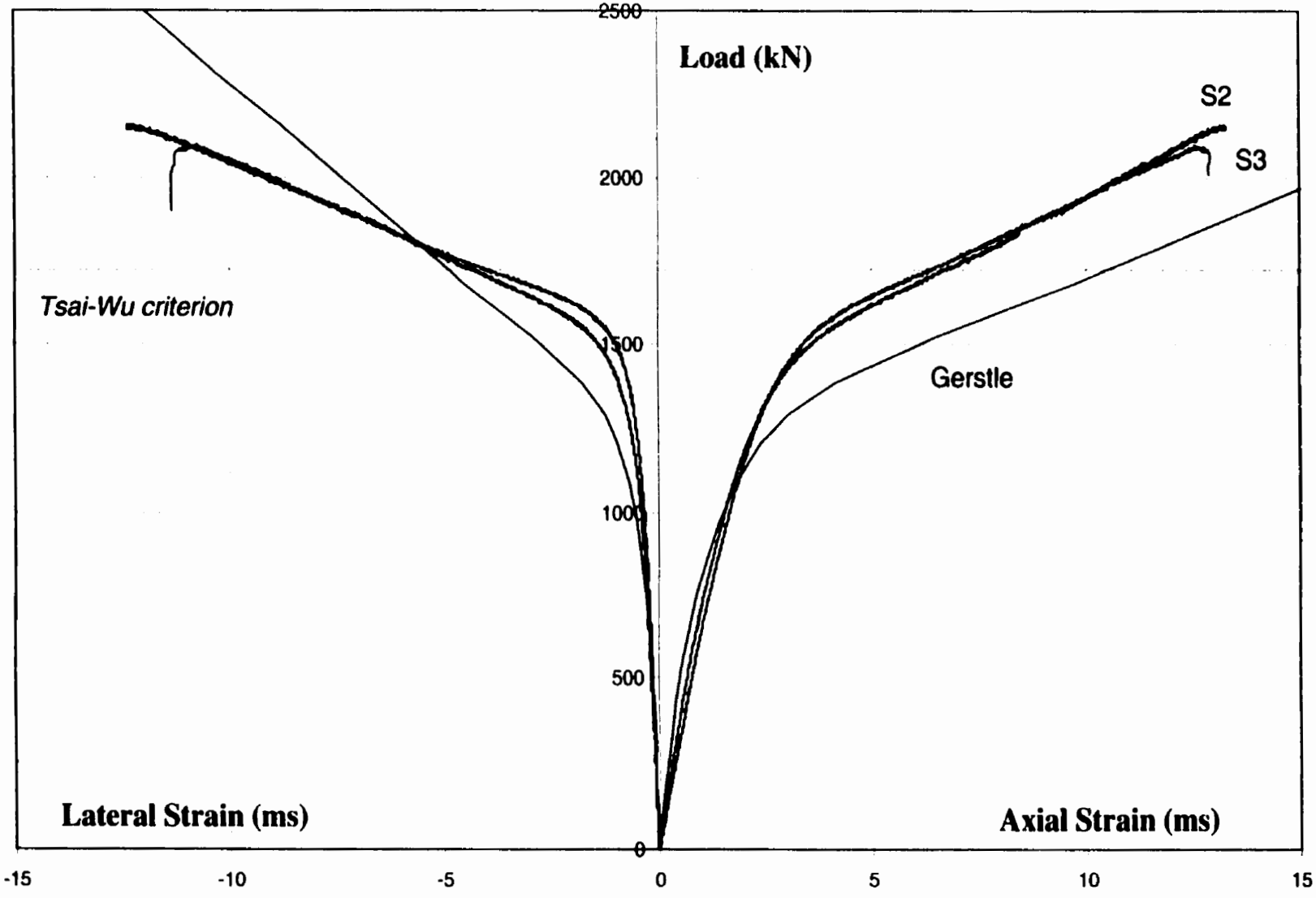

Fig. V - 12 : Modeling of Stub Column Tests S2 and S3

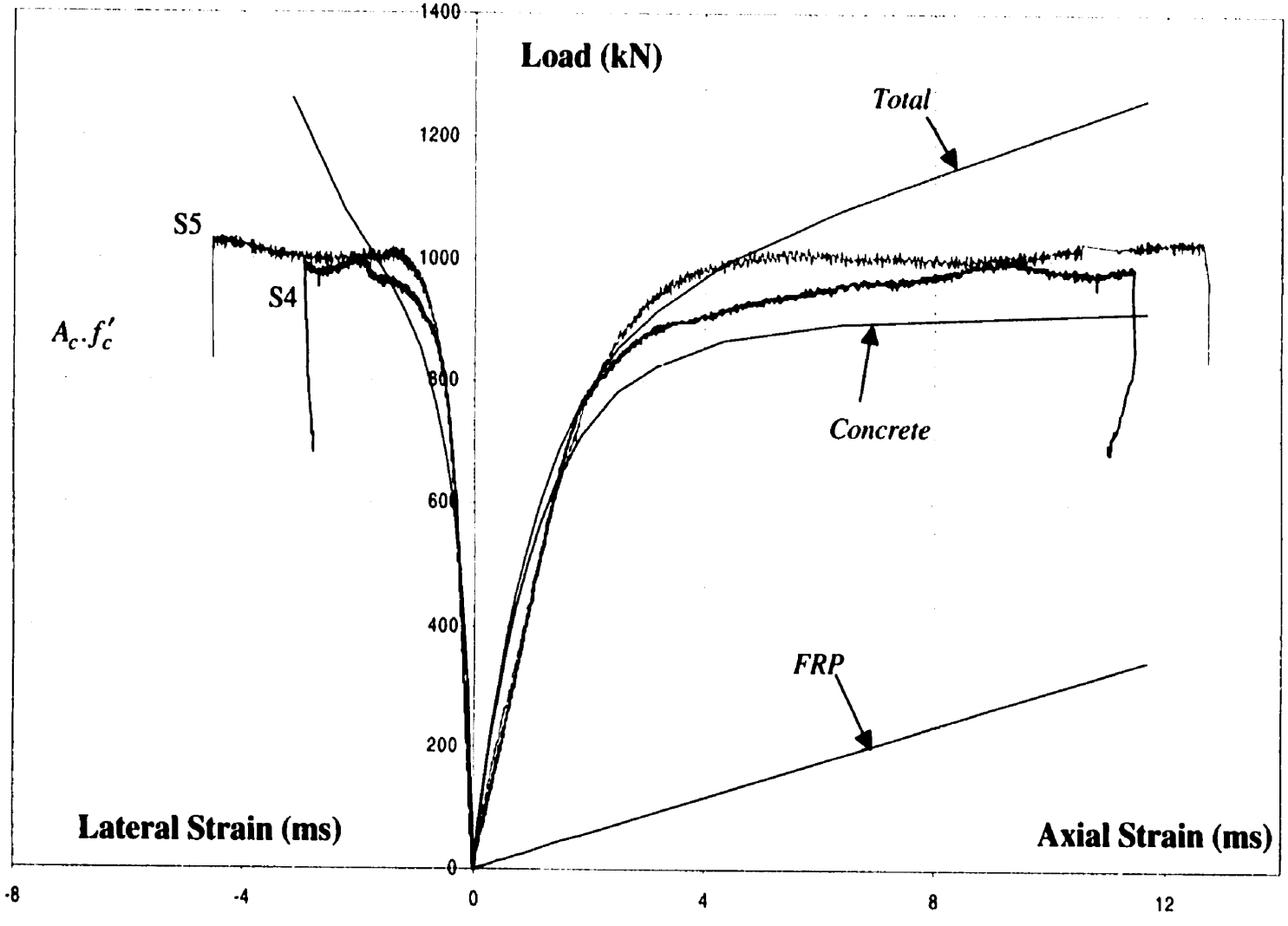

Fig. V - 13 : Modeling of Stub Column Tests S4 and S5

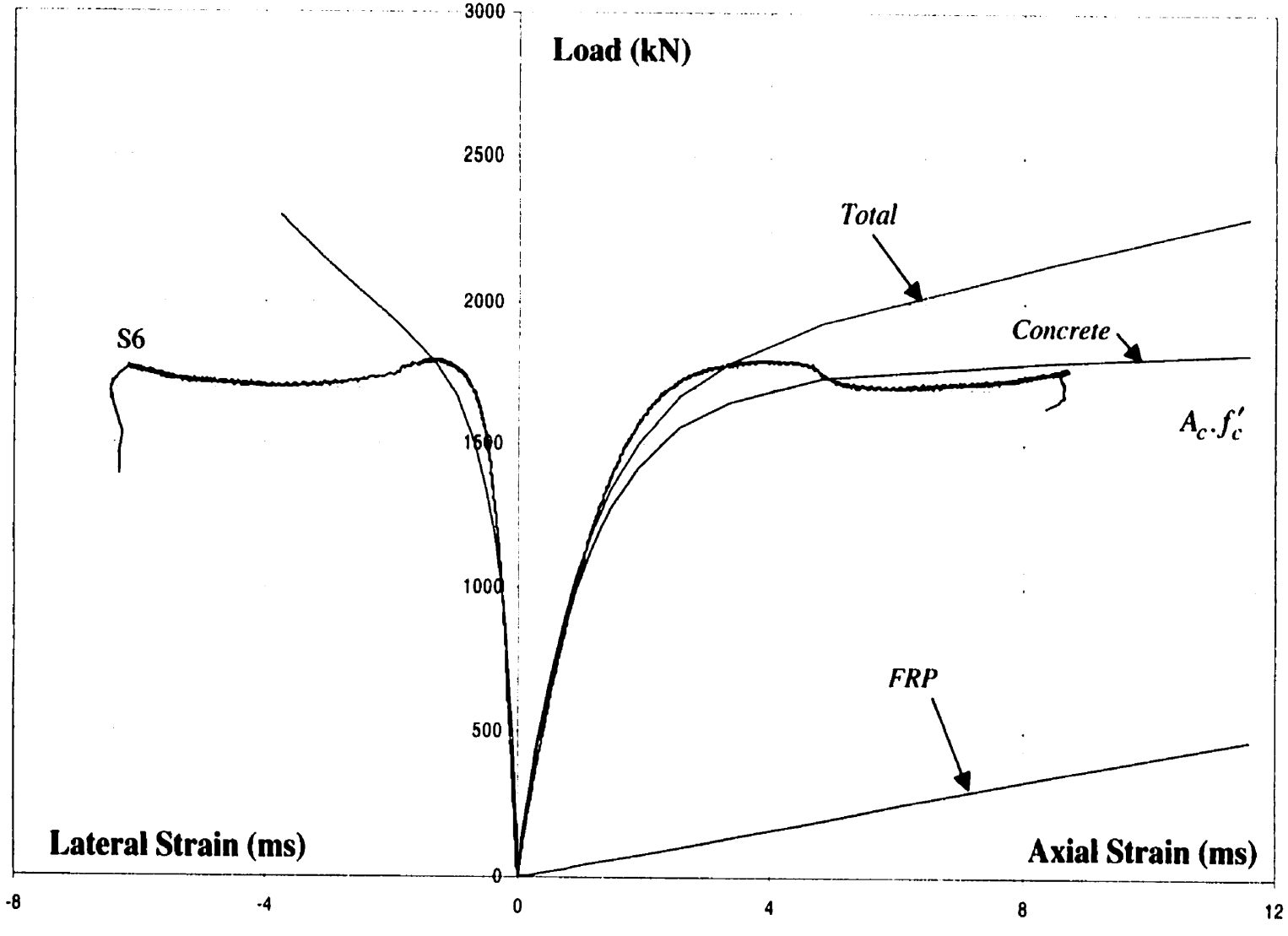

Fig. V - 14 : Modeling of Stub Column Test S6

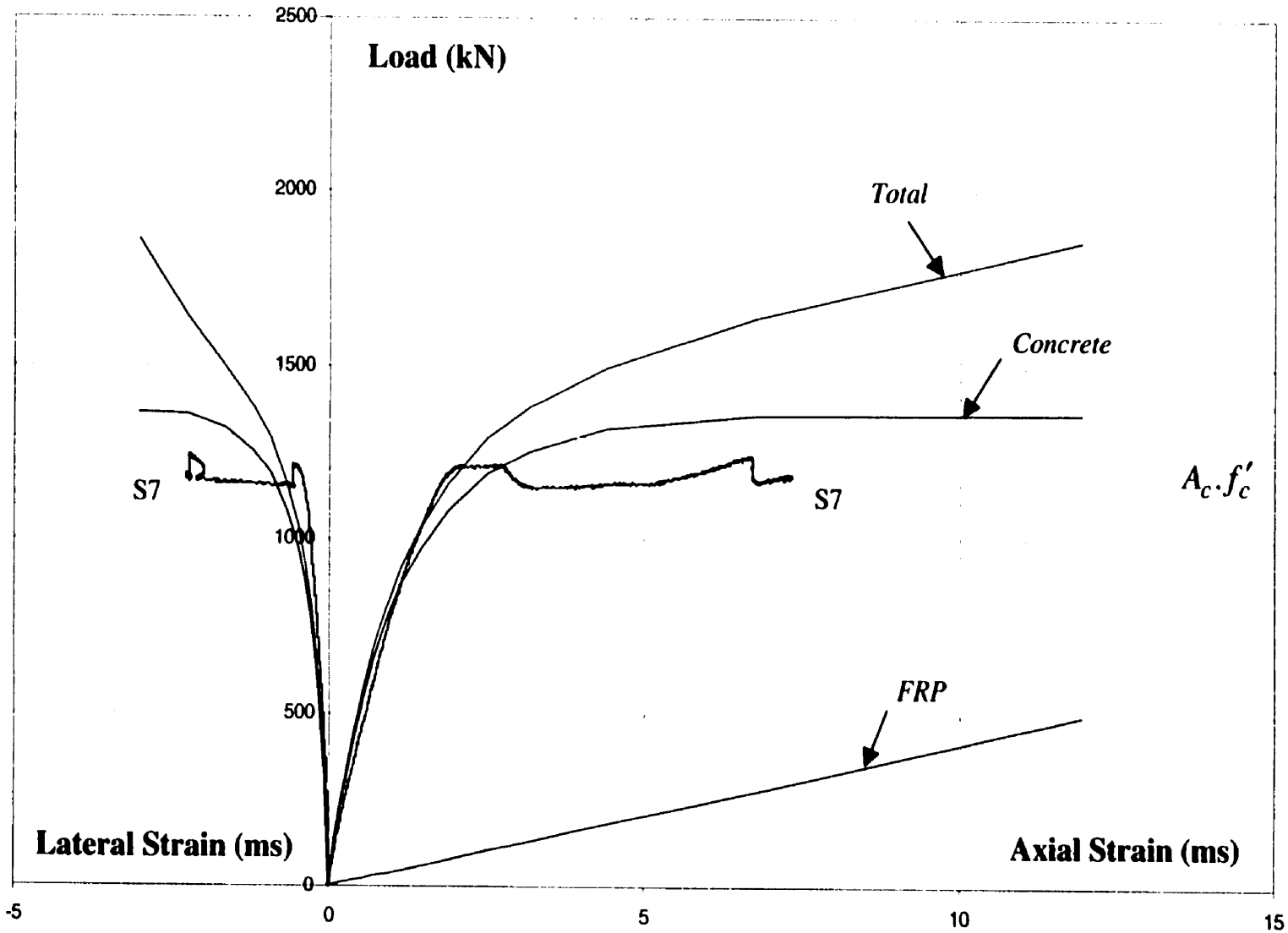

Fig. V - 15 : Modeling of Stub Column Test S7

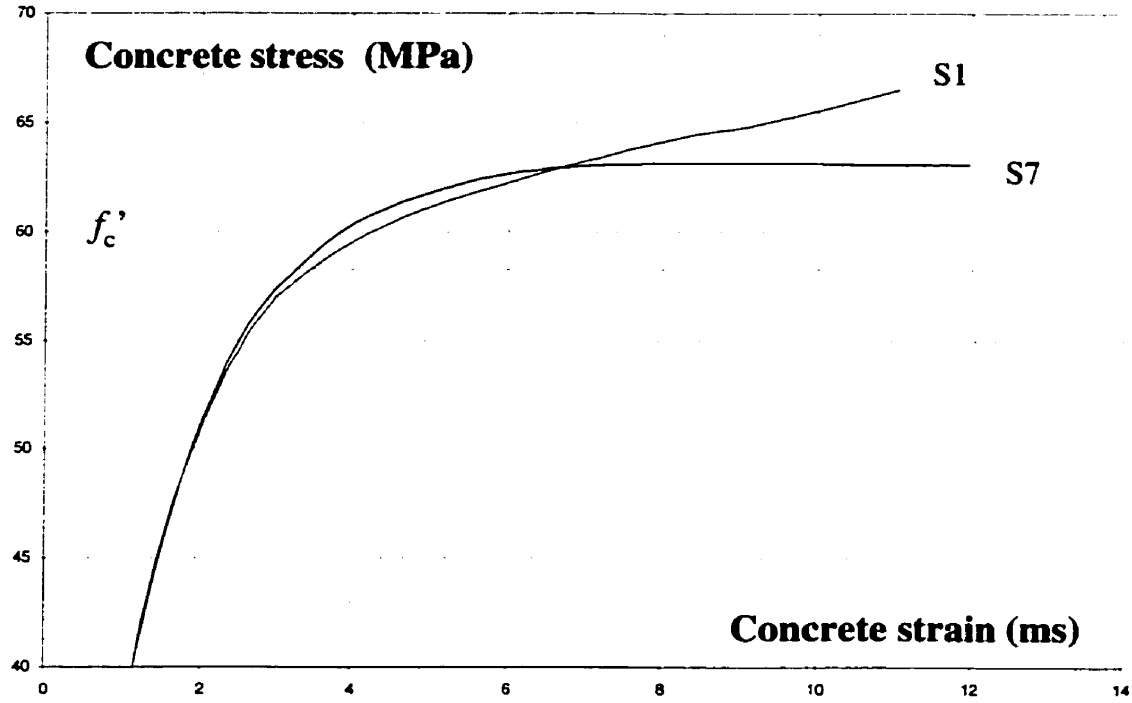

Fig. V - 16 : Concrete stress-strain curves for S1 and S7

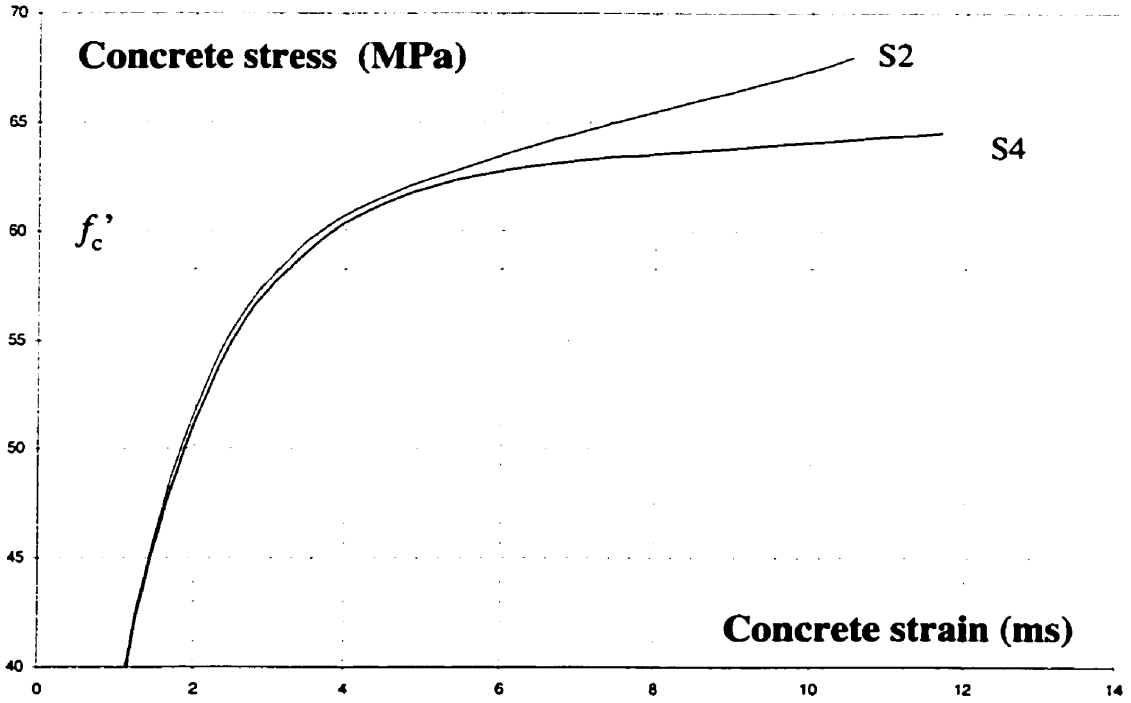

Fig. V - 17 : Concrete stress-strain curves for S2 and S4

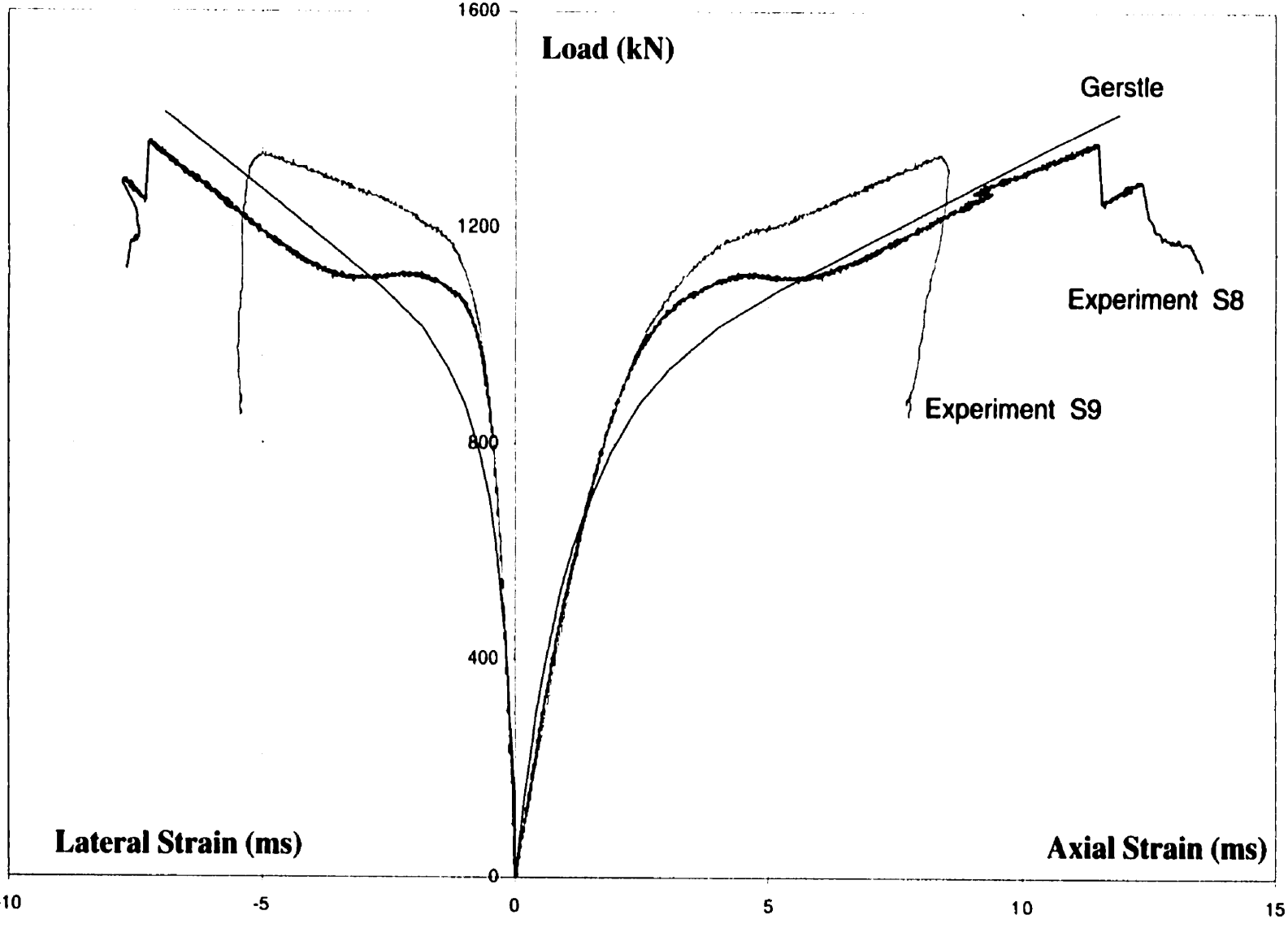

Fig. V - 18 : Modeling of Stub Column Tests S8 and S9

Chapter VI :

Finite Element Model

6.1 Introduction

In this chapter a finite element model is presented for FRP-confined concrete columns. The analysis predicts the behaviour of FRP/concrete columns in the case where the load is applied to the concrete only, and in the case where both the concrete and the shell are loaded simultaneously.

Most finite element packages like ANSYS have no built-in concrete confinement models. However, a model can be constructed using standard ANSYS features that is fairly simple but recognizes the main mechanisms of confinement by an outer FRP shell.

6.2 Theory

6.2.1 Failure Criterion

The model is based on the Drucker-Prager (DP) failure criterion, which is available under the ANSYS program version R5.4. In the three-dimensional principal stress space the DP criterion is represented by a circular cone along the hydrostatic axis $\sigma_1 = \sigma_2 = \sigma_3$ (Fig. VI - 1). Any point on the hydrostatic axis represents a hydrostatic stress state. Any plane perpendicular to the hydrostatic axis is a hydrostatic plane where the hydrostatic stress, as defined by Eq. (III - 8), is constant. The conic shape of the DP criterion implies that with increasing hydrostatic stresses the deviatoric strength will increase.

The DP criterion was originally developed for soil where a hydrostatic pressure increases the friction between the grains and bring the soil in a state which is further away from failure.

The parameters defining the cone's shape can be calibrated in order to represent a failure criterion for confined concrete.

The DP cone is defined by the cohesion c and the friction angle ϕ through the following equation :

$$F = 3\beta\sigma_o + \sqrt{\frac{1}{2}\{s\}^T\{s\}} - \sigma_y = 0 \qquad \text{(VI-1)}$$

where β is a material parameter, given by the following equation :

$$\beta = \frac{2\sin\phi}{\sqrt{3}(3-\sin\phi)} \qquad \text{(VI-2)}$$

σ_y is the material yield parameter, given by the following equation :

$$\sigma_y = \frac{6c(\cos\phi)}{\sqrt{3}(3-\sin\phi)} \qquad (VI-3)$$

σ_o is the hydrostatic component of the stress vector as defined in Eq. (III - 8).

The vector {s} contains the remaining (deviatoric) part of the stress vector :

$$\{s\} = \begin{Bmatrix} \sigma_x \\ \sigma_y \\ \sigma_z \\ \tau_{xy} \\ \tau_{yz} \\ \tau_{xz} \end{Bmatrix} - \begin{Bmatrix} \sigma_o \\ \sigma_o \\ \sigma_o \\ 0 \\ 0 \\ 0 \end{Bmatrix} \qquad (VI-4)$$

c and ϕ will be expressed in terms of the uniaxial concrete strength f_c' and the confinement effectiveness k by enforcing the following two conditions, illustrated in Fig. (VI – 2) :

1. The uniaxial strength equals f_c'. Consequently, the point with coordinates

   $(\sigma_1,\sigma_2,\sigma_3) = (f_c',0,0)$

   must be located on the cone surface.

2. The confinement effectiveness equals k. Consequently, the slope of the cone in the $(\sigma_2 = \sigma_3)$-plane must be $k/\sqrt{2}$, or the point with coordinates

   $(\sigma_1,\sigma_2,\sigma_3) = (f_c' + k\underline{\sigma}, \underline{\sigma}, \underline{\sigma})$

   must be on the cone for any value of $\underline{\sigma}$. $\underline{\sigma}$ indicates a lateral pressure.

Substituting these two conditions into Eq. (VI - 1) results in the following equation :

$$c = \frac{1-\sin\phi}{2\cos\phi} f_c' \qquad (VI-5)$$

$$\sin\phi = \frac{k-1}{k+1} \qquad (VI-6)$$

6.2.2 Behaviour

It was mentioned before that the large volumetric dilation of plain concrete does not occur until the peak strength is neared. This fact will be used in the model.

A linearly elastic element will be combined with the DP criterion in an elastic-perfectly plastic element, where the yield level depends on the level of confinement (Fig. VI - 3). Consider the plane where $\sigma_2 = \sigma_3$, shown in Fig. (VI - 4). Initially the element behaves perfectly linear. At point *A* the strength capacity under the current confining stresses is reached. However, the DP criterion still allows for an increase in the strength under increasing hydrostatic pressure, while plastic flow occurs on the failure surface.

Plastic flow is controlled by a parameter ϕ_f called the plastic flow angle. It determines the flow rule and the amount of volumetric straining during the occurrence of plastic flow.

According to the plastic theory, the plastic strain increment vector $d\bar{\varepsilon}_{pl}$ is perpendicular to the flow surface at any point. If the flow surface and the yield surface are assumed the same, the flow rule is called associated or associative (Fig. VI - 5), and ϕ_f is equal

to ϕ. If flow surface and yield surface are not coincident the flow rule is non-associated, as presented in Fig. (VI - 6).

Placing $d\bar{\varepsilon}_{pl}$ in the 3D strain space it can be seen that ϕ_f controls the volumetric behaviour. This is illustrated in Fig. (VI - 7) :

Fig. (VI - 7 a) : $\phi_f < 0$ means volumetric compression

Fig. (VI - 7 b) : $\phi_f = 0$ means yielding with no volume change

Fig. (VI - 7 c) : $\phi_f > 0$ means volumetric expansion

In this way the model can be calibrated to obtain a realistic volumetric response. It was already mentioned before that FRP-confined concrete fails with a decrease in volume whereas steel-confined concrete undergoes a volume increase at failure.

Fig. (VI - 8) leads to the following relationships :

$$\gamma = arctg\left(\frac{d\varepsilon_{1,pl}}{\sqrt{2}\ d\varepsilon_{2,pl}}\right) = arctg\left(\frac{1}{\sqrt{2}\mu}\right) \qquad (VI-7)$$

and :

$$\phi_f = 90^o - \gamma - arctg\left(\frac{1}{\sqrt{2}}\right) = 54.74^o - arctg\left(\frac{1}{\sqrt{2}\mu}\right) \qquad (VI-8)$$

The above indicates that an ANSYS model for FRP composite sections can be based on the Drucker-Prager criterion, which has 3 parameters : the cohesion c, the friction angle

ϕ and the flow angle ϕ_f. To adapt the model to confined concrete behaviour, these parameters are determined using the following formulas :

$$\sin\phi = \frac{k-1}{k+1}$$

$$c = \frac{1-\sin\phi}{2\cos\phi} f_c'$$

$$\phi_f = 54.74^o - arctg\left(\frac{1}{\sqrt{2}\mu}\right)$$

Finally it should be noted that the derivation was made for the case of triaxial compression with none of the principal stresses being a tensile stress.

6.3 Examples

6.3.1 Nanni and Bradford (1995)

The proposed model was used to predict the behaviour of Example 3, introduced in Chapter II. The concrete core is confined by a GFRP shell and the load is applied on the concrete only.

The finite element model was developed in ANSYS version R5.4.

8-Node elastic brick elements SOLID45 were used to model the concrete core. For the FRP shell 4-node elastic shell elements SHELL63 were used. Only a quarter of the cross-section was modeled and appropriate symmetry boundary conditions were

imposed. A total of 162 elements were used for the core together with 36 elements for the shell. Compatible meshes were established for the core and the shell so that the degrees of freedom of the coinciding shell and brick nodes could be coupled. The finite element mesh is shown in Fig. (VI - 9).

The FRP was modeled as a perfectly linear material with orthotropic material properties. The elastic modulus is assumed to be 52 GPa in the circumferential direction of the shell and to be negligible in the axial direction, since the shell was meant to be used as a jacket and carries no load in the axial direction. The Poisson's ratios ν_f and ν_f' are assumed to be zero.

The confinement effect in the concrete was accounted for using the DP criterion.

Using $k = 3.09$, Eq. (II - 4) yields :

$$\mu_u = 0.30$$

Eqs. (VI - 5) to (VI - 8) result in :

$$\sin \phi = 0.511 \quad \text{or} \quad \phi = 30.73^\circ$$

$$c = 10.32$$

$$\phi_f = -12.4^\circ$$

The calculations were performed with the Load Control Option. This results in a load step size, selected by the program, of 5 MPa in the second part of the stress-strain curve. The elastic modulus of the concrete is taken as the secant modulus at failure :

$$E_c = 36.3 / 0.002 \text{ MPa}$$

$$= 18.1 \text{ GPa}$$

The predicted results are presented in Fig. (VI - 10).

The point where both branches of the concrete stress-strain curve intersect is determined by c and ϕ. The slope of the second branch of the curve depends on ϕ and ϕ_f. ϕ_f is dependent on μ.

It should be noted that Eq. (II - 4) is a modified version of an equation originally proposed by the same authors (Mirmiran and Shahawy (1997)) :

$$\mu_u = -0.1375 Ln\left(\frac{2E_{FRP}t}{f_c'D}\right) + 0.8646 \qquad (VI-9)$$

This equation yields a value of 0.43 for μ_u in the case of example 3.

6.3.2 Mirmiran and Shahawy (1998)

The proposed model is used to predict the behaviour of Example 2 (Chapter II), a GRFP-confined specimen, loaded on the core only.

Eq. (II - 4) yields :

$$\mu_u = 0.18$$

whereas Eq. (VI - 9) yields :

$$\mu_u = 0.35$$

Since the difference, the accuracy of Eq. (II - 4) might be questionable in this case. Using a value of 0.18 for μ_u, the variables in the DP criterion were calculated as follows :

$$\sin \phi = 0.435 \quad \text{or} \quad \phi = 25.78^{\circ}$$

$$c = 8.28$$

$$\phi_f = -20^{\circ}$$

A load step size of 2 MPa was used in this case. The results of the analysis are shown in Fig. (VI - 11).

The maximum axial concrete stress was predicted to be 71.2 MPa, in comparison to a measured value of 74.6 MPa. The error is 4.5 percent. The predicted ultimate strain was 0.066, in comparison to a measured value of 0.043.

The confinement effect was underestimated by the model. This example illustrates the dependence of the model on a realistic estimation of the dilation rate μ_u.

6.3.3 Specimen S1

Specimen S1, introduced in the previous chapter as part of the experimental program at the University of Manitoba (1999), is used to examine the FE for the case where the load is applied on both the concrete and the shell. The specimen has an 8.625 inches diameter and is totally filled with concrete.

The mesh shown in Fig. (VI – 9) was used, with 162 elements for the concrete core and 36 elements for the shell. The degrees of freedom of the coinciding shell- and core nodes were coupled to ensure strain compatibility in both axial and circumferential directions. The shell was modeled as an orthotropic material with E_{hoop} and E_{long} as listed in Table (V - 5). The major Poisson's ratio v_f was taken as 0.1.

The Tsai-Wu criterion is also available under ANSYS R5.4 and was used to detect failure in this case.

The model is based on Eq. (II - 4) for μ_u to control the plastic properties of the concrete.

In this case the model parameters have the following values :

ϕ = 26.78°

c = 17.94

ϕ_f = -7.575°

The predicted behaviour is shown in Fig. (VI - 12). Good agreement with the measured behaviour was obtained for the load vs. axial strain curve. The predicted ultimate load is 2612 kN, in comparison to a measured value of 2636. The error is 0.9 percent.

The predicted axial strain at failure is 10.6 ms, in comparison to a measured value of 11 ms. The error is 6 percent. The lateral strains are somewhat underestimated.

6.3.4 Specimens S2 and S3

Specimens S2 and S3, introduced in Chapter V as part of the experimental program conducted at the University of Manitoba, are used as another verification. Both specimens are totally filled sections with an outer diameter of 6.625". The geometrical and material properties of the model are adjusted according to the values in Table (V – 7).

The parameters of the model have the following values :

ϕ = 25.89°

c = 18.25

$\phi_f = -10.04°$

Fig. (VI - 13) shows the results of the finite element approach. The predicted failure load is 1855 kN, in comparison to an average measured value of 2121 kN. The error is 12.5 percent. The predicted ultimate axial strain is 13.72 ms, compared to a measured value of 13 ms. The error is 4.6 percent.

6.4 Conclusions

The FE model, based on the Drucker-Prager criterion and the Tsai-Wu failure criterion, is capable of predicting the behaviour of an FRP/concrete composite column, in case the load is applied to the concrete core only, and in case the load is acting on both the FRP shell and the concrete.

The predictions are based on an idealized concrete behaviour and are not as accurate as the two models proposed in Chapters IV and V.

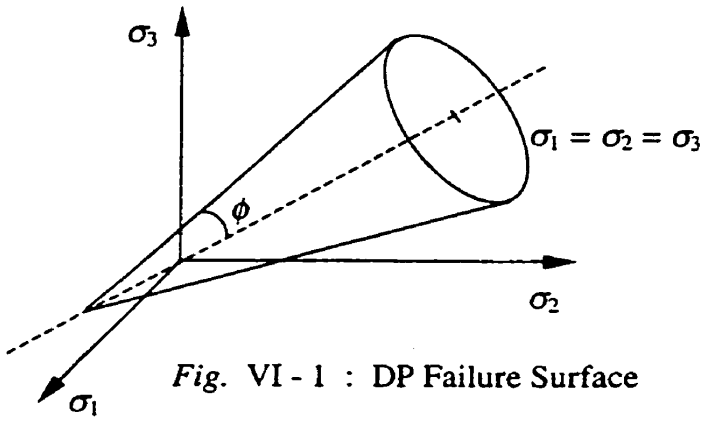

Fig. VI - 1 : DP Failure Surface

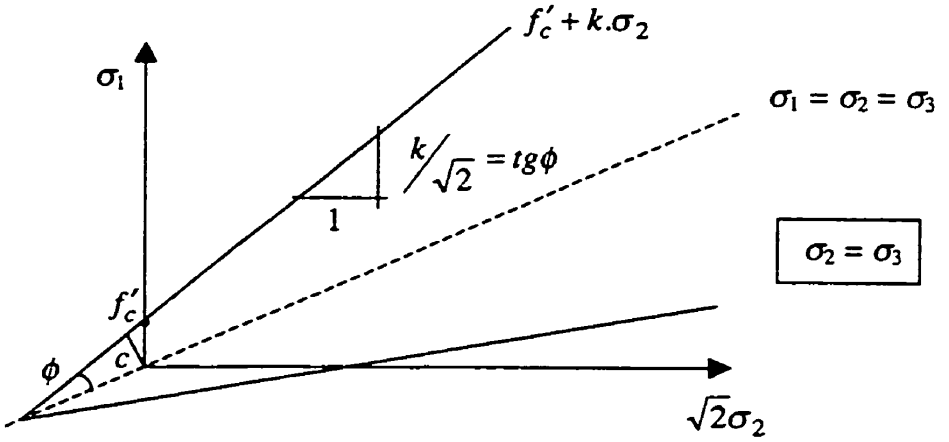

Fig. VI - 2 : Calibration of the Failure Surface

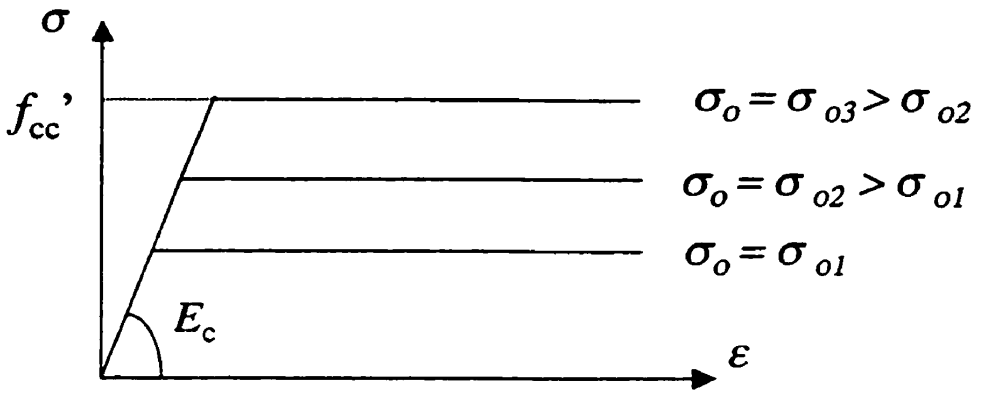

Fig. VI - 3 : Stress-Strain Relationship

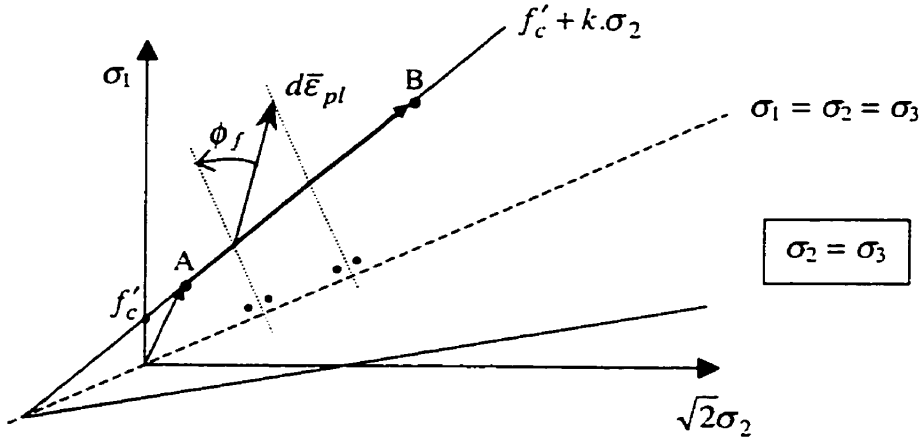

Fig. VI - 4 : Plastic Flow on the Failure Surface

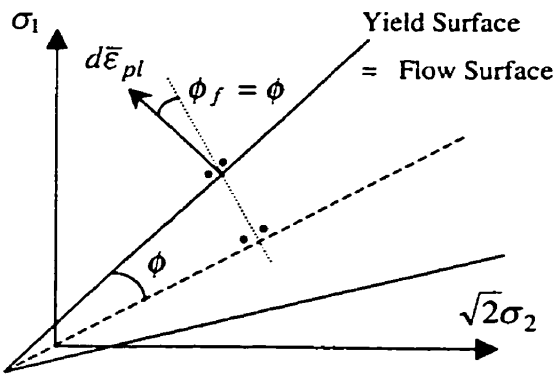

Fig. VI - 5 Associative Flow rule

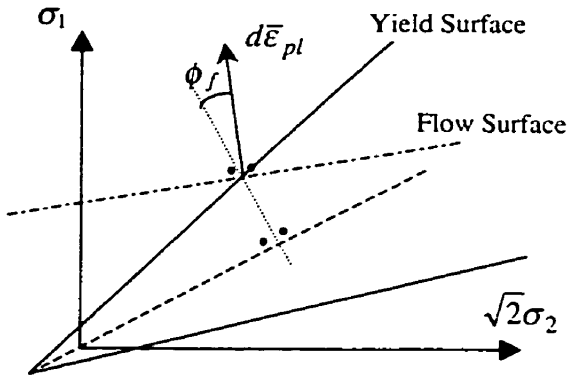

Fig. VI - 6 Non - associative Flow rule

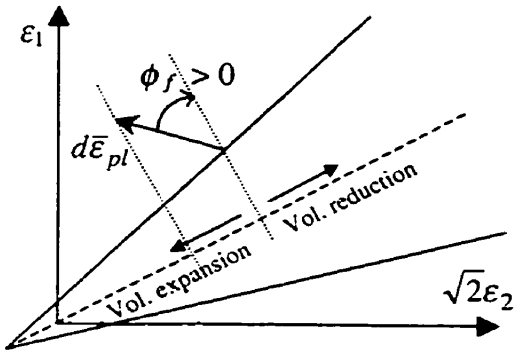

Fig. VI - 7 a

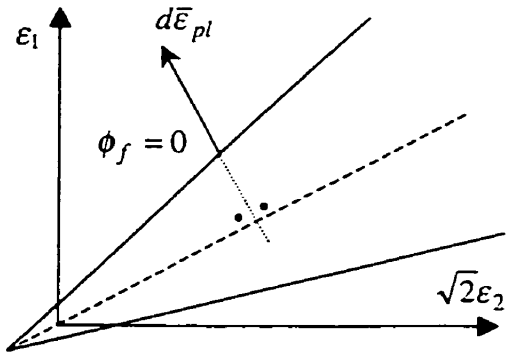

Fig. VI - 7 b

Plastic Flow and Volumetric Behaviour

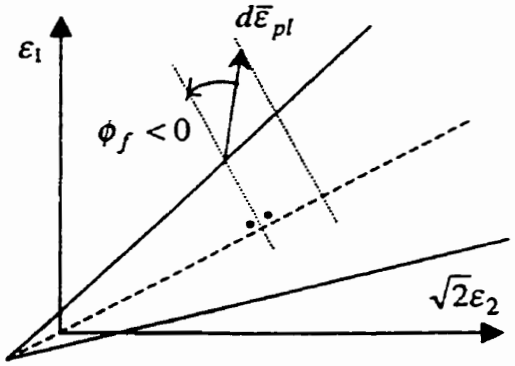

Fig. VI - 7 c : Plastic Flow and Volumetric Behaviour

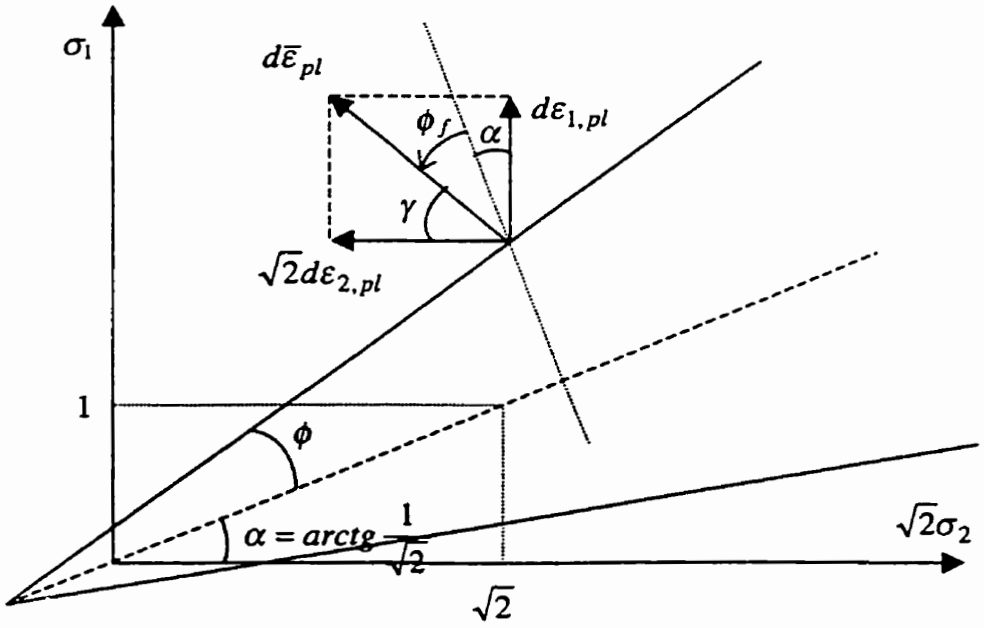

Fig. VI - 8 : Determination of ϕ

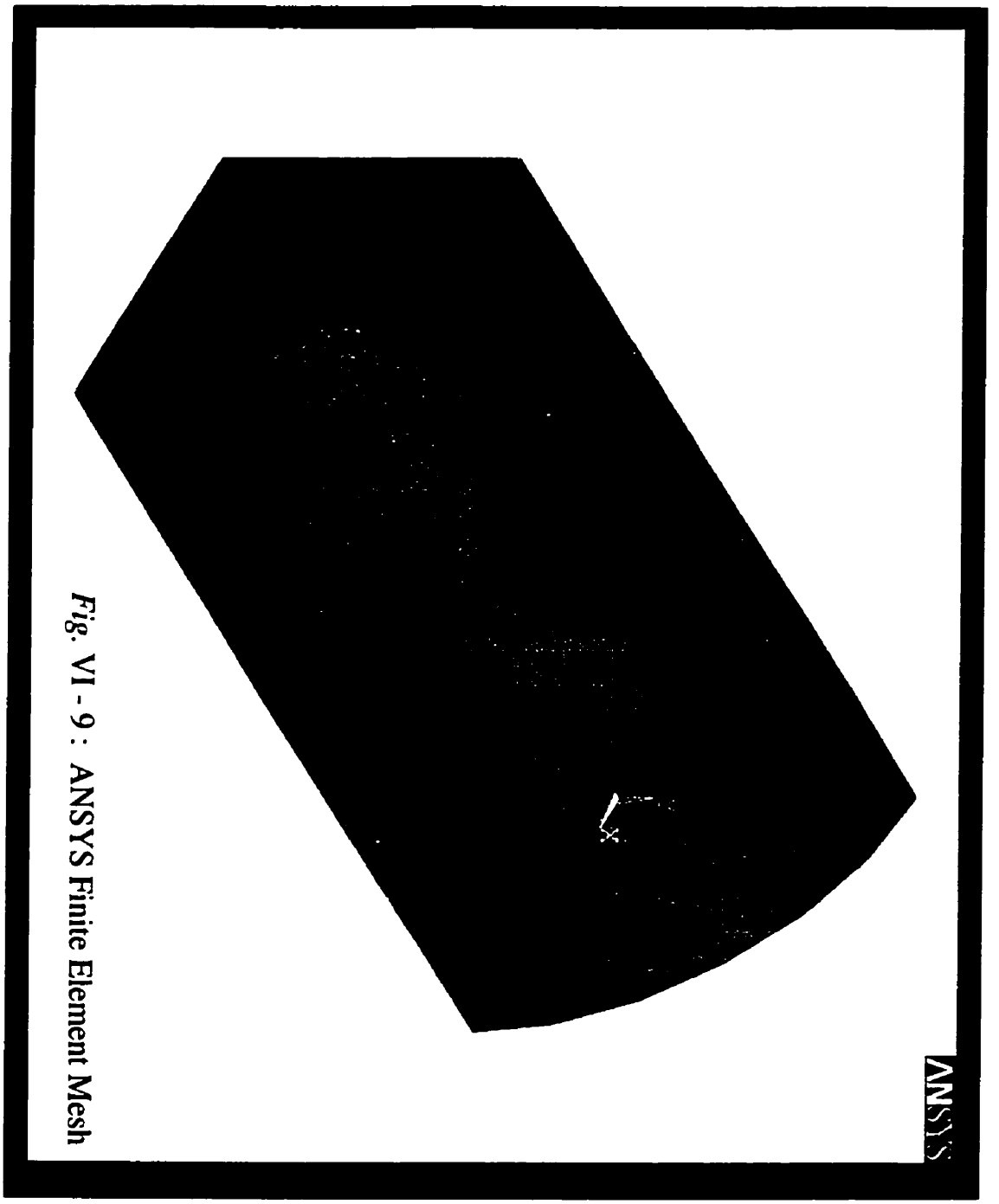

Fig. VI - 9 : ANSYS Finite Element Mesh

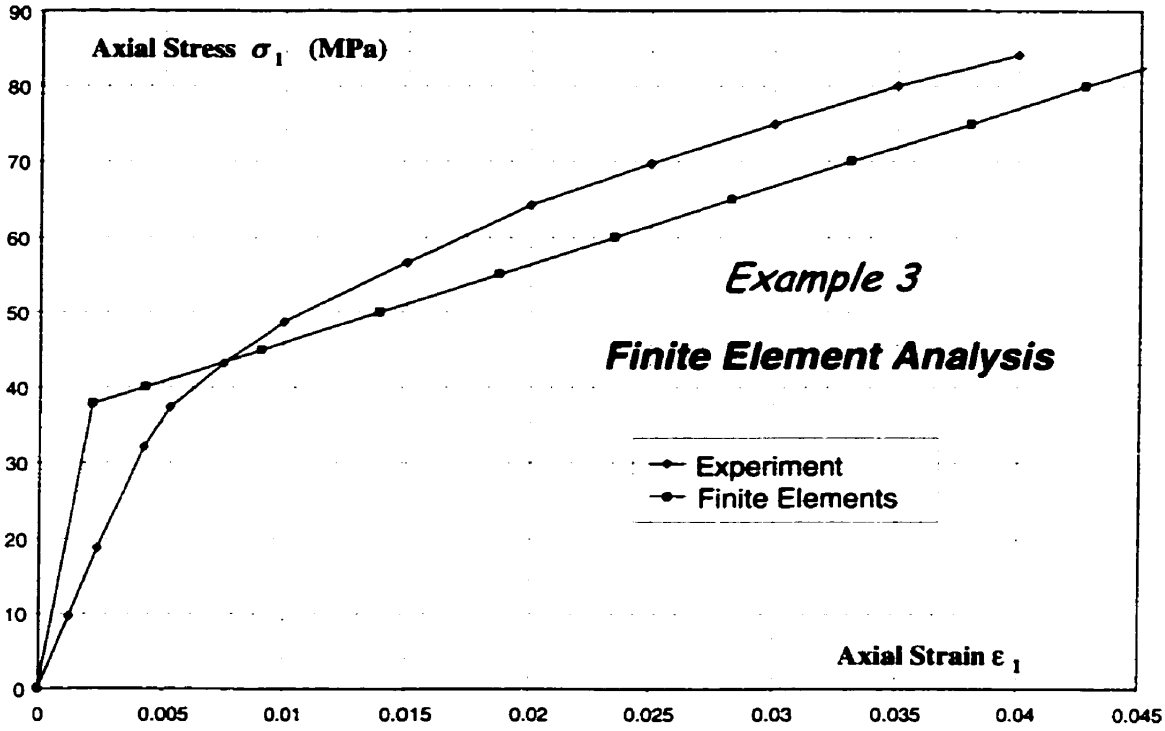

Fig. VI - 10 : Axial concrete stress-strain curve : FE analysis

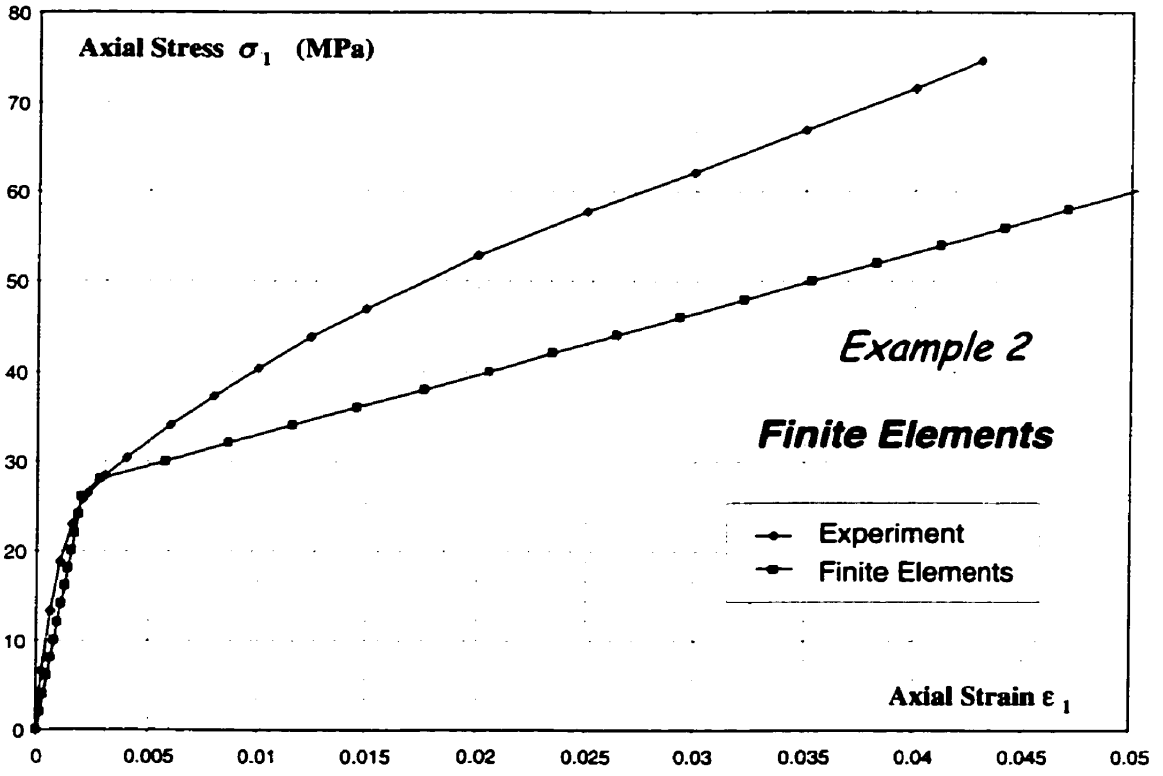

Fig. VI - 11 : Axial concrete stress-strain curve : FE analysis

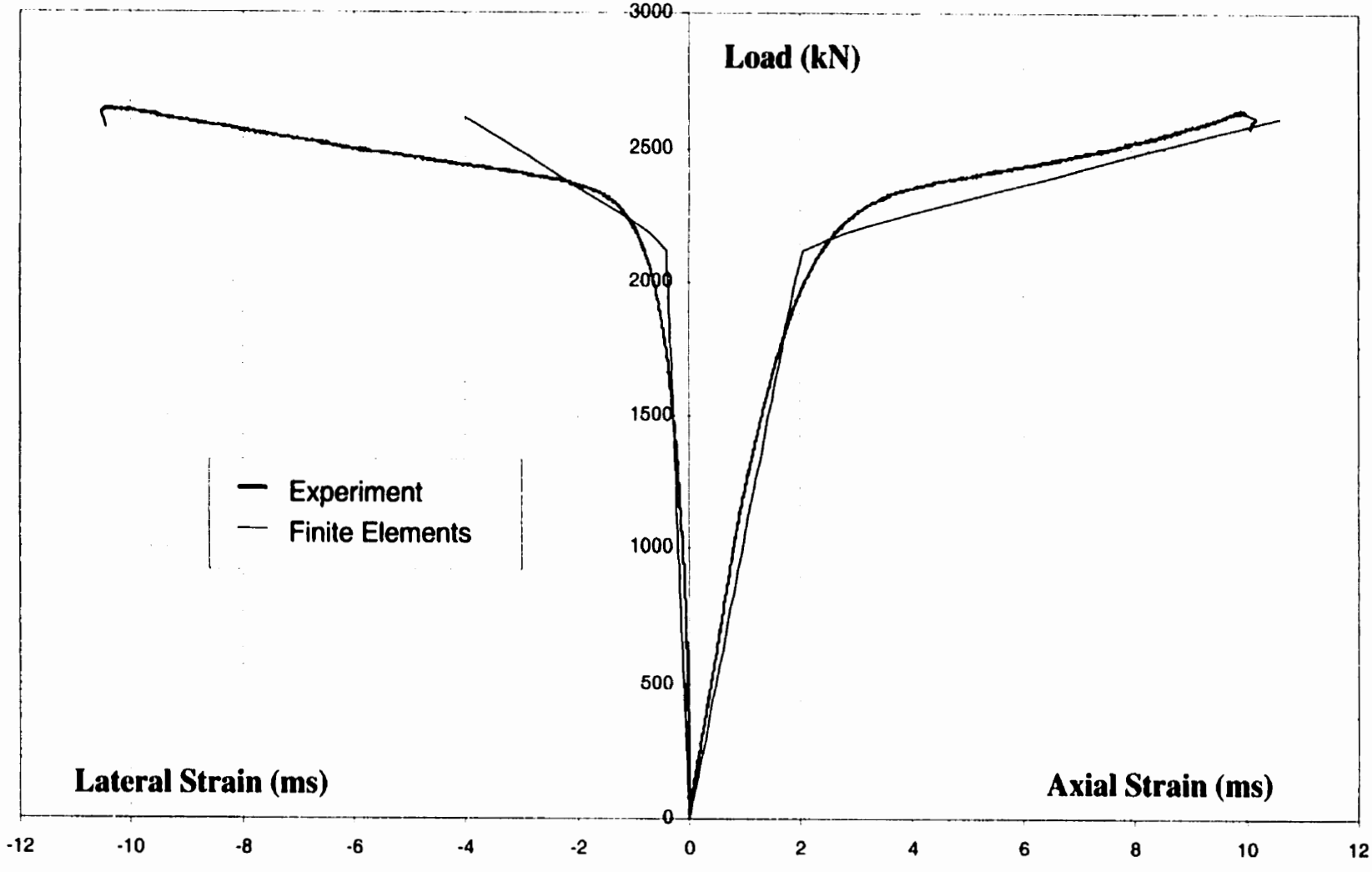

Fig.* VI - 12 : *Modeling of Stub Column Test S1 : Finite Elements

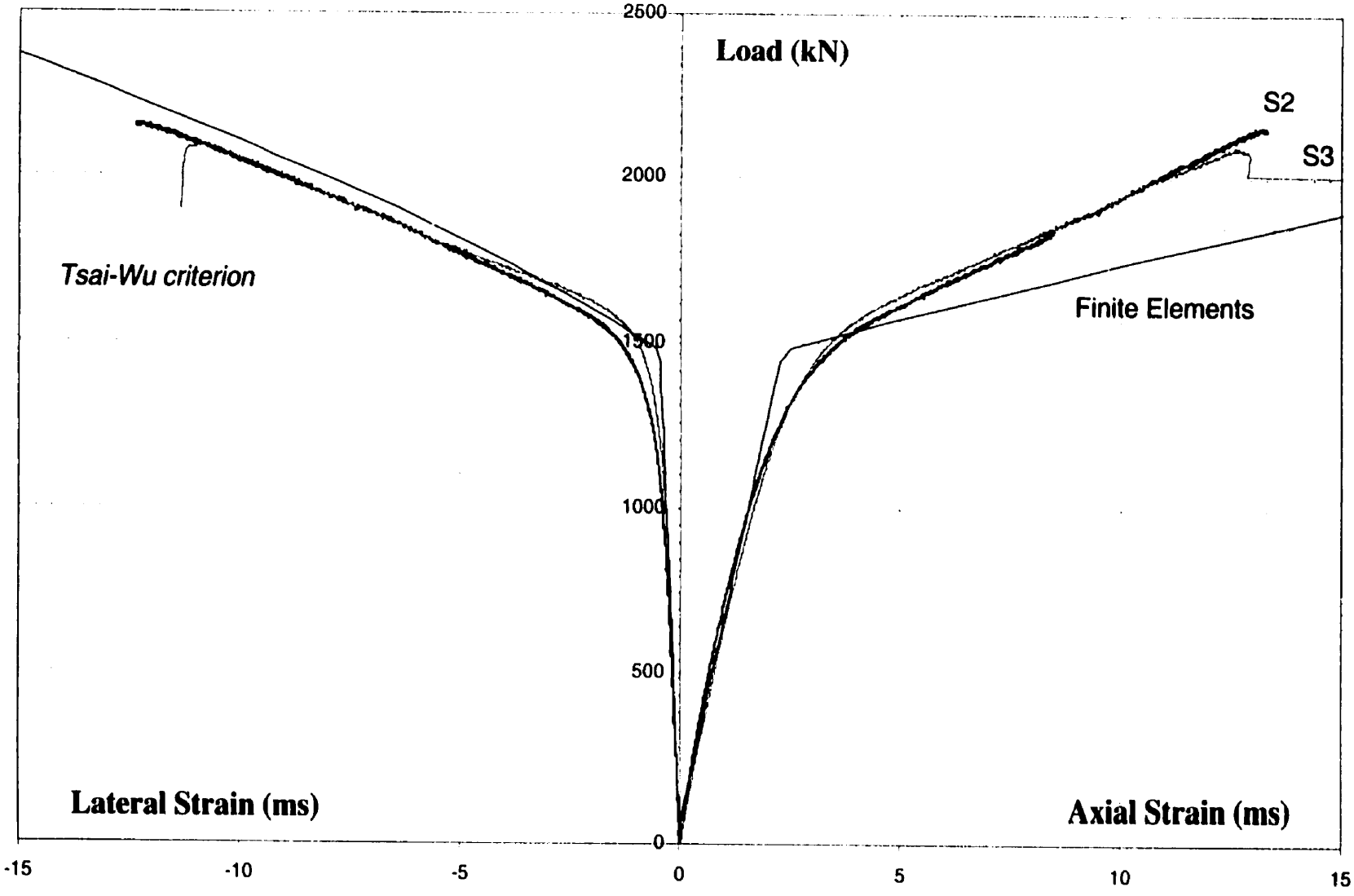

Fig. VI - 13 : Modeling of Stub Column Tests S2 & S3 : Finite Elements

Chapter VII :

Parametric Studies

7.1 Introduction

In order to extend the knowledge on the behaviour of confined columns with FRP, this chapter presents parametric studies for the key parameters believed to affect the behaviour. The following parameters were selected in this thesis :

- type of material of the outer shell
- size of the inner void
- number of confining FRP layers

7.2 Type of the Material of the Outer Shell

7.2.1 Steel, GFRP and CFRP

The proposed model 1 in this thesis was used to examine the behaviour of concrete confined with three different jacket materials : steel, carbon-FRP (CFRP) and glass-FRP (GFRP). The load is applied only to the concrete core and the shell is used mainly to provide the confinement.

The specimen geometry and concrete properties were the same for the three materials used in this study. The shell thickness t, which reflects the reinforcement ratio ρ, was also kept constant:

$$\rho \equiv \frac{2\pi Rt}{\pi R^2}$$

$$= \frac{2t}{R}$$

The concrete properties are listed in Table (VII –1). The material properties of the shell are listed in Table (VII – 2) and were taken over from examples by Spoelstra and Monti (1999).

Fig. (VII - 1) shows the analysis results, presented as normalized stress σ_1 / f_c' versus normalized strain $\varepsilon_1 / \varepsilon_p$. ε_p is the unconfined peak strain and is assumed to be 0.002. The steel-confined concrete initially exhibits a behaviour similar to the CFRP-confined concrete, even demonstrating a slightly higher stiffness because of the high elastic modulus of the steel. However, yielding of the steel will curtail the performance of the

section and the maximum confined concrete strength will be reached shortly after the steel starts yielding.

Because of the linear characteristics of the FRP, the fiber-confined concrete will be subjected to an increasing confining pressure up to failure. The GFRP-confined concrete curve reveals the bilinear behaviour that was discussed before. The gain in ductility in comparison to the unconfined concrete is tremendous, with an ultimate concrete strain that is more than twenty times the unconfined peak strain ε_p.

The CFRP-confined concrete will reach a strength more than 2.25 times the unconfined concrete strength and an ultimate strain more than eight times ε_p. For clarity, it is noted again that the point of failure is determined by the hoop strength of the CFRP.

7.2.2 Effect of the Elastic Modulus

A parametric study was performed for an FRP-confined concrete section where the elastic modulus of the FRP was gradually varied from 5 GPa up to 240 GPa.

The reinforcement ratio ρ used is 0.04. This value represents a typical value that, for instance, corresponds to a shell thickness of 2 mm and a shell diameter of 200 mm. The concrete strength is 35 MPa for a concrete modulus of 29.6 GPa.

The results of the parametric study are shown in Fig. (VII - 2). The notation of each curve is given in Table (VII – 3).

It should be noted that the elastic modulus of the FRP E_{hoop}, the thickness of the shell t and the radius R are always combined in a factor ψ, defined as follows :

$$\psi = \frac{E_{hoop} t}{R}$$

$$= \frac{E_{hoop} \cdot \rho}{2}$$

The factor ψ is the main parameter which controls the behaviour. The same value can be obtained using various combinations of E, t and R, resulting in the same behaviour. As such the curve D represents the behaviour of a column confined by a material with an elastic modulus of 40 GPa and a reinforcement ratio of 4 %, as well as the behaviour of another column with a reinforcement ratio of 8 % and an elastic modulus of 20 GPa, since the factor ψ is identical for both cases. This indicates, for instance, that the same behaviour can be obtained by reducing the thickness of a shell by one half and increasing the modulus by a factor of 2. Thus Fig. (VII - 2) can be used as a general design chart for concrete confined by FRP material. The ultimate strength of the section however will be controlled by the hoop strength of the FRP material and the thickness t. The behaviour of the GFRP-confined concrete given in Fig. (VII - 1) corresponds to a curve with a ψ value of 310 in Fig. (VII – 2).

7.3 Effect of the Void Size

This section describes the influence of the size of an inner void on the confinement effect of concrete casted in an FRP tube. The experimental program discussed in Chapter V is thereby used in this study. Using specimen S2, given in Table (V – 7) and

loaded on the composite section of concrete and FRP, the proposed model 2 is used to predict the behaviour in the cases of having an inner void with radius R_i of 10 mm, 20 mm, 30 mm and 46 mm. These selected values represent R_i/R_o ratios of 0.12, 0.24, 0.37 and 0.56. An inner radius of 46 mm corresponds to the configuration of specimens S4 and S5, given in Table (V – 1).

The behaviour of the specimens with different void sizes is compared to that of a solidly filled cylinder in Fig. (VII – 3).

Based on the conclusions drawn from the behaviour of specimens S4 and S5, an inner void diameter larger than 46 mm is not expected to give realistic predictions. This is due to Gerstle's assumption of totally ductile failure for the concrete and the incapability to deal with a descending branch of the stress-strain curve.

The influence of the void size is shown in Fig. (VII - 3), in terms of the axial load resistance as related to the axial strain. Fig. (VII - 4) also shows the stress-strain curves of the confined concrete for the different void sizes.

The presence of a void considerably alters the stress state of the confined concrete. For small values of R_i the axial load-strain behaviour as well as the stress-strain curve of the confined concrete are close to the corresponding ones for the solidly filled cylinder. Thus it can be concluded that a small void has a minor effect on the strength and the ultimate strain.

While increasing the void size, the confinement effect will gradually be reduced, as shown in Fig. (VII - 4).

7.4 Number of Confining FRP Layers

In this study, a 162 mm diameter concrete cylinder is considered, confined by a GFRP shell. The shell is solidly filled with concrete. The uniaxial unconfined strength of the concrete is 58.3 MPa. The FRP shell is glassfiber-epoxy composite with a fiber volume fraction of 0.5. The layer structure is built up from layers with horizontally oriented fibers (± 86.4° winding angle) and layers with axially oriented fibers (± 7.7° winding angle). The thickness of each layer is 0.01" (0.254 mm).

A total of 10 layers was assumed with 5 layers out of 10 oriented in the hoop direction. This is denoted as specimen 5/10 in Fig. (VII – 6).

More layers with hoop oriented fibers were then added in order to study the effect of increasing confinement. Specimen 6/11 has 6 layers out of 11 oriented in the hoop direction.

The classical laminate theory was used to compute the properties of the different shell configurations. The shell properties are shown in Table (VII – 4).

The results of the calculations are presented in Fig. (VII - 6) in terms of the axial load and the corresponding axial strain. Table (VII - 5) shows the same results in numerical form.

It can be seen from Fig. (VII - 6) that adding more hoop fibers is an effective way to increase the confinement effect in a section, leading to both higher strength and ductility.

In this case adding 5 more layers of hoop fibers increased the ultimate load by more than 1000 kN (42 %) in comparison to the original configuration. The ultimate strain increased by 73 %.

Concrete Elastic Modulus E_o	29.6 GPa
Unconfined Concrete Strength f_c'	35 MPa
Reinforcement Ratio ρ	1.6 %

Table VII – 1 : Specimen Properties

Material	E	f_{hoop} or f_y
Steel	200 GPa	440 MPa
Carbonfiber (CFRP)	138 GPa	1447 MPa
Glassfiber (GFRP)	38.6 GPa	1062 MPa

Table VII – 2 : Material Properties

	E_{FRP}	ψ
A	5 GPa	100 MPa
B	10 GPa	200 MPa
C	20 GPa	400 MPa
D	40 GPa	800 MPa
E	80 GPa	1600 MPa
F	120 GPa	2400 MPa
G	160 GPa	3200 MPa
H	200 GPa	4000 MPa
I	240 GPa	4800 MPa

Table VII – 3 : Legend to Fig. (VII – 2)

	E_{long} (MPa)	E_{hoop} (MPa)	f_{long} (MPa)	f_{hoop} (MPa)	t (mm)
5/10	16,234	16,372	198.8	198.1	2.54
6/11	17,545	22,166	220.0	360.4	2.79
7/12	18,469	24,745	250.9	460.0	3.05
8/13	18,841	26,228	290.8	518.9	3.30
9/14	18,690	27,214	337.8	553.2	3.56
10/15	18,179	27,938	388.8	572.9	3.81

Table VII - 4 : Shell Properties

	P_{max} (kN)	ε_{cu} (ms)
5/10	2405	10.3
6/11	2560	11.0
7/12	2742	12.1
8/13	2928	14.0
9/14	3151	15.5
10/15	3410	17.8

Table VII - 5 : Ultimate Loads and Strains

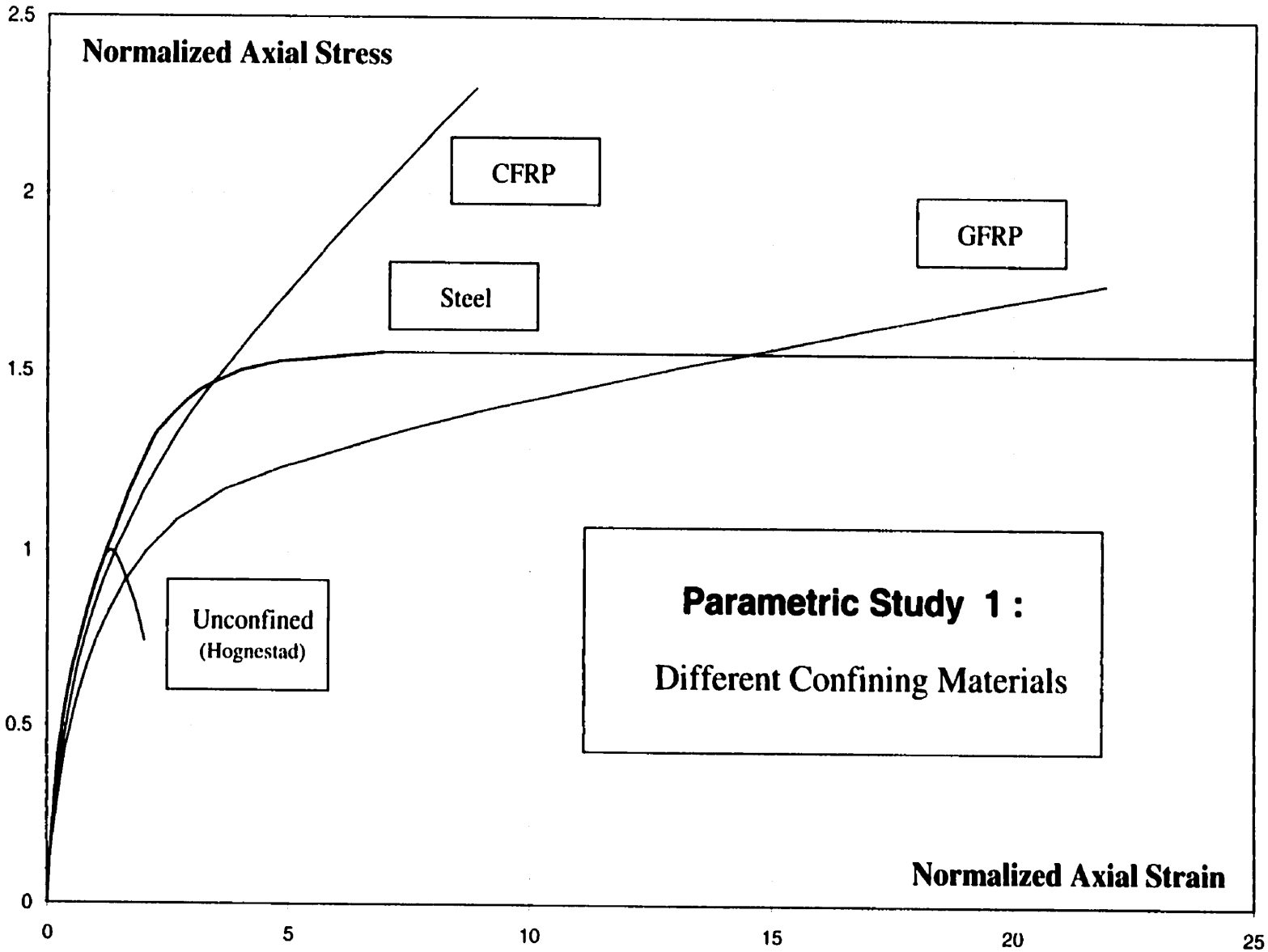

Fig. VII - 1 : Behaviour of columns confined by different materials

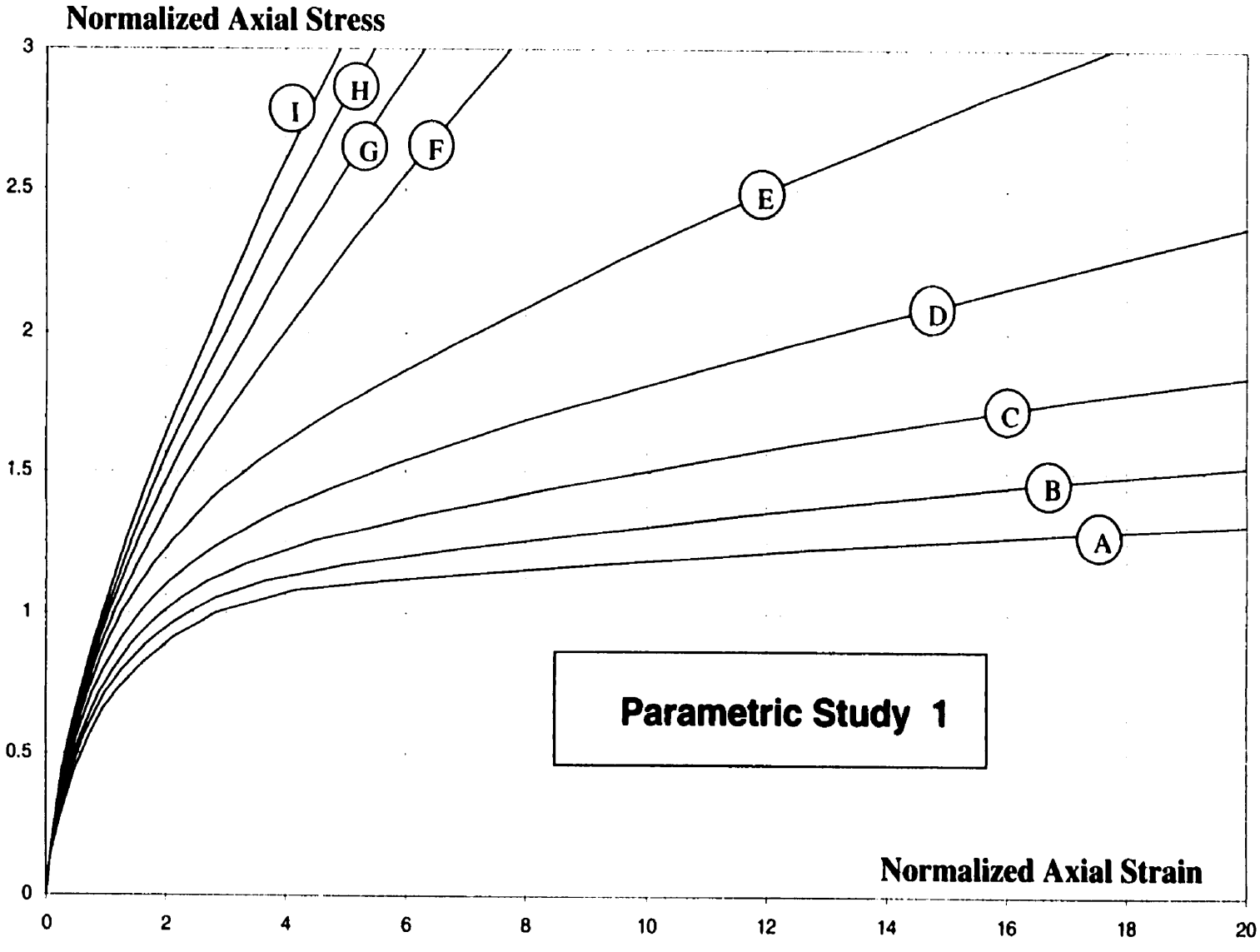

Fig. VII - 2 : Effect of ψ on the behaviour of confined columns

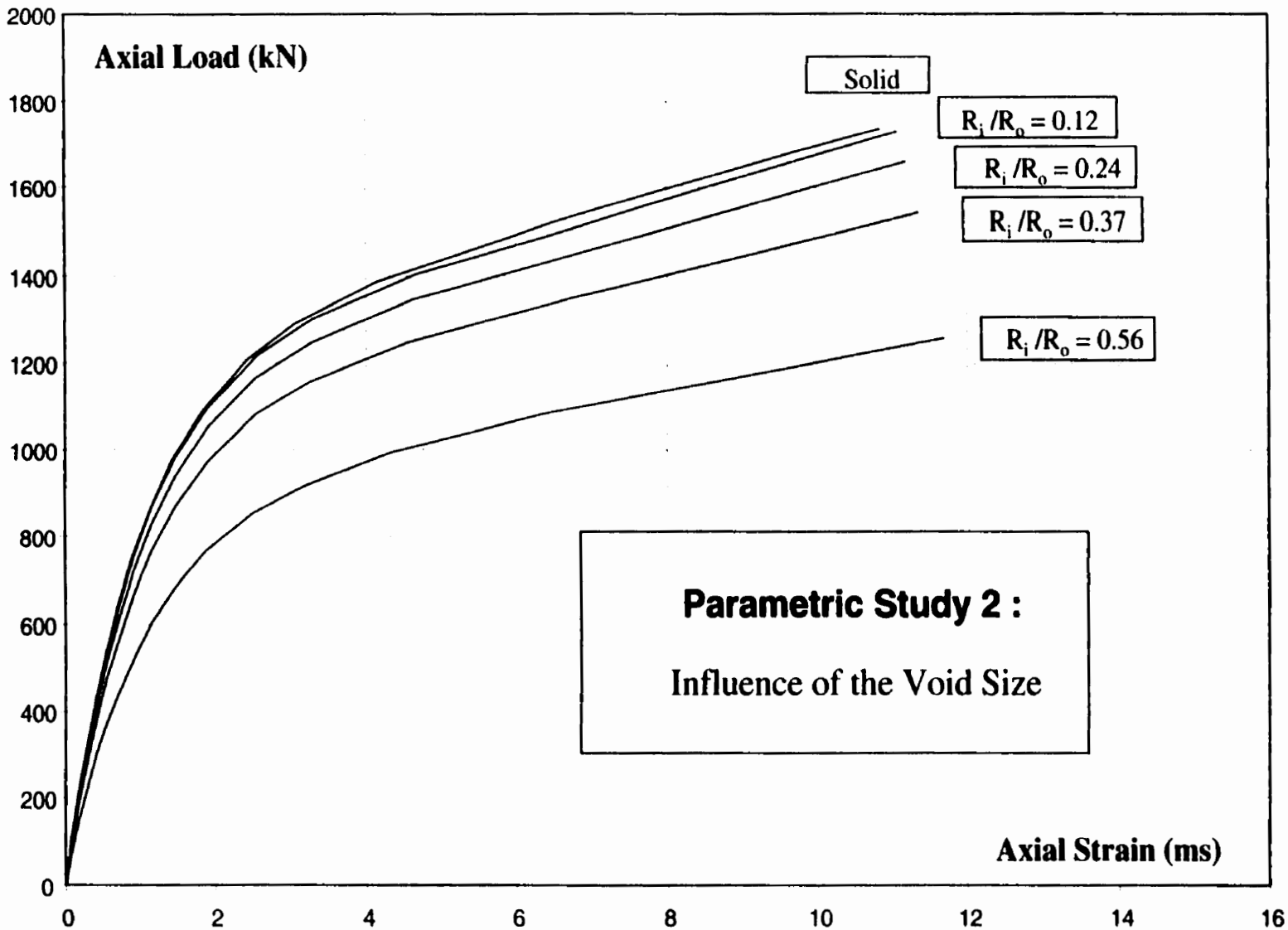

Fig. VII - 3 : Load vs. axial concrete strain for cylinders with different void sizes

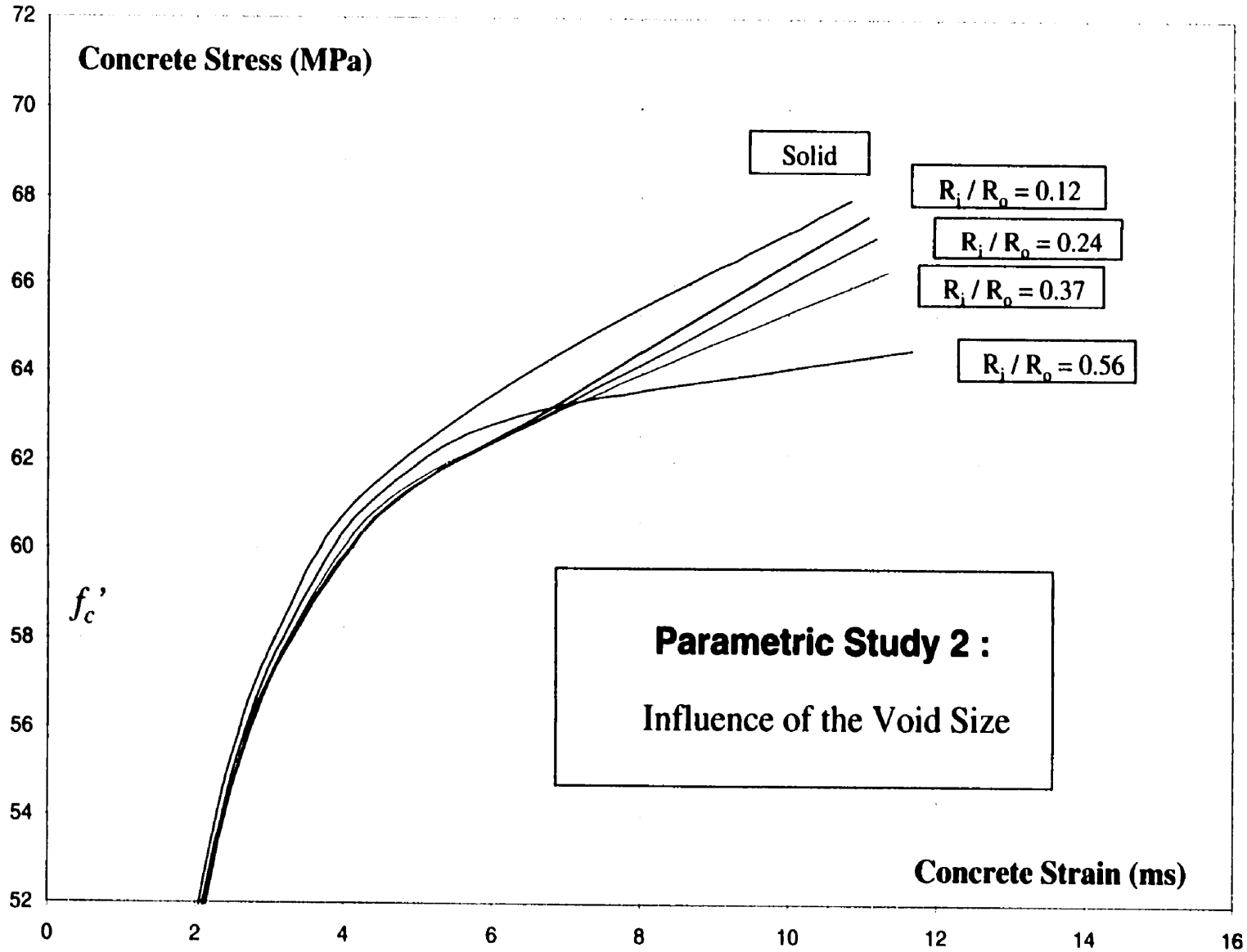

Fig. VII - 4 : Concrete stress-strain curve of cylinders with different void sizes

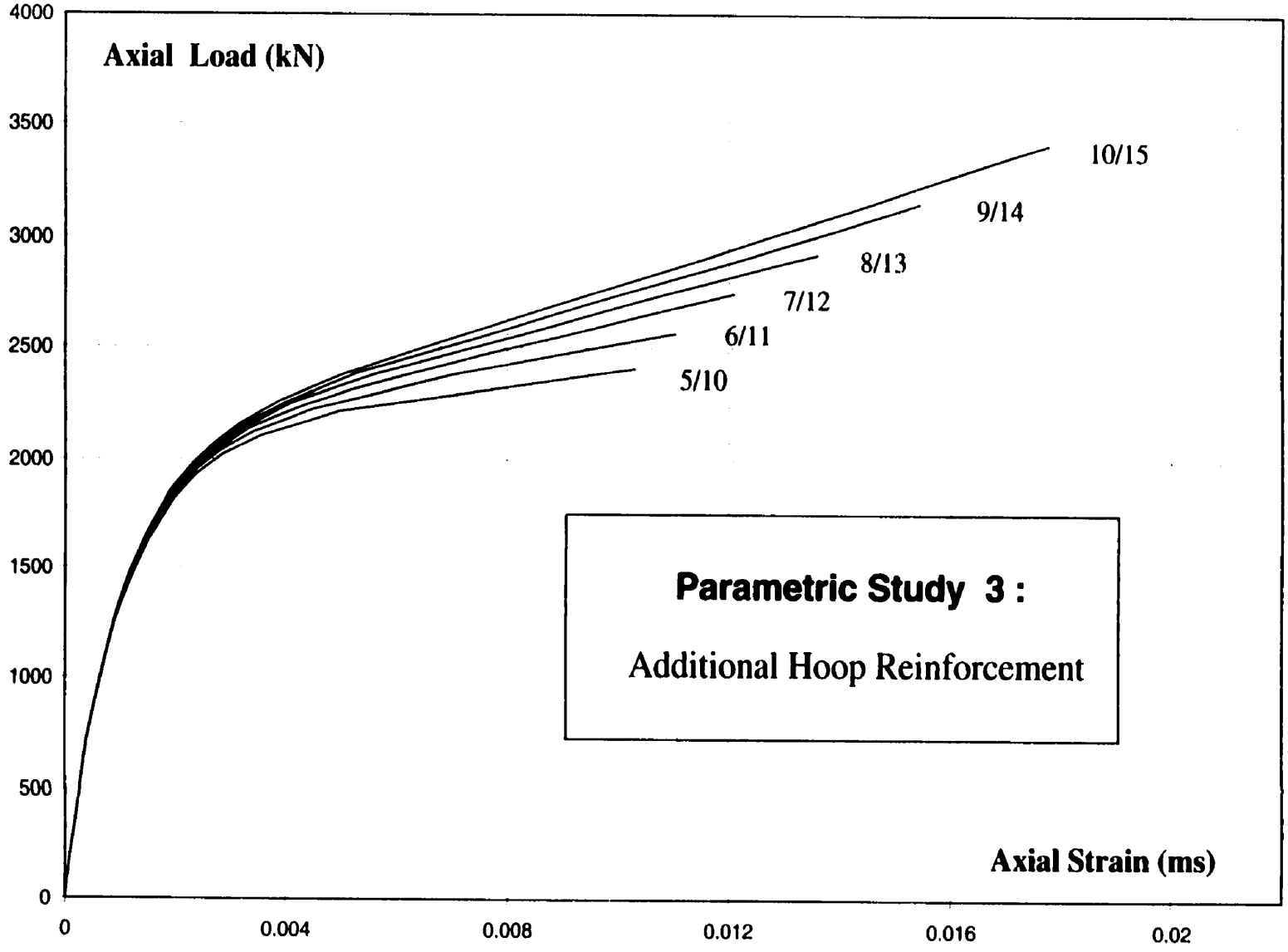

Fig. VII - 6 : Effect of additional layers of hoop fibers on the confinement

Chapter VIII :

Summary and Conclusions

Two analytical models are proposed for FRP/concrete hybrid columns in this thesis. The first model deals with the case where the load is applied only to the concrete core and the shell is used as a jacket to provide confinement. The proposed model is based on equilibrium and strain compatibility at the interface surface. The concrete is modeled using different triaxial constitutive relations presented in literature. The octahedral stress-strain relations presented by Gerstle are proven to be the most suitable ones to use. The model agreed very well with the experimental data, both for steel-confined and FRP-confined columns.

The second model, based on equilibrium and strain compatibility, is proposed for hybrid FRP/concrete columns for the case when the load is applied to both the concrete and the FRP shell. The triaxial state of stresses in the concrete is modeled using Gerstle's octahedral constitutive relations. Failure of the FRP shell under a biaxial stress state was

predicted by the Tsai-Wu quadratic failure criterion. The model was verified using an experimental program conducted at the University of Manitoba. Good to excellent agreement with the experimental data was obtained.

The model was modified to include hybrid sections with an inner void and hybrid sections with a double shell. This implied a study of the state of stresses, which is no longer uniform over the cross-section. Very good agreement with the experiment was obtained for the double shell. However, the confinement effect in the columns with an inner void was overestimated. This is due to Gerstle's assumption of totally ductile failure.

The proposed models were used to examine the key parameters believed to influence the behaviour, including the type of the shell material, the size of the inner void and the number of confining FRP layers. It was found that :

- FRP-confined concrete demonstrates a major gain in strength and ductility and, unlike steel-confined concrete, benefits from an ever-increasing confining pressure up to failure.

- the presence of an inner void reduces the confinement effect, but the effect of a small void is negligible.

- increasing the number of confining FRP layers greatly increases both the strength and the ultimate strain of the concrete core.

A finite element model is proposed, based on the Drucker-Prager criterion and the Tsai-Wu failure criterion. It is capable of predicting the behaviour of an FRP/concrete composite section, in the case where the shell is directly loaded and in the case where the shell is used as a confining jacket only. The model is not as accurate as the two proposed analytical models.

References

1. Ahmad, S. H., *Properties of Confined Concrete under Static and Dynamic Loads.* Ph.D. thesis, 1980, University of Illinois, Chicago
2. Ahmad, S. H., and Shah, S. P., *Complete Triaxial Stress-Strain Curves for Concrete* Proceedings of the ASCE, Vol. 108, April 1982 ; pp.728- 742
3. Argyris, J. H., Krempl, E. and William K. J., *Constitutive Models and Finite Element Solution of Inelastic Behaviour.* United States-German Symposium on Formulations and Computational Algorithms in FE Analysis, Aug. 1976, MIT, Boston
4. Cedolin, L., Crutzen, Y. R. J., and Dei Poli, S., *Triaxial Stress-Strain Relationship for Concrete* ; ASCE Proceedings Jun 1977 ; pp. 423-439
5. Darwin D. and Pecknold, D., *Nonlinear Biaxial Law for Concrete.* Journal of the Engineering Mechanics Division, ASCE, Vol. 103, April 1977, pp. 229-241
6. Elwi, A. A., and Murray, D. W., *A 3D Hypoelastic Concrete Constitutive Relationship* ; Proceedings of the ASCE, Vol. 105, August 1979 ; pp. 623-641
7. Gerstle, K. H., et al., *Strength of Concrete under Multiaxial Stress States* ; Douglas McHenry International Symposium on Concrete and Concrete Structures ; American Concrete Institute, Detroit, 1978, pp. 103-131
8. Gerstle, K. H., *Behaviour of Concrete under Multiaxial Stress States* ; ASCE Proceedings Dec 1980 ; pp. 1383-1403
9. Gerstle, K. H., *Simple Formulation of Biaxial Concrete Behaviour* ; ACI Journal Jan-Feb 1981; pp. 62-68

10. Gerstle, K. H., *Simple Formulation of Triaxial Concrete Behaviour* ; ACI Journal Sep-Oct 1981; pp.382-387

11. Hognestad, E., *A Study of Combined Bending and Axial Load in Reinforced Concrete Members*. Bulletin Series No. 399, University of Illinois, Nov. 1951

12. Kotsovos, M. D., and Newman, J. B., *Generalized Stress-Strain Relations for Concrete* ; ASCE Proceedings Aug 1978 ; pp. 845-856

13. Kupfer, H., Hilsdorf, H. K., and Rush, H., *Behavior of Concrete under Biaxial Stresses* ; ACI Journal Aug 1969 ; pp. 656-666

14. Mander, J. B., Priestley, M., and Park, R., *Theoretical Stress-Strain Model for Confined Concrete*. J. Struct. Eng., ASCE, 114(8), 1988, pp. 1804-1826

15. Mills, L. L., and Zimmerman, R. M., Compressive Strength of Plain Concrete Under Multiaxial Loading Conditions, Proceedings ACI, Vol. 68, No. 4, April 1971, pp. 300-303

16. Mirmiran, A., and Shahawy, M., *Behaviour of Concrete Columns Confined by Fiber Composites* ; Journal of Structural Engineering ; May 1997 ; pp. 583-590

17. Nanni, A., and Bradford, N. M., *FRP jacketed concrete under uniaxial compression,* Construction and Building Materials, 1995, 9(2), 115-124

18. Orito, Y., Sato, T., Tanaka, N., and Watanabe, Y., *Study on the unbounded steel tube structure*. Proc. Int. Conference on Composite Structures in Steel and Concrete, ASCE, 1987, pp. 786-804

19. Parent S., and Labossiere, P., *Finite Element Analysis of Reinforced Concrete Columns Confined with Composite Materials* ; M. Sc. thesis ; Universite de Sherbrooke

20. Popovics, S. , *Analytical Approach to Complete Stress-Strain Curves.* Cement and Concrete Res., 3(5), 1973, pp. 583-599

21. Purba, B. K., and Mufti, A. A., *Reinforcement of Circular Concrete Columns with Carbon Fiber Reinforced Polymer Jackets* ; Nova Scotia CAD/CAM Centre

22. Razvi, S., and Saatcioglu, M., *Confinement Model for High-Strength Concrete* ; Journal of Structural Engineering, March 1999 ; pp. 281-289

23. Richart, F. E., Brandtzaeg, A., and Brown, R. L., *A Study of the Failure of Concrete under Combined Compressive Stresses.* Bulletin No. 185, 1928, University of Illinois

24. Saatcioglu, M., and Razvi, S. R., *Strength and Ductility of Confined Concrete* ; Journal of Structural Engineering, Vol. 118, June 1992 ; pp. 1590-1607

25. Saenz, L. P., *Equation for the Stress-Strain Curve of Concrete.* Journal of the American Concrete Institute, Vol. 61, Sept. 1964, pp. 1229-1235

26. Samaan, M., Mirmiran, A., and Shahawy, M., *Model of Concrete Confined by Fiber Composites* ; Journal of Structural Engineering ; September 1998 ; pp. 1025-1032

27. Spoelstra, M. R., and Monti, G., *FRP-Confined Concrete Model* ; Journal of Composites for Construction ; August 1999 ; pp. 143-150

28. Tomii, M., Yan, X., and Sakino, K., *Experimental Study on the Properties of Concrete Confined in Circular Steel Tubes* ; Proceedings of the International Conference on Concrete Filled Steel Tubular Structures. 1988, China

29. Tomii, M., Yoshimura, K., and Morishita, Y., *Experimental Studies on Concrete Filled Steel Tubular Stub Columns under Concentric Loads.* International Colloquium on Stability of Structures under Static and Dynamic Loads, May 17-19, 1977, Washington D.C.

30. Tsai, S.W. and Wu, E.M., *A General Theory of Strength for Anisotropic Materials.* Journal of Composite Materials, Vol. 5, Jan 1971, pp. 58-80

Appendix

Calculation Examples

Octahedral theory / Gerstle

Modeling of a Test by Orito (1987) involving a Steel-Confined Concrete Cylinder under Compression

LABELS							
	R	57.15					
	t	5.2					
	E	200000					
STRESS							
	$\Delta\sigma 1$	10	10	10	10	10	10
	$\Delta\sigma 2$	0.77	1.29	1.84	2.36	2.24	3.22
	$\Delta\sigma 3$	0.77	1.29	1.84	2.36	2.24	3.22
	$\sigma 1$	10	20	30	40	50	60
	$\sigma 2$	0.77	2.06	3.9	6.26	8.5	11.72
	$\Delta\tau o$	3.846667	4.193333	4.56	4.906667	4.826667	5.48
	$\Delta\tau o$	4.351064	4.105933	3.846661	3.601531	3.658099	3.196123
	σo	3.846667	8.04	12.6	17.50667	22.33333	27.81333
	τo	4.351064	8.456997	12.30366	15.90519	19.56329	22.75941
CONST							
	K	18111.11	18111.11	18111.11	18111.11	18111.11	18111.11
	$\tau o,max$	15.60948	18.40224	21.4392	24.70704	27.9216	31.57128
	G	13583.33	9797.048	7340.93	5788.048	4839.045	4066.162
STRAIN							
	$\Delta\varepsilon o$	7.08E-05	7.72E-05	8.39E-05	9.03E-05	8.88E-05	0.000101
	$\Delta\gamma o$	0.00016	0.00021	0.000262	0.000311	0.000378	0.000393
	B	-0.5	-0.5	-0.5	-0.5	-0.5	-0.5
	C	1.414214	1.414214	1.414214	1.414214	1.414214	1.414214
	$\Delta\varepsilon 1$	0.000297	0.000374	0.000454	0.00053	0.000623	0.000657
	$\Delta\varepsilon 2$	-4.25E-05	-7.1E-05	-0.000101	-0.00013	-0.000178	-0.000177
	$\Delta\varepsilon 3$	-4.25E-05	-7.1E-05	-0.000101	-0.00013	-0.000178	-0.000177
	$\Delta\sigma 2'$	0.772566	1.291965	1.844089	2.360005	3.247129	3.221806
	$\varepsilon 1$	0.000297	0.000671	0.001125	0.001656	0.002279	0.002936
	$\varepsilon 2$	-4.25E-05	-0.000113	-0.000215	-0.000344	-0.000523	-0.0007
	εv	0.000212	0.000444	0.000696	0.000967	0.001233	0.001536

10	10	10	10	10	10	2.9	10
3.4	3.52	3.59	3.64	3.67	3.69	1.07	0
3.4	3.52	3.59	3.64	3.67	3.69	1.07	0
70	80	90	100	110	120	122.9	132.9
15.12	18.64	22.23	25.87	29.54	33.23	34.3	34.3
5.6	5.68	5.726667	5.76	5.78	5.793333	1.68	3.333333
3.11127	3.054701	3.021703	2.998133	2.983991	2.974563	0.86267	4.714045
33.41333	39.09333	44.82	50.58	56.36	62.15333	63.83333	67.16667
25.87068	28.92538	31.94708	34.94522	37.92921	40.90377	41.76644	46.48049
18111.11	18111.11	18111.11	18111.11	18111.11	18111.11	18111.11	18111.11
35.30088	39.08376	42.89772	46.73388	50.58336	54.44172	55.5606	57.7806
3791.248	3628.622	3530.485	3467.46	3426.408	3398.065	3377.749	3372.366
0.000103	0.000105	0.000105	0.000106	0.000106	0.000107	3.09E-05	6.13E-05
0.00041	0.000421	0.000428	0.000432	0.000435	0.000438	0.000128	0.000699
-0.5	-0.5	-0.5	-0.5	-0.5	-0.5	-0.5	-0.5
1.414214	1.414214	1.414214	1.414214	1.414214	1.414214	1.414214	1.414214
0.000683	0.0007	0.000711	0.000717	0.000722	0.000726	0.000212	0.00105
-0.000187	-0.000193	-0.000197	-0.0002	-0.000202	-0.000203	-5.94E-05	-0.000433
-0.000187	-0.000193	-0.000197	-0.0002	-0.000202	-0.000203	-5.94E-05	-0.000433
3.404329	3.513867	3.588657	3.633849	3.667247	3.691664	1.080518	7.877126
0.003619	0.004319	0.005029	0.005747	0.006469	0.007195	0.007406	0.008456
-0.000887	-0.00108	-0.001277	-0.001477	-0.001679	-0.001881	-0.001941	-0.002374
0.001845	0.002159	0.002475	0.002793	0.003112	0.003432	0.003525	0.003709

10	10	10	10	5.3	Δσ1
0	0	0	0	0	Δσ2
0	0	0	0	0	Δσ3
142.9	152.9	162.9	172.9	178.2	σ1
34.3	34.3	34.3	34.3	34.3	σ2
3.333333	3.333333	3.333333	3.333333	1.766667	Δσo
4.714045	4.714045	4.714045	4.714045	2.498444	Δτo
70.5	73.83333	77.16667	80.5	82.26667	σo
51.19453	55.90858	60.62262	65.33667	67.83511	τo
18111.11	18111.11	18111.11	18111.11	18111.11	*K*
60.0006	62.2206	64.4406	66.6606	67.8372	τou
2656.484	1993.576	1377.973	804.7857	269.776	*G*
6.13E-05	6.13E-05	6.13E-05	6.13E-05	3.25E-05	Δεo
0.000887	0.001182	0.00171	0.002929	0.004631	Δγo
-0.5	-0.5	-0.5	-0.5	-0.5	B
1.414214	1.414214	1.414214	1.414214	1.414214	C
0.001316	0.001733	0.00248	0.004203	0.006581	Δε1
-0.000566	-0.000775	-0.001148	-0.00201	-0.003242	Δε2
-0.000566	-0.000775	-0.001148	-0.00201	-0.003242	Δε3
10.30075	14.09721	20.89383	36.57006	58.9935	Δσ2'
0.009772	0.011505	0.013986	0.018189	0.02477	ε1
-0.00294	-0.003714	-0.004863	-0.006872	-0.010114	ε2
0.003893	0.004077	0.004261	0.004445	0.004542	εv

Octahedral theory / Kotsovos and Newman

Modeling of a Test by Orito (1987) involving a Steel-Confined Concrete Cylinder under Compression

LABELS							
	R	57.14					
	t	5.2					
	E	200000					
STRESS							
	Δσ1	10	10	10	10	10	10
	Δσ2	0.77	0.91	1.25	1.67	2.11	2.54
	Δσ3	0.77	0.91	1.25	1.67	2.11	2.54
	σ1	10	20	30	40	50	60
	σ2	0.77	1.68	2.93	4.6	6.71	9.25
	Δσo	3.846667	3.94	4.166667	4.446667	4.74	5.026667
	Δτo	4.351064	4.285067	4.12479	3.9268	3.719382	3.516678
	σo	3.846667	7.786667	11.95333	16.4	21.14	26.16667
	τo	4.351064	8.636131	12.76092	16.68772	20.4071	23.92378
CONST							
	K	18097.22	17029.87	15942.1	14886.47	13873.33	12912.48
	τou	15.60948	18.23352	21.00852	23.97	27.12684	30.4746
	G	13572.92	11905.23	9365.358	7248.576	5710.834	4619.517
STRAIN							
	Δεo	7.09E-05	7.71E-05	8.71E-05	9.96E-05	0.000114	0.00013
	Δγo	0.00016	0.00018	0.00022	0.000271	0.000326	0.000381
	B	-0.5	-0.5	-0.5	-0.5	-0.5	-0.5
	C	1.414214	1.414214	1.414214	1.414214	1.414214	1.414214
	Δε1	0.000298	0.000332	0.000399	0.000483	0.000574	0.000668
	Δε2	-4.25E-05	-5.01E-05	-6.86E-05	-9.2E-05	-0.000116	-0.000139
	Δε3	-4.25E-05	-5.01E-05	-6.86E-05	-9.2E-05	-0.000116	-0.000139
	Δσ2'	0.773159	0.912353	1.248271	1.673525	2.117787	2.536498
	ε1	0.000298	0.000629	0.001028	0.00151	0.002085	0.002753
	ε2	-4.25E-05	-9.26E-05	-0.000161	-0.000253	-0.00037	-0.000509
	εv	0.000213	0.000444	0.000705	0.001004	0.001346	0.001735

10	10	10	10	10	10	6.7	10
2.93	3.27	3.58	3.85	4.1	4.3	3.02	0
2.93	3.27	3.58	3.85	4.1	4.3	3.02	0
70	80	90	100	110	120	126.7	136.7
12.18	15.45	19.03	22.88	26.98	31.28	34.3	34.28
5.286667	5.513333	5.72	5.9	6.066667	6.2	4.246667	3.333333
3.33283	3.172552	3.026417	2.899138	2.781287	2.687006	1.734769	4.714045
31.45333	36.96667	42.68667	48.58667	54.65333	60.85333	65.1	68.43333
27.25661	30.42916	33.45558	36.35472	39.136	41.82301	43.55778	48.28125
12011.65	11176.86	10410.54	9710.287	9073.027	8493.48	7968.043	7641.698
33.99552	37.6674	41.47692	45.40632	49.44672	53.57592	56.4042	58.6242
3834.537	3254.862	2814.454	2471.771	2198.866	1977.604	1794.408	1689.528
0.000147	0.000164	0.000183	0.000203	0.000223	0.000243	0.000178	0.000145
0.000435	0.000487	0.000538	0.000586	0.000632	0.000679	0.000483	0.001395
-0.5	-0.5	-0.5	-0.5	-0.5	-0.5	-0.5	-0.5
1.414214	1.414214	1.414214	1.414214	1.414214	1.414214	1.414214	1.414214
0.000761	0.000854	0.000944	0.001032	0.001117	0.001204	0.000861	0.002118
-0.000161	-0.00018	-0.000197	-0.000212	-0.000224	-0.000237	-0.000164	-0.000841
-0.000161	-0.00018	-0.000197	-0.000212	-0.000224	-0.000237	-0.000164	-0.000841
2.922289	3.278968	3.585545	3.860613	4.082065	4.313868	2.987129	-
0.003514	0.004368	0.005311	0.006343	0.00746	0.008665	0.009526	0.011644
-0.00067	-0.00085	-0.001047	-0.001259	-0.001483	-0.00172	-0.001884	-0.002725
0.002175	0.002668	0.003218	0.003825	0.004494	0.005224	0.005757	0.006193

10	10	10	10	1.4	Δσ1
0	0	0	0	0	Δσ2
0	0	0	0	0	Δσ3
146.7	156.7	166.7	176.7	178.1	σ1
34.28	34.28	34.28	34.28	34.28	σ2
3.333333	3.333333	3.333333	3.333333	0.466667	Δσo
4.714045	4.714045	4.714045	4.714045	0.659966	Δτo
71.76667	75.1	78.43333	81.76667	82.23333	σo
52.9953	57.70934	62.42339	67.13743	67.7974	τo
7402.466	7176.801	6963.624	6761.966	6570.949	*K*
60.8442	63.0642	65.2842	67.5042	67.815	τou
1447.177	1254.809	1099.288	971.7555	865.8491	*G*
0.00015	0.000155	0.00016	0.000164	2.37E-05	Δεo
0.001629	0.001878	0.002144	0.002426	0.000381	Δγo
-0.5	-0.5	-0.5	-0.5	-0.5	B
1.414214	1.414214	1.414214	1.414214	1.414214	C
0.002453	0.002811	0.003192	0.003595	0.000563	Δε1
-0.001002	-0.001173	-0.001357	-0.001551	-0.000246	Δε2
-0.001002	-0.001173	-0.001357	-0.001551	-0.000246	Δε3
-	-	-	-	-	Δσ2'
0.014098	0.016909	0.020101	0.023695	0.024258	ε1
-0.003727	-0.0049	-0.006257	-0.007808	-0.008054	ε2
0.006643	0.007108	0.007587	0.00808	0.008151	εv

Octahedral theory / Cedolin

Modeling of a Test by Orito (1987) involving a Steel-Confined Concrete Cylinder under Compression

LABELS								
	R	57.15						
	t	5.2						
	E	200000						
STRESS								
	Δσ1	10	10	10	10	10	10	10
	Δσ2	0.77	0.97	1.26	1.67	2.3	3.26	4.67
	Δσ3	0.77	0.97	1.26	1.67	2.3	3.26	4.67
	σ1	10	20	30	40	50	60	70
	σ2	0.77	1.74	3	4.67	6.97	10.23	14.9
	Δσo	3.84667	3.98	4.17333	4.44667	4.86667	5.50667	6.44667
	Δτo	4.35106	4.25678	4.12008	3.9268	3.62981	3.17727	2.51259
	σo	3.84667	7.82667	12	16.4467	21.3133	26.82	33.2667
	τo	4.35106	8.60785	12.7279	16.6547	20.2845	23.4618	25.9744
CONST								
	K	18111.1	16733.5	15301.2	13792.5	12178.9	10410.5	8417.94
	τo,max	8.21774	11.5729	15.091	18.8395	22.9421	27.5843	33.0188
	G	13583.3	11315.4	9096.9	6959.24	4950.29	3158.96	1734.54
STRAIN								
	εo	7.1E-05	0.00015	0.00024	0.00035	0.00048	0.00066	0.00091
	Δεo	7.1E-05	7.9E-05	9.1E-05	0.00011	0.00013	0.00018	0.00026
	Δγo	0.00016	0.00019	0.00023	0.00028	0.00037	0.0005	0.00072
	γo	0.00016	0.00035	0.00057	0.00086	0.00122	0.00173	0.00245
	B	-0.5	-0.5	-0.5	-0.5	-0.5	-0.5	-0.5
	C	1.41421	1.41421	1.41421	1.41421	1.41421	1.41421	1.41421
	Δε1	0.0003	0.00035	0.00041	0.00051	0.00065	0.00089	0.00128
	Δε2	-4.2E-05	-5.4E-05	-6.9E-05	-9.2E-05	-0.00013	-0.00018	-0.00026
	Δε3	-4.2E-05	-5.4E-05	-6.9E-05	-9.2E-05	-0.00013	-0.00018	-0.00026
	Δσ2'	0.77257	0.97763	1.25952	1.67472	2.29373	3.26257	4.67442
	ε1	0.0003	0.00064	0.00105	0.00156	0.00221	0.0031	0.00438
	ε2	-4.2E-05	-9.6E-05	-0.00017	-0.00026	-0.00038	-0.00056	-0.00082
	εv	0.00021	0.00045	0.00072	0.00105	0.00144	0.00197	0.00274

10	10	5	5	5	5	5	5	2.12
6.03	5.45	1.643	0.578	0.388	1.1	1.556	1.816	0.839
6.03	5.45	1.643	0.578	0.388	1.1	1.556	1.816	0.839
80	90	95	100	105	110	115	120	122.12
20.93	26.38	28.023	28.601	28.989	30.089	31.645	33.461	34.3
7.35333	6.96667	2.762	2.052	1.92533	2.4	2.704	2.87733	1.266
1.87148	2.14489	1.5825	2.08455	2.17412	1.83848	1.62352	1.50095	0.60387
40.62	47.5867	50.3487	52.4007	54.326	56.726	59.43	62.3073	63.5733
27.8459	29.9908	31.5733	33.6578	35.8319	37.6704	39.2939	40.7949	41.3987
6126.99	3636.25	1529.98	777.373	690.109	1075.66	1443.45	1722.93	1934.93
39.2177	45.0906	47.4189	49.1488	50.7718	52.795	55.0745	57.5001	58.5673
904.152	808.245	808.245	808.245	808.245	808.245	808.245	808.245	808.245
0.00131	0.00195	0.00255	0.00343	0.00436	0.00511	0.00573	0.00629	0.00651
0.0004	0.00064	0.0006	0.00088	0.00093	0.00074	0.00062	0.00056	0.00022
0.00103	0.00133	0.00098	0.00129	0.00134	0.00114	0.001	0.00093	0.00037
0.00349	0.00481	0.00579	0.00708	0.00843	0.00956	0.01057	0.0115	0.01187
-0.5	-0.5	-0.5	-0.5	-0.5	-0.5	-0.5	-0.5	-0.5
1.41421	1.41421	1.41421	1.41421	1.41421	1.41421	1.41421	1.41421	1.41421
0.00186	0.00252	0.00199	0.0027	0.00283	0.00235	0.00204	0.00187	0.00075
-0.00033	-0.0003	-9E-05	-3.2E-05	-2.1E-05	-6E-05	-8.6E-05	-1E-04	-4.6E-05
-0.00033	-0.0003	-9E-05	-3.2E-05	-2.1E-05	-6E-05	-8.6E-05	-1E-04	-4.6E-05
6.03724	5.45234	1.64668	0.58171	0.38335	1.10058	1.56044	1.81783	0.83813
0.00624	0.00876	0.01074	0.01345	0.01628	0.01863	0.02068	0.02255	0.02329
-0.00115	-0.00145	-0.00154	-0.00157	-0.00159	-0.00165	-0.00174	-0.00184	-0.00189
0.00394	0.00586	0.00766	0.0103	0.01309	0.01532	0.0172	0.01887	0.01952

10	10	10	10	5	5	6.08	Δσ1
0	0	0	0	0	0	0	Δσ2
0	0	0	0	0	0	0	Δσ3
132.12	142.12	152.12	162.12	167.12	172.12	178.2	σ1
34.3	34.3	34.3	34.3	34.3	34.3	34.3	σ2
3.33333	3.33333	3.33333	3.33333	1.66667	1.66667	2.02667	Δσο
4.71405	4.71405	4.71405	4.71405	2.35702	2.35702	2.86614	Δτο
66.9067	70.24	73.5733	76.9067	78.5733	80.24	82.2667	σο
46.1128	50.8268	55.5409	60.2549	62.6119	64.969	67.8351	το
2007.86	2168.37	2288.27	2379.85	2450.79	2480.02	2505.96	*K*
61.3773	64.1873	66.9973	69.8073	71.2123	72.6173	74.3258	το,max
808.245	808.245	808.245	808.245	808.245	808.245	808.245	*G*
0.00706	0.00757	0.00806	0.00852	0.00875	0.00898	0.00924	εο
0.00055	0.00051	0.00049	0.00047	0.00023	0.00022	0.00027	Δεο
0.00292	0.00292	0.00292	0.00292	0.00146	0.00146	0.00177	Δγο
0.01479	0.0177	0.02062	0.02353	0.02499	0.02645	0.02822	γο
-0.5	-0.5	-0.5	-0.5	-0.5	-0.5	-0.5	B
1.41421	1.41421	1.41421	1.41421	1.41421	1.41421	1.41421	C
0.00468	0.00464	0.00461	0.00459	0.00229	0.00229	0.00278	Δε1
-0.00151	-0.00155	-0.00158	-0.0016	-0.0008	-0.00081	-0.00098	Δε2
-0.00151	-0.00155	-0.00158	-0.0016	-0.0008	-0.00081	-0.00098	Δε3
27.4549	28.2003	28.6889	29.029	14.6375	14.6861	17.9096	Δσ2'
0.02797	0.03261	0.03722	0.04181	0.0441	0.04638	0.04916	ε1
-0.0034	-0.00495	-0.00652	-0.00812	-0.00892	-0.00973	-0.01071	ε2
0.02118	0.02272	0.02417	0.02557	0.02625	0.02693	0.02773	εv

Ahmed and Shah

Modeling of a Test by Orito on a Steel-Concrete Column

ε1a	-0.037443	-0.061282	-0.090714	-0.126481	-0.169901	-0.222916	-0.288325
ε1b	0.000539	0.001026	0.001479	0.001917	0.002346	0.002771	0.003191
ε1p	0.006276	0.008073	0.009871	0.011669	0.013466	0.015264	0.017061
a	-0.530186	-0.436457	-0.369365	-0.318055	-0.27631	-0.240782	-0.209558
b	-3.117557	-3.257492	-3.339078	-3.395278	-3.438047	-3.472768	-3.502227
c	0.271906	0.420947	0.508733	0.566442	0.607453	0.638274	0.662427
Y	0.271906	0.420947	0.508733	0.566442	0.607453	0.638274	0.662427
X1a	0.085961	0.127061	0.149873	0.164303	0.174245	0.18151	0.187051
X1b	-5.966076	-7.590542	-9.18992	-10.83943	-12.61696	-14.60439	-16.89947
ε2	-0.0001	-0.0002	-0.0003	-0.0004	-0.0005	-0.0006	-0.0007
ε2p	-0.00081	-0.001326	-0.001842	-0.002357	-0.002873	-0.003389	-0.003905
X2	0.123449	0.150847	0.162899	0.169676	0.174021	0.177042	0.179266
γo,o	0.003912	0.003912	0.003912	0.003912	0.003912	0.003912	0.003912
εo,o	0.007622	0.007622	0.007622	0.007622	0.007622	0.007622	0.007622
γo,u	0.006681	0.008862	0.011043	0.013224	0.015405	0.017586	0.019767
εo,u	0.001552	0.001807	0.002063	0.002318	0.002573	0.002829	0.003084
τo,u	26.99205	29.28251	31.57297	33.86342	36.15388	38.44434	40.73479
σo,u	20.90604	24.34541	27.78478	31.22415	34.66352	38.10289	41.54226
E1	33275.91	33977.3	34678.68	35380.06	36081.45	36782.83	37484.22
E2	166379.6	169886.5	173393.4	176900.3	180407.2	183914.2	187421.1
E1p	9413.517	8144.837	7338.219	6780.12	6371.019	6058.274	5811.43
E2p	72932.1	49596.48	39332.24	33559.53	29859.43	27285.6	25391.74
A1	3.534908	4.171636	4.725763	5.218206	5.663372	6.071503	6.450085
A2	2.281294	3.425374	4.408429	5.271239	6.041886	6.740338	7.381184
D1	2.101632	2.480703	2.787414	3.040091	3.251352	3.430172	3.583105
D2	1.348532	1.328363	1.283557	1.220354	1.143049	1.054699	0.957535
σ2	1.819773	3.639545	5.459318	7.27909	9.098863	10.91864	12.73841
σp	59.07857	65.75713	72.4357	79.11426	85.79283	92.47139	99.14996
σ1	16.0638	27.68029	36.85041	44.81365	52.11507	59.0221	65.67964
ε1	0.000539	0.001026	0.001479	0.001917	0.002346	0.002771	0.003191
ε2	-0.0001	-0.0002	-0.0003	-0.0004	-0.0005	-0.0006	-0.0007
εv	0.000339	0.000626	0.000879	0.001117	0.001346	0.001571	0.001791

-0.3702	-0.4749	-0.6121	-1.0647	-2.1687	-8.4437	4.50491	1.438	0.37406
0.00361	0.00403	0.00444	0.00527	0.0061	0.00693	0.0081	0.00854	0.01043
0.01886	0.02066	0.02245	0.02605	0.02964	0.03324	0.03836	0.03836	0.03836
-0.1815	-0.1558	-0.132	-0.0888	-0.0499	-0.0145	0.03154	0.0954	0.31944
-3.528	-3.5511	-3.5721	-3.6096	-3.6426	-3.6723	-3.7104	-3.5975	-3.2019
0.68198	0.69821	0.71197	0.73422	0.75164	0.76582	0.78222	0.79658	0.84696
0.68198	0.69821	0.71197	0.73422	0.75164	0.76582	0.78222	0.79658	0.84696
0.19142	0.19495	0.19787	0.2024	0.20577	0.20837	0.2112	0.22274	0.2719
-19.632	-22.989	-27.262	-40.873	-73.157	-254.03	117.431	37.4876	9.75147
-0.0008	-0.0009	-0.001	-0.0012	-0.0014	-0.0016	-0.0019	-0.002	-0.0025
-0.0044	-0.0049	-0.0055	-0.0065	-0.0075	-0.0085	-0.01	-0.01	-0.01
0.18097	0.18232	0.18341	0.18508	0.18628	0.1872	0.18818	0.19968	0.2496
0.00391	0.00391	0.00391	0.00391	0.00391	0.00391	0.00391	0.00391	0.00391
0.00762	0.00762	0.00762	0.00762	0.00762	0.00762	0.00762	0.00762	0.00762
0.02195	0.02413	0.02631	0.03067	0.03503	0.0394	0.04561	0.04561	0.04561
0.00334	0.00359	0.00385	0.00436	0.00487	0.00538	0.00611	0.00611	0.00611
43.0253	45.3157	47.6062	52.1871	56.768	61.3489	67.8767	67.8733	67.8733
44.9816	48.421	51.8604	58.7391	65.6178	72.4966	82.2988	82.2937	82.2937
38185.6	38887	39588.4	40991.1	42393.9	43796.7	45795.6	45794.6	45794.6
190928	194435	197942	204956	211970	218983	228978	228973	228973
5611.64	5446.63	5308.03	5088.23	4921.73	4791.26	4647.58	4647.65	4647.65
23939.8	22791.3	21860.1	20442.2	19413.5	18633.2	17798.9	17799.3	17799.3
6.80471	7.13965	7.4582	8.05608	8.61361	9.14096	9.85365	9.85328	9.85328
7.97533	8.53109	9.05493	10.0261	10.9186	11.7523	12.8647	12.8642	12.8642
3.71505	3.82975	3.9301	4.09644	4.22743	4.33198	4.44699	4.44693	4.44693
0.85323	0.74304	0.62798	0.38614	0.13227	-0.1306	-0.5168	-0.5166	-0.5166
14.5582	16.378	18.1977	21.8373	25.4768	29.1164	34.3027	34.3	34.3
105.829	112.507	119.186	132.543	145.9	159.257	178.291	178.281	178.281
72.1725	78.5534	84.8566	97.3155	109.664	121.962	139.463	142.015	150.997
0.00361	0.00403	0.00444	0.00527	0.0061	0.00693	0.00775	0.00854	0.01043
-0.0008	-0.0009	-0.001	-0.0012	-0.0014	-0.0016	-0.0018	-0.002	-0.0025
0.00201	0.00223	0.00244	0.00287	0.0033	0.00373	0.00415	0.00454	0.00543

0.22006	0.158	0.12432	0.10308	0.08841	0.07763	0.06935	0.06278	0.05743
0.01227	0.01408	0.01587	0.01765	0.01942	0.0212	0.023	0.0248	0.02663
0.03836	0.03836	0.03836	0.03836	0.03836	0.03836	0.03836	0.03836	0.03836
0.48141	0.60236	0.69477	0.76652	0.82281	0.86724	0.90236	0.93003	0.95165
-2.9158	-2.7022	-2.539	-2.4123	-2.3129	-2.2345	-2.1724	-2.1236	-2.0854
0.88338	0.91058	0.93136	0.9475	0.96015	0.97015	0.97804	0.98427	0.98913
0.88338	0.91058	0.93136	0.9475	0.96015	0.97015	0.97804	0.98427	0.98913
0.31985	0.367	0.41364	0.46001	0.50633	0.55277	0.59948	0.64661	0.69429
5.73692	4.11903	3.24084	2.68712	2.30466	2.02373	1.80801	1.6367	1.49705
-0.003	-0.0035	-0.004	-0.0045	-0.005	-0.0055	-0.006	-0.0065	-0.007
-0.01	-0.01	-0.01	-0.01	-0.01	-0.01	-0.01	-0.01	-0.01
0.29951	0.34943	0.39935	0.44927	0.49919	0.54911	0.59903	0.64895	0.69887
0.00391	0.00391	0.00391	0.00391	0.00391	0.00391	0.00391	0.00391	0.00391
0.00762	0.00762	0.00762	0.00762	0.00762	0.00762	0.00762	0.00762	0.00762
0.04561	0.04561	0.04561	0.04561	0.04561	0.04561	0.04561	0.04561	0.04561
0.00611	0.00611	0.00611	0.00611	0.00611	0.00611	0.00611	0.00611	0.00611
67.8733	67.8733	67.8733	67.8733	67.8733	67.8733	67.8733	67.8733	67.8733
82.2937	82.2937	82.2937	82.2937	82.2937	82.2937	82.2937	82.2937	82.2937
45794.6	45794.6	45794.6	45794.6	45794.6	45794.6	45794.6	45794.6	45794.6
228973	228973	228973	228973	228973	228973	228973	228973	228973
4647.65	4647.65	4647.65	4647.65	4647.65	4647.65	4647.65	4647.65	4647.65
17799.3	17799.3	17799.3	17799.3	17799.3	17799.3	17799.3	17799.3	17799.3
9.85328	9.85328	9.85328	9.85328	9.85328	9.85328	9.85328	9.85328	9.85328
12.8642	12.8642	12.8642	12.8642	12.8642	12.8642	12.8642	12.8642	12.8642
4.44693	4.44693	4.44693	4.44693	4.44693	4.44693	4.44693	4.44693	4.44693
-0.5166	-0.5166	-0.5166	-0.5166	-0.5166	-0.5166	-0.5166	-0.5166	-0.5166
34.3	34.3	34.3	34.3	34.3	34.3	34.3	34.3	34.3
178.281	178.281	178.281	178.281	178.281	178.281	178.281	178.281	178.281
157.491	162.339	166.044	168.921	171.177	172.959	174.367	175.476	176.343
0.01227	0.01408	0.01587	0.01765	0.01942	0.0212	0.023	0.0248	0.02663
-0.003	-0.0035	-0.004	-0.0045	-0.005	-0.0055	-0.006	-0.0065	-0.007
0.00627	0.00708	0.00787	0.00865	0.00942	0.0102	0.011	0.0118	0.01263

0.05297	0.04919	0.04311	0.03843	0.06239	0.0683	0.09787
0.02849	0.03037	0.03425	0.03829	0.02493	0.02326	0.01821
0.03836	0.03836	0.03836	0.03836	0.03836	0.03836	0.03836
0.96827	0.98072	0.99558	1	0.93167	0.90684	0.78587
-2.056	-2.034	-2.0078	-2	-2.1207	-2.1645	-2.3781
0.99287	0.99567	0.999	1	0.98463	0.97905	0.95185
0.99287	0.99567	0.999	1	0.98463	0.97905	0.95185
0.74263	0.79175	0.89277	0.99825	0.6498	0.60635	0.47472
1.38077	1.28227	1.12397	1.00175	1.62642	1.78053	2.5514
-0.0075	-0.008	-0.009	-0.01	-0.015	-0.016	-0.02
-0.01	-0.01	-0.01	-0.01	-0.01	-0.01	-0.01
0.74879	0.79871	0.89854	0.99838	1.49757	1.59741	1.99677
0.00391	0.00391	0.00391	0.00391	0.00391	0.00391	0.00391
0.00762	0.00762	0.00762	0.00762	0.00762	0.00762	0.00762
0.04561	0.04561	0.04561	0.04561	0.04561	0.04561	0.04561
0.00611	0.00611	0.00611	0.00611	0.00611	0.00611	0.00611
67.8733	67.8733	67.8733	67.8733	67.8733	67.8733	67.8733
82.2937	82.2937	82.2937	82.2937	82.2937	82.2937	82.2937
45794.6	45794.6	45794.6	45794.6	45794.6	45794.6	45794.6
228973	228973	228973	228973	228973	228973	228973
4647.65	4647.65	4647.65	4647.65	4647.65	4647.65	4647.65
17799.3	17799.3	17799.3	17799.3	17799.3	17799.3	17799.3
9.85328	9.85328	9.85328	9.85328	9.85328	9.85328	9.85328
12.8642	12.8642	12.8642	12.8642	12.8642	12.8642	12.8642
4.44693	4.44693	4.44693	4.44693	4.44693	4.44693	4.44693
-0.5166	-0.5166	-0.5166	-0.5166	-0.5166	-0.5166	-0.5166
34.3	34.3	34.3	34.3	34.3	34.3	34.3
178.281	178.281	178.281	178.281	178.281	178.281	178.281
177.009	177.508	178.104	178.281	175.541	174.546	169.697
0.02849	0.03037	0.03425	0.03829	0.06239	0.0683	0.09787
-0.0075	-0.008	-0.009	-0.01	-0.015	-0.016	-0.02
0.01349	0.01437	0.01625	0.01829	0.03239	0.0363	0.05787

Elwi and Murray (a Hypoelastic Model)

Orito

Δσ1		10	10	10	10	10	10	10	10
Δσ2		0.77	0.81	0.82	0.85	0.926	1.11	1.48	2.146
σ1	0	10	20	30	40	50	60	70	80
σ2	0	0.77	1.58	2.4	3.25	4.176	5.286	6.766	8.912
ω1		12.987	12.658	12.5	12.308	11.973	11.351	10.346	8.9767
Δε1u		0.0003	0.0003	0.0003	0.0003	0.0003	0.0003	0.0004	0.0005
Δε2u		2E-05	2E-05	2E-05	2E-05	3E-05	4E-05	6E-05	0.0001
ε1u		0.0003	0.0006	0.0009	0.0012	0.0015	0.0018	0.0022	0.0027
ε2u		2E-05	5E-05	7E-05	9E-05	0.0001	0.0002	0.0002	0.0003
ω2		12.987	12.669	12.516	12.328	11.985	11.298	10.066	8.1853
φ		0.864	0.8358	0.8246	0.8157	0.7962	0.7496	0.6497	0.4735
φΔe1u		0.0003	0.0002	0.0002	0.0002	0.0002	0.0002	0.0003	0.0002
φΔε2u		2E-05	2E-05	2E-05	2E-05	2E-05	3E-05	4E-05	5E-05
$\phi B11$		0.96	0.9522	0.9492	0.9467	0.9415	0.9291	0.9033	0.8596
$2\phi B12$		0.48	0.5326	0.5528	0.5684	0.6013	0.6748	0.8126	1.0083
$\phi B21$		0.24	0.2663	0.2762	0.2839	0.3001	0.3369	0.4091	0.5263
$2\phi B22$		1.2	1.2185	1.2255	1.2308	1.2419	1.2663	1.311	1.3747
Δε1		0.0003	0.0003	0.0003	0.0003	0.0003	0.0003	0.0004	0.0004
Δε2		-4E-05	-4E-05	-5E-05	-5E-05	-5E-05	-6E-05	-8E-05	-0.0001
ε1	0	0.0003	0.0006	0.0008	0.0011	0.0014	0.0017	0.0021	0.0025
ε2	0	-4E-05	-9E-05	-0.0001	-0.0002	-0.0002	-0.0003	-0.0004	-0.0005
Δσ2'		0.7726	0.8096	0.8213	0.8474	0.9272	1.1077	1.4799	2.1465
A	0.249	0.249	0.249	0.249	0.249	0.249	0.249	0.249	0.249
B	0.666	0.666	0.666	0.666	0.666	0.666	0.666	0.666	0.666
σ1c		72.925	73.679	74.062	74.546	75.441	77.316	81.079	88.501
*Re*1		1.3687	1.3682	1.368	1.3678	1.3681	1.3717	1.39	1.4668
ε1u	0	0.0003	0.0006	0.0009	0.0012	0.0015	0.0018	0.0022	0.0027
ε1c		0.0031	0.0031	0.0031	0.0031	0.0032	0.0033	0.0035	0.004
ε1u/ε1c		0.1002	0.1919	0.2806	0.3689	0.4582	0.5472	0.6273	0.6666
*R*1		0.2062	0.2061	0.206	0.2059	0.206	0.2072	0.2133	0.2389
*E*1	32600	34894	35880	35504	33671	30351	25747	20583	16676
ν1	0.2	0.2185	0.2255	0.2308	0.2419	0.2663	0.311	0.3747	0.4158
σ2c		5.6152	5.8206	5.9249	6.0568	6.3009	6.8115	7.8369	9.859
*Re*2		1.3687	1.367	1.3662	1.3656	1.3667	1.3781	1.4286	1.6086
ε2u	0	2E-05	5E-05	7E-05	9E-05	0.0001	0.0002	0.0002	0.0003
ε2c		0.0002	0.0002	0.0002	0.0003	0.0003	0.0003	0.0003	0.0005
ε2u/ε2c		0.1002	0.1919	0.2806	0.3689	0.4582	0.5472	0.6273	0.6666
*R*2		0.2062	0.2057	0.2054	0.2052	0.2056	0.2094	0.2262	0.2862
*E*2	32600	34894	35901	35546	33733	30392	25571	19715	14387
ν2	0.2	0.2185	0.2255	0.2308	0.2419	0.2663	0.311	0.3747	0.4158
μ12	0.2	0.2185	0.2255	0.2308	0.2419	0.2663	0.311	0.3747	0.4158
μ23	0.2	0.2185	0.2255	0.2308	0.2419	0.2663	0.311	0.3747	0.4158

10	10	10	10	10	10	10	10	Δσ1
2.81	2.47	2.114	1.93	1.817	1.776	1.398	5.723	Δσ2
90	100	110	120	130	140	150	160	σ1
11.722	14.192	16.306	18.236	20.053	21.829	23.227	28.95	σ2
7.6779	7.0462	6.746	6.5804	6.4828	6.4135	6.458	5.5268	ω1
0.0006	0.0007	0.0008	0.0009	0.0013	0.002	0.0059	-0.0104	Δε1u
0.0002	0.0002	0.0002	0.0003	0.0004	0.0007	0.0021	-0.0088	Δε2u
0.0033	0.0039	0.0047	0.0056	0.0069	0.0089	0.0148	0.0044	ε1u
0.0005	0.0007	0.001	0.0013	0.0017	0.0024	0.0046	-0.0042	ε2u
6.2626	5.2694	4.7127	4.3169	3.9887	3.641	3.2374	-1.0488	ω2
0.3376	0.513	0.6608	0.7406	0.7916	0.8193	0.8782	7.4299	ϕ
0.0002	0.0003	0.0005	0.0007	0.001	0.0016	0.0052	-0.0775	ϕΔe1u
7E-05	0.0001	0.0002	0.0002	0.0003	0.0006	0.0019	-0.065	ϕΔε2u
0.8271	0.8692	0.9061	0.9268	0.9403	0.9477	0.964	-3.743	*B*11
1.0936	0.8401	0.6423	0.5274	0.4481	0.3963	0.2815	-4.2359	2*B*12
0.6338	0.5774	0.4989	0.4485	0.4129	0.3982	0.3625	-3.1067	*B*21
1.4158	1.3617	1.3064	1.2706	1.2444	1.2286	1.1899	-1.1778	2*B*22
0.0004	0.0005	0.0006	0.0008	0.0011	0.0018	0.0054	0.0211	Δε1
-0.0002	-0.0001	-0.0001	-0.0001	-1E-04	-1E-04	-8E-05	-0.0003	Δε2
0.0029	0.0034	0.0041	0.0049	0.006	0.0078	0.0132	0.0342	ε1
-0.0006	-0.0008	-0.0009	-0.001	-0.0011	-0.0012	-0.0013	-0.0016	ε2
2.8085	2.4676	2.1143	1.9399	1.8187	1.7758	1.4059	5.7048	Δσ2'
0.249	0.249	0.249	0.249	0.249	0.249	0.249	0.249	A
0.666	0.666	0.666	0.666	0.666	0.666	0.666	0.666	B
100.23	109.19	114.75	118.3	120.59	122.31	121.2	155.75	σ1c
1.7259	2.161	2.8213	4.0412	7.4403	-72.688	-4.4182	0.1022	*R*e1
0.0033	0.0039	0.0047	0.0056	0.0069	0.0089	0.0148	0.0044	ε1u
0.0053	0.0072	0.0099	0.0147	0.0275	-0.2727	-0.0164	0.0005	ε1c
0.6132	0.5399	0.4695	0.3819	0.2496	-0.0325	-0.9016	8.9776	ε1u/ε1c
0.3253	0.4703	0.6904	1.0971	2.2301	-24.479	-1.7227	-0.2159	*R*1
15288	13265	10650	7884.5	5000.5	1683.7	-959.12	1866.5	*E*1
0.3617	0.3064	0.2706	0.2444	0.2286	0.1899	-2.1778	1158.8	ν1
13.054	15.497	17.01	17.977	18.601	19.071	18.767	28.181	σ2c
2.116	2.8897	4.0385	6.1601	12.093	-128.04	-8.8134	-0.5384	*R*e2
0.0005	0.0007	0.001	0.0013	0.0017	0.0024	0.0046	-0.0042	ε2u
0.0008	0.0014	0.0021	0.0034	0.0069	-0.0749	-0.0051	-0.0005	ε2c
0.6132	0.5399	0.4695	0.3819	0.2496	-0.0325	-0.9016	8.9776	ε2u/ε2c
0.4553	0.7132	1.0962	1.8034	3.7809	-42.929	-3.1878	-0.4295	*R*2
11123	8539.2	6262.3	4277.8	2488.5	653.8	-653.86	442.67	*E*2
0.3617	0.3064	0.2706	0.2444	0.2286	0.1899	-2.1778	1158.8	ν2
0.3617	0.3064	0.2706	0.2444	0.2286	0.1899	2.1778	1158.8	μ12
0.3617	0.3064	0.2706	0.2444	0.2286	0.1899	-2.1778	1158.8	μ23

Razvi & Saatcioglu

Modeling of a Test by Orito (1987) involving a Steel-Confined Concrete Cylinder under Compression

t	5.2	k_1	3.673903	K	2.403141
R	57.15	f_c	52.4	ε_{cc}	0.026031
f_y	376.7	f_{cc}	178.3246		
σ_2	34.27542			E	32574.53
				E_{sec}	6850.362
				r	1.266301

ε_1	$\varepsilon_1 / \varepsilon_{cc}$	σ_1
0	0	0
0.001	0.038462	30.74816
0.002	0.076923	56.9216
0.003	0.115385	78.66186
0.004	0.153846	96.56397
0.006	0.230769	123.3448
0.008	0.307692	141.4753
0.01	0.384615	153.8485
0.012	0.461538	162.346
0.014	0.538462	168.1888
0.016	0.615385	172.1801
0.018	0.692308	174.8579
0.02	0.769231	176.5898
0.022	0.846154	177.6317
0.024	0.923077	178.165
0.026	1	178.32

Octahedral theory / Gerstle

Modeling of a compression test on an FRP-concrete column stub by Mirmiran (1997)

LABELS							
	R	72.5					
	t	2.2					
	E	37000					
STRESS							
	Δσ1	5	5	5	5	3	3
	Δσ2	0.046	0.077	0.13	0.21	0.225	0.34
	Δσ3	0.046	0.077	0.13	0.21	0.225	0.34
	σ1	5	10	15	20	23	26
	σ2	0.046	0.123	0.253	0.463	0.688	1.028
	Δσo	1.697333	1.718	1.753333	1.806667	1.15	1.226667
	Δτo	2.335338	2.320724	2.29574	2.258028	1.308148	1.253936
	σo	1.697333	3.415333	5.168667	6.975333	8.125333	9.352
	τo	2.335338	4.656062	6.951802	9.20983	10.51798	11.77191
CONST							
	K	12845	12845	12845	12845	12845	12845
	τo,max	9.05152	9.87616	10.71776	11.58496	12.13696	12.72576
	G	9633.75	7148.194	5091.97	3385.063	1975.096	1285.072
STRAIN							
	Δεo	4.4E-05	4.46E-05	4.55E-05	4.69E-05	2.98E-05	3.18E-05
	Δγo	0.000121	0.000162	0.000225	0.000334	0.000331	0.000488
	B	-0.5	-0.5	-0.5	-0.5	-0.5	-0.5
	C	1.414214	1.414214	1.414214	1.414214	1.414214	1.414214
	Δε1	0.000215	0.000274	0.000364	0.000519	0.000498	0.000722
	Δε2	-4.2E-05	-7E-05	-0.00011	-0.00019	-0.0002	-0.00031
	Δε3	-4.2E-05	-7E-05	-0.00011	-0.00019	-0.0002	-0.00031
	Δσ2'	0.045794	0.077169	0.125207	0.207712	0.224603	0.344237
	uz	0.065715	0.149331	0.260443	0.418605	0.570548	0.790699
	ur	-0.00302	-0.00509	-0.00826	-0.0137	-0.01481	-0.0227
	ε1	0.000215	0.00049	0.000854	0.001372	0.001871	0.002592
	ε2	-4E-05	-0.00011	-0.00022	-0.00041	-0.00062	-0.00093

3	3	3	3	3	3	3	5
0.575	1.015	1.29	1.17	1.22	1.21	1.21	2.02
0.575	1.015	1.29	1.17	1.22	1.21	1.21	2.02
29	32	35	38	41	44	47	52
1.603	2.618	3.908	5.078	6.298	7.508	8.718	10.738
1.383333	1.676667	1.86	1.78	1.813333	1.806667	1.806667	3.013333
1.143156	0.935738	0.806102	0.86267	0.8391	0.843814	0.843814	1.404785
10.73533	12.412	14.272	16.052	17.86533	19.672	21.47867	24.492
12.91507	13.85081	14.65691	15.51958	16.35868	17.20249	18.04631	19.45109
12845	12845	12845	12845	12845	12845	12845	12845
13.38976	14.19456	15.08736	15.94176	16.81216	17.67936	18.54656	19.99296
722.0879	341.5332	233.3024	274.8562	255.1274	259.8545	259.8516	259.8489
3.59E-05	4.35E-05	4.83E-05	4.62E-05	4.71E-05	4.69E-05	4.69E-05	7.82E-05
0.000792	0.00137	0.001728	0.001569	0.001644	0.001624	0.001624	0.002703
-0.5	-0.5	-0.5	-0.5	-0.5	-0.5	-0.5	-0.5
1.414214	1.414214	1.414214	1.414214	1.414214	1.414214	1.414214	1.414214
0.001155	0.001981	0.002491	0.002266	0.002373	0.002343	0.002343	0.003901
-0.00052	-0.00093	-0.00117	-0.00106	-0.00112	-0.0011	-0.0011	-0.00183
-0.00052	-0.00093	-0.00117	-0.00106	-0.00112	-0.0011	-0.0011	-0.00183
0.575814	1.01699	1.289784	1.169038	1.226508	1.210496	1.21051	2.015125
1.143077	1.747237	2.507129	3.198117	3.921788	4.636415	5.351051	6.540835
-0.03798	-0.06707	-0.08507	-0.0771	-0.08089	-0.07984	-0.07984	-0.1329
0.003748	0.005729	0.00822	0.010486	0.012858	0.015201	0.017544	0.021445
-0.00145	-0.00238	-0.00355	-0.00462	-0.00573	-0.00683	-0.00793	-0.00977

5	5	5	1.7	$\Delta\sigma 1$
2.01	2.02	2.02	0.68	$\Delta\sigma 2$
2.01	2.02	2.02	0.68	$\Delta\sigma 3$
57	62	67	68.7	$\sigma 1$
12.748	14.768	16.788	17.468	$\sigma 2$
3.006667	3.013333	3.013333	1.02	$\Delta\sigma o$
1.4095	1.404785	1.404785	0.480833	$\Delta\tau o$
27.49867	30.512	33.52533	34.54533	σo
20.86059	22.26538	23.67016	24.151	τo
12845	12845	12845	12845	K
21.43616	22.88256	24.32896	24.81856	$\tau o,max$
261.1023	258.669	259.8387	260.8693	G
7.8E-05	7.82E-05	7.82E-05	2.65E-05	$\Delta\varepsilon o$
0.002699	0.002715	0.002703	0.000922	$\Delta\gamma o$
-0.5	-0.5	-0.5	-0.5	B
1.414214	1.414214	1.414214	1.414214	C
0.003895	0.003918	0.003901	0.00133	$\Delta\varepsilon 1$
-0.00183	-0.00184	-0.00183	-0.00063	$\Delta\varepsilon 2$
-0.00183	-0.00184	-0.00183	-0.00063	$\Delta\varepsilon 3$
2.012246	2.024709	2.015208	0.687253	$\Delta\sigma 2'$
7.728863	8.923965	10.1138	10.51939	uz
-0.13271	-0.13354	-0.13291	-0.04533	ur
0.025341	0.029259	0.03316	0.03449	$\varepsilon 1$
-0.0116	-0.01344	-0.01527	-0.0159	$\varepsilon 2$

Octahedral theory / Gerstle (Refined)

Modeling of a compression test on an FRP-concrete column stub by Mirmiran (1997)

LABELS							
	R	72.5					
	t	2.2					
	E	37000					
STRESS							
	Δσ1	5	5	5	5	3	3
	Δσ2	0.046	0.16	0.23	0.32	0.27	0.33
	Δσ3	0.046	0.16	0.23	0.32	0.27	0.33
	σ1	5	10	15	20	23	26
	σ2	0.046	0.206	0.436	0.756	1.026	1.356
	Δσo	1.697333	1.773333	1.82	1.88	1.18	1.22
	Δτo	2.335338	2.281598	2.2486	2.206173	1.286934	1.25865
	σo	1.697333	3.470667	5.290667	7.170667	8.350667	9.570667
	τo	2.335338	4.616936	6.865535	9.071709	10.35864	11.61729
CONST							
	K	12845	12845	12845	12845	12845	12845
	k	15.11207	9.638092	7.696713	6.525213	5.953975	5.476125
	A	0.082644	0.121516	0.145845	0.165886	0.1778	0.189164
	B	1.166281	1.049666	0.97668	0.916556	0.880815	0.846722
	τou	4.161375	6.85106	9.017585	10.9517	12.0493	13.09762
	G	9633.75	4227.349	3141.557	2299.097	1653.753	1351.727
STRAIN							
	Δεo	4.4E-05	4.6E-05	4.72E-05	4.88E-05	3.06E-05	3.17E-05
	Δγo	0.000121	0.00027	0.000358	0.00048	0.000389	0.000466
	B	-0.5	-0.5	-0.5	-0.5	-0.5	-0.5
	C	1.414214	1.414214	1.414214	1.414214	1.414214	1.414214
	Δε1	0.000215	0.000428	0.000553	0.000727	0.000581	0.00069
	Δε2	-4.17E-05	-0.000145	-0.000206	-0.00029	-0.000245	-0.000298
	Δε3	-4.17E-05	-0.000145	-0.000206	-0.00029	-0.000245	-0.000298
	Δσ2'	0.045794	0.159175	0.226259	0.319309	0.26878	0.327083
	*u*z	0.065715	0.196151	0.364922	0.586753	0.763923	0.974396
	*u*r	-0.00302	-0.010498	-0.014923	-0.02106	-0.017727	-0.021572
	ε1	0.000215	0.000643	0.001196	0.001924	0.002505	0.003195
	ε2	-3.96E-05	-0.000184	-0.00039	-0.000681	-0.000925	-0.001223

3	3	3	3	3	3	3	5
0.4	0.5	0.61	0.74	0.89	1.02	1.13	2.03
0.4	0.5	0.61	0.74	0.89	1.02	1.13	2.03
29	32	35	38	41	44	47	52
1.756	2.256	2.866	3.606	4.496	5.516	6.646	8.676
1.266667	1.333333	1.406667	1.493333	1.593333	1.68	1.753333	3.02
1.225652	1.178511	1.126657	1.065374	0.994664	0.933381	0.881526	1.400071
10.83733	12.17067	13.57733	15.07067	16.664	18.344	20.09733	23.11733
12.84294	14.02146	15.14811	16.21349	17.20815	18.14153	19.02306	20.42313
12845	12845	12845	12845	12845	12845	12845	12845
5.067502	4.700559	4.374903	4.083603	3.822112	3.594711	3.39925	3.138018
0.200101	0.211059	0.221841	0.232463	0.242904	0.252777	0.261928	0.275245
0.813911	0.781036	0.748691	0.716824	0.685502	0.655883	0.62843	0.588479
14.10329	15.07769	16.02183	16.94004	17.83587	18.70483	19.54467	20.87052
1088.831	860.9214	674.8726	525.3545	413.1909	339.0502	290.1197	257.1053
3.29E-05	3.46E-05	3.65E-05	3.88E-05	4.13E-05	4.36E-05	4.55E-05	7.84E-05
0.000563	0.000684	0.000835	0.001014	0.001204	0.001376	0.001519	0.002723
-0.5	-0.5	-0.5	-0.5	-0.5	-0.5	-0.5	-0.5
1.414214	1.414214	1.414214	1.414214	1.414214	1.414214	1.414214	1.414214
0.000829	0.001003	0.001217	0.001473	0.001744	0.00199	0.002194	0.003929
-0.000365	-0.000449	-0.000554	-0.000678	-0.00081	-0.00093	-0.001029	-0.001847
-0.000365	-0.000449	-0.000554	-0.000678	-0.00081	-0.00093	-0.001029	-0.001847
0.40135	0.493981	0.608693	0.745542	0.890126	1.021991	1.130882	2.03023
1.22719	1.532969	1.904146	2.353321	2.885103	3.492118	4.161299	5.359624
-0.02647	-0.03258	-0.040146	-0.049171	-0.058707	-0.067404	-0.074586	-0.133901
0.004024	0.005026	0.006243	0.007716	0.009459	0.01145	0.013644	0.017573
-0.001588	-0.002037	-0.002591	-0.003269	-0.004079	-0.005009	-0.006037	-0.007884

5	5	5	2.7	Δσ1
2.3	2.43	2.6	1.5	Δσ2
2.3	2.43	2.6	1.5	Δσ3
57	62	67	69.7	σ1
10.976	13.406	16.006	17.506	σ2
3.2	3.286667	3.4	1.9	Δσo
1.272792	1.21151	1.131371	0.565685	Δτo
26.31733	29.604	33.004	34.904	σo
21.69592	22.90743	24.0388	24.60449	τo
12845	12845	12845	12845	*K*
2.924274	2.753984	2.611358	2.542115	
0.287192	0.29748	0.306681	0.311356	
0.552637	0.521775	0.494172	0.480146	
22.1258	23.30008	24.40602	24.97882	τou
206.5155	187.1721	162.3459	144.9513	*G*
8.3E-05	8.53E-05	8.82E-05	4.93E-05	Δεo
0.003082	0.003236	0.003484	0.001951	Δγo
-0.5	-0.5	-0.5	-0.5	B
1.414214	1.414214	1.414214	1.414214	C
0.004441	0.004662	0.005016	0.002809	Δε1
-0.002096	-0.002203	-0.002376	-0.00133	Δε2
-0.002096	-0.002203	-0.002376	-0.00133	Δε3
2.304012	2.421835	2.611443	1.462526	Δσ2'
6.714149	8.136115	9.665989	10.52269	*uz*
-0.151958	-0.159729	-0.172234	-0.096459	*ur*
0.022014	0.026676	0.031692	0.034501	ε1
-0.00998	-0.012183	-0.014559	-0.01589	ε2

Octahedral theory / Gerstle

Modeling of test S1
(large diameter ; solidly filled)
Amir Fam (1999)

LABELS								
R	106							
t	3.5							
E	27000							
STRESS								
Δσ1	5	5	5	5	5	5	5	5
Δσ2	0.0088	0.0126	0.017	0.023	0.03	0.039	0.05	0.067
Δσ3	0.0088	0.0126	0.017	0.023	0.03	0.039	0.05	0.067
σ1	5	10	15	20	25	30	35	40
σ2	0.0088	0.0214	0.0384	0.0614	0.0914	0.1304	0.1804	0.2474
Δσo	1.67253	1.67507	1.678	1.682	1.68667	1.69267	1.7	1.71133
Δτo	2.35287	2.35108	2.34901	2.34618	2.34288	2.33864	2.33345	2.32544
σo	1.67253	3.3476	5.0256	6.7076	8.39427	10.0869	11.7869	13.4983
τo	2.35287	4.70396	7.05297	9.39915	11.742	14.0807	16.4141	18.7396
CONST								
K	32388.9	32388.9	32388.9	32388.9	32388.9	32388.9	32388.9	32388.9
τo,max	18.3263	19.1638	20.0028	20.8438	21.6871	22.5335	23.3835	24.2391
G	24291.7	21172.9	18329	15726.5	13337.8	11139.5	9112.34	7240.04
STRAIN								
Δεo	1.7E-05	1.7E-05	1.7E-05	1.7E-05	1.7E-05	1.7E-05	1.7E-05	1.8E-05
Δγo	4.8E-05	5.6E-05	6.4E-05	7.5E-05	8.8E-05	0.0001	0.00013	0.00016
B	-0.5	-0.5	-0.5	-0.5	-0.5	-0.5	-0.5	-0.5
C	1.41421	1.41421	1.41421	1.41421	1.41421	1.41421	1.41421	1.41421
Δε1	8.6E-05	9.6E-05	0.00011	0.00012	0.00014	0.00017	0.0002	0.00024
Δε2	-2E-05	-2E-05	-3E-05	-4E-05	-4E-05	-6E-05	-7E-05	-1E-04
Δε3	-2E-05	-2E-05	-3E-05	-4E-05	-4E-05	-6E-05	-7E-05	-1E-04
Δσh	-0.2674	-0.38	-0.5161	-0.6831	-0.8934	-1.1658	-1.5326	-2.05
Δσ2'	0.00883	0.01255	0.01704	0.02255	0.0295	0.03849	0.0506	0.06769
uz	0.0294	0.03284	0.03701	0.04212	0.04856	0.05689	0.06811	0.08394
ur	-0.0018	-0.0023	-0.003	-0.0038	-0.0047	-0.006	-0.0077	-0.0102
ε1	8.6E-05	0.00018	0.00029	0.00041	0.00055	0.00072	0.00092	0.00116
ε2	-2E-05	-4E-05	-7E-05	-0.0001	-0.0001	-0.0002	-0.0003	-0.0004
LOAD								
conc.	176.495	352.989	529.484	705.979	882.473	1058.97	1235.46	1411.96
Δσl	1.52768	1.70236	1.91313	2.17218	2.49818	2.9204	3.48842	4.29033
σl	1.52768	3.23004	5.14317	7.31534	9.81352	12.7339	16.2223	20.5127
FRP	3.56112	7.52941	11.989	17.0525	22.8759	29.6836	37.8153	47.8163
Total	180.056	360.519	541.473	723.031	905.349	1088.65	1273.28	1459.77
TSAIWU								
σh	-0.2674	-0.6474	-1.1635	-1.8465	-2.7399	-3.9057	-5.4382	-7.4882
A	5.1E-05	0.00023	0.00059	0.00121	0.00221	0.00377	0.00622	0.0101

5	5	5	3	3	2	2	1.5	Δσ1
0.094	0.14	0.22	0.28	0.55	1.03	0.58	0.62	Δσ2
0.094	0.14	0.22	0.28	0.55	1.03	0.58	0.62	Δσ3
45	50	55	58	61	63	65	66.5	σ1
0.3414	0.4814	0.7014	0.9814	1.5314	2.5614	3.1414	3.7614	σ2
1.72933	1.76	1.81333	1.18667	1.36667	1.35333	1.05333	0.91333	Δσo
2.31271	2.29103	2.25331	1.28222	1.15494	0.45726	0.66939	0.41484	Δτo
15.2276	16.9876	18.8009	19.9876	21.3543	22.7076	23.7609	24.6743	σo
21.0523	23.3433	25.5966	26.8788	28.0338	28.491	29.1604	29.5753	τo
32388.9	32388.9	32388.9	32388.9	32388.9	32388.9	32388.9	32388.9	*K*
25.1038	25.9838	26.8905	27.4838	28.1671	28.8438	29.3705	29.8271	τo,max
5511.5	3920.46	2468.55	1168.82	534.709	115.017	297.096	173.722	*G*
1.8E-05	1.8E-05	1.9E-05	1.2E-05	1.4E-05	1.4E-05	1.1E-05	9.4E-06	Δεo
0.00021	0.00029	0.00046	0.00055	0.00108	0.00199	0.00113	0.00119	Δγo
-0.5	-0.5	-0.5	-0.5	-0.5	-0.5	-0.5	-0.5	B
1.41421	1.41421	1.41421	1.41421	1.41421	1.41421	1.41421	1.41421	C
0.00031	0.00043	0.00066	0.00079	0.00154	0.00283	0.0016	0.0017	Δε1
-0.0001	-0.0002	-0.0003	-0.0004	-0.0007	-0.0014	-0.0008	-0.0008	Δε2
-0.0001	-0.0002	-0.0003	-0.0004	-0.0007	-0.0014	-0.0008	-0.0008	Δε3
-2.8318	-4.1403	-6.7512	-8.4147	-16.862	-31.389	-17.702	-18.823	Δσh
0.0935	0.13671	0.22292	0.27785	0.55677	1.03643	0.58451	0.62152	Δσ2'
0.10788	0.14795	0.22779	0.27026	0.52869	0.96901	0.55019	0.58239	*u*z
-0.0138	-0.02	-0.0322	-0.0398	-0.0795	-0.1475	-0.0833	-0.0885	*u*r
0.00148	0.00191	0.00257	0.00336	0.0049	0.00773	0.00933	0.01103	ε1
-0.0005	-0.0007	-0.001	-0.0014	-0.0021	-0.0035	-0.0043	-0.0051	ε2
1588.45	1764.95	1941.44	2047.34	2153.24	2223.83	2294.43	2347.38	conc.
5.50261	7.53208	11.576	13.7114	26.8005	49.0942	27.8814	29.5085	Δσl
26.0153	33.5474	45.1234	58.8348	85.6353	134.73	162.611	192.119	σl
60.6432	78.201	105.185	137.148	199.621	314.063	379.056	447.842	FRP
1649.1	1843.15	2046.63	2184.49	2352.86	2537.9	2673.49	2795.22	Total
-10.32	-14.46	-21.211	-29.626	-46.488	-77.877	-95.58	-114.4	σh
0.01652	0.02798	0.05171	0.08952	0.19375	0.48888	0.71597	1.00362	A

Octahedral theory / Gerstle

Modeling of Test S6
Experimental work
by Amir (1999)

LABELS								
	R	106						
	t	3.5						
	E	27000						
STRESS								
	Δσ1	5	5	5	5	5	5	5
	Δσ2	0.01302	0.01849	0.02514	0.03254	0.04289	0.05621	0.07396
	Δσ3	0.0088	0.0125	0.017	0.022	0.029	0.038	0.05
	σ1	5	10	15	20	25	30	35
	Dpo	0.0088	0.0125	0.017	0.022	0.029	0.038	0.05
	po	0.0088	0.0213	0.0383	0.0603	0.0893	0.1273	0.1773
	Δσo	1.67397	1.67704	1.68077	1.68492	1.69073	1.6982	1.70816
r = Ro	Δτo	2.35216	2.35012	2.34764	2.34488	2.34102	2.33605	2.32944
r = Ri	Δτo2	2.35341	2.35189	2.35005	2.348	2.34514	2.34147	2.33658
	σo	1.67397	3.35101	5.03178	6.7167	8.40743	10.1056	11.8138
r = Ro	τo	2.35216	4.70229	7.04992	9.3948	11.7358	14.0719	16.4013
r = Ri	to2	2.35341	4.70531	7.05536	9.40336	11.7485	14.09	16.4266
CONST								
	K	32388.9	32388.9	32388.9	32388.9	32388.9	32388.9	32388.9
	τo,max	18.327	19.1655	20.0059	20.8484	21.6937	22.5428	23.3969
	G	24291.7	21174	18331.7	15731.5	13345.2	11150.4	9128.11
STRAIN								
	Δεo	1.7E-05	1.7E-05	1.7E-05	1.7E-05	1.7E-05	1.7E-05	1.8E-05
	Δγo	4.8E-05	5.6E-05	6.4E-05	7.5E-05	8.8E-05	0.0001	0.00013
	B	-0.49938	-0.49912	-0.4988	-0.49844	-0.49795	-0.4973	-0.49644
	C	1.41421	1.41421	1.41421	1.41421	1.41421	1.41421	1.4142
	Δε1	8.6E-05	9.6E-05	0.00011	0.00012	0.00014	0.00017	0.0002
	Δε2	-1.7E-05	-2.2E-05	-2.8E-05	-3.5E-05	-4.4E-05	-5.6E-05	-7.2E-05
	Δε3	-1.7E-05	-2.2E-05	-2.8E-05	-3.6E-05	-4.5E-05	-5.7E-05	-7.4E-05
	Δσh	-0.26596	-0.37783	-0.51257	-0.67825	-0.88576	-1.15358	-1.51175
	Δpo	0.00878	0.01248	0.01692	0.02239	0.02925	0.03809	0.04992
	ε1	8.6E-05	0.00018	0.00029	0.00041	0.00055	0.00072	0.00092
	ε2	-1.7E-05	-3.9E-05	-6.7E-05	-0.0001	-0.00015	-0.0002	-0.00028
LOAD								
	conc.	141.8	283.6	425.4	567.2	709	850.8	992.6
	Δσl	1.52831	1.70326	1.91433	2.17385	2.50026	2.92271	3.4898
	σl	1.52831	3.23157	5.14589	7.31975	9.82001	12.7427	16.2325
	FRP	3.56257	7.53298	11.9954	17.0628	22.8911	29.7041	37.839
	total	145.363	291.133	437.395	584.263	731.891	880.504	1030.44
TSAIWU								
	σh	-0.26596	-0.64379	-1.15636	-1.8346	-2.72036	-3.87394	-5.38569
	A	5.1E-05	0.00023	0.00059	0.00121	0.00221	0.00377	0.00621

5	5	5	5	3	3	2	1.2	Δσ1
0.09762	0.1346	0.19228	0.31061	0.36978	0.6656	0.991	0.67299	Δσ2
0.066	0.091	0.13	0.21	0.25	0.45	0.66999	0.455	Δσ3
40	45	50	55	58	61	63	64.2	σ1
0.066	0.091	0.13	0.21	0.25	0.45	0.67	0.455	Dpo
0.2433	0.3343	0.4643	0.6743	0.9243	1.3743	2.0443	2.4993	po
1.72143	1.74218	1.77454	1.84092	1.20745	1.37341	1.22263	0.77756	Δσo
2.32062	2.30685	2.28539	2.24146	1.28351	1.18166	0.64145	0.4043	Δτo
2.33008	2.31996	2.30427	2.27247	1.34687	1.30242	0.92635	0.68322	Δτo2
13.5352	15.2774	17.0519	18.8929	20.1003	21.4737	22.6964	23.4739	σo
18.7219	21.0288	23.3142	25.5556	26.8391	28.0208	28.6622	29.0665	τo
18.7566	21.0766	23.3809	25.6533	27.0002	28.3026	29.229	29.9122	to2
32388.9	32388.9	32388.9	32388.9	32388.9	32388.9	32388.9	32388.9	*K*
24.2576	25.1287	26.016	26.9364	27.5402	28.2269	28.8382	29.227	τo,max
7263.12	5543.45	3963.36	2522.73	1245.23	618.334	177.343	148.204	*G*
1.8E-05	1.8E-05	1.8E-05	1.9E-05	1.2E-05	1.4E-05	1.3E-05	8E-06	Δεo
0.00016	0.00021	0.00029	0.00045	0.00054	0.00105	0.00261	0.0023	Δγo
-0.49528	-0.49345	-0.49055	-0.48442	-0.46731	-0.43515	-0.29797	-0.24753	B
1.41419	1.41417	1.41413	1.41398	1.41321	1.41027	1.37723	1.35769	C
0.00024	0.00031	0.00043	0.00066	0.00078	0.0015	0.00361	0.00314	Δε1
-9.5E-05	-0.00013	-0.00018	-0.00029	-0.00034	-0.00063	-0.00106	-0.00077	Δε2
-9.7E-05	-0.00013	-0.00019	-0.00031	-0.00039	-0.00082	-0.00251	-0.00235	Δε3
-2.0147	-2.76619	-4.00618	-6.37572	-7.59968	-13.7652	-20.5571	-13.6797	Δσh
0.06652	0.09134	0.13228	0.21052	0.25093	0.45451	0.67877	0.45169	Δpo
0.00116	0.00148	0.00191	0.00256	0.00334	0.00484	0.00845	0.01159	ε1
-0.00037	-0.0005	-0.00068	-0.00097	-0.00132	-0.00195	-0.00301	-0.00377	ε2
1134.4	1276.2	1418	1559.8	1644.88	1729.96	1786.68	1820.71	conc.
4.28925	5.49437	7.50388	11.4474	13.5551	26.2181	63.8206	55.7084	Δσl
20.5218	26.0161	33.52	44.9674	58.5225	84.7406	148.561	204.27	σl
47.8375	60.6452	78.1372	104.822	136.42	197.536	346.305	476.165	FRP
1182.24	1336.85	1496.14	1664.62	1781.3	1927.5	2132.99	2296.88	total
-7.40039	-10.1666	-14.1728	-20.5485	-28.1482	-41.9134	-62.4704	-76.1501	σh
0.01008	0.01647	0.02781	0.05099	0.08749	0.1848	0.54568	1.0056	A

Octahedral theory / Gerstle

Modeling of Test S8 / S9
Test by Amir Fam (1999)

LABELS										
	Ro	81	Ri	44						
	t	3.2	E	27000						
STRESS										
	Δσ1	5	5	5	5	5	5	5	5	5
r = Ro	Δσ2	0.009	0.013	0.018	0.024	0.031	0.041	0.053	0.07	0.094
	Δσ3	0.02407	0.03502	0.04814	0.06419	0.08291	0.10881	0.14007	0.18218	0.24218
r = Ri	Δσ2	-0.009	-0.0133	-0.018	-0.024	-0.031	-0.04	-0.051	-0.064	-0.083
	Δσ3	0.04207	0.06132	0.08414	0.11219	0.14491	0.18981	0.24407	0.31618	0.41918
	σ1	5	10	15	20	25	30	35	40	45
	Dpo	0.009	0.013	0.018	0.024	0.031	0.041	0.053	0.07	0.094
	po	0.009	0.022	0.04	0.064	0.095	0.136	0.189	0.259	0.353
	Dpi	-0.009	-0.0133	-0.018	-0.024	-0.031	-0.04	-0.051	-0.064	-0.083
	pi	-0.009	-0.0223	-0.0403	-0.0643	-0.0953	-0.1353	-0.1863	-0.2503	-0.3333
	Δσo	1.67769	1.68267	1.68871	1.69606	1.70464	1.7166	1.73102	1.75073	1.77873
r = Ro	Δτo	2.34924	2.34572	2.34147	2.33629	2.33027	2.32188	2.31179	2.29804	2.27859
r = Ri	Δτo2	2.34932	2.3459	2.3418	2.3369	2.33128	2.32361	2.31465	2.30282	2.28699
	σo	1.67769	3.36036	5.04908	6.74514	8.44977	10.1664	11.8974	13.6481	15.4269
	τo	2.34924	4.69496	7.03642	9.37272	11.703	14.0249	16.3367	18.6347	20.9133
	to2	2.34932	4.69522	7.03703	9.37393	11.7052	14.0288	16.3435	18.6463	20.9333
CONST										
	K	32388.9	32388.9	32388.9	32388.9	32388.9	32388.9	32388.9	32388.9	32388.9
	τo,max	18.3288	19.1702	20.0145	20.8626	21.7149	22.5732	23.4387	24.3141	25.2034
	G	24291.7	21178.2	18342.4	15751.6	13378.4	11200	9199.1	7360.5	5674.14
STRAIN										
	Δεo	1.7E-05	1.7E-05	1.7E-05	1.7E-05	1.8E-05	1.8E-05	1.8E-05	1.8E-05	1.8E-05
	Δγo	4.8E-05	5.5E-05	6.4E-05	7.4E-05	8.7E-05	0.0001	0.00013	0.00016	0.0002
r = Ro	B	-0.50227	-0.50332	-0.50455	-0.50608	-0.50788	-0.51033	-0.51332	-0.51726	-0.523
	C	1.41421	1.4142	1.41419	1.41418	1.41416	1.41411	1.41405	1.41393	1.41372
	Δε1	8.6E-05	9.6E-05	0.00011	0.00012	0.00014	0.00016	0.0002	0.00024	0.0003
	Δε2	-1.7E-05	-2.2E-05	-2.8E-05	-3.6E-05	-4.5E-05	-5.7E-05	-7.3E-05	-9.6E-05	-0.00013
	Δε3	-1.7E-05	-2.2E-05	-2.7E-05	-3.4E-05	-4.3E-05	-5.4E-05	-6.9E-05	-8.9E-05	-0.00012
	Dsh	-0.22379	-0.32778	-0.4521	-0.60306	-0.79081	-1.02778	-1.33934	-1.76344	-2.36937
	Δpo	0.00884	0.01295	0.01786	0.02382	0.03124	0.0406	0.05291	0.06967	0.0936
r = Ri	B	-0.50769	-0.51125	-0.51542	-0.52061	-0.52669	-0.535	-0.54513	-0.5585	-0.57795
	C	1.41416	1.41409	1.41399	1.41381	1.41354	1.41306	1.4123	1.411	1.40852
	Δε1	8.6E-05	9.6E-05	0.00011	0.00012	0.00014	0.00016	0.0002	0.00024	0.0003
	Δε2	-1.7E-05	-2.2E-05	-2.8E-05	-3.6E-05	-4.5E-05	-5.7E-05	-7.3E-05	-9.6E-05	-0.00013
	Δε3	-1.6E-05	-2.1E-05	-2.6E-05	-3.3E-05	-4.1E-05	-5E-05	-6.3E-05	-7.9E-05	-0.0001
	Δσh	-0.20073	-0.29198	-0.39947	-0.52726	-0.68307	-0.87191	-1.11145	-1.41948	-1.81774
	Δpi	0.00912	0.01327	0.01816	0.02397	0.03105	0.03963	0.05052	0.06452	0.08262
	ε1	8.6E-05	0.00018	0.00029	0.00041	0.00055	0.00072	0.00091	0.00115	0.00145
	ε2	-1.7E-05	-3.9E-05	-6.7E-05	-0.0001	-0.00015	-0.00021	-0.00028	-0.00037	-0.0005
LOAD										
	conc.	70.92	141.84	212.76	283.68	354.6	425.52	496.44	567.36	638.28
r = Ro	Δσl	1.52678	1.69867	1.90593	2.15945	2.47641	2.88243	3.421	4.16593	5.25721
	σl	1.52678	3.22544	5.13138	7.29083	9.76724	12.6497	16.0707	20.2366	25.4938
r = Ri	Δσl	1.3577	1.51168	1.69688	1.92362	2.20732	2.57122	3.05428	3.723	4.70324
	σl	1.3577	2.86937	4.56625	6.48987	8.69718	11.2684	14.3227	18.0457	22.7489
	FRP	3.31567	7.00526	11.1455	15.837	21.2179	27.4821	34.9183	43.9757	55.4086
	total	74.2357	148.845	223.905	299.517	375.818	453.002	531.358	611.336	693.689
TSAIWU										
r = Ro	sh	-0.22379	-0.55158	-1.00368	-1.60673	-2.39754	-3.42533	-4.76466	-6.52811	-8.89748
	A	5E-05	0.00023	0.00058	0.00119	0.00216	0.00368	0.00602	0.00969	0.01561
r = Ri	sh	-0.20073	-0.49271	-0.89217	-1.41943	-2.1025	-2.97441	-4.08586	-5.50534	-7.32308
	A	2.7E-05	0.00012	0.00031	0.00064	0.00116	0.00198	0.00325	0.00522	0.00839

5	5	3	3	2	1.5	1.5	1.5	1 Δσ1
0.13	0.19	0.195	0.3	0.355	0.419	0.481	0.49	0.32 Δσ2
0.33093	0.46627	0.44197	0.61395	0.61034	0.6149	0.67272	0.68088	0.44809 Δσ3
-0.11	-0.14	-0.1	-0.075	0.05	0.185	0.252	0.262	0.167 Δσ2
0.57093	0.79627	0.73697	0.98895	0.91534	0.8489	0.90172	0.90888	0.60109 Δσ3
50	55	58	61	63	64.5	66	67.5	68.5 σ1
0.13	0.19	0.195	0.3	0.355	0.419	0.481	0.49	0.32 Dpo
0.483	0.673	0.868	1.168	1.523	1.942	2.423	2.913	3.233 po
-0.11	-0.14	-0.1	-0.075	0.05	0.185	0.252	0.262	0.167 Dpi
-0.4433	-0.5833	-0.6833	-0.7583	-0.7083	-0.5233	-0.2713	-0.0093	0.1577 pi
1.82031	1.88542	1.21232	1.30465	0.98845	0.84463	0.88457	0.89029	0.58936 Δσo
2.24988	2.20522	1.26809	1.20563	0.72283	0.47026	0.44216	0.43811	0.29504 Δτo
2.2655	2.23526	1.30945	1.27506	0.79776	0.53685	0.50964	0.50558	0.34017 Δτo2
17.2472	19.1326	20.3449	21.6496	22.638	23.4826	24.3672	25.2575	25.8469 σo
23.1632	25.3684	26.6365	27.8421	28.5649	29.0352	29.4774	29.9155	30.2105 τo
23.1988	25.434	26.7435	28.0185	28.8163	29.3532	29.8628	30.3684	30.7085 to2
32388.9	32388.9	32388.9	32388.9	32388.9	32388.9	32388.9	32388.9	32388.9 *K*
26.1136	27.0563	27.6625	28.3148	28.809	29.2313	29.6736	30.1188	30.4134 τo,max
4134.95	2744.58	1515.44	900.96	405.517	205.799	162.981	160.658	163.956 *G*
1.9E-05	1.9E-05	1.2E-05	1.3E-05	1E-05	8.7E-06	9.1E-06	9.2E-06	6.1E-06 Δεo
0.00027	0.0004	0.00042	0.00067	0.00089	0.00114	0.00136	0.00136	0.0009 Δγo
-0.5316	-0.54435	-0.56908	-0.59259	-0.62621	-0.64946	-0.65576	-0.65653	-0.65597 B
1.41327	1.41236	1.40974	1.4062	1.39943	1.39361	1.39188	1.39166	1.39182 C
0.0004	0.00059	0.0006	0.00095	0.00126	0.0016	0.0019	0.00191	0.00126 Δε1
-0.00019	-0.00029	-0.00032	-0.00054	-0.00077	-0.00103	-0.00123	-0.00124	-0.00082 Δε2
-0.00016	-0.00024	-0.00024	-0.00037	-0.00046	-0.00055	-0.00064	-0.00064	-0.00042 Δε3
-3.30111	-4.92143	-4.94895	-7.48526	-9.00783	-10.6189	-12.3034	-12.3247	-8.15257 Dsh
0.13041	0.19443	0.19551	0.29571	0.35586	0.41951	0.48606	0.4869	0.32208 Δpo
-0.60707	-0.6503	-0.73409	-0.81378	-0.92773	-1.00651	-1.02786	-1.03048	-1.02856 B
1.40353	1.39338	1.36522	1.32963	1.26799	1.22075	1.20758	1.20595	1.20714 C
0.0004	0.00058	0.00058	0.0009	0.00114	0.0014	0.00165	0.00165	0.00109 Δε1
-0.00019	-0.00029	-0.00032	-0.00054	-0.00077	-0.00103	-0.00123	-0.00124	-0.00082 Δε2
-0.00013	-0.00018	-0.00014	-0.00015	-7.1E-05	1.8E-05	5.5E-05	5.9E-05	3.7E-05 Δε3
-2.33785	-3.03444	-2.07642	-1.58681	1.08965	4.05139	5.62278	5.75562	3.74853 Δσh
0.10627	0.13793	0.09438	0.07213	-0.04953	-0.18415	-0.25558	-0.26162	-0.17039 Δpi
0.00186	0.00244	0.00304	0.004	0.00526	0.00686	0.00875	0.01066	0.01192 ε1
-0.00069	-0.00098	-0.0013	-0.00185	-0.00262	-0.00364	-0.00487	-0.00611	-0.00692 ε2
709.2	780.12	822.672	865.224	893.592	914.868	936.144	957.42	971.604 conc.
6.99378	10.143	10.3633	16.3613	21.4604	27.2436	32.2589	32.4187	21.3964 Δσl
32.4876	42.6306	52.9938	69.3552	90.8156	118.059	150.318	182.737	204.133 σl
6.2617	9.07556	9.20777	14.3487	18.313	22.7106	26.7089	26.8186	17.7113 Δσl
29.0106	38.0862	47.2939	61.6427	79.9556	102.666	129.375	156.194	173.905 σl
70.6209	92.6797	115.181	150.599	196.768	255.075	324.013	393.279	439.001 FRP
779.821	872.8	937.853	1015.82	1090.36	1169.94	1260.16	1350.7	1410.61 total
-12.1986	-17.12	-22.069	-29.5542	-38.5621	-49.181	-61.4843	-73.809	-81.9616 sh
0.02573	0.04495	0.07005	0.12064	0.20668	0.34769	0.56126	0.82706	1.03068 A
-9.66093	-12.6954	-14.7718	-16.3586	-15.269	-11.2176	-5.59479	0.16083	3.90936 sh
0.01375	0.0237	0.03603	0.05935	0.09513	0.14894	0.22712	0.3224	0.39467 A